การลดสัญญาณรบกวนในการสื่อสัญญาณซีดีเอ็มเอแสงชนิดแผ่ทางเวลาแบบโคฮีเรนต์ความเร็ว 40 กิกะบิตต่อวินาทีบนโครงข่ายเชิงแสงแบบพาสซีฟ

นายรชฎ มณีขัติ

วิทยานิพนธ์นี้เป็นส่วนหนึ่งของการศึกษาตามหลักสูตรปริญญาวิศวกรรมศาสตรดุษฎีบัณฑิต
สาขาวิชาวิศวกรรมไฟฟ้า ภาควิชาวิศวกรรมไฟฟ้า
คณะวิศวกรรมศาสตร์ จุฬาลงกรณ์มหาวิทยาลัย
ปีการศึกษา 2558

NOISE SUPPRESSION IN 40 GIGABIT-PER-SECOND COHERENT TIME-SPREADING OCDMA SIGNAL TRANSMISSION OVER PASSIVE OPTICAL NE TWORK

Mr. Rachata Maneekut

A Dissertation Submitted in Partial Fulfillment of the Requirements
for the Degree of Doctor of Philosophy Program in Electrical Engineering
Department of Electrical Engineering
Faculty of Engineering
Chulalongkorn University
Academic Year 2015

Thesis Title	NOISE SUPPRESSION IN 40 GIGABIT-PER-SECOND COHERENT TIME-SPREADING OCDMA SIGNAL TRANSMISSION OVER PASSIVE OPTICAL NETWORK
By	Mr. Rachata Maneekut
Field of Study	Electrical Engineering
Thesis Advisor	Assistant Professor Pasu Kaewplung, Ph.D.

Accepted by the Faculty of Engineering, Chulalongkorn University in Partial Fulfillment of the Requirements for the Doctoral Degree

.....Dean of the Faculty of Engineering
(Associate Professor Supot Teachavorasinskun, D.Eng.)

THESIS COMMITTEE

.....Chairman
(Assistant Professor Tuptim Angkaew, D.Eng.)
.....Thesis Advisor
(Assistant Professor Pasu Kaewplung, Ph.D.)
.....Examiner
(Associate Professor Lunchakorn Wuttisittikulkij, Ph.D.)
.....External Examiner
(Associate Professor Poompat Saengudomlert, Ph.D.)
.....External Examiner
(Assistant Professor Norrarat Wattanamongkhol, Ph.D.)

รชฎ มณีขัติ : การลดสัญญาณรบกวนในการสื่อสัญญาณซีดีเอ็มเอแสงชนิดแผ่ทางเวลาแบบโคฮีเรนต์ความเร็ว 40 กิกะบิตต่อวินาทีบนโครงข่ายเชิงแสงแบบพาสซีฟ (NOISE SUPPRESSION IN 40 GIGABIT-PER-SECOND COHERENT TIME-SPREADING OCDMA SIGNAL TRANSMISSION OVER PASSIVE OPTICAL NETWORK) อ.ที่ปรึกษาวิทยานิพนธ์หลัก: พสุ แก้วปลั่ง, หน้า.

วิทยานิพนธ์ฉบับนี้ศึกษาการลดสัญญาณรบกวนของการส่งสัญญาณแบบซีดีเอ็มเอแสงบนโครงข่ายเชิงแสงแบบพาสซีฟความเร็ว 40 กิกะบิตต่อวินาทีต่อผู้ใช้บริการโดยใช้อัตราส่วนการแผ่ทางเวลาต่อระยะเวลา 1 บิต (spreading-time to bit period ratio : SBR) ควบคู่กับชุดรหัสฟูเรียร์ที่มีค่าความเปรียบต่างกำลังสัญญาณ (power contrast ratio: PCR) ที่สูงกว่าชุดรหัสแบบอื่น ผลการศึกษาปรากฏว่าการใช้ตัวเข้า/ถอดรหัสที่มีจำนวนชิปเท่ากับ 32 สามารถลดผลกระทบจากสัญญาณรบกวนในการส่งสัญญาณแบบซีดีเอ็มเอแสงได้ดีที่สุด ผลการคำนวณทางคณิตศาสตร์ของสัญญาณรบกวนและอัตราบิตผิดพลาดของระบบซีดีเอ็มเอแสงโดยใช้ตัวแปร SBR ที่ต่างกัน พบว่า ในสถานการณ์ที่แย่ที่สุดและสถานการณ์การเข้าถึงแบบสุ่มเมื่อใช้ SBR เท่ากับ 0.6, 0.4 และ 0.2 สามารถลดผลกระทบของสัญญาณรบกวนได้มากกว่าระบบซีดีเอ็มเอแสงแบบเดิมที่ใช้ SBR เท่ากับ 1.0 และ 0.8 นอกจากนี้ยังได้ใช้การจำลองทางคอมพิวเตอร์เพื่อการยืนยันผลการคำนวณทางคณิตศาสตร์ ผลการเปรียบเทียบปรากฏว่าระบบซีดีเอ็มเอแสงบนโครงข่ายเชิงแสงแบบพาสซีฟมีประสิทธิภาพที่ดีกว่าในแง่ของต้นทุนกำลัง อัตราบิตต่อผู้ใช้บริการและมีความซับซ้อนของระบบที่ดีกว่าระบบทีดีเอ็มเอ ท้ายสุดการยืนยันผลของการคำนวณทางคณิตศาสตร์และการจำลองทางคอมพิวเตอร์ด้วยการทดลองจริงที่ใช้ตัวเข้า/ถอดรหัสแบบ AWG สำหรับค่า SBR เท่ากับ 0.8 และใช้ตัวเข้า/ถอดรหัสแบบ PLC สำหรับค่า SBR เท่ากับ 0.1 ผลการทดลองสามารถยืนยันได้ว่าการลด SBR สามารถลดผลของสัญญาณรบกวนในการสื่อสัญญาณแบบซีดีเอ็มเอแสงได้

ภาควิชา วิศวกรรมไฟฟ้า ลายมือชื่อนิสิต .....

สาขาวิชา วิศวกรรมไฟฟ้า ลายมือชื่อ อ.ที่ปรึกษาหลัก .....

ปีการศึกษา 2558

5471422621 : MAJOR ELECTRICAL ENGINEERING
KEYWORDS: OPTICAL COMMUNICATION / OPTICAL FIBER TRANSMISSION / OPTICAL CODE DIVISION MULTIPLE ACCESS / OPTICAL CODE DIVISION MULTIPLEXING / FIBER TO THE HOME

RACHATA MANEEKUT: NOISE SUPPRESSION IN 40 GIGABIT-PER-SECOND COHERENT TIME-SPREADING OCDMA SIGNAL TRANSMISSION OVER PASSIVE OPTICAL NETWORK. ADVISOR: ASST. PROF. PASU KAEWPLUNG, Ph.D., pp.

In this dissertation, we studied the OCDMA system over PON at the bit rate per channel of 40 Gbps using Fourier code in order to suppress the noise. We proposed the spreading-time to bit period ratio (SBR) as a factor that can suppress the noise. Our results showed that the highest chip number was resulting in the lowest noise and the BER due to its highest PCR. We further investigated the performance of the system with the different SBR. We performed the mathematical calculation to obtain the noise variance and the BER. The results showed that, in the worst case, and the average case, the BER of the system employing SBR = 0.6, 0.4, and 0.2 was greater than the conventional system using SBR = 1.0, and 0.8. The simulation results confirmed the validity of our mathematical values. Moreover, the comparison between the TDMA and the OCDMA-PON was demonstrated. We showed that the OCDMA-PON was superior in terms of bit rate per subscriber, power budget, and the system complexity at the same bit rate, respectively. Finally, the system verification was proved by performing the experiment. We used the AWG and the PLC en/decoder with the SBR = 0.1 and 0.8. The results had reached and agreement with our mathematical calculation and the simulation, respectively.

Department:	Electrical Engineering	Student's Signature	.....
Field of Study:	Electrical Engineering	Advisor's Signature	.....
Academic Year:	2015		

ACKNOWLEDGEMENTS

At first, I would like to thank Assistant Professor Dr. Pasu Kaewplung, my thesis advisor for giving me a valuable discussion in my work. Without their professional supervision and powerful encouragement throughout my whole period of the course, this entire work can be hardly completed.

I would like to thank Assistant Prfessor Dr. Tuptim Angkaew, Associate Professor Dr. Lunchakorn Wuttisittikulkij, Associate Professor Dr. Poompat Saengudomlert, and Assistant Professor Dr. Norrarat Wattanamongkol for their careful reading and valuable comments on this dissertation.

I also would like to thank the National Institute of Communication and Technology (NICT), Japan for granting me a research Fellowship. Especially, I would like to thank Dr. Naoya Wada, Dr. Satoshi Shimizu and all great staffs from NICT, Japan for giving me their expertise in the research discussion.

To my family, I could have never achieved my achievement without my most powerful inspiration and support from my parents.

This dissertation is supported by the 90th Anniversary of Chulalongkorn University, Rachadapisek Sompote Fund.

Finally, I would like to express my sincere thankful to Ms. Saweeya Dejitikul, my girlfriend, all of my friends at the department of the Telecommunication 13th floor, MLC research group, GZC group for their helps.

CONTENTS

Page

Page

Page

FIGURE CONTENTS

TABLE CONTENTS

CHAPTER 1 Introduction

1.1 Background Knowledge

The fabulous increasing of the demand in data communication is growing rapidly due to the number of end-subscribers is also growing up and many types of widespread internet media such as social media applications, online gaming, telemedicine service, full-HDTV, 3D-TV and super hi-vision (4k) digital video format have been developed to have a greater performance which could bring a dramatically huge amount of bandwidth as well [1, 2]. The main key to satisfy the bandwidth hunger is the excellence in data transmission for the last mile. Fiber to the home (FTTH) based passive optical network (PON) has been stately stated as one of the most powerful access network for decades since FTTH can provide a gigabit-class data rate to the customers [3]. Institute of electrical and electronics engineers (IEEE) and international telecommunication union telecommunication standardization sector (ITU-T) has been already standardized the 10G-PON technology in the name of 10G-EPON and XG-PON, released in 2009 and 2010, respectively [4, 5]. However, in the upcoming years, PON should be able to provide at the bit rate 40 Gbps or beyond with the major architecture platform employing a prospective time-wavelength division multiplexing (TWDM) at least 40 km [6, 7]. These requirements are recently being discussed in the next generation PON stage 2 (NG-PON2) as the main aiming system enhancements that could have a possibility to start a deployment later than 2015 [6].

However, most of current PON standardizations, the multiple access scheme for an upstream is based on the time-division multiple access (TDMA) which the time-slots for each subscriber is dynamically assigned by optical line terminal. Hence, each subscriber is able to transmit their own information without any collisions via an efficient dynamic bandwidth allocation (DBA) protocol, but the total amount of bandwidth per subscriber is sharing among all subscribers in each PON [8]. Due to this tight control in time-slot synchronization and bandwidth sharing among subscribers, it is difficult to increase the individual bandwidth. In order to increase the system line rate, the bit period is reduced so we have to compete with the serious pulse broadening due to the dispersive effect in a fiber. Moreover, the complexity in an electronic circuit design that could increase the system cost is not preferable in the last-mile network.

Wavelength division multiple access (WDMA) is another multiple access scheme that can increase the bandwidth per subscriber by assigning an individual wavelength to each subscriber. Therefore, there is no need in time-slot synchronization and no bandwidth sharing that could let each subscriber to obtain maximum bandwidth at all time [9]. Anyway, the total number of subscribers is depended on the number of wavelength according to WDM standardization. In ITU-T G.694-2 or coarse wavelength division multiplexing (CWDM) with 20 nm channel spacing, from 1270-1610 nm, has reserved only 18 wavelengths. That is not enough for the access network. One of the solutions is choosing a WDM with narrower channel spacing to increase the number of wavelengths. For instance, a WDM with

0.8 nm (100 GHz) channel spacing can provide approximately 73 wavelengths simultaneously in C-band from 1520-1577 nm. However, the major drawbacks of this solution are the serious crosstalk between consecutive channels and we need to apply high-priced optical sources with a good stability in temperature control and narrow linewidth [10]. Consequently, we need another multiple access scheme to break this bandwidth limitation.

Optical code-division multiple access (OCDMA) is neither time nor wavelength multiple access scheme, but it proposes another dimension to access to the network. The unique code, which is orthogonal to the others, is assigned to each subscriber. The code is used to encode the original optical signal to exhibit a unique temporal waveform. With this scheme, each subscriber can transmit their own information using same wavelength simultaneously with the full capacity in bandwidth allocation of the system. Therefore, OCDMA is a promising multiple access technology that can increase system bit rate and the total number of subscribers [11-14].

Many of current researches on access and non-access network are also paying attention on the OCDMA. In a backbone optical network technology, the OCDMA has been introduced to increase the system capacity over WDM network [15]. A field trial of 3-WDM channel in cooperating with 10-OCDMA subscribers/wavelength at a bit rate of 10 Gbps/subscriber was successfully demonstrated over 111 km with a bit error rate (BER) lower than 10^{-9} [16]. Another interesting experiment was done by the employing of 4-OCDMA subscribers/wavelength over 8 WDM channels simultaneously. The bit rate per subscribers is 40 Gbps. Moreover, a polarization division multiplexing (PDM) technique is also used in this paper. A largest capacity of 2.56 Tbps with asynchronous transmission has been achieved over 50 km [17]. Moreover, in order to increase the node-throughput in a backbone network, it is necessary to pay attention on the packet routing and the switching technology. Most of the conventional core-node router is based on the optical-electrical-optical (OEO) conversion which the signal routing and the signal processing are done in the electrical domain. Therefore, the limitation of the routing and the switching are restricted by the electronic processing. Another solution to enhance the node-throughput and the packet processing speed are to process the packet in the optical domain, called the optical packet switching (OPS) [18, 19]. An OPS is consisted of the optical label and the payload which the optical label is employing OCDMA technology. For example, the research in [20] has shown the Ethernet-to-optical-packet convertor in OPS network while using OCDMA as the optical label and the work in [21] has demonstrated a transparent OPS system with 64 DWDM channels in cooperate with 10-Gbps NRZ-DPSK data format and performed OCDMA optical label by a multiport en/decoder.

In an access network, OCDMA is stated as one of an attractive option that can enhance the system performance of NG-PON2 and also one of a candidate for the next evolution of PON [22]. This multiple access scheme performs both the encoding and the decoding process in the optical domain, so there is no need any complex electrical circuits as an electrical en/decoder at the transmitter and the receiver. With this technique, we can allow all subscribers to experience the most favorable property of OCDMA by accessing to the system without any contention as a truly

asynchronous manner due to the reduction in tight synchronization between the optical line terminal (OLT) and the optical network units (ONUs).

Since 1999, many laboratories have paid attention on employing OCDMA over PON. In the first era, the overall system performance of OCDMA is quite fair due to the impairments in optical devices and the bad correlation property [23, 24]. In a nature of OCDMA, a signal from a desired subscriber will be code-multiplexed with other subscribers, called interferers. In the mathematical analysis, we can see three OCDMA noise terms in the expression. The study in [25] in 2004 has categorized the OCDMA into 3 different regimes: the incoherent, the coherent and the partially coherent, respectively and analyzed how these noise terms affected to these 3 types of the OCDMA system. The main idea of this paper is stated that the primary beat noise (PBN) which is the beat term between desired and interfered signals is the main noise source that limits the system performance in the coherent regime. On the other hand, the multiple access interference (MAI) noise is the dominant noise source that limits the system performance in incoherent regime. In order to increase the system performance in the total bit rate and the total number of subscribers, the key technologies that enable OCDMA work proficiently is an optical en/decoder and its code to suppress noise. Many kinds of en/decoders and optical codes are proposed [23, 26-29]. In 2006, a record of 511-chip of superstructure fiber bragg grating (SSFBG) has been proposed for the first time as a passive en/decoding device that can reduce beat noise [30]. Moreover, this paper also used super-continuum generation-based optical thresholder to reduce the effect of MAI as well. Moreover, a multiport en/decoder based array waveguide grating (AWG) is mathematical modeled in 2006 and first demonstrated in a hybrid OPS system with SSFBG [31-33]. Then, this multiport en/decoder and SSFBG is fabricated with a new code set. A multi-level phase shifted keying optical code, known as Fourier code [34], is one of a breakthrough in reducing the number of chips while maintaining high contrast between auto-correlation and cross-correlation peak among other codes has been implemented over a multiport en/decoder and a SSFBG en/decoder that has been successfully demonstrated in many papers [16, 17], [27], [33-36]. For example, a paper in [37] has successfully demonstrated an experiment setup of a hybrid OCDMA over PON by using only single multiport en/decoder at the OLT and 8 SSFBG as decoders at the ONU. Recently, both multiport en/decoder and SSFBG has announced their newly developed prototype that is able to encode and decode OCDMA signal at a bit rate of 40-Gbps per subscriber [22], [38].

Nevertheless, the studies in [23], [30], [35], and [39] have proposed an experiment using a whole bit period as a total encoded signal, respectively. On the other hand, the studies in [37], [40], and [41] have conducted the experiment with only 80 percent is used as an encoding period, respectively. The total encoding period is determined by the number of chips and the chip period which the latter one is corresponding to the chip rate (chips/s) or free-spectral range (Hz) of the en/decoder. To our knowledge, the primary beat noise is occurred when desire signal and interfered signals are superimposed in optical field. Therefore, to decrease the encoding period, we can avoid the interference between them, leading to the suppression of beat noise.

It is extremely necessary to explore the suppression of primary beat noise with various values of encoding periods corresponding to the bit period, in order to find out the most appropriate encoding period for OCDMA-PON.

1.2 Objectives

The main objective of this thesis is to find the suppression of primary beat noise and also to find the optimum value of spreading time per bit period to be used in OCDMA-PON. We can categorized our goal as follows,

1. Feasibility study of employing several chip numbers over OCDMA-PON.
2. Feasibility study of applying various SBRs over OCDMA-PON.
3. Analysis of the noise variance and bit error rate in OCDMA according to using various SBRs.
4. Analysis of maximum number of subscribers, total bit rate and spectrum efficiency of OCDMA-PON per 1 wavelength according to the limitation of the system.
5. A design approach to achieve the maximum performance of the 40-Gbps OCDMA-PON.
6. Comparison of OCDMA-PON and TDM-PON in an identical scenario with respect to maximum number of subscribers, bit rate and spectrum efficiency.

1.3 Methodology

This research is started with studying the encoding and decoding scheme of optical signal as used in recent OCDMA network. Then, we will formulate and generate OCDMA signals in order to investigate the system performance. Next, we consider one of the solutions to reduce primary beat noise which is the limitation in OCDMA network by the change in number of chips and the reduction in total spreading time of encoded signal. With this method, we could mitigate primary beat noise due to the large difference between desired and interfered signals and the lower number of interfered chips between desired and interfered subscribers.

According to our research plan, all of works are mainly based on some of theoretical mathematics derivations. Therefore, we will evaluate our derivations and hypothesis by numerical simulations. As following,

1. Studying the principle of PON and OCDMA technology regarding to the PON history, current PON technology and the trend of the next generation access network based optical fiber.
2. Studying the principle of encoding and decoding scheme based on coherent time-spreading technique.
3. Studying the effect of number of encoded chips to the system performance. Collecting the results and presenting in an international conference.

4. Formulating and Generating OCDMA signals corresponding to the standard work, using computational software. Then, starting to generate OCDMA signal according to our proposed method, reducing the encoding period while constraining the number of encoded chips and coherent ratio of the signal. Next, collecting data and summarizing their results.
5. Analyzing the results and evaluating the system performance due to the maximum number of subscribers, total bit rate and spectrum efficiency of OCDMA-PON. Then, using computer simulation to verify our propose method. Moreover, a power penalty due to an imperfectly dispersion slope mismatched at each value of SBR will be proposed.
6. Summarizing all works and presenting the work in an international periodical journal.
7. Writing a Ph.D. thesis.

1.4 Scopes

1. System bit rate is fixed at 40 Gbps/subscriber.
2. An OCDMA-PON encoding and decoding method is only a coherent time-spreading scheme using a programmable multi-level phase shifted en/decoder.
3. Optical fiber specification is according to ITU-T G.652.D standardization.
4. Signal deteriorations are including only fiber attenuation, fiber dispersion, dispersion slope, multiple access interference (MAI), primary beat noise, secondary beat noise and receiver's noise, respectively.
5. Through out this study, we use only MATLAB and a simulation software, OptiSystem, to investigate, analyze and verify the results without performing an experiment.

1.5 Expected outcomes

1. To be able to understand the current situation of access network based on FTTH technology and realize the massive advantages of employing OCDMA over PON as the next-generation PON.
2. A novel effective method to reduce primary beat noise.
3. A result of parameter analysis how SBR does affect to the overall system performance.
4. A guideline for designing OCDMA-PON with high efficiency.
5. Publications on international conference and periodicals.

CHAPTER 2 Principle of Optical Communication, Passive Optical Network and Optical Code Division Multiple Access

In this chapter, we will introduce the optical fiber ITU-T G.652 which will be used in this thesis. Moreover, the principle of optical communication system will be discussed. The signal transmission over an optical fiber will be suffered from fiber loss, dispersion, dispersion slope and non-linearity of a fiber. However, in an optical access network, the total reach does not exceed one hundred kilometers so we can neglect the effect of fiber non-linearity. One of the most powerful short reach optical networks in nowadays is a passive optical network which is considered as a breakthrough in the transmission rate to the last-mile subscribers. Passive optical network standardizations that are currently being deployed and the roadmap of the next generation of passive optical network will be discussed in this chapter. Finally, we will focus on the optical code division multiple access technology about its potential, system architecture and also describe how this technique works, respectively.

2.1 Single-Mode Fiber ITU-T G.652

An optical fiber is a communication medium made of SiO_2. It has developed to be one of the most important parts in optical communication. In the early 1970's, it was called the first window of optical communication. The fiber attenuation was found to be 4.8-5.0 dB/km at wavelength 800 nm. Then, in 1980's, the fiber was improved in lower attenuation at 1310 nm band and 1550 nm band. Therefore, ITU-T has standardized the fiber ITU-T G.652 whose attenuation and dispersion at 1310 nm is typically 0.3 dB/km and 0 ps/nm·km, respectively. Actually it has a high attenuation around 1400 nm due to water-peak attenuation. This problem is then eliminated by the ultrahigh purifying in silica fiber production, so it is compatible with a broad range of optical bandwidth from 1300-1600 nm. This new fiber is known for a low water-peak non-dispersion shifted fiber or ITU-T G.652.C-D [42]. Here, some specifications of most commonly deployed fiber G.652.D in the last mile has shown in Table 2.1 respectively.

Table 2.1 Specifications of an optical fiber ITU-T G.652.D.

Fiber attribute		
Attribute	**Detail**	**Value**
Mode field diameter	Wavelength	1310 nm
	Range of nominal values	8.6-9.5 μm
	Tolerance	$\pm$ 0.6 μm
Cladding Diameter	Nominal	125.0 μm
	Tolerance	$\pm$ 1 μm
Core Concentricity error	Maximum	0.6 μm
Cladding noncircularity	Maximum	1.0%
Cable cut-off wavelength	Maximum	1260 nm
Macrobend loss	Radius	30 mm
	Number of turns	100
	Maximum at 1550 nm	0.1 dB
Proof stress	Minimum	0.69 GPa
Chromatic dispersion coefficient	$\lambda_{0\min}$	1300 nm
	$\lambda_{0\max}$	1324 nm
	$S_{0\max}$	0.092 ps/nm^2 x km
Cable attributes		
Attribute	**Detail**	**Value**
Attenuation coefficient	Maximum from 1310 nm to 1625 nm (Note 2)	0.4 dB/km
	Maximum at 1383 nm $\pm$ 3 nm	(Note 3)
	Maximum at 1550 nm	0.3 dB/km
PMD coefficient	M	20 cables
	Q	0.01%
	Maximum PMD	0.20 ps/$\sqrt{km}$
NOTE 1 – According to 6.2, a maximum PMD$_Q$ value on uncabled is specified in order to support the primary requirement on cable PMD$_Q$.		
NOTE 2 - This wavelength region can be extended to 1260 nm by adding 0.07 dB/km		

induced Rayleigh scattering loss to the attenuation value at 1310 nm. In this case, the cable cut-off wavelength should not exceed 1250 nm.

NOTE 3 - The sampled attenuation average at this wavelength shall be less than or equal to the maximum value specified for the range, 1310 nm to 1625 nm, after hydrogen ageing according to IEC 60793-2-50 regarding the B1.3 fibre category.

2.2 Theory of Optical Signal Transmission over a Fiber

In order to model a signal propagating in an optical fiber, a nonlinear Schrodinger equation (NLSE) has described the propagation of light in an optical fiber as shown in (2.1).

$$\frac{\partial A}{\partial z} = -\frac{1}{2}\alpha A - \frac{i}{2}\beta_2 \frac{\partial^2 A}{\partial T^2} + i\gamma |A|^2 A, \tag{2.1}$$

where A is an envelope of the signal, α is the fiber attenuation coefficient, β_2 is the group velocity dispersion, γ is the nonlinear coefficient and z is the distance that light propagating in fiber, respectively [43, 44]. The first term represents an attenuation of a signal. The second term is a group velocity dispersion which represents how much a pulse is broadened along the distance. The last term is a nonlinear effect generated by signal with high peak power travelling along the fiber. This nonlinear effect can cause a change in refractive index of fiber that will also cause a self-induced phase-shifted during the propagation along the fiber. In this study, we consider only the effect of fiber loss and fiber dispersion in cooperate with on-off keying data format over OCDMA network.

2.2.1 Fiber Loss

In an optical fiber, a signal power P_T in dBm at a distance L km apart from can be expressed as

$$P_T = P_i \cdot \exp[-\alpha L], \tag{2.2}$$

where P_i is signal power launched into a fiber, α is the fiber attenuation coefficient, respectively. It's obviously seen that signal power is decayed exponentially along the distance L. In general, we usually express α in terms of dB/km by using

$$\alpha_{dB} = -\frac{10}{L}\log\left(\frac{P_T}{P_i}\right) = 4.343\alpha. \tag{2.3}$$

The fiber attenuation coefficient α_{dB} depends on the wavelength of light. In a single-mode fiber ITU-T G.652.D, its attenuation coefficient comes from Rayleigh scattering and the absorption in material induced by OH ion Moreover, an additional

loss in a fiber comes from micro-bending, macro-bending, splice loss and connector loss as well.

2.2.2 Dispersion

Dispersion is a phenomenon that light occupying different wavelength components travel in a fiber with different velocity. Therefore, each wavelength component will reach the destination with different time delay that can cause the pulse broadening in time-domain. This issue is an enormous limitation in system bit rate and reaches in an optical communication based optical fiber.

2.2.2.1 Second Order Dispersion

The mathematically expression of a dispersion can be expressed by taking an expansion of signal propagation constant $\beta(\omega)$ in a Taylor series around center carrier frequency ω_0 as

$$\beta(\omega) \approx \beta_0 + \beta_1(\omega-\omega_0) + \frac{1}{2}\beta_2(\omega-\omega_0)^2 + \frac{1}{6}\beta_3(\omega-\omega_0)^3 + ..., \quad (2.4)$$

where $\beta_m = \left(d^m\beta / d\omega^m\right)_{\omega=\omega_0}$. Therefore, β_1 refers to the inversely to the group velocity $\beta_1 = 1/v_g$ as known as first order group velocity dispersion (GVD). In additions, β_2 is defined as a second order dispersion (SOD) which causes pulse broadening in a fiber and β_3 is known as a third order dispersion (TOD) which will affect to both system bit rate and reaches at a bit rate beyond 40Gbps.

More specially, the second order dispersion β_2 can be expressed as the dispersion parameter D which is more commonly use in optical communication. The relation between β_2 and D is

$$D = \frac{d}{d\lambda}\left(\frac{1}{v_g}\right) = -\frac{2\pi c}{\lambda^2}\beta_2. \quad (2.5)$$

The unit of D is ps/nm·km and it varies with wavelength. Its physical meaning describes the total amount of the pulse broadening in ps over a given spectral width of a light source which is propagating over one kilometer of a fiber. The relation between pulse broadening $\Delta\tau$ and dispersion parameter D is

$$\Delta\tau = |D_\lambda| L\sigma_\lambda, \quad (2.6)$$

where L is the length of a fiber and σ is the spectral width of optical source, respectively.

Fig. 2.1 illustrated the relation of dispersion parameter as a function of wavelength in a fiber ITU-T G.652.D. At 1310 nm we can obtain that D is equal to zero, so we call this wavelength as a zero dispersion wavelength λ_0. Moreover, the dispersion below 1310 nm has the negative value while it is positive value over λ_0. We define the dispersion region with negative value of D as normal dispersion region and the dispersion region with positive value of D as anomalous dispersion, respectively. Both normal and anomalous dispersion with the identical absolute value of D will exhibit the same amount in pulse broadening. The effect of pulse broadening due to SOD is shown in Fig. 2.2. Three bits of electrical signal corresponding to bit sequence "101" are modulated with light source and then return optical pulses which we can obtain as "101" as well. These pulses are launched into a fiber with a proper distance. Then, due to the presence of dispersion, pulses are broadened and the outcome of superimposed pulse can be obtained as a new pulse. This phenomenon is called inter-symbol interference (ISI). The bit detection can be misleading if the intensity of superimposed pulses caused by ISI is more than a decision threshold level and this error will cause a poor system bit error rate. It should be noted that the effect of dispersion does not change the output spectrum of the signal.

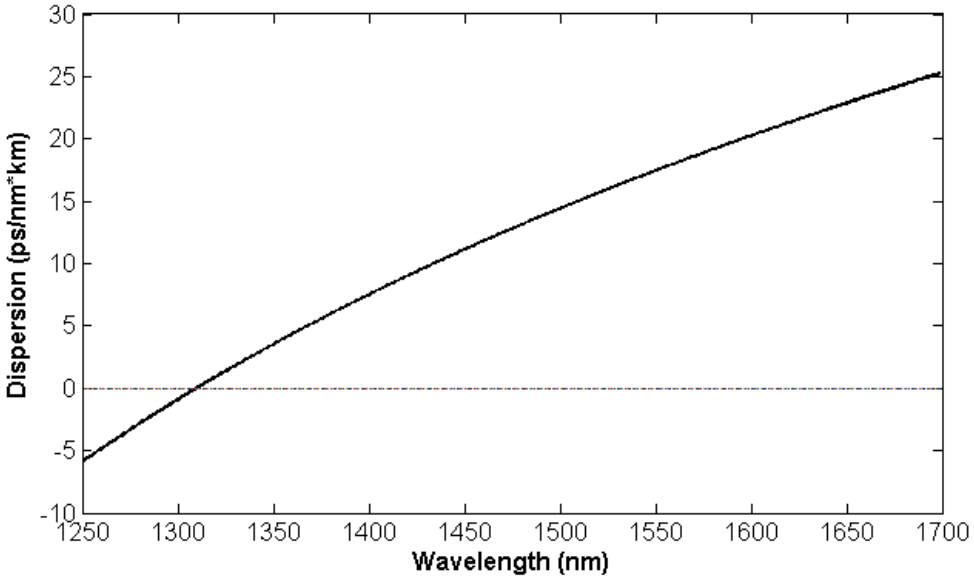

Fig. 2.1 Dispersion characteristic of a single-mode fiber ITU-T G.652.D.

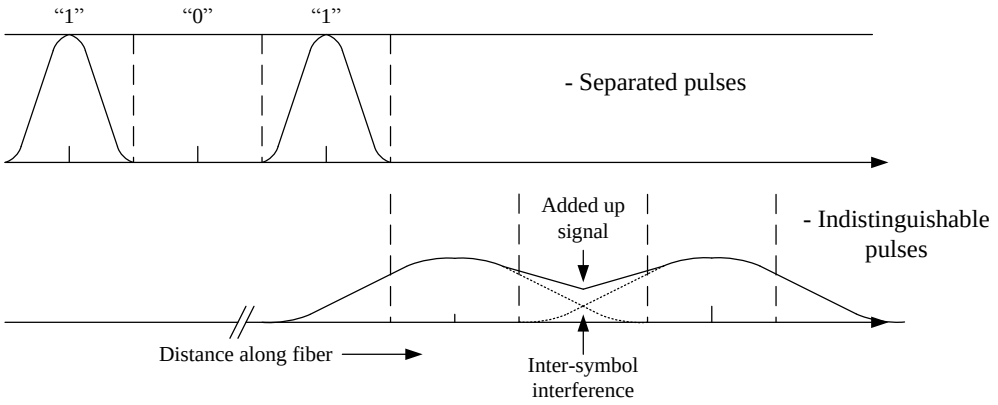

Fig. 2.2 Evolution of optical pulses propagating in a fiber with the effect of dispersion.

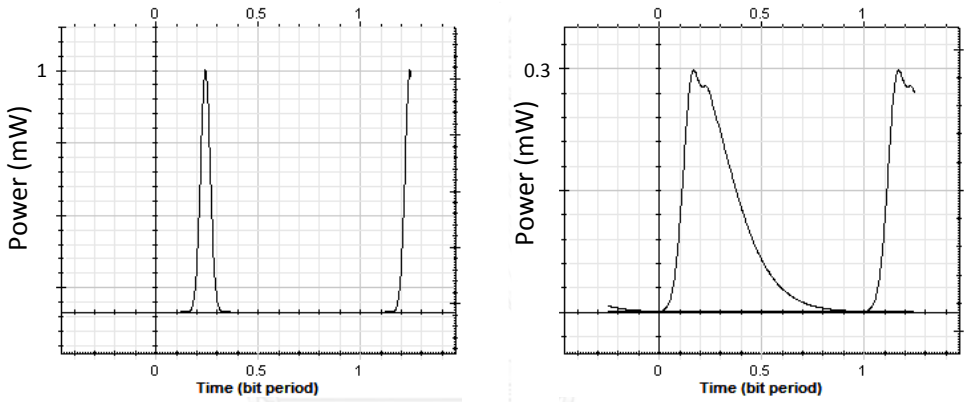

Fig. 2.3 TOD pulse broadening.

In an optical transmission link design considering the effect of SOD, the dispersion-limited length L_{D2} governed by the dispersive effect is defined as

$$L_{D2} = \frac{T_0^2}{|\beta_2|}. \tag{2.7}$$

2.2.2.2 Third Order Dispersion

In (2.4), we have another high-order term of β which also causes a pulse broadening, it is called β_3. The derivation of β_3 can be done by taking derivative of β_2 by frequency ω

$$\beta_3 = \frac{d\beta_2}{d\omega}. \tag{2.8}$$

The physical meaning of taking derivative at a point is the slope of the line tangent to the function β_2 at the point. In general, we usually represent the effect of β_3 as the third-order dispersion (TOD) or dispersion slope, defined as

$$TOD = \frac{dD}{d\lambda}. \tag{2.9}$$

The unit of TOD is ps/nm$^2 \cdot$km. This parameter is quite significant around the wavelength which its dispersion parameter is equal to zero because TOD can still cause a pulse broadening. Fig. 2.3 shows a single pulse travelling along fiber is suffered from the effect of positive TOD. Its original pulse is transformed to become asymmetric with oscillatory pulse as its tail. Anyway, it does not change the output spectrum. Therefore, the system reach limited by TOD can be expressed as

$$L_{D3} = \frac{T_0^3}{|\beta_3|}. \tag{2.10}$$

2.3 Passive Optical Network

Although many of electrical-based technologies such as digital sub-scriber line (DSL), data over cable service interface specification (DOCSIS) are already deployed extensively, a fiber-to-the-home based passive optical network (PON) is a promising access network that can provide much more bandwidth than previous technologies [45, 46]. A PON is an optical fiber-based network which is a gateway between internet service providers and end-users in the last-mile. Its significant point is to keep away from using active switching components between the transmitter side and the receiver side. The most popular network topology of PON is a tree topology as expressed in Fig. 2.4.

The system architecture of PON is consisted of an optical line terminal (OLT), an optical fiber with a passive power splitter and an optical network unit (ONU) or optical network terminal (ONT), respectively. An OLT is located at a central office of the internet service provider where it is an inter-connection to the backbone network [47, 48]. Then, signals sent from OLT will be fed into a fiber to the destination area. A passive splitter located at the remote node or distribution point will split optical signal into many branches. Each split signal is then arrived the ONU, located at a house or building, and convert optical signal into electrical signal with a proper interface to the user's equipment.

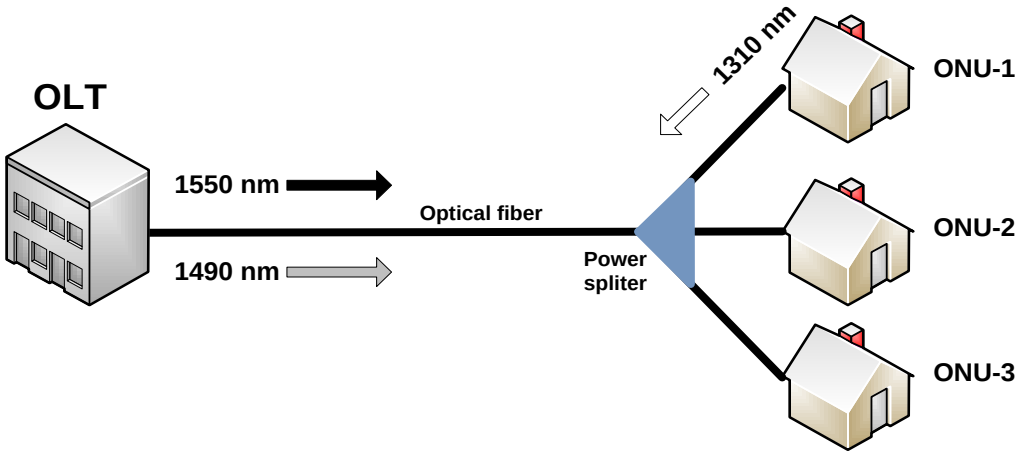

Fig. 2.4 Basic PON architecture.

2.3.1 PON's Evolution

A passive optical network was founded in 1995 by a Full-Service Access Network (FSAN) working group. The first standardization is APON with the transmission rate 155 Mbps has been announced in 1998 by ITU. Then, in 2000, the revision of PON standardization has been completed in the name BPON ITU-T G.983 with the improvement in transmission rate up to 622 Mbps. Afterwards, IEEE has announce its first PON standardization IEEE 802.3ah or Ethernet-PON (EPON) in 2004 with the maximum bit rate of 1.25 Gbps in both downstream and upstream direction. It was a great deal to transmit Ethernet over optical network. EPON has been widely deployed in Japan and China. At the same period, ITU has also announced its standardization of ITU-T G.983.x or Gigabit-PON (GPON) with the maximum transmission rate of 2.5 Gbps. This GPON is deployed most of the world outside Japan and China. The competition in PON technology between IEEE and ITU has not been finished yet until now. In 2009, IEEE has announced a new standard of IEEE 802.3av or 10G-EPON and follow by ITU who has announced ITU-T G.987 or XG-PON in 2010, respectively. Both of two 10G-PON is capable of providing up to 10 Gbps in downstream and upstream as well. This dramatic breakthrough is according to a next-generation PON stage 1(NG-PON1) conducted by FSAN in order to increase the transmission rate especially in the downstream with a coexistence with existing PON. In the upcoming years, a beyond 10G-PON will be announced with an enhancement in a long reach and a record transmission rate for access network according to a next-generation PON stage 2 (NG-PON2). The commercial PON standardization and its evolution is shown in Fig. 2.5 [3]-[8]

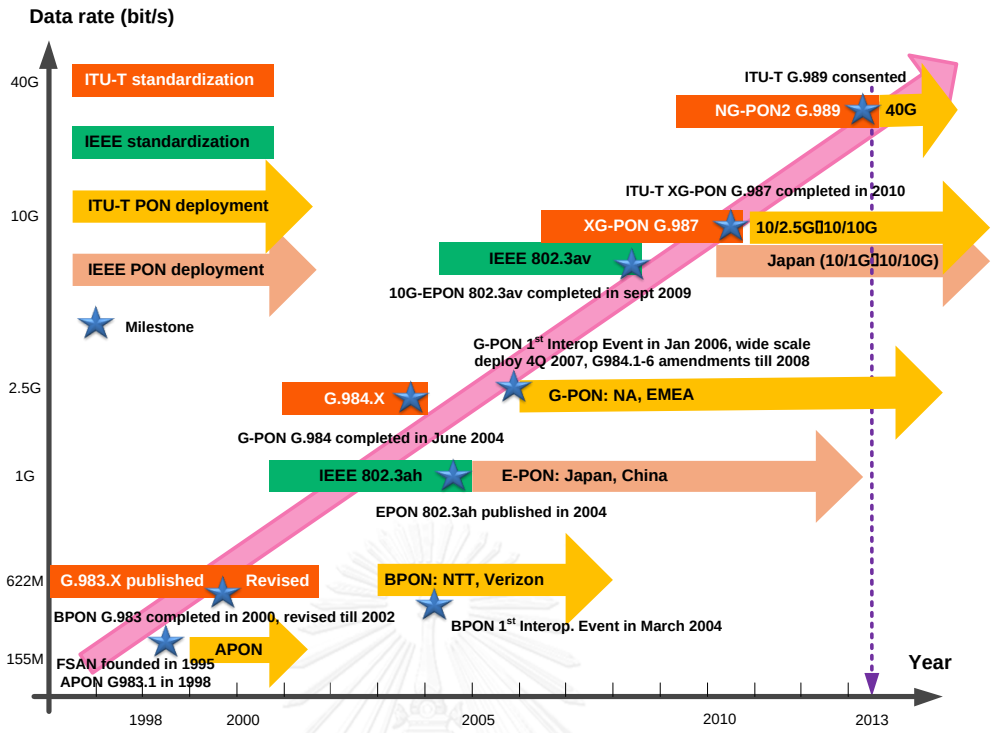

Fig. 2.5 Commercial PON standardization.

2.3.2 XG-PON and 10G-EPON Standardization

This standardization is based on TDMA which each time-slot assigning to subscribers is conducted dynamically by OLT, therefore the maximum bit rate of each subscriber is depended on the total numbers of subscribers in each individual PON. In order to coexist with the existed EPON or GPON, different wavelengths used for 10G in both downstream and upstream are assigned. In the downstream direction, a 1490 nm wavelength is used for 1G as always, a 1550 nm wavelength is used for 2.5G and a newly assigned wavelength for 10G is 1577 nm, respectively. on the other hand, in the upstream, a 1310 nm wavelength is assigned for 1G and a 1270 nm wavelength is assigned for 10G, respectively. The wavelength assignment for 10G-PON in the coexistence with conventional 1G-EPON and GPON is shown in Fig. 2.6.

Table 2.2 System parameter of XG-PON ITU-T G.987.

Specification	**Power budget class**					
Name	N1	N2a	E1	E2a	N2b	E2b
OLT Tx power (max) [dBm]	+6	+8	+10	+12	+12.5	+16.5
OLT Tx power (min) [dBm]	+2	+4	+6	+8	+10.5	+14.5
OLT Rx sensitivity (max) [dBm]	-7	-9	-11	-11	-9	-13
OLT Rx sensitivity (min) [dBm]	-27.75	-29.5	-31.5	-31.5	-29.5	-33.5
ONU Tx power (max) [dBm]	+7				+7	
ONU Tx power (min) [dBm]	+2				+2	
ONU photodetector type	APD				PIN	
ONU Rx sensitivity (max) [dBm]	-8				-3.5	
ONU Rx sensitivity (min) [dBm]	-28				-22.5	
System power budget [dB]	29	31	33	35	31	35

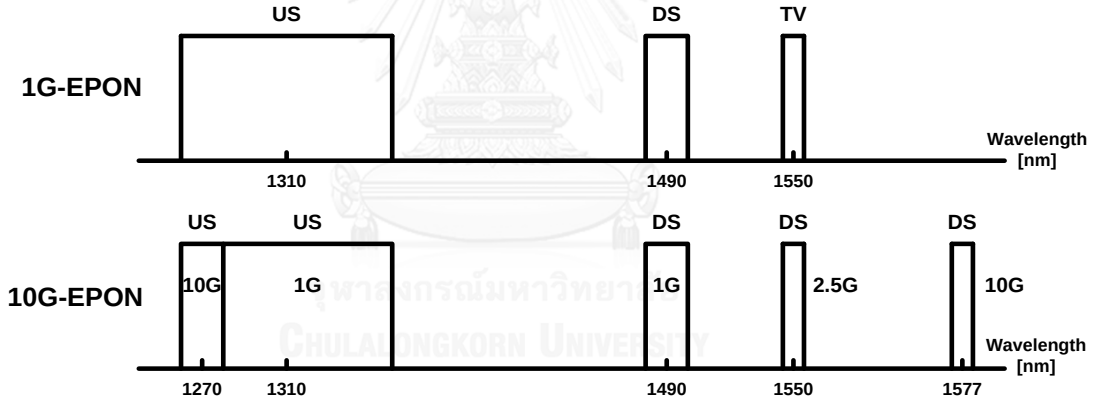

Fig. 2.6 Wavelength assignment for 1G-PON (EPON and GPON) and 10G-PON (10G-EPON and XG-PON).

One of a tight control parameter in PON system design is a power budget. The power budget is total effective amount of signal power in dB that can achieve the desired quality of received signal at the receiver. It can be calculated from

$$P_T = P_{tx} - P_{rx} = \alpha L + \sum l_c + \sum l_s + \sum l_{other} + G_{margin}, \qquad (2.11)$$

where P_T is a system power budget in dB, P_{tx} is a transmitted power in dBm, P_{rx} is a received optical power at the receiver in dBm, α is the fiber attenuation coefficient, L is the system reach, l_c connector loss, l_s is the loss due to fiber splicing, l_{other} is

reserved for the other loss such as insertion loss from optical devices and G_{margin} is the reserved system margin, respectively. The power budget must be satisfied in order to meet the successful transmission with acceptable error rate. In ITU-T G.987, the power budget is categorized into two main groups, the nominal class and the extended class. There are 4 types of OLTs and 2 types of ONU with various combinations of power budget as clearly shown in Table 2.2 [5].

2.4 Optical Code Division Multiple Access (OCDMA)

A code division multiple access technique, as known as CDMA, was first used in military due to resistance jamming. Then, it was developed its performance and universally deployed as a commercial use in a satellite network and a third generation of mobile telecommunication network or 3G. In a wireless 3G network, the coding procedure is based on a spread spectrum technique which each signal is divided into several small time periods called chips and then is coded with a unique set of chip sequence or code. After encoding process, each signal is transformed into a temporal waveform due to its assigned code. Then, at the decoding process, detected signal at the receiver's end will be decoded by the code which is identical to the encoder. The correctly decoded signal will achieve very high signal power called auto-correlation peak whereas the mismatched decoded signal will be obtained in a very small amount in signal power, called cross-correlation peak, respectively.

The first proposal in applying CDMA technique over optical network has started since 1970s and its demonstration has demonstrated by 1980s. At the first era of OCDMA demonstration, the system stability was restricted by the immaturity of optical devices such as insertion loss and an inaccuracy in phase coding owing to the imperfectness fabrication. In the 2000s, many of newly developed en/decoders with great correlation property have introduced to the researchers. Since the signal interference beat noise between desired and interfered subscribers is the critical problem in OCDMA network, some laboratories have proposed interesting solutions to suppress this issue by employing time-gating technique and optical-threshold devices. Anyway, some of en/decoders developed by [30]-[33] show the possibility to suppress beat noise effectively and we will discuss further about this technique in the next session below.

Due to each subscriber is coding with a code which it is orthogonal among other codes. Therefore, individual subscribers can transmit their information over a fiber using same wavelength at the same time, respectively. This asynchronous property is the most attractive property of OCDMA which allows everyone can access to the network without any strict synchronizations between the transmitter side and the receiver side, in the medium access protocol (MAC) layer. Moreover, OCDMA can be named as a truly all optical processing due to its coding operation is performed in optical domain. This also prevents eavesdropping because it's hardly to tap the coded optical signal. Therefore, these significant benefits become a desirable reason to be implemented on optical network and PON as well.

2.4.1 System Architecture and Working Principle

The basic system configuration of OCDMA system is shown as Fig. 2.7. At the transmitter side, Optical signals from N subscribers are transmitted and encoded via each transmitter and encoder. Then, all signals are combined together and launched into a network. Finally, the signals which are multiplexed by code will be detected by each decoder at the receiver end. Only a detected signal which its encoded phase is matched to the code sequence of a decoder will be detected as an ACP while the others are detected as CCP.

Types of OCDMA are clearly categorized by both processing dimension and working principle as illustrated in Fig. 2.8. In the processing dimension, there are 1-D and 2-D processing. Optical signal is coded in even frequency-domain or time-domain in 1-D OCDMA while 2-D OCDMA is performing in both frequency and time-domain simultaneously. By considering at working principle, there are 2 types of OCDMA processing. The first one is incoherent OCDMA. Coding operation is performed in an optical intensity basis (0,+1). For an example, the single bit with mark "1" is encoded by a 4-chip encoder with code "1101". After coding process, encoded signal is a series of 4 chips with chip mark "1101", respectively. These 4 chips are spread over the whole bit period as shown in Fig. 2.9(a). Due to the incoherence of light source, this operation gives the poor overall system performance such as small number of code size, low bandwidth efficiency and bad correlation property [25].

On the other hand, the coherent OCDMA performs the coding in amplitude basis (+1,-1) of optical signal. This means each chip have the equal intensity but different in phases. Fig. 2.9(b) illustrates the coherent OCDMA. The single bit is encoded by a 4-chip encoder with chip mark "$00\pi0$". After the signal processing, we can obtain 4 chips with the same intensity are spread over the whole bit where the phase of the 1^{st}-4^{th} chip is stated as "$00\pi0$" respectively. With this coding operation, the overall performance of coherent OCDMA is superior to the incoherent OCDMA.

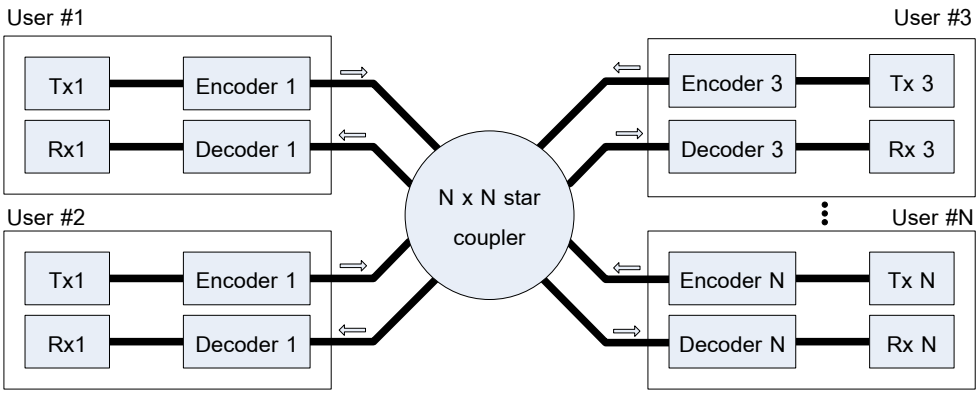

Fig. 2.7 Basic System Configuration of OCDMA networks.

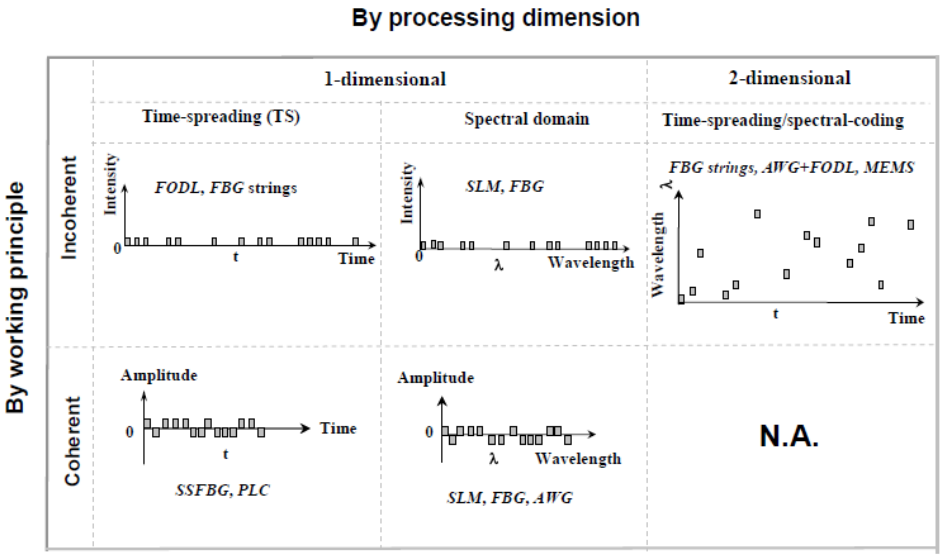

Fig. 2.8 OCDMA coding principle.

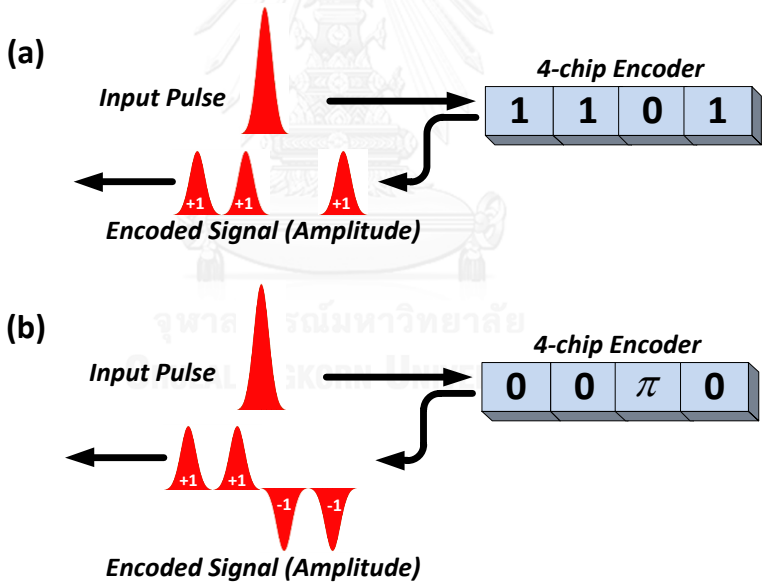

Fig. 2.9 Basic coding principle of (a) incoherent OCDMA (b) coherent OCDMA.

2.4.2 Coherent Time-Spreading OCDMA

The coherent property in OCDMA network is defined by the ratio between chip period T_{chip} and the coherence time of light source τ_c , called coherent ratio, as expressed in (2.12)

$$kt = \frac{T_{chip}}{\tau_c}. \tag{2.12}$$

The coherence time of light is corresponding to the optical bandwidth B_o of the light source where $\tau_c = 1/B_o$. It is considered as a time interval that light propagating in the optical path with predictable phase, may be called coherent. In order to perform coherent OCDMA, we have to control the phase of each chip with a certain predictable phase sequence. A study in [25] has considered a coherent ratio of "1" as a definition of a coherent regime of OCDMA. It reveals that we require the coherence time of light to be at least constant within a chip period.

Therefore, the coherent time-spreading OCDMA can be described as the coding operation in time-domain of a single input pulse returns a series of N chips as an output. The output chips from the encoder are spread over a whole bit period and the phase of each chip is determined by the phase mask of the encoder. In the next section, we will describe the en/decoding scheme of coherent time-spreading OCDMA.

2.4.3 Coherent Time-Spreading OCDMA Transmitter

An OCDMA transmitter is basically consisted of a light source, an electrical signal generator and an optical modulator. Most of light sources used in OCDMA are mainly based on a Mode-locked laser diode (MLLD). A MLLD can generate a narrow width optical pulse at a certain repetition rate. Then, series of generated pulses are intensity modulated with an incoming electrical signal. Fig. 2.10 has shown the intensity modulation of a 40-Gbps OCDMA signal transmission. An optical Gaussian pulse generator generated a pulse at a repetition rate of 40 GHz (1 pulse every 25 ps) which is corresponding to the bit period of 40 Gbps electrical signal. Therefore, the sequence of modulated optical pulses is governed by bit sequence of electrical signal.

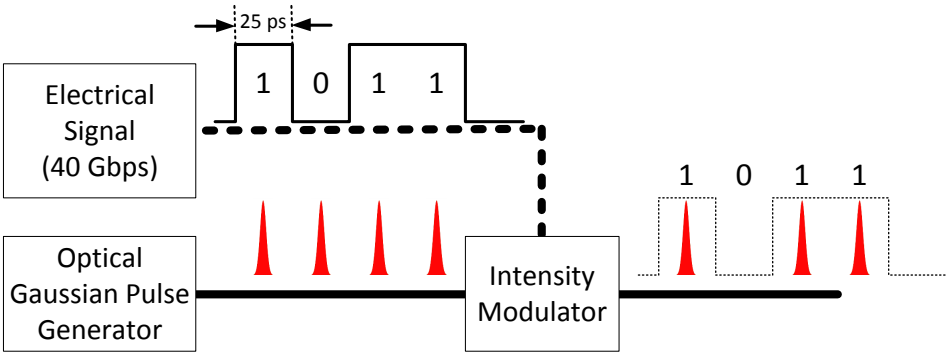

Fig. 2.10 The OCDMA Transmitter.

2.4.4 Coherent Time-Spreading Encoding and Decoding Scheme

Coherent time-spreading OCDMA has become one of a leading research topic in OCDMA code processing due to the advantages of the coding performance. There are many optical devices that have used as an en/decoder such as a fiber delay line, planar lightwave circuit (PLC), fiber Bragg grating (FBG), array waveguide grating (AWG) and superstructure fiber Bragg grating (SSFBG). Anyway, the researchers have currently focused on both a novel multiport en/decoder based AWG and a SSFBG, respectively. The SSFBG used in OCDMA network is a FBG which its refractive index is changed slowly and its refractive index modulation profile is also changed along the grating length [30], [46]. A phase shifter can be also fabricated onto each segment of an FBG so that the phase of the output signal is determined by this phase-shifted sequence. Optical signal with center frequency f_0 can penetrate through the whole length of the SSFBG but this signal will be reflected by each segment of SSFBG with different value corresponding to the reflectivity of the grating. Dissimilarity in each segment's reflectivity let us can control the intensity of encoded pulses

Fig. 2.11 illustrates a simple diagram of a coherent time-spreading by a 7-chip SSFBG encoder. The phase-shifted sequence from the 1^{st} - 7^{th} chip is $0\pi\pi00\pi0$, respectively. Firstly, a single pulse with very narrow pulse-width is fed into a decoder. The pulse is first reflected at the first chip and its phase is still not change. Then, the rest of pulse goes through to the second chip and its phase is shifted by π radian and reflected with the same intensity as the first reflection. The rest of pulse with phase π radian goes through the third chip and its phase is shifted by π radian again. The phase of pulse is now changed to 2π or 0 radian and then is reflected again. This mechanism occurs until the pulse goes through the last chip of the encoder and we finally can obtain 7 chips of encoded signal with the amplitude in optical field as +1 -1 +1 +1 +1 -1 -1. On the other hand, the phase of each chip can be expressed as $0\pi000\pi\pi$, respectively.

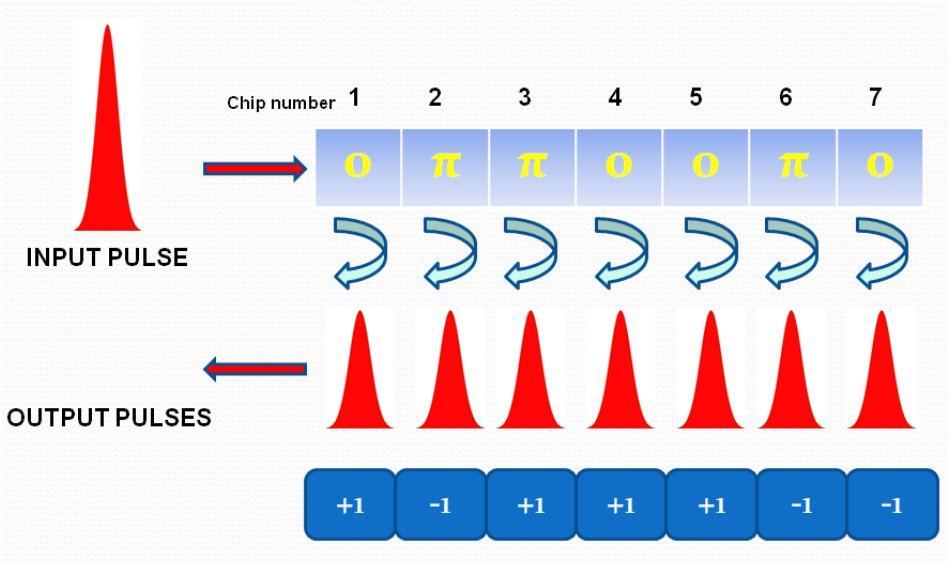

Fig. 2.11 Coherent time-spreading encoding scheme.

This train of chips will be decoded by a decoder. In order to detect the received signal with maximized signal to noise ratio, a matched-filtering has been used. We introduce h_e and $H_e(\omega)$ are the impulse response and the Fourier spectrum of the encoder, respectively [47]. A matched-filter Fourier spectrum of the decoder $H_d(\omega)$ is the complex conjugate of its Fourier spectrum at the encoder, as shown by

$$H_d(\omega) = H_e(\omega)^* \exp[-j\omega t_0], \tag{2.13}$$

$$h_d(t) = h_e(t_0 - t), \tag{2.14}$$

where h_d is the impulse response of the matched-filter of decoder, respectively. Therefore, the output between an encoder and a decoder can be expressed by a convolution

$$\begin{aligned} Output &= \int_{-\infty}^{\infty} H_e(\omega) \cdot H_d(\omega) \exp[j\omega t] df \\ &= \int_{-\infty}^{\infty} |H_e(\omega)|^2 \exp[j\omega(t - t_0)] dt \\ &= \int_{-\infty}^{\infty} h_e(t') \cdot h_e(t' - t + t_0) dt' \\ &\equiv \psi(t - t_0) \quad ; (t_0 : \text{arbitary}). \end{aligned} \tag{2.15}$$

The output from the convolution is the auto-correlation function of the encoder's impulse response h_e. Therefore, the physical meaning of the matched-filtering of the decoder can be performed coding with time-reversing sequence in time-domain.

Fig. 2.12 shows a graphical decoding process by the SSFBG decoder with code $0\pi00\pi\pi0$ which is the time-reversing sequence in comparison to the encoder. The input signal is the encoded signal from the encoder. The first pulse is phase-shifted by π radian and then some of its intensity is reflected out. The rest of the first pulse goes through the second chip of the decoder. At the same time, the second pulse reaches the first chip of the decoder. The 2nd reflected pulse from the first input pulse and the 1st reflected pulse from the second input pulse will be arrived the output branch of the decoder at the same time. So, the second output pulse is the combination between these 2 reflected pulses, respectively. This decoding process will be finished until the 7th input pulse is reflected by the last chip of the decoder. All combination of reflected pulses will return a series of decoded pulses in field amplitude and we can obtain their optical intensity by taking a square over the amplitude. The correctly decoded signal by a match-filtering gives a very high intensity at the central position of the decoded pulses whereas both two sides of the central peak are relative low as shown in Fig. 2.12, respectively.

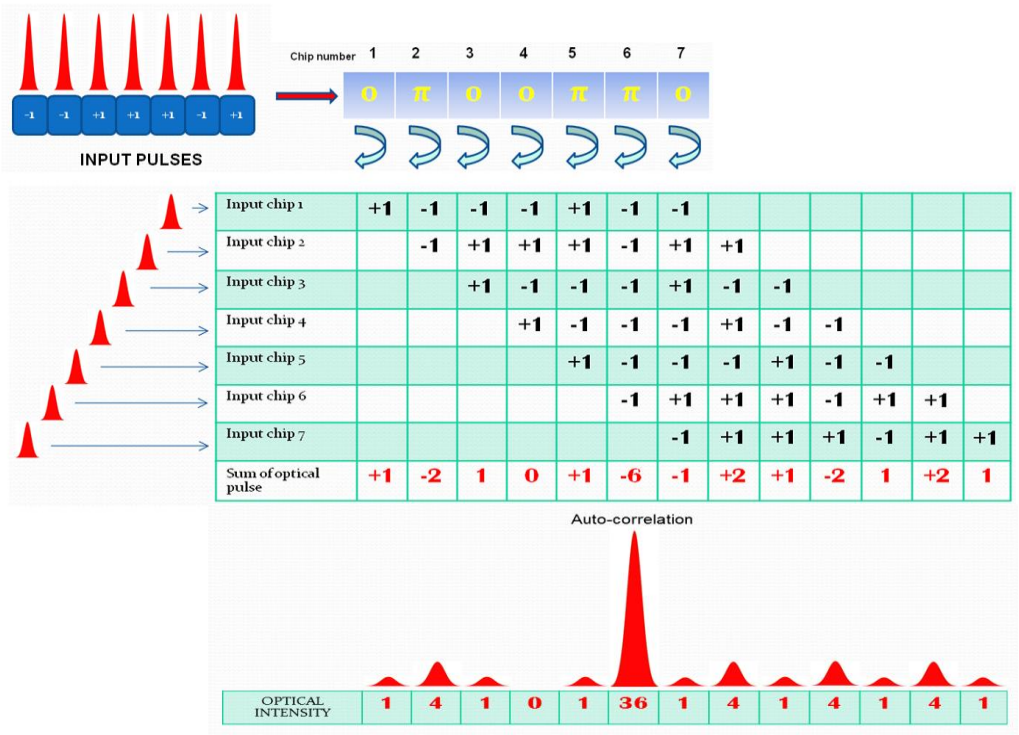

Fig. 2.12 Matched-filtering decoder.

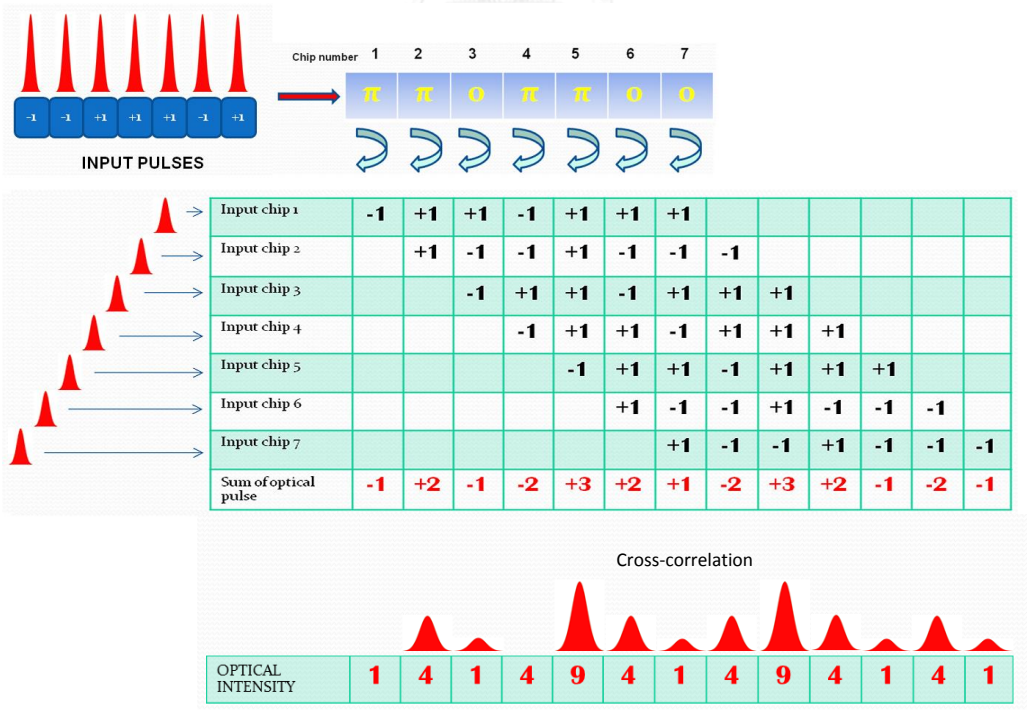

Fig. 2.13 Unmatched-filtering decoder.

On the other sides, Fig. 2.13 shows a decoding process with the unmatched code sequence. We use a decoder with code $\pi\pi 0\pi\pi 00$. As expected, the incorrectly decoded signal returns no high intensity peak but low intensity peaks instead.

2.4.5 OCDMA Receiver Using Direct Detection

After the OCDMA signal is launched into a fiber, at the receiver end, decoded optical signal is converted back to electrical signal. One of the most significant components in this part is a photodetector or photodiode. A photodetector is a semiconductor-based device. Its fundamental function is to convert an incident photon into signal current. There are two types of most commonly use nowadays, a PIN and an APD photodetector. One of the significant parameter of a photodetector is a responsivity R. It is a ratio between output signal current from the photodetector in Ampere and incident optical signal power in Watt. It informs us how much a signal current is given by an optical signal input power as shown in (2.16)

$$R = \frac{I}{P_0} = \frac{\eta q}{h\nu}, \tag{2.16}$$

where η is the electron-hole pair generated, q is the electron charge, $h\upsilon$ is the photon energy, respectively.

Once the electrical signal is converted back from photon, electrical noise is also generated here. The main noise sources (sometimes called noise variance) in optical receiver are quantum or shot noise, bulk dark current noise, surface dark current noise and thermal noise, respectively. Therefore, in order to maintain the signal quality, an electrical signal-to-noise ratio should be considered. A signal-to-noise ratio is a ratio between a square of generated photo current to the sum of noise variance.

The addition in photo current and noise current causes a fluctuation in signal level. A high fluctuated current brings a serious perturbation to the decision circuit which will make a judge whether an incoming signal is bit mark “1” or “0”. Thus, we measure the performance of the decision circuit, and also a whole individual lightwave system, through a BER.

A BER is ratio between error bits that are occurred over total bits sent in one second. It can be calculated by using an average probability of misunderstood bit sequence. One of the most formal expressions of BER can be obtained as

$$BER = p(1)\cdot P(0/1) + p(0)\cdot P(1/0), \tag{2.17}$$

where $p(1)$, $p(0)$ are the probabilities of bit generated with mark “1” and “0” , $P(0/1)$ is the probability of bit mark “1” is decided to “0” and $P(1/0)$ is the probability of bit mark “0” is decided to “1”, respectively. Furthermore, the error probabilities of $P(0/1)$ and $P(1/0)$ can be derived as conditional error probabilities with Gaussian random variables. Then, the BER becomes a classic form as

$$BER = \frac{1}{4}\left[erfc\left(\frac{I_1 - I_D}{\sigma_1\sqrt{2}} \right) + erfc\left(\frac{I_D - I_0}{\sigma_0\sqrt{2}} \right) \right], \tag{2.18}$$

where I_0, I_1, I_D, σ_0^2 and σ_1^2 are mean signal level of bit "0", mean signal level of bit "1", threshold level, noise variance at bit "0" and noise variance of bit "1", respectively.

CHAPTER 3 OCDMA over PON Using a Programmable Multi-Level Phase-Shifted En/Decoder with Various Numbers of Chips

When N subscribers are multiplexed together, this will cause a serious primary beat noise that that is the main noise source that limits the overall performance of the system. Therefore, this section will show an OCDMA over PON simulation result in using various number of en/decoding chips.

3.1 System model

The system configuration using in this section is shown in Fig. 3.1. At the transmitter side, an intensity modulator is replaced by a phase modulator and a simple electrical non-return-to-zero (NRZ) data format is replace by a differential phase shift keying (DPSK) data format instead. The study in [37] has shown the potential of DPSK in the receiver sensitivity improvement. In comparison to the OOK data format, by using DPSK can achieve approximately 6 dB in power penalty. Then, N signals after encoded are mixed by a power combiner and fed into a SMF followed by a dispersion compensating fiber. At the ONU, signals are split by 1: N passive splitter and then are decoded by a decoder. Optical signals are delayed by a 1-bit delay interferometer and are detected by a balanced detector in order to perform a DPSK decoder. Finally, detected signals are filtered by a 30-GHz low pass filter and the BER is numerical calculated from the obtained eye-opening by the BER tester, respectively.

3.2 En/decode scheme

In section 2.5.4, we have already shown the en/decoding scheme by using Gold code with 7 chips. The auto-correlation peak is like a needle shape as presented in Fig. 2.14 while the cross-correlation behaves like a waveform of noise as shown in Fig. 2.15, respectively. Nevertheless, in this section we will use a cyclic code which the phase of each consecutive chip is shifted by a step of $\frac{2(n-1)\pi}{N}$ radian. Here, n is stated as a number of codes and N is the total number of chips. For instance, Fig. 3.2 shows the encoding process by a 4 chip encoder with code number 2. A single pulse with peak power of 16 and initial phase of 0, expressed as $16\angle 0$, is fed into an encoder. The phase-shifted sequence of an encoder is $\pi/2$, $\pi/2$, $\pi/2$ and $\pi/2$ so that each reflected pulse is phase-shifted by a step of $\pi/2$. After encoded, we can obtain 4 chips with equal power and the phase of the 1^{st}-4^{th} chip is $\pi/2$, π, $3\pi/2$ and 2π, respectively. We can also expressed all 4 chips as $4\angle\pi/2$, $4\angle\pi$, $4\angle 3\pi/2$ and $4\angle 2\pi$, respectively.

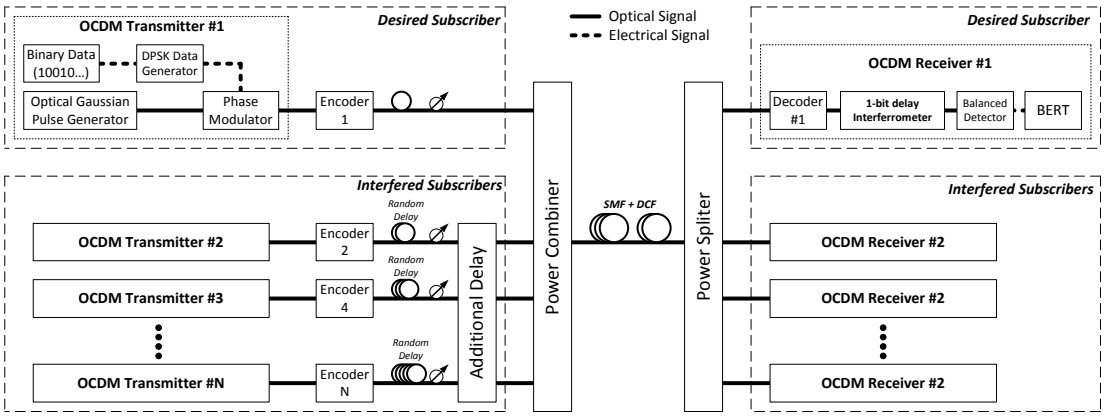

Fig. 3.1 The OCDMA system used in this section.

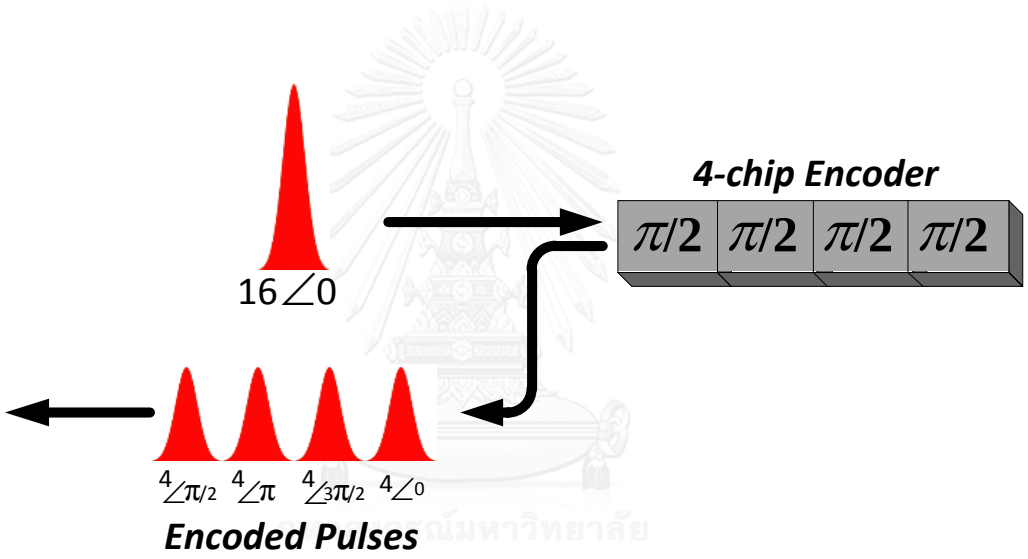

Fig. 3.2 The encoding process of a 4-chip encoder.

At the decoding process, a matched-filtering with time-reversal sequence of a decoder is $\pi/2$, $\pi/2$, $\pi/2$ and $\pi/2$ which is identical to the encoder. By employing the same operation, the output signal as a convolution between encoded signal and a decoder impulse response is depicts in Fig. 3.3. Finally, the combination of all of reflected pulses gives an auto-correlation signal like a triangle shape. Whereas the decoding process is done by an unmatched code (code number 4) is shown in Fig. 3.4 which the phase-shifted sequence of a decoder is $3\pi/2$, $3\pi/2$, $3\pi/2$ and $3\pi/2$, respectively. The combination of decoded pulsed is illustrated and the cross-correlation signal is a noise-like waveform as expected.

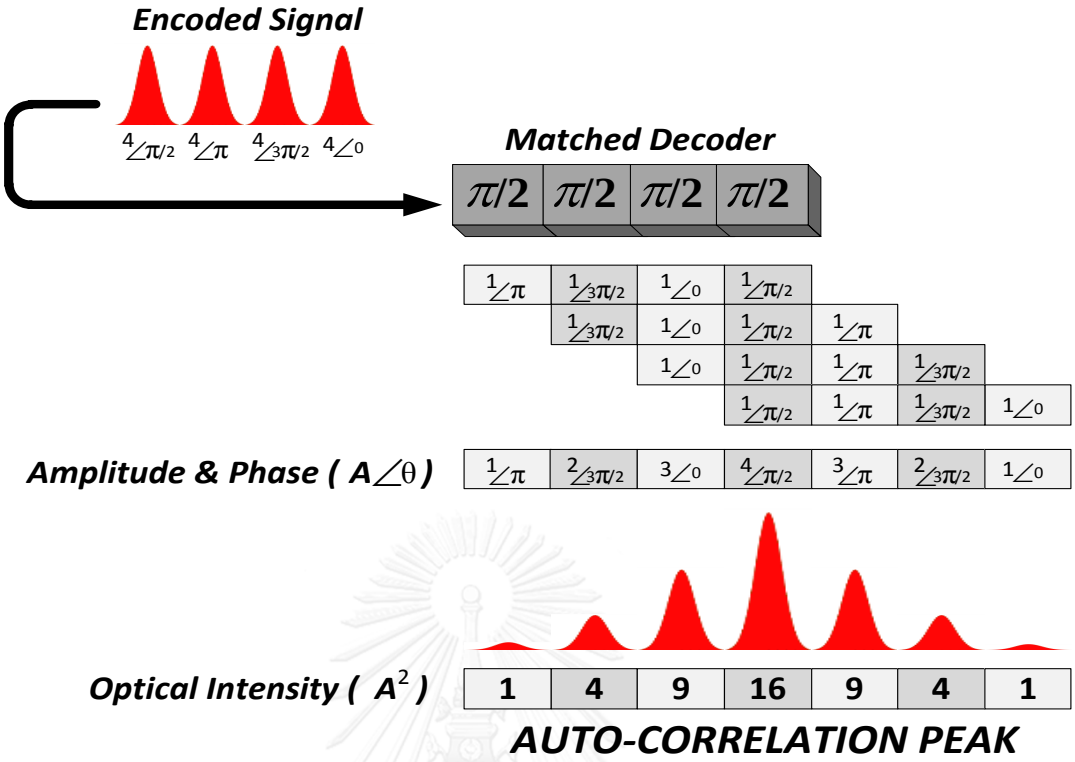

Fig. 3.3 Matched-filtering decoder.

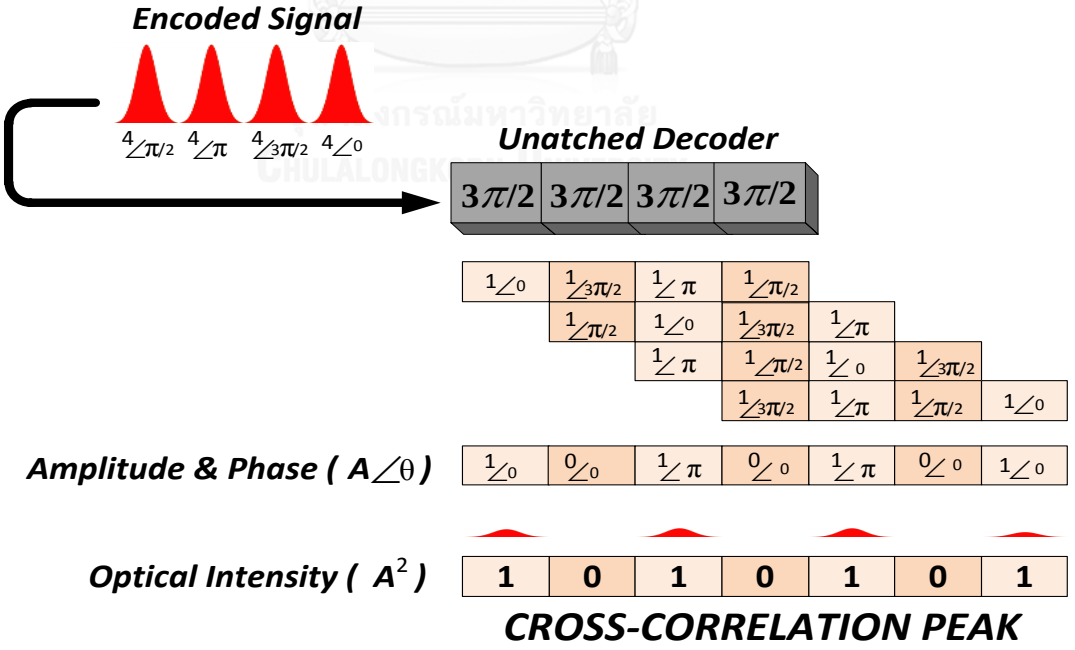

Fig. 3.4 Unmatched-filtering decoder.

3.3 The 8, 16, and 32 multi-level phase-shifted en/decoder

To go further in analyzing the performance of this code, the paper in [49] has propose peak to maximum cross correlation (P/C) ratio. It is a variable to measure the difference between auto-correlation peak and the maximum peak of the cross-correlation, as shown in

$$P/C = \frac{A_{ACP}^2}{A_{CCP-\max}^2}, \tag{3.1}$$

where A_{ACP} is an amplitude or magnitude of auto-correlation peak and $A_{CCP-\max}$ is the amplitude of the maximum of cross-correlation peak, respectively. Moreover, the ratio between auto correlation peak power and the cross correlation power or power contrast ration (PCR) is also proposed in [32] and it is one of the typical value to measure the performance of code in OCDMA. The PCR is calculated by

$$PCR_i = \frac{P_{ccp-i}}{P_{acp}}. \tag{3.2}$$

We have illustrated a graphical expression of the encoding process by 8-chip encoder. The code number is 3 with a phase-shifted sequence of is $\pi/2$, $\pi/2$, $\pi/2$ $\pi/2$, $\pi/2$, $\pi/2$, $\pi/2$ and $\pi/2$, respectively. As usual, we can obtain a series of 8 chips as an encoded signal which the phases of each chip are $\pi/2, \pi, 3\pi/2, 2\pi, \pi/2,$ $\pi, 3\pi/2$ and 2π, respectively. Then, this encoded signal will be decode by code #3 to obtain auto-correlation signal while it will be decoded by code #7 (phase-shifted sequence is a step of $3\pi/2$). The encoded signal, auto-correlation signal, cross-correlation signal, highest auto-correlation peak and maximum peak of cross-correlation are already shown in Fig. 3.5.

For the case of a 16-chip en/decoder, we selected code #5 as an en/decoder with a phase-shifted sequence is changed by a step of $\pi/2$. Then, the auto-correlation and cross-correlation is obtained by decoding with code #5 and #13 which its phase-shifted sequence is a step of $\pi/2$ and $3\pi/2$, respectively. The encoded signal, auto-correlation signal, cross-correlation signal, highest auto-correlation peak and maximum peak of cross-correlation are already shown in Fig. 3.6.

For the case of a 32-chip en/decoder, code #9 is chose as an encoder and a decoder with code #9 (phase-shifted sequence is a step of $\pi/2$) is used to obtain auto-correlation signal and code #25 (phase-shifted sequence is a step of $3\pi/2$) is used to obtain a cross-correlation signal, respectively. The encoded signal, auto-correlation signal, cross-correlation signal, highest auto-correlation peak and maximum peak of cross-correlation are already shown in Fig. 3.7.

Table 3.1 Peak to maximum cross-correlation ratio.

Attributes	Value		
	8-chip	16-chip	32-chip
Auto-correlation peak power	64	256	1024
Max cross-correlation peak power	1	1	1
P/C	64	256	1024
P/C [dB]	18.06	24.08	30.10

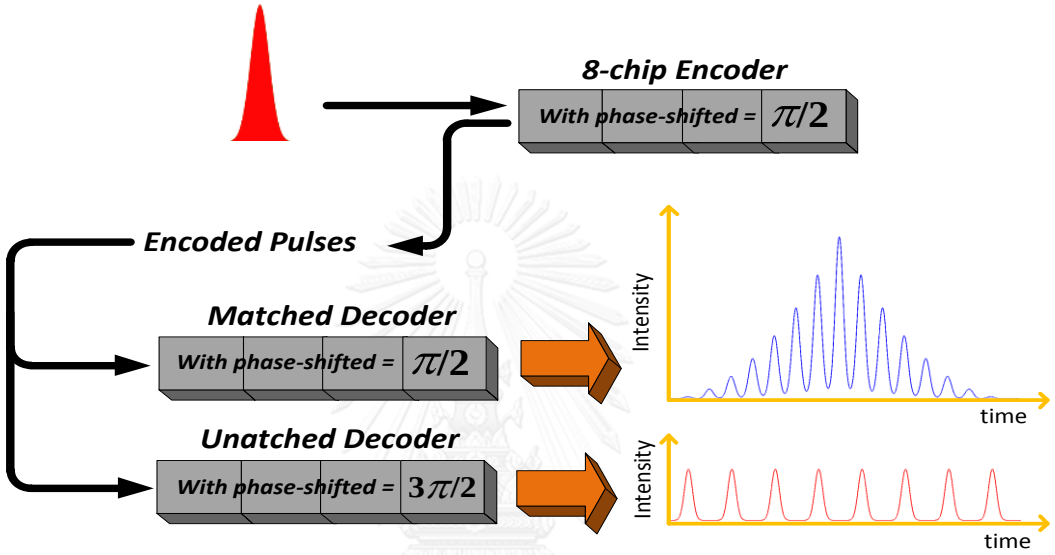

Fig. 3.5 Auto-correlation and cross-correlation signal from an 8-chip en/decoder.

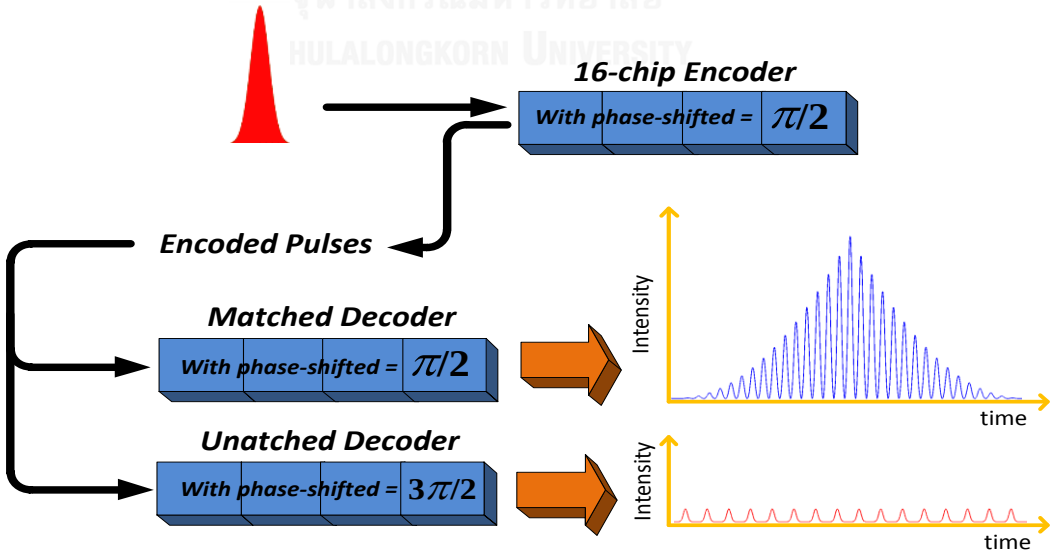

Fig. 3.6 Auto-correlation and cross-correlation signal from a 16-chip en/decoder.

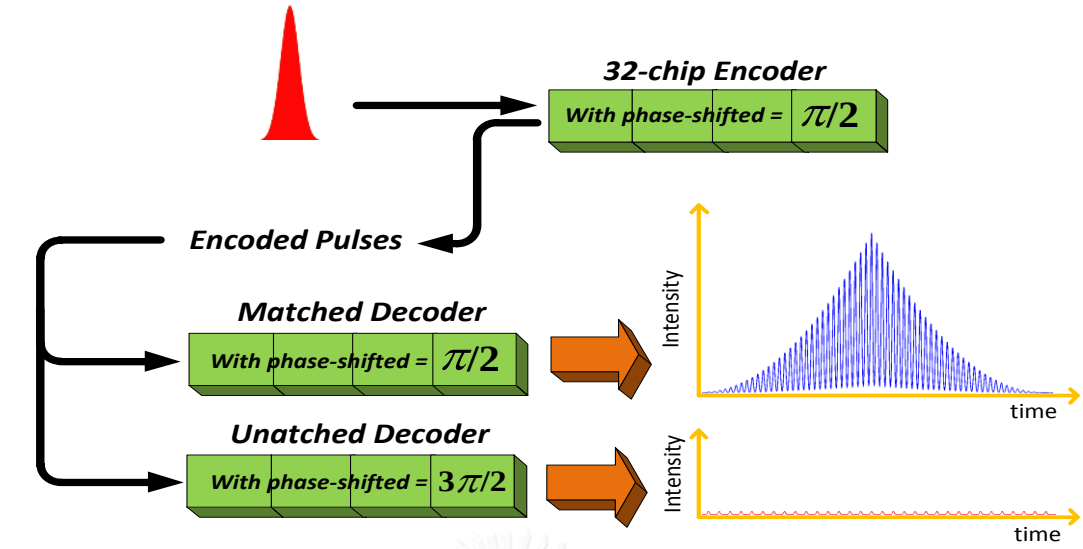

Fig. 3.7 Auto-correlation and cross-correlation signal from a 32-chip en/decoder.

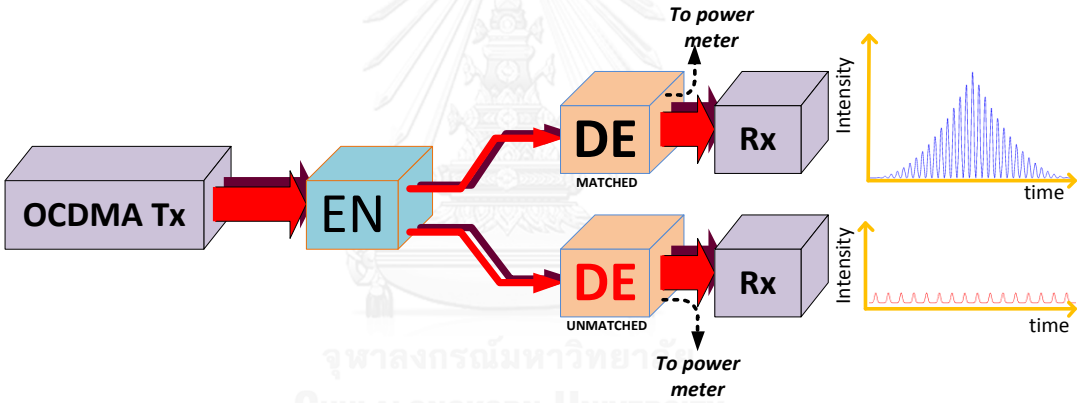

Fig. 3.8 Block diagram to measure PCR.

All of the codes from the case of 8, 16 and 32-chip en/decoder that we have selected to obtain auto-correlation and cross-correlation signal have the same phase-shifted sequence because we want to measure P/C according to the identical is the phase difference between two codes. Moreover, the P/C ratio calculation is already shown in Table 3.1, respectively.

In addition, we have performed a computer simulation to verify our expression. A simple block diagram is shown in Fig. 3.8. Firstly, OCDMA signal is generated at a transmitter and then encoded by an 8, 16 and 32-chip encoder, respectively. The code fabricated in these 3 types of encoder is the same code we have discussed above. The auto-correlation and cross-correlation is captured after the decoder and the signal power is measured in front of OCDMA receiver, respectively.

Fig. 3.9 has already expressed the auto-correlation and cross-correlation from the 8, 16 and 32 en/decoder at the same power level of the highest auto-correlation

peak. Hence, the P/C ratio and power contrast ratio from the computer simulation are calculated and are shown in Table 3.2. The results show that the P/C ratio is 18.06, 24.08 and 30.1 while the PCR is -16.33, -22.33 and -28.34 for the case of 8, 16 and 32-chip en/decoder, respectively. From the results, it confirms that using 32-chip en/decoder is the best point from our experiment that is capable in the reduction of the cross-correlation peak.

Although Fourier codes have a good correlation property, its orthogonality among other codes is not the same. The orthogonality is the maximum while the phase difference between two codes is equal to π. For example, a system using 4-chip en/decoder and encoded by code #2 (phase-shifted sequence is a step of $\pi/2$) will be achieved the best correlation property with code #4 (phase-shifted sequence is a step of $3\pi/2$) and the correlation property among code #1 (phase-shifted sequence is a step of 0) and code #3 (phase-shifted sequence is a step of π) mitigated. Therefore, a maximum in orthogonality will result in the strongest difference between auto-correlation and cross-correlation signal and Fig. 3.10 has shown the auto-correlation of code #2 and the cross-correlation signal corresponding to code #1, #3 and #4, respectively.

In the meanwhile, this phenomenon is dealt with a PCR value due to the contrast power in auto-correlation and cross-correlation signal. Therefore the measured PCR as a function of code number for the case of using 16-chip en/decoder is already illustrated in Fig. 3.11. The maximum PCR is found to be approximately 23 dB and the lowest is found at the adjacent codes with the PCR value of 7 dB, respectively.

Table 3.2 The P/C ratio and PCR obtain from the simulation.

Parameter	Value		
	8-chip	16-chip	32-chip
Auto-correlation peak power	64	256	1024
Max cross-correlation peak power	1	1	1
P/C [dB]	18.06	24.08	30.10
PCR [dB]	-16.33	-22.33	-28.34

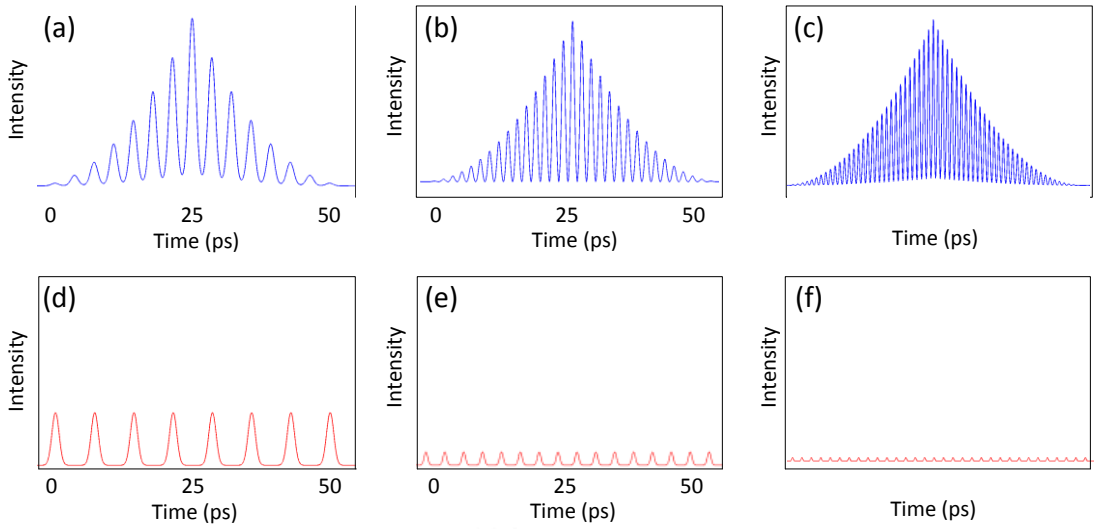

Fig. 3.9 An auto-correlation signal from (a) 8-chip en/decoder (b) 16-chip en/decoder (c) 32-chip en/decoder and a cross-correlation signal from (d) 8-chip en/decoder (e) 16-chip en/decoder and (f) 32-chip en/decoder.

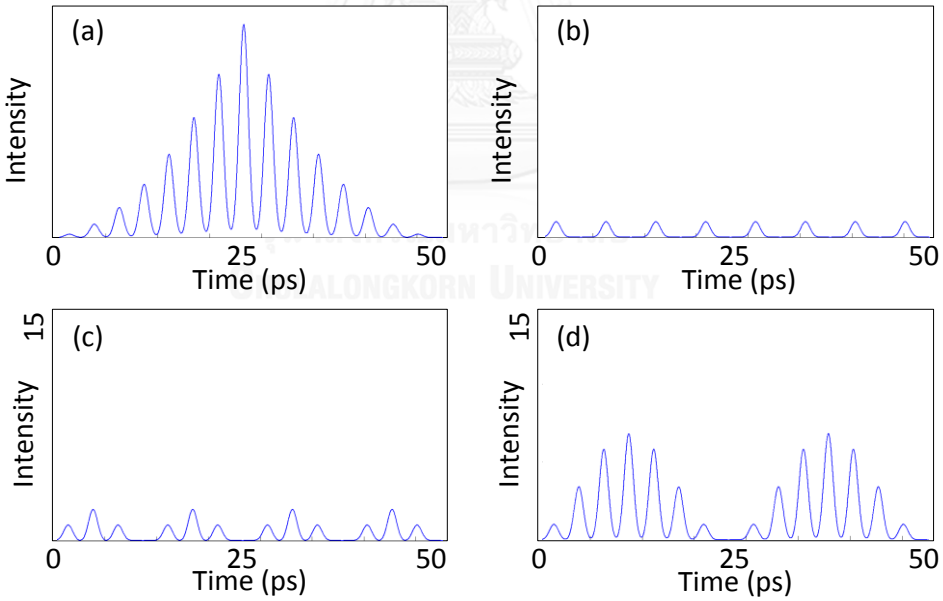

Fig. 3.10 Decoding Signal of code #2 (a) auto-correlation (b) cross-correlation between code 2# vs code #4 (c) cross-correlation between code 2# vs code #1and (d) cross-correlation between code 2# vs code #3.

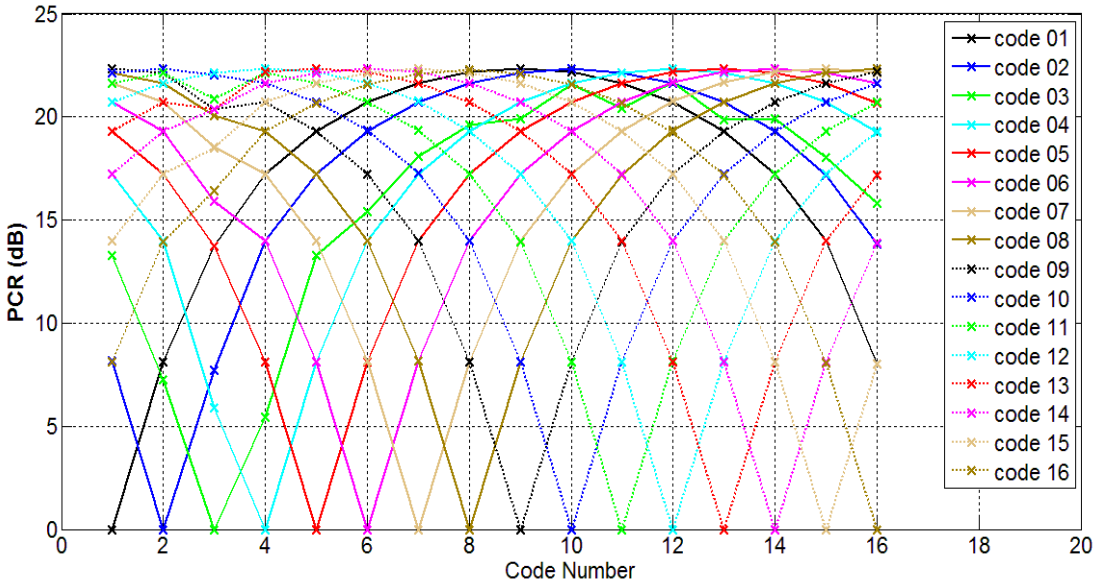

Fig. 3.11 The PCR as a function of code number for the case of 16-chip en/decoder.

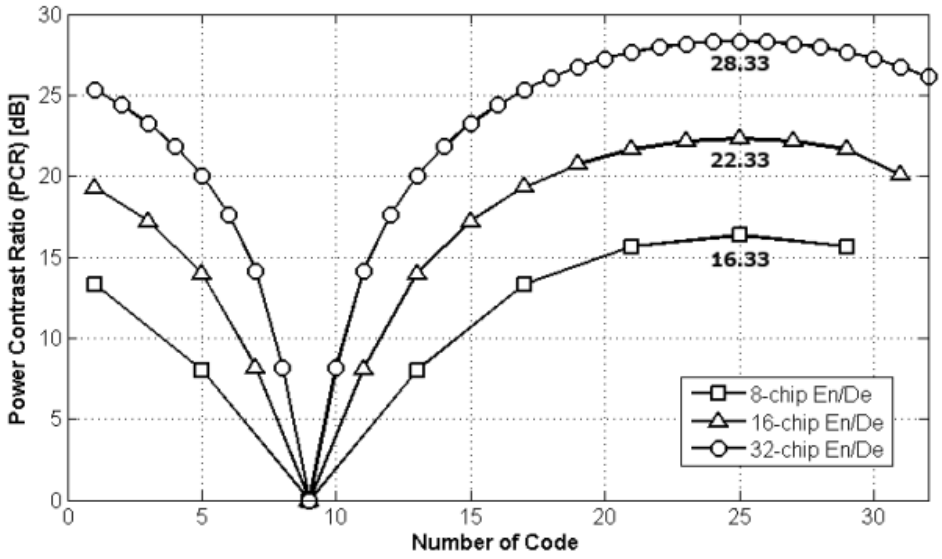

Fig. 3.12 The PCR for the case of 8, 16 and 32-chip en/decoder.

In comparison to the case of 8, 16 and 32-chip en/decoder, the great 32-chip case is found to be the best among others due to its maximum PCR of 28.33 dB. It is better than 12 and 6 dB, for the case of 8 and 16-chip en/decoder. However, the lowest PCR from these 3 cases are found to be the same by 7 dB, as shown in Fig. 3.12.

We finalized our computer simulation with a 40-Gbps OCDMA signal transmission with DPSK data format in the back-to-back case. The simulation setup for this experiment is already shown in Fig. 3.1. In order to find the maximum number of subscribers without any signal deteriorations from optical fiber, system parameter setup is shown in Table 3.3.

Table 3.3 System parameter setup for measuring the maximum number of subscribers

Parameter	Unit	Value		
		8-chip	16-chip	32-chip
System bit rate	Gbps	40		
Optical power	dBm	10		
Center wavelength	nm	1552.52		
Full-width half maximum	ps	1.33	0.687	0.332
Number of en/decoder chip	chip	8	16	32
Chip period	ps	3.125	1.5625	0.78125
Split Ratio of splitter	-	1:8	1:16	1:32
Splitter insertion loss	dB	9	12	15
PIN responsivity	A/W	1		
Dark current	nA	10		
Thermal noise	$pA/Hz^{1/2}$	1.52		
Cut-off frequency	GHz	30		

Table 3.4 System parameter setup for measuring the BER for the case of 8-chip en/decoder after a signal transmission over 20 km of OCDMA-PON.

Attributes	Unit	Value
System bit rate	Gbps	40
Minimum number of subscribers	-	1
Maximum number of subscriber	-	5
Optical power	dBm	10
Center wavelength	nm	1552.52
Full-width half maximum	ps	1.33
Number of en/decoder chip	chip	8
Chip period	ps	3.125
SMF G.652 length @ 1552 nm	km	20
SMF G.652 Attenuation @ 1552 nm	dB/km	0.2
SMF G.652 Dispersion @ 1552 nm	$ps/nm \cdot km$	17.577
SMF G.652 Dispersion slope @ 1552 nm	$ps/nm^2 \cdot km$	0.0581
DCF length	km	2.3127
DCF Attenuation @ 1552 nm	dB/km	-
DCF Dispersion @ 1552 nm	$ps/nm \cdot km$	-152
DCF Dispersion slope @ 1552 nm	$ps/nm^2 \cdot km$	-0.5022
Split Ratio of splitter	-	1:8
Splitter insertion loss	dB	9
PIN responsivity	A/W	1
Dark current	nA	10
Thermal noise	$pA/Hz^{1/2}$	1.52
Cut-off frequency	GHz	30

The relation between numerical bit error rate (BER) as a function of total number of subscribers in the system is shown in Fig. 3.13. By employing the more number of subscribers simultaneously, the more severe interference among subscribers can cause higher beat noise and MAI which is resulted in poor BER. An FEC limit is obtained at BER is lower than 10^{-3}. It should be mentioned that by employing a forward error correction (FEC) with Reed-Solomon RS(255, 239) can improve the BER from 10^{-3} to 10^{-9}. The simulation result shows that the maximum number supported by 8, 16 and 32-chip en/decoder is 7, 15 and 19, respectively.

Moreover, we also investigate the number of subscriber in the system and find out how it affects to the BER for the case of 8-chip en/decoder. We perform the signal transmission over 20 km of SMF followed by an appropriate length of DCF in order to cancel all accumulated chromatic dispersion in the link. The system parameter setup in shown in Table 3.4.

In this scenario, Fig. 3.14 illustrates the relation between the numerical BER and the ROP, obtained for both the back-to-back (B-B) detection and the 20-km transmission, for the cases of 1-5 subscribers. From the simulation result, only the cases of 1-4 subscribers can achieve the BER lower than 10^{-3} without using forward-error correction (FEC) at the ROP of -28.28, -27.9, -27.49, and -26.56 dBm for the B-B detection, and -28.06, -27.83, -27.44, and -26.5 dBm for the case of 20-km transmission, respectively. The insets (i)-(v) display the eye diagrams from the case of 1-5 subscribers, obtained from the auto-correlation of the detected DPSK-OCDMA signal, at the same ROP of -26.56 dBm. Although we set up the condition that minimizes the MAI, the simulation results show that when more subscribers are added into the system, the residual MAI also arises, and the large amount of beat noise becomes severe to cause the interference among OCDMA signals of different subscribers. Fig. 3.15 shows that the power penalties for 2, 3, and 4 subscribers at the BER of 10^{-3} are 0.39, 0.79, and 1.72 dB, for the case of B-B detection, and are 0.22, 0.61, and 1.54 dB for the case of 20-km transmission, respectively. These values of power penalties can be further used as the power budget considering MAI and beat noise for OCDMA-PON design.

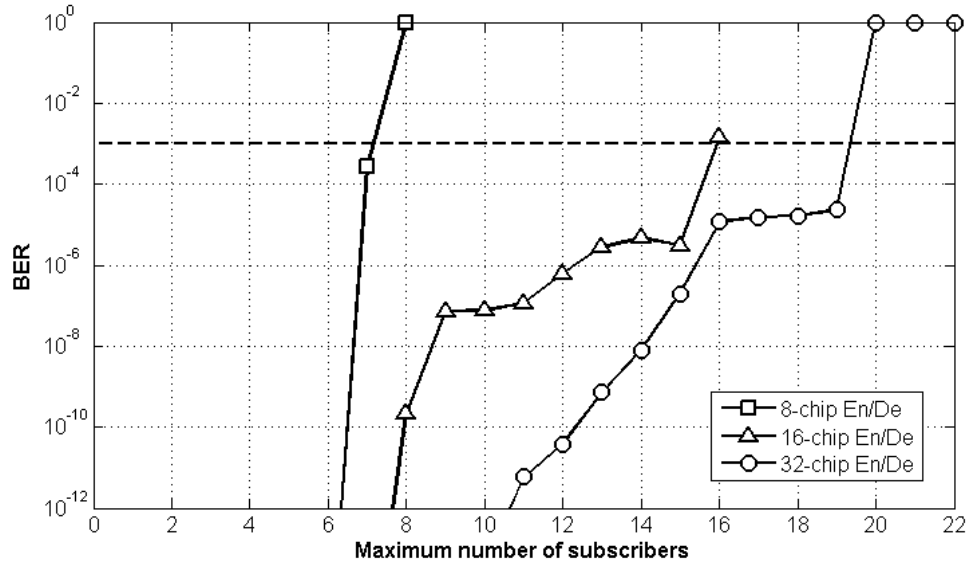

Fig. 3.13 The maximum number of subscribers in the back-to-back scenario.

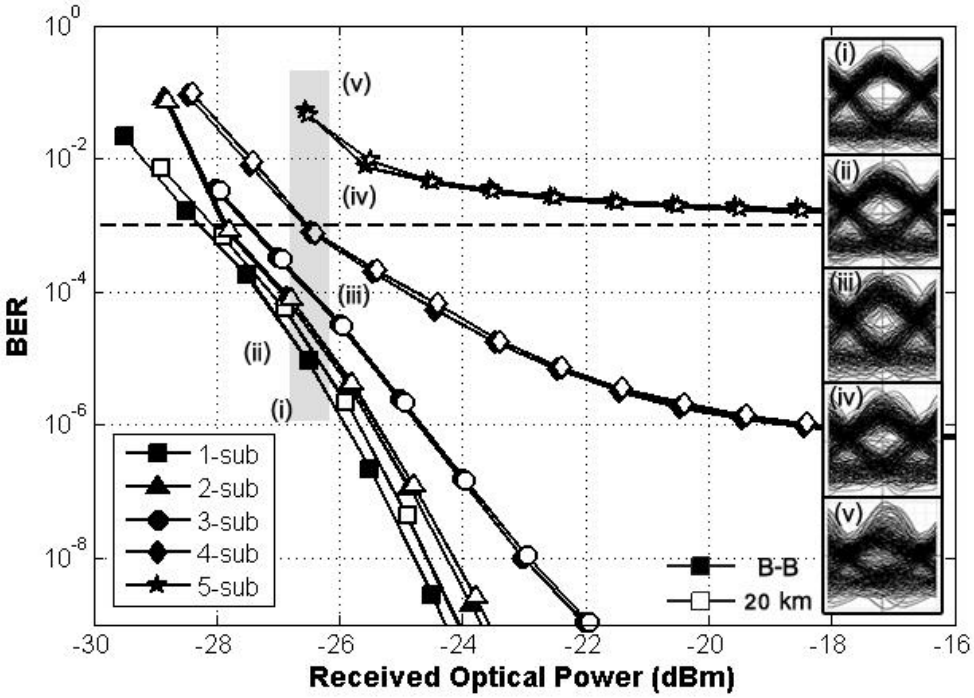

Fig. 3.14 Numerical BER as a function of received optical power, obtained for both the back-to-back (B-B) detection and the 20-km transmission, for the cases of 1-5 subscribers.

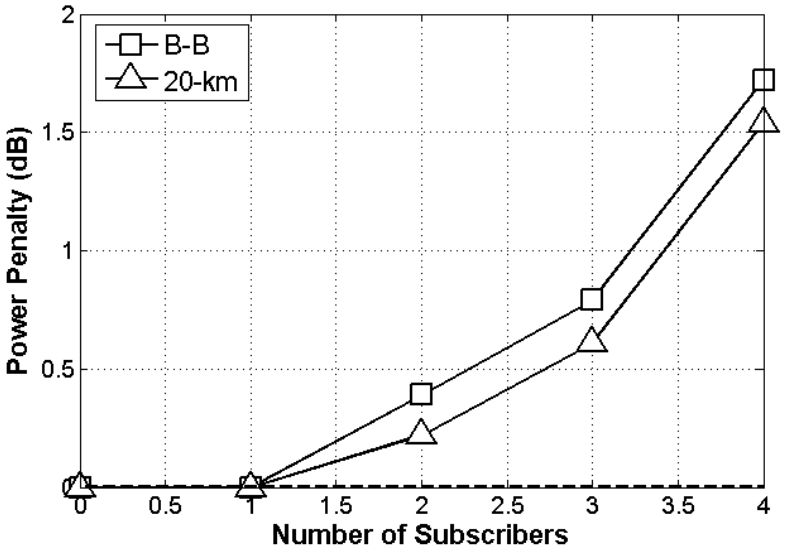

Fig. 3.15 Power penalties for 2, 3, and 4 subscribers for the cases of B-B and 20-km transmission.

CHAPTER 4 Proposed Model of OCDMA over PON with Various Spreading-Time to Bit-Period Ratio

In OCDMA networks, one of the most serious problems in both synchronous and asynchronous signal transmission over an optical fiber is primary beat noise and MAI. In order to mitigate those tragedy defects, many of effective solutions have already proposed. In this chapter, our proposed system model of OCDMA over PON will be described and we will illustrate some of key enabling techniques that could reduce noise in OCDMA network. Finally, the system parameters that are used to determine the system performance will be discussed, respectively.

4.1 System Model

Our basic system configuration of 40G OCDMA over PON is illustrated in Fig. 4.1. At OLT side, the first section is the light source which generates optical pulses exhibit Gaussian shape at a repetition rate of 40-GHz. So, our Gaussian pulse can be written as

$$A(t) = A_{\max} \exp\left[-\frac{1}{2}\left(\frac{t}{T_{FWHM}} \right)^2 \right], \tag{4.1}$$

where T_{FWHM} is a full-width half maximum of the optical pulse which is corresponding to an optical bandwidth B_0. Next, these pulses which are 25 ps apart from each other will be intensity modulated by an intensity modulator with non-return to zero (NRZ) electrical signal $D(t)$ employing random binary bit sequence “0” and “1” corresponding to the system bit rate. As optical pulses were driven into our programmable 8-level phase-shifted time-spreading en/decoder, we will obtain a series of 8 pulses as an encoded signal which the phases of each consecutive pulses or chips are determined by

$$h_c(t) = \sum_{k=0}^{N-1} \exp\left[-j\frac{2\pi k}{N}(c-1) \right] \cdot \delta(t - kt_{chip}), \tag{4.2}$$

where c is the number of code ordered from 1 to N, and the chip period t_{chip} is expressed as

$$t_{chip} = \frac{T_{bit}}{N}. \tag{4.3}$$

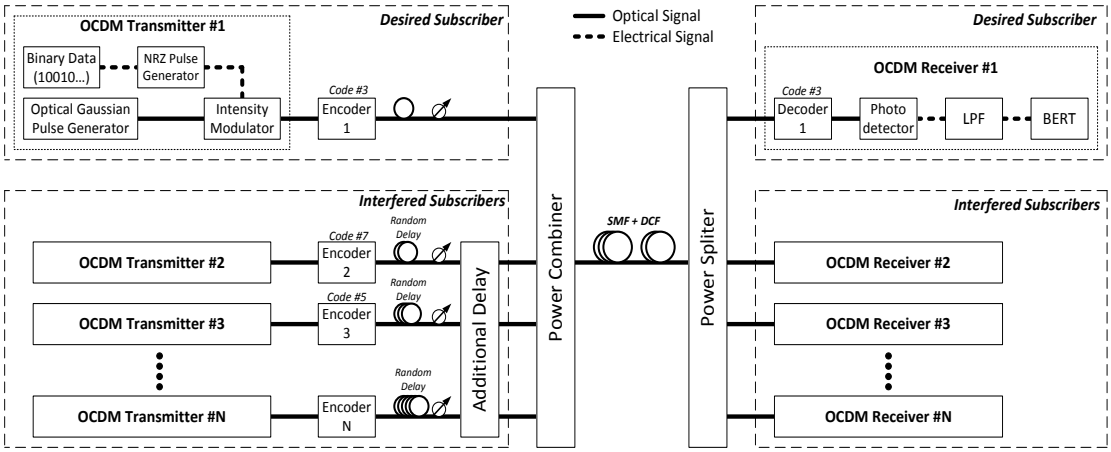

Fig. 4.1 Basic system model of OCDMA-PON.

Therefore, the optical field of encoded signal can be evaluated by the convolution between optical signal and the impulse response, given by

$$E_{en-c}(t) = (D(t) \cdot G(t)) \otimes h_c(t). \tag{4.4}$$

It should be noted that in order to operate TS-OCDMA in coherent regime, the ratio between t_{chip} and the coherence time of light source $\tau_c = 1/B_0$ called coherent ratio $kt = t_{chip} / \tau_c$ should be equal or greater than 1. Nevertheless, in order to perform the worst case of the coherent regime, we set the coherent ratio equal to 1.

Encoded signals from each subscriber are then combined and launched into a finite length of single-mode fiber and followed with perfect dispersion compensation in order to cancel accumulated dispersion.

At the decoding process at ONU side, the incoming series of encoded signal will be decoded by the decoder, which is still the convolution product between encoded signal and impulse response of the decoder. The correctly decoded signal from the decoder is defined as auto-correlation peak (ACP) signal if the code between en/de is identical while it is defined as cross-correlation peak (CCP) signal if the code between en/de is not matched. So, the optical field of the decoded signal is

$$E_{acp}(t) = E_{en-c}(t) \otimes h_c(t), \tag{4.5}$$

$$E_{ccp}(t) = E_{en-c}(t) \otimes h_d(t), \tag{4.6}$$

where c and d is the code number of the encoder and decoder, respectively. For example, subscriber with code #3 whose 8-chip E/D have the phase-shifted sequence by a step of $\pi/2$ (0, $\pi/2$, π, $\pi/2$, $3\pi/2$, 2π, $5\pi/2$, 3π). The input pulses, encoded signal, correctly decoded (decoded by code #3) and incorrect decoded signal (decoded by code #5) which is corresponding to the input bit-sequence "11010" are clearly shown in Fig. 4.2, respectively.

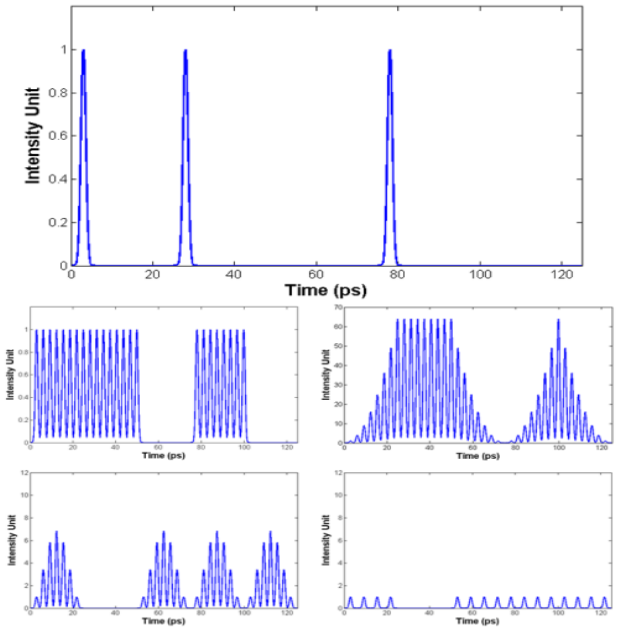

Fig. 4.2 Optical signal from a subscriber using code #3 with bit-sequence "11010" (a) input Gaussian pulses (b) encoded signal (c) ACP (code #3 vs code #3) (d) CCP (code #4 vs code #3) and (e) CCP (code #7 vs code #3).

4.2 Bit Error Rate and Signal to Noise Ratio Calculation

In order to evaluate the system performance based on the signal quality. In physical layer, we usually use the bit error rate and the signal to noise ratio to determine whether the quality of detected signal is acceptable or not. The methodologies to accomplish these two parameters are described below.

4.2.1 Bit Error Rate

The bit error rate (BER) is one of the most important parameters to measure the quality of the detected signal at the optical receiver. It is basically a ratio between the number of error transmitted bit over total sent bits. Nevertheless, in the numerical method, a BER approximation can be evaluate by a calculation of error probability. Firstly, the incident optical field $E_{PIN}(t)$ at the photodetector which is the summation of a desired ACP signal and m interfered signals or CCP as shown as

$$E_{PIN}(t) = E_{acp}(t) + \sum_{i=1}^{m} E_{ccp-i}(t). \tag{4.7}$$

At the photodetector, a converted electrical signal is produced by a square-law photodetector, the detected electrical signal over a total transmission time T is

$$
\begin{aligned}
Z &= \int_0^T (E_{PIN}(t)\cdot E_{PIN}{}^{*}(t))dt + \int_0^T n_0(t)dt \\
&= R\cdot\int_0^T (E_{acp}(t)\cdot E_{acp}^{*}(t))dt + R\cdot\sum_{i=1}^{m}\int_0^T (E_{ccp-i}(t)\cdot E_{ccp-i}^{*}(t))dt + 2R\cdot\sum_{i=1}^{m}\int_0^T (E_{acp}(t)\cdot E_{ccp-i}^{*}(t))dt \\
&\quad + 2R\cdot\sum_{j=i+1}^{m}\sum_{i=1}^{m-1}\int_0^T (E_{ccp-i}(t)\cdot E_{ccp-j}^{*}(t))dt + \int_0^T n_0(t)dt,
\end{aligned}
\tag{4.8}
$$

where R is the photodetector responsivity. The first term in (4.8) is the desired ACP signal. The second term is the beat term between each CCP signal themselves, called multiple access interference (MAI). The third term is the beat term between desired ACP and CCP called primary beat noise (PBN). The fourth term is the cross beat term between each individual CCP called secondary beat noise (SBN). Finally, the last term is the Gaussian random noise at the photodetector. It should be noted that the last term in (4.8) is related to dark current noise σ_d^2, shot noise σ_{sh}^2 and thermal noise σ_{th}^2 which can be evaluated as

$$\sigma_d^2 = 2qI_d B, \tag{4.9}$$

$$\sigma_{sh}^2 = 2qBRP_{acp}(1+\sum_{i=1}^{m}\xi_i), \tag{4.10}$$

$$\sigma_{th}^2 = \frac{4k_B BT}{R_L}, \tag{4.11}$$

where B is the receiver bandwidth, k_B is the Boltzmann's constant, T is the temperature and R_L is the load resistance of the receiver, P_{acp} is the average power of ACP and ξ_i is crosstalk level which is the ratio between average power of CCP to ACP as shown as

$$\xi_i = \frac{P_{ccp-i}}{P_{acp}}. \tag{4.12}$$

The converted electrical signal regardless of Gaussian random noise of photodetector is shown in Fig. 4.3. The needle-shape signal formed a triangular envelope is the desired ACP signal. As expected, the signal in grey tone stands for a most critical PBN which is generated by the beat between the desired ACP and CCP signal inside the ACP period only. Moreover, the MAI is illustrated in a black tone and it is generated at interfered CCP's position itself.

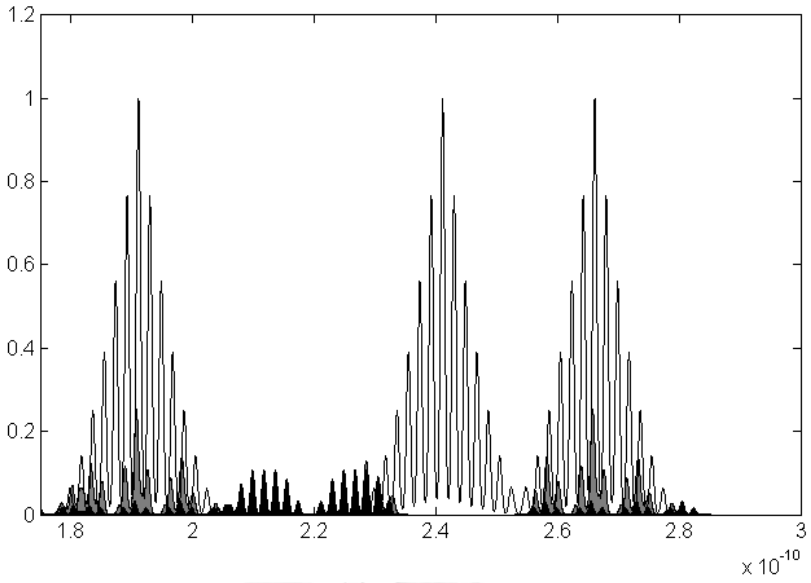

Fig. 4.3 The detected electrical signal at the photodetector.

Since the nature of the optical-to-electrical (O/E) conversion at the photodetector behaves like a low-pass filter itself, the signals after O/E will be filtered their high frequency components out and only the baseband signals are kept for the bit error rate detection, respectively. Therefore, the baseband signals after filtered with a desired impulse response $\Gamma(t)$ of a photodetector can be derived as

$$\begin{aligned} Z_{LPF} &= R\cdot\int_0^T \Gamma(t)\otimes(E_{acp}(t)\cdot E_{acp}^*(t))dt \\ &\quad + R\cdot\sum_{i=1}^{m}\int_0^T \Gamma(t)\otimes(E_{ccp-i}(t)\cdot E_{ccp-i}^*(t))dt \\ &\quad + 2R\cdot\sum_{i=1}^{m}\int_0^T \Gamma(t)\otimes(E_{acp}(t)\cdot E_{ccp-i}^*(t))dt \\ &\quad + 2R\cdot\sum_{j=i+1}^{m}\sum_{i=1}^{m-1}\int_0^T \Gamma(t)\otimes(E_{ccp-i}(t)\cdot E_{ccp-j}^*(t))dt \\ &\quad + \int_0^T \Gamma(t)\otimes n_0(t)dt. \end{aligned} \tag{4.13}$$

The signal Z_{LPF} is the convolution product between $\Gamma(t)$ and Z. Consequently, the high frequency components of all terms in (4.8) are filtered out by a low pass filter resulting in a smooth-shape signal in time domain as illustrated in Fig. 4.4

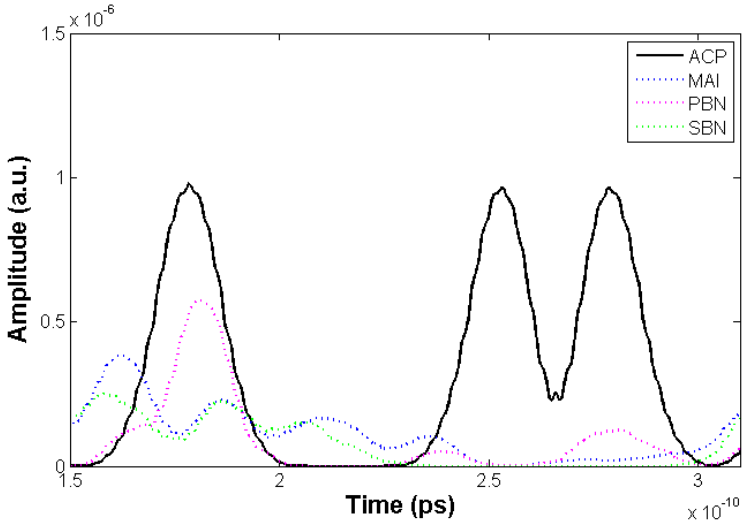

Fig. 4.4 Converted electrical signals after been filtered by a LPF.

Then, we use signal Z_{LPF} in (4.13) to investigate the stability of the system by the computation of BER under the Gaussian approximation. To calculate the BER, the general form of BER calculation at the sampling point is commonly represented by

$$BER = \frac{1}{4}\left[erfc\left(\frac{I_1 - D}{\sigma_1\sqrt{2}}\right) + erfc\left(\frac{D - I_0}{\sigma_0\sqrt{2}}\right)\right], \tag{4.14}$$

where I_1 is the mean electrical signal level at bit "1", I_0 is the mean electrical signal level of bit "0" and D is the decision threshold electrical signal level which can be optimized by

$$D = \frac{\sigma_0 I_1 + \sigma_1 I_0}{\sigma_0 + \sigma_1}. \tag{4.15}$$

Therefore, in order to modify (4.15) to be compatible with OCDMA system, the equation (4.15) has been derived by [50] as,

$$BER = \frac{1}{4}\left(erfc\left[\frac{RP_{acp}(1+\sum_{i=1}^{m}\xi_i - D)}{\sqrt{2}\sigma_1}\right] + erfc\left[\frac{RP_{acp}(D-\sum_{i=1}^{m}\xi_i)}{\sqrt{2}\sigma_0}\right]\right). \tag{4.16}$$

In (4.16), by discarding D, the term $RP_{acp}(\sum_{i=1}^{m}\xi_i)$ represents average current obtained from CCP signal power over a whole bit period. The integration of square of the 2nd term in (4.7) resulting in a signal power of MAI, SBN and receiver noise

which are the 2nd, 4th and 5th term in (4.8), respectively. The term $RP_{acp}(\sum_{i=1}^{m}\xi_i)$ is used as the mean current level of bit with mark "0" or cross correlation signal current I_{ccp}. Similarly, the term $RP_{acp}(1+\sum_{i=1}^{m}\xi_i)$ represents average current obtained from the sum of ACP signal power and CCP signal power over a whole bit period which are the power of the 1st, and 2nd terms in (4.8). The term RP_{acp} can be stated as the auto correlation signal current I_{acp}. Finally, the term $RP_{acp}(1+\sum_{i=1}^{m}\xi_i)$ is used as the mean current level of bit with mark "1" as well [50]. Both of I_{ccp} and I_{acp} can be written as

$$I_{ccp} = R\cdot\sum_{i=1}^{m}\int_{0}^{T}\Gamma(t)\otimes(E_{ccp-i}(t)\cdot E^{*}_{ccp-i}(t))dt, \tag{4.17}$$

$$I_{acp} = R\cdot\int_{0}^{T}\Gamma(t)\otimes(E_{acp}(t)\cdot E^{*}_{acp}(t))dt, \tag{4.18}$$

respectively.

Moreover, total noise variances are MAI noise σ^2_{MAI}, PBN noise σ^2_{PBN}, SBN noise σ^2_{SBN} and receiver's noise σ^2_{Rx} which are the variances of the 2nd, 3rd, 4th and 5th terms in (4.13), respectively. All noise variances are calculated by MATLAB using variance function. For bit "0", the total noise variance is expressed in (4.19) as

$$\sigma_1^2 = \sigma^2_{MAI} + \sigma^2_{SBN} + \sigma^2_{PBN} + \sigma^2_{Rx}. \tag{4.19}$$

The total noise variance for bit "0" is a subtraction of (4.19) by PBN noise as shown in (4.20) as

$$\sigma_0^2 = +\sigma^2_{MAI} + \sigma^2_{SBN} + \sigma^2_{Rx}. \tag{4.20}$$

Therefore, the threshold current level can be modified from (4.16) as

$$I_D = \frac{\left(\sigma_0\cdot\left(I_{acp}+\sum_{i=i}^{m}I_{ccp-i}\right)\right)+\left(\sigma_1\cdot\sum_{i=i}^{m}I_{ccp-i}\right)}{\sigma_0+\sigma_1}. \tag{4.21}$$

Finally, the BER is evaluated as

$$BER = \frac{1}{4}\left(erfc\left[\frac{\left(I_{acp} + \sum_{i=i}^{m} I_{ccp-i} \right) - I_D}{\sqrt{2}\sigma_1} \right] + erfc\left[\frac{I_D - \sum_{i=i}^{m} I_{ccp-i}}{\sqrt{2}\sigma_0} \right] \right). \quad (4.22)$$

4.3 Key Enabling Technique

There are many works have proposed a solution to reduce the effect of PBN since the PBN is stated as the most crucial noise in OCDMA [25]. Some of them have performed the experiment by using longer codes and another has performed by using an en/de with high power contrast ratio. Those works are accomplished by reducing the crosstalk level ξ that resulting in the PBN, MAI and SBN reduction, respectively. Moreover, in [51] has shown the model of imperfectly overlapped chips in OCDMA system as a real asynchronous transmission scenario and we could learn that the reduction in the interference between subscribers could reduce the effect of PBN as well. The imperfect overlapped model in [51] has shown another solution to reduce PBN by reducing the pulse width of optical pulse over a certain t_{chip} and this also caused a lower coherence time of light source τ_c. In this case, the kt ratio is increased and the BER is improved through its statistical independence. Nevertheless, the OCDMA criteria would be changed from coherent to incoherent regime due to the very large value of kt ratio as well.

In this section, we propose a parameter that can reduce the interference between desired ACP and interfered CCP signals and can improve system BER while constraining the same $kt = 1$(the coherent limit).

4.3.1 Spreading-Time to Bit-Period Ratio

We introduce the spreading-time to bit-period ratio (SBR) as the ratio between the total encoding periods to the total bit-period,

$$SBR = \frac{T_{en}}{T_{bit}}, \quad (4.23)$$

where T_{en} is evaluated as

$$T_{en} = N \cdot t_{chip}. \quad (4.24)$$

Then, substitute T_{en} into (4.24) and re-arrange in term of t_{chip}, we get

$$t_{chip} = \frac{T_{bit} \cdot SBR}{N}. \quad (4.25)$$

We finally substitute (4.25) into (4.2), so the impulse response and the frequency response of the modified encoder corresponding to the SBR is expressed as

$$h_{code-c}(t) = \sum_{k=0}^{N-1} \exp\left[-j \frac{2\pi k}{N}(c-1) \right] \cdot \delta(t - k\frac{T_{bit} \cdot SBR}{N}), \tag{4.26}$$

$$H_{code-c}(f) = \sum_{k=0}^{N-1} \exp\left[-j2\pi k \left(\left(\frac{c-1}{N} \right) + f \frac{T_{bit} \cdot SBR}{N} \right) \right] \tag{4.27}$$

respectively.

For example, OCDMA-based 40G-PON has a bit period of 25 ps, if we sent a short pulse to the encoder in order to construct series of encoded pulses and they took whole 25 ps, their SBR is 1. On the other hand, if we spread encoded pulses to 20, 15, 10 and 5 ps, their SBR is 0.8, 0.6, 0.4 and 0.2 respectively. The encoded signals from the encoder are stated as

$$E_{code-c}(t) = \sum_{k=0}^{N-1} \exp\left[-j \frac{2\pi k}{N}(c-1) \right] \cdot \exp\left[-\frac{(t - k(T_{bit} \cdot SBR/N))^2}{2T_0^2} \right] \tag{4.28}$$

Fig. 4.5 shows a comparison of encoded and decoded signal using different SBR of 1, 0.8, 0.6, 0.4 and 0.2, respectively. It is clearly seen that, with SBR equals to 1, encoded signals are spread over a whole bit period as shown in Fig. 4.5(a). On the other hand, while pulses are spread with other values of SBR, we will have some blank spaces between each consecutive bit as a guard-time interval, respectively. This method allow us to avoid the inter-symbol interference (ISI) between consecutive bits while using low value of SBR by reducing the total period of encoded pulses. In the decoding process, the auto correlation peak signal and the cross correlation peak signal which are depended on the codes between the en/decoder, are governed by,

$$\begin{aligned} E_{acp}(t) = &\sum_{k=0}^{N-1} \exp\left[-j \frac{\pi(2k+N+1)}{N}(c-1) \right] \cdot (k+1) \cdot \exp\left[-\left(t - k\left(\frac{T_{bit} \cdot SBR}{N} \right) \right)^2 \Big/ 2T_0^2 \right] \\ &+ \sum_{k=N}^{2N-2} \exp\left[-j \frac{\pi(2k+N+1)}{N}(c-1) \right] \cdot (2N-k-1) \cdot \exp\left[-\left(t - k\left(\frac{T_{bit} \cdot SBR}{N} \right) \right)^2 \Big/ 2T_0^2 \right] \end{aligned} \tag{4.29}$$

$$\begin{aligned} E_{ccp-i}(t) = &\exp\left[-j \frac{\pi d}{2N} \right] \times \sum_{k=0}^{2N-2} \exp\left[-j \frac{\pi(2k+N+1)}{N} \right] \times \left(\frac{\sin[\pi(k) \cdot (d)/N]}{\sin[\pi \cdot d/N]} \right) \\ &\times \exp\left[-\left(t - k\left(\frac{T_{bit} \cdot SBR}{N} \right) \right)^2 \Big/ 2T_0^2 \right] \end{aligned} \tag{4.30}$$

we can obtain that the ACP from the first bit is overlapped to the second bit, shown in Fig. 4.5(b) for the case of SBR = 1.0, 0.8 and 0.6, while there is not any overlapped intervals between 2 consecutive bits for the case of SBR = 0.4 and 0.2. These guard-time intervals also allow us to avoid the interference between ACP and CCP which bring us serious noise problem by the reduction of overlapped chips between desired and interfered subscribers.

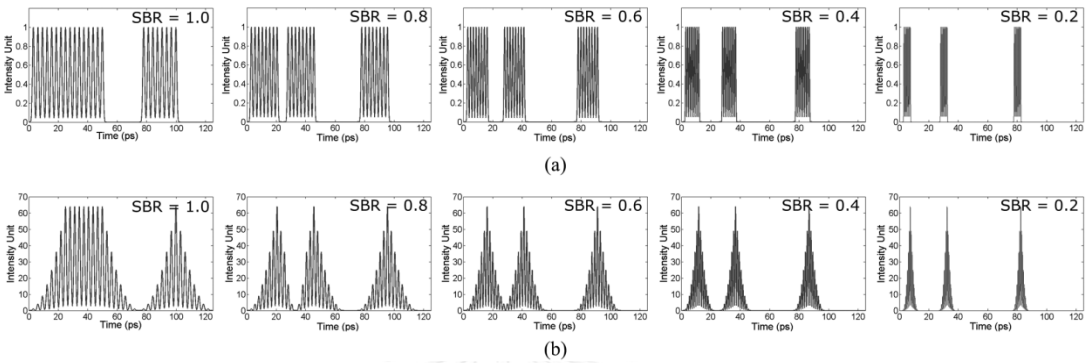

Fig. 4.5 ACP from code #3 at different value of SBR (a) encoded signals and (b) decoded signals.

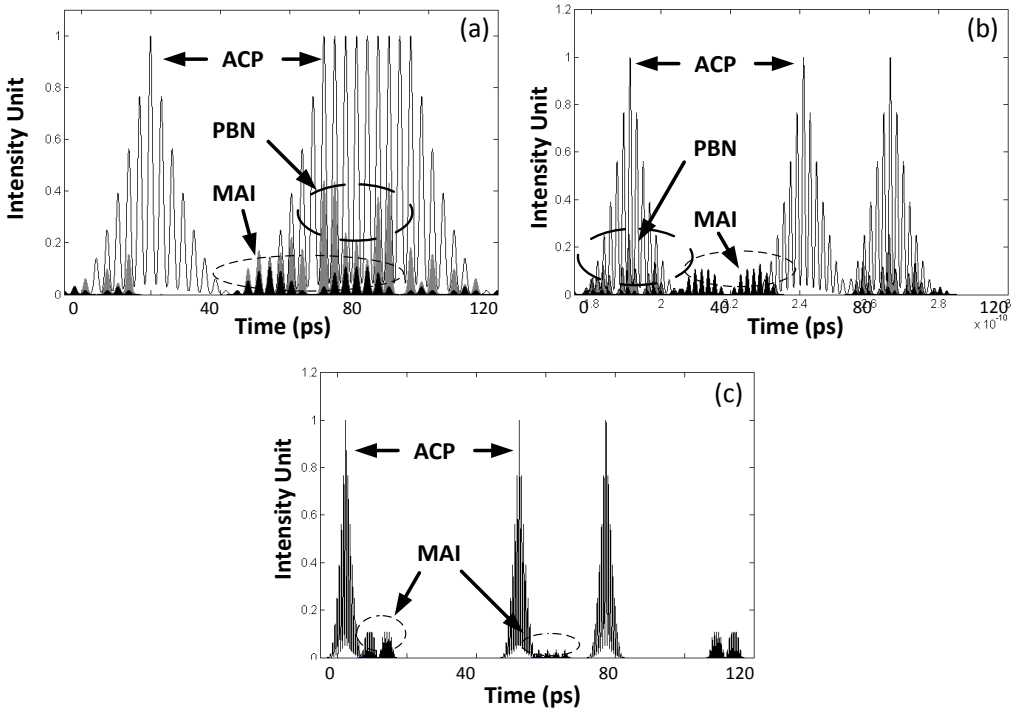

Fig. 4.6 The ACP, MAI, and PBN signal from (a) SBR = 1.0 (b) SBR = 0.6 and (c) SBR = 0.2.

Fig. 4.6 shows the difference of employing various SBR. In each case, The thin-black line of desired ACP signal with bits mark "1011" is launched together with two interfered CCP signals which are 15-chip delayed apart from the first chip of the desired ACP. In Fig. 4.6(a), the SBR = 1.0, the CCP signals cause MAIs as depicted in dark solid color and cause PBNs as depicted in grey solid color, respectively. Although we can obtain that the first bit of CCP is shifted 15 chips apart and it does not interfered the first bit of ACP, it causes interference at the third bit of ACP signal instead and the PBN is produced. For the case of SBR = 0.6, after the first bit of CCP signal is shifted, it is positioned at the beginning of the second bit of ACP signal. Therefore, only the rear part of CCP signal causes interference at the front part of the third ACP bit. In this case, the number of chips that produce PBN has been decreased in comparison to the case of SBR = 1.0, as shown in Fig. 4.6(b). The last case, SBR = 0.2, the first bit of CCP signal has shifted 15-chip apart and it does not cause any interferences with the ACP signal at all due to its shortening decoding period. Consequently, the PBN is not generated but only MAI is produced as illustrated in Fig. 4.6(c).

4.4 System Performance

We analyze the system's BER of subscriber using code #3 while the code of m interfered subscribers are started from code #4, #2, #5, #1, #6, #8 and #7 for the case of simultaneously transmitting 2-8 subscribers, respectively. With this orientation, code #3 will be experienced the maximum crosstalk level among the other codes for total N -1 subscribers. To investigate the system performance with the system configuration shown in Fig. 4.5, we organized the experiment to obtain the worst and the average performance. Note that this calculation is considering a dispersion-free transmission in order to investigate signal deterioration caused by employing various value of SBR.

Firstly, at each SBR, we perform the calculation for the case of 1-8 subscribers, respectively. All noise variances and BER will be analyzed further in the next session. In order to perform the calculation, some of useful parameters used in this chapter are stated in Table 4.1.

4.4.1 Worst Performance

In this case, all m interfered subscribers were aligned to experience the maximum CCP signals. Moreover, we investigated the BERs at all available chip positions in one bit period by adding the delay Δt_n which is define as

$$\Delta t_n = n \cdot t_{chip} \tag{4.31}$$

, where n is the set of index chip number in one bit period at each SBR. The index n is stated as

$$n = \left\{ x \in (\mathrm{I} - \mathrm{I}^{-}) \middle| 0 \le x \le T_{bit} / t_{chip} \right\}. \tag{4.32}$$

Then, we substitute t_{chip} from (4.25) into (4.32) and we get

$$n = \left\{ x \in (\mathrm{I} - \mathrm{I}^{-}) \middle| 0 \le x \le N/SBR \right\}. \tag{4.33}$$

Therefore, the additional delay Δt_n for all interfered subscribers are varied from 0-8, 0-10, 0-13, 0-20 and 0-40 chips respected to the desired subscribers, in order to find the worst case scenario of each cases, for the case of SBR equals 1.0, 0.8, 0.6, 0.4 and 0.2 as shown in Fig. 4.7, respectively.

Table 4.1 System parameters of the OCDMA using various SBR.

Attributes	Unit	Value				
		SBR = 1.0	SBR = 0.8	SBR = 0.6	SBR = 0.4	SBR = 0.2
System bit rate	Gbps	40				
Center wavelength of optical source	Nm	1552.52				
Repetition rate	GHz	40				
Optical power	dBm	10				
Full width half maximum	ps	1.33	1.07	0.78	0.54	0.28
Coherence time of optical source	ps	3.089	2.487	1.881	1.246	0.623
Number of en/de chip	chip	8				
Chip period	ps	3.125	2.500	1.875	1.250	0.625
Coherent ratio	-	1				
Optical receiver type	-	PIN photodiode				
Responsivity	A/W	0.6				
Dark current	nA	50				
Thermal noise	$pA/Hz^{-0.5}$	1.52				
Cut-off frequency	GHz	30				

Since we have added the additional delay in each SBR as mentioned above, the position of CCPs has been changed in each delay and this causes different interference levels. Therefore, we could obtain several values of MAI, PBN and SBN, respectively. Fig. 4.8 shows a relation between numerical value of PBN variance σ_{PBN}^2 as a function of delayed time. The variance of PBN, in each SBR, is normalized with its maximum value in a case that employing SBR = 1.0 with $m = 7$. We can see clearly in Fig. 4.8(a)-(c) that σ_{PBN}^2 is increased as a function of number of subscribers and is increased as we reduce the SBR. In addition, σ_{PBN}^2 is also a function of time delay related to the ACP. For the case of SBR = 1.0, all 8 encoded chips are spread over a whole bit period and its ACP are spread over one bit and a half (15 chips). Unfortunately, the CCPs are 15-chip spread at the decoder as well. A PBN generation is generated at every additional delays and always causes high σ_{PBN}^2. For the case of SBR = 0.6 as shown, all 8 encoded chips are spread over 60% of a bit period or 8 of 13.33 chips. Anyway, all 15 chips of ACP are 13 chips located in its own bit whereas another 2 chips are placed at the consecutive bit. Fortunately, for the case of SBR = 0.2, all 8 encoded chips are spread over 20% of a bit period or 8 of 40 chips. Although the ACP occupies for 15 chips, the remained 25 chips are vacant. As expected, the σ_{PBN}^2 is decreased since the additional delay is applied to the CCPs and the PBN is zero due to none of interfered chips between ACP and CCP in the left and the right-side of the ACP in one bit period as shown in Fig. 4.8, respectively.

From our numerical value, obtained from each SBR, the BER as a function of received optical power (ROP) at the photodetector for the case of 1-8 subscribers are illustrated in Fig. 4.9. The FEC limit is considered at the BER lower than 10^{-3}. It should be noted that employing a forward error correction (FEC) can enhance the system performance by improving the BER from 10^{-3} to 10^{-9}, respectively. For the case of single subscriber, the receiver sensitivity at BER of 10^{-3} is -21.8, -24.05, -24.54, -25.04 and -25.48 dBm, respectively. The receiver sensitivity is improved when employing low SBR because the narrower pulse width gives the lower ROP at the same value of ACP [52]. For the multi-subscribers case, at each SBR, the BERs are increased since the noise variances σ_0^2 and σ_1^2 have been increased due to the more number of m interfered subscribers. We can see in Fig. 4.9(c)-(e) that, by employing lower SBR can improve the receiver sensitivity at BER = 10^{-3}. Since we have fixed the cut-off frequency of the LPF at 75 percent of the bit rate or 30 GHz, the noise fluctuations with high frequency which are corresponding to the chip rate of 533, 800, and 1600 GHz, for the case of SBR = 0.6, 0.4, and 0.2 can be eliminated. Nevertheless, for the case of SBR = 0.8 in Fig. 4.9(b), the BERs are the worst among all SBRs.

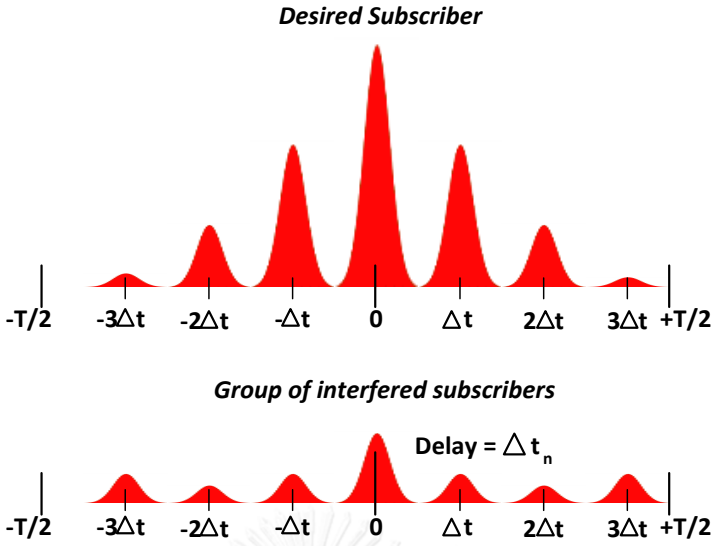

Fig. 4.7 Using additional delay with group of interfered subscribers.

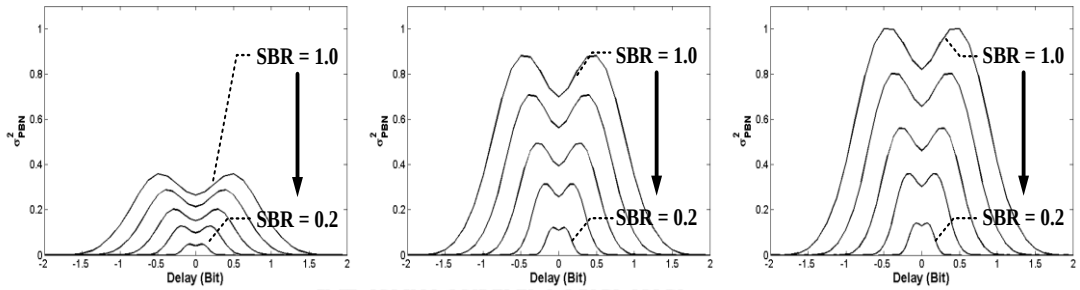

Fig. 4.8 Relation between variance of PBN and time delay for the case of (a) m = 1, (b) m = 4, and (c) m = 7, respectively.

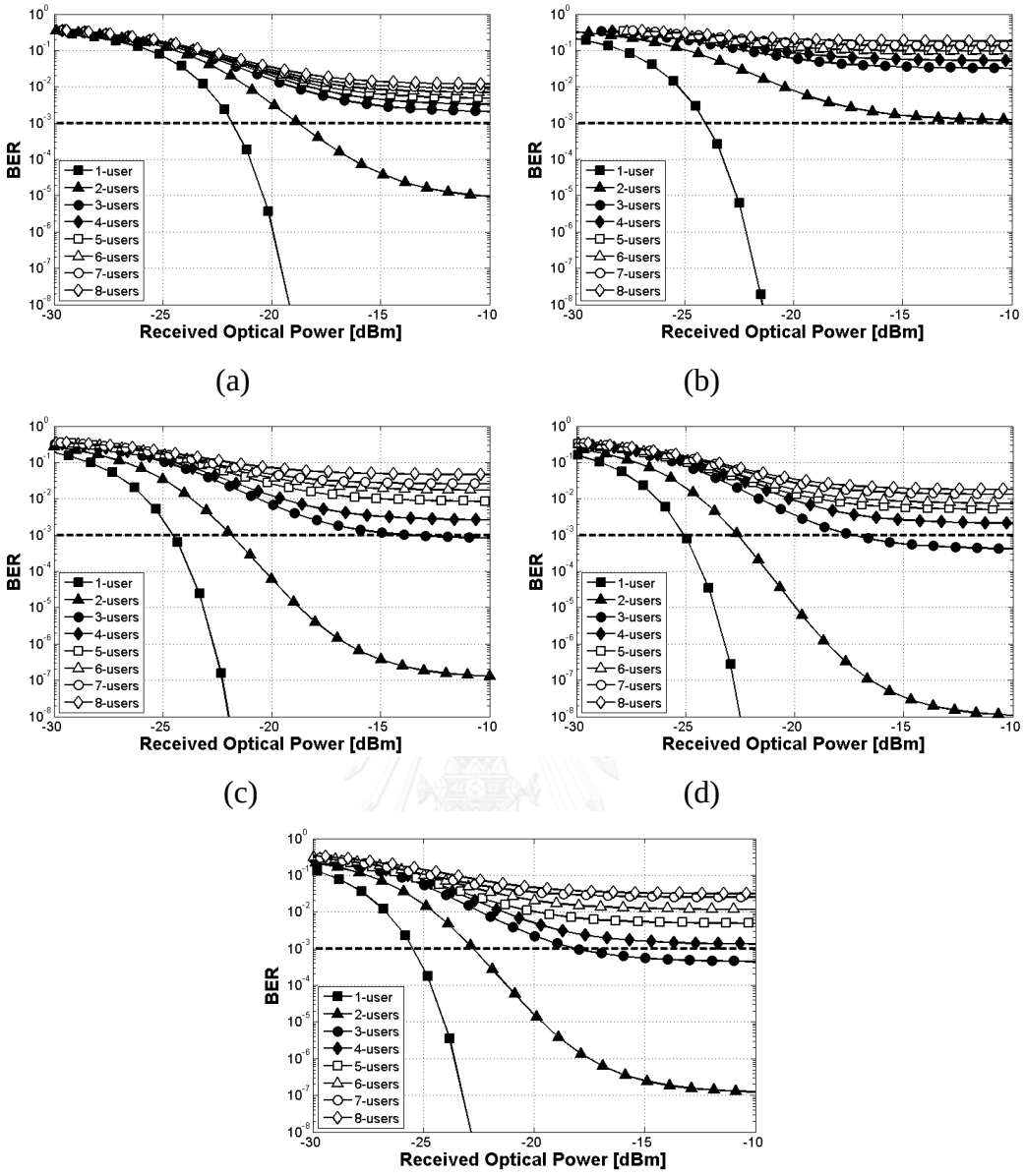

Fig. 4.9 Relation between numerical BER and ROP of the worst case (a) SBR = 1.0, (b) SBR = 0.8, (c) SBR = 0.6, (d) SBR = 0.4 and (e) SBR = 0.2.

The effect of varying the SBR causes the internal interferences between the consecutive CCPs. In Fig. 4.10, we illustrate 3 consecutive decoded signals using the adjacent code with respected to the desired code. By employing SBR = 1.0 and 0.8, there are 8 and 10 chips in one bit period. As a result, the sum of the optical field causes the destructive interference in the case of SBR = 1.0, as shown in Fig. 4.10(a). On the other hand, the interference becomes constructive in the case of SBR = 0.8 as shown in Fig. 4.10(b). Due to the large CCP in the case of SBR = 0.8, the σ^2_{PBN}, σ^2_{MAI}, and σ^2_{SBN} can be increased and this is resulting in the high BER as shown in Fig. 4.9.

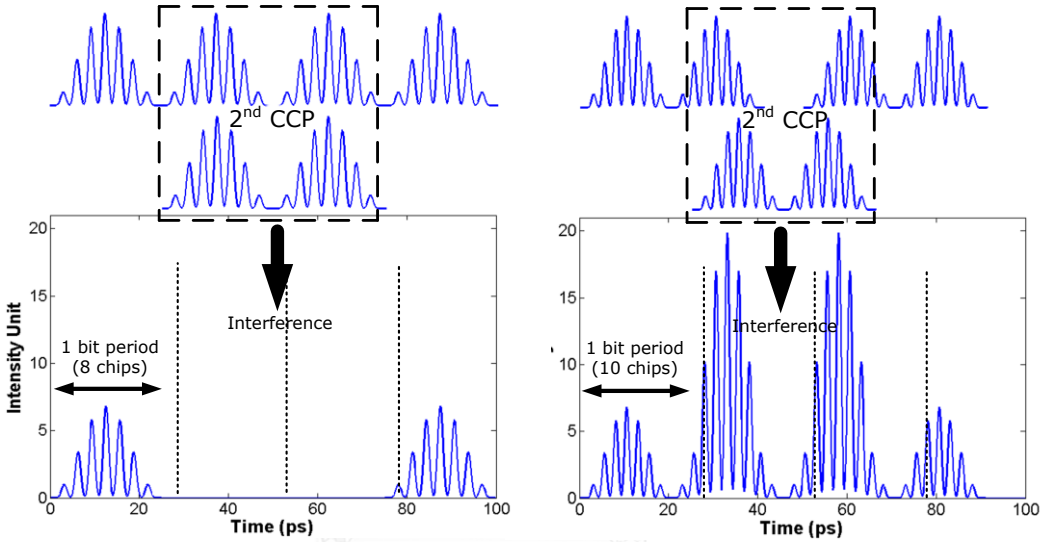

Fig. 4.10 The internal interference of the consecutive CCP signals (a) SBR = 1.0, and (b) SBR = 0.8.

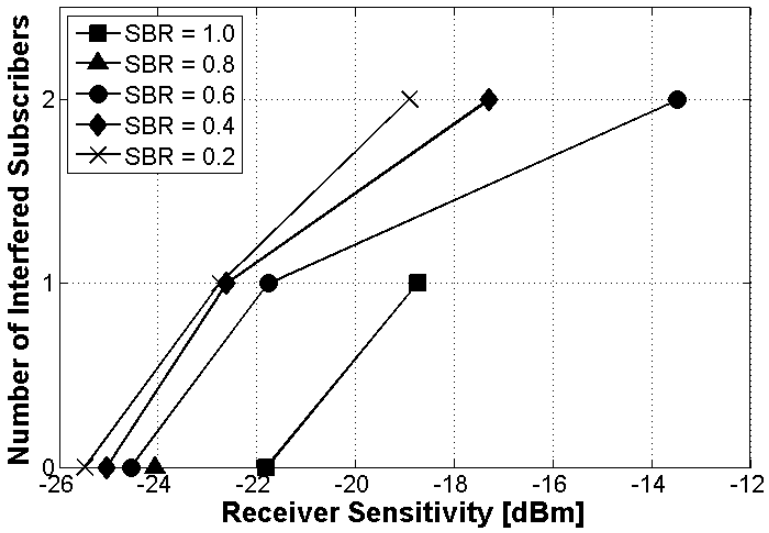

Fig. 4.11 Relation between ROP and the numbers of achieved error-free subscribers from the worst case.

The receiver sensitivity of all cases are collected from Fig. 4.9 and then shown in Fig. 4.11. It reveals the maximum of subscriber that can achieved the BER lower than 10^{-3} are 1, 0, 2, 2, and, 2 and the total subscribers are found to be 2, 1, 3, 3 and 3 for the case of SBR = 1.0, 0.8, 0.6, 0.4 and 0.2, respectively.

The computed noise variances as a function of m are shown in Fig. 4.12. All values are obtained at the MLLD peak power of 0 dBm. The results show that the SBR = 0.8 experiences the highest noise variances due to the largest CCPs. We can confirm that the σ_{PBN}^2 is the most severe noise variance due to its largest value in comparison to the σ_{MAI}^2 and the σ_{SBN}^2, respectively.

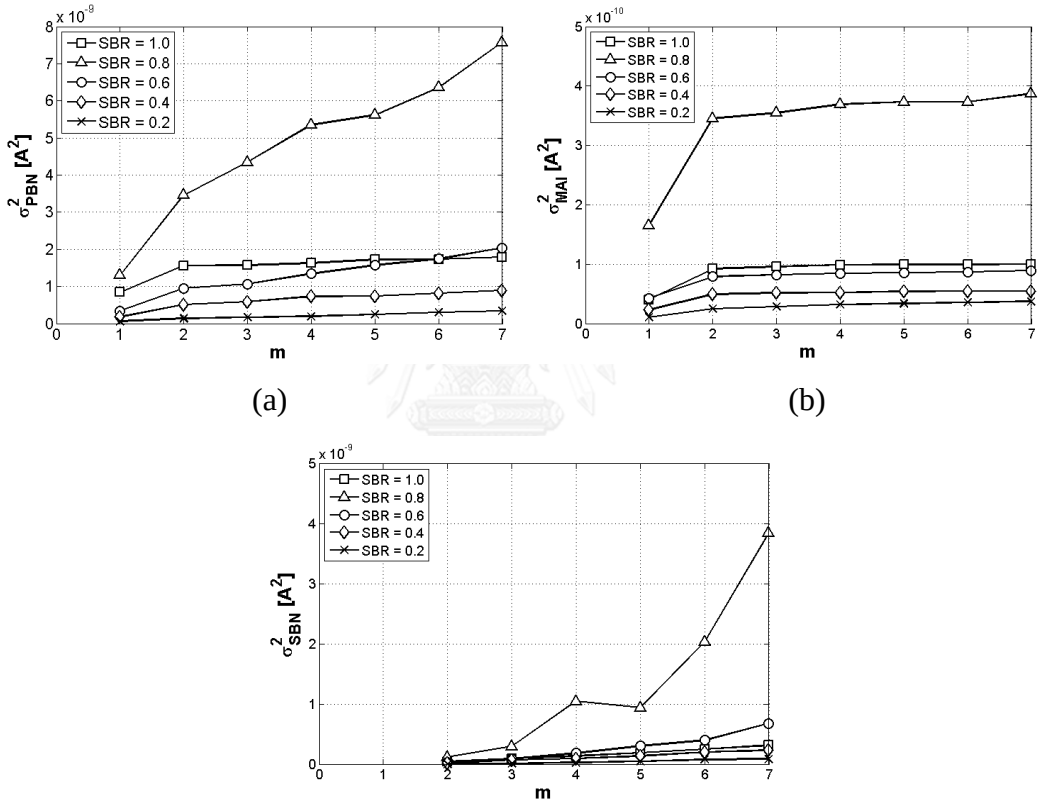

Fig. 4.12 Noise variances of the worst performance (a) σ_{PBN}^2, (b) σ_{MAI}^2, and (c) σ_{SBN}^2
.

4.4.2 Average Performance

In this case, we assume that all m interfered subscribers are launched to the system randomly. With the random delays of the interfered subscribers, the noise variance can be reduced through their statistical properties and the BER can be improved. We will organize to obtain the average performance by two methods. The first method is to find the BER with the aid of the probability and the second one is to find the average BER through the many possible events.

4.4.2.1 First Method

The total BER of the system can be calculate by using the average BER of each m interfered subscribers, defines as $BER(m)$ and the probability of each m will be launched to the system $p(m)$. Therefore, the average BER can be written as,

$$BER = \sum_{m=1}^{N-1} p(m) \cdot BER(m). \tag{4.34}$$

$p(m)$ obeys the binomial distribution with its probability of

$$p(m) = \frac{(N-1)!}{(N-m-1)!m!} \cdot 2^{N-1}. \tag{4.35}$$

$BER(m)$ is the average BER computed from all $BER(i)$ of all available chips in one bit period where all m interfered subscribers are aligned together to have the greatest CCP. The BER at each chip position is assumed to have the uniform distribution with probability $p(i)$. The probability is,

$$p(i) = \frac{1}{n}. \tag{4.36}$$

Therefore, the $BER(m)$ can be obtained as,

$$BER(m) = \sum_{i=1}^{n} p(i) \cdot BER(i), \tag{4.37}$$

where i is the index number of the chip and n is the total chips in one bit period.

The BERs of the OCDM system in the average case are illustrated in Fig. 4.13. We can see that the BERs of all cases are improved in comparison with the worst case. As a result, the receiver sensitivities are improved and the numbers of subscribers that can achieve the FEC limit are increased, respectively.

The receiver sensitivities as a function of m are also shown in Fig. 4.14. In comparison to the worst performance, the numbers of possible m subscribers are 4, 1, 5, 6, and 6. For the case of 2 subscribers (m = 1), by employing lower SBR can also

improve the receiver sensitivity with the power penalty of 1.0, 2.86, 3.61, and 4.03 dB in comparison to the single subscriber case for the case of SBR = 0.8, 0.6, 0.4, and 0.2, respectively. Moreover, the power penalty in each SBR can obtain in Fig. 4.14, respectively.

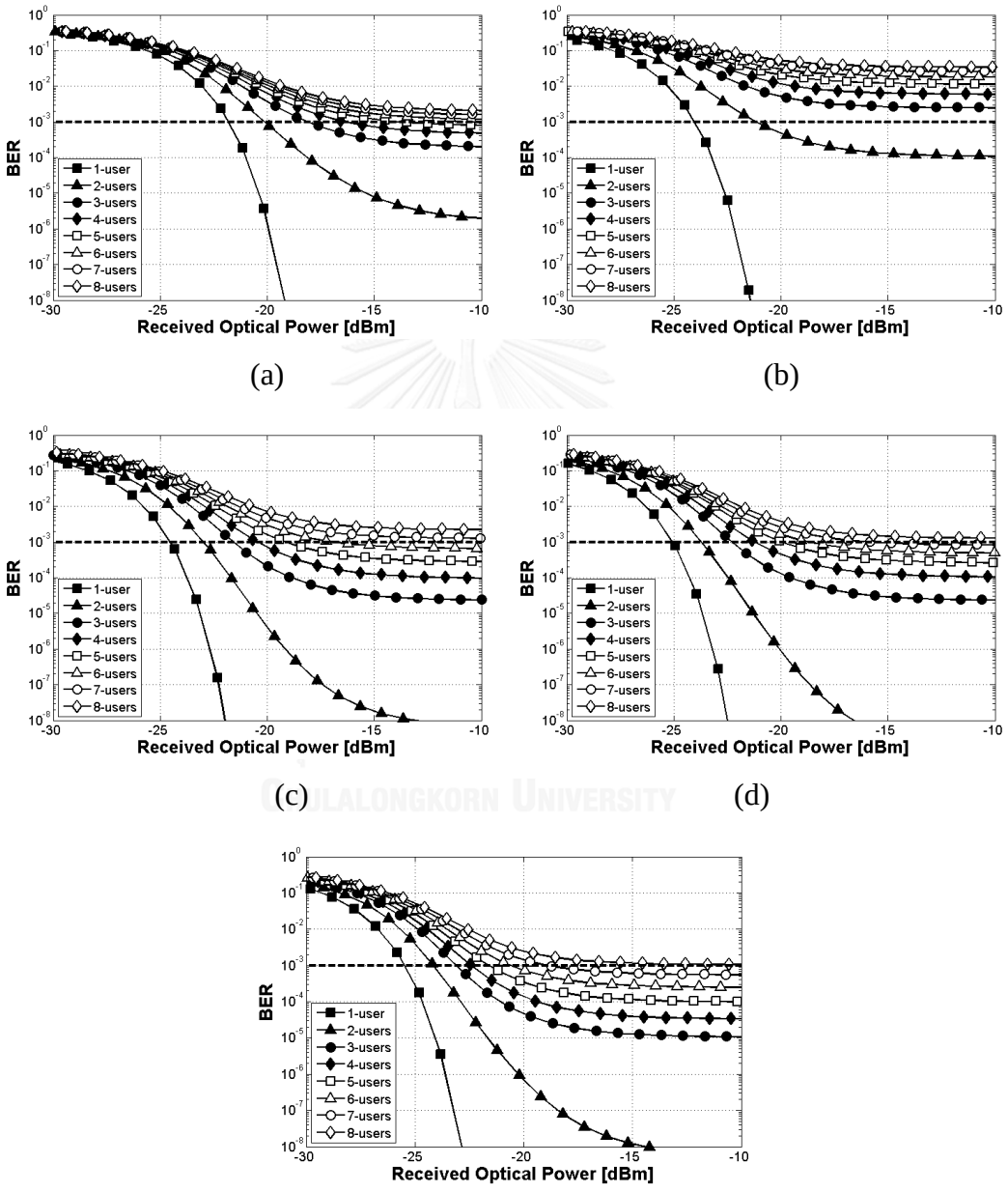

Fig. 4.13 Relation between numerical BER and ROP of the average performance from the first method (a) SBR = 1.0, (b) SBR = 0.8, (c) SBR = 0.6, (d) SBR = 0.4 and (e) SBR = 0.2.

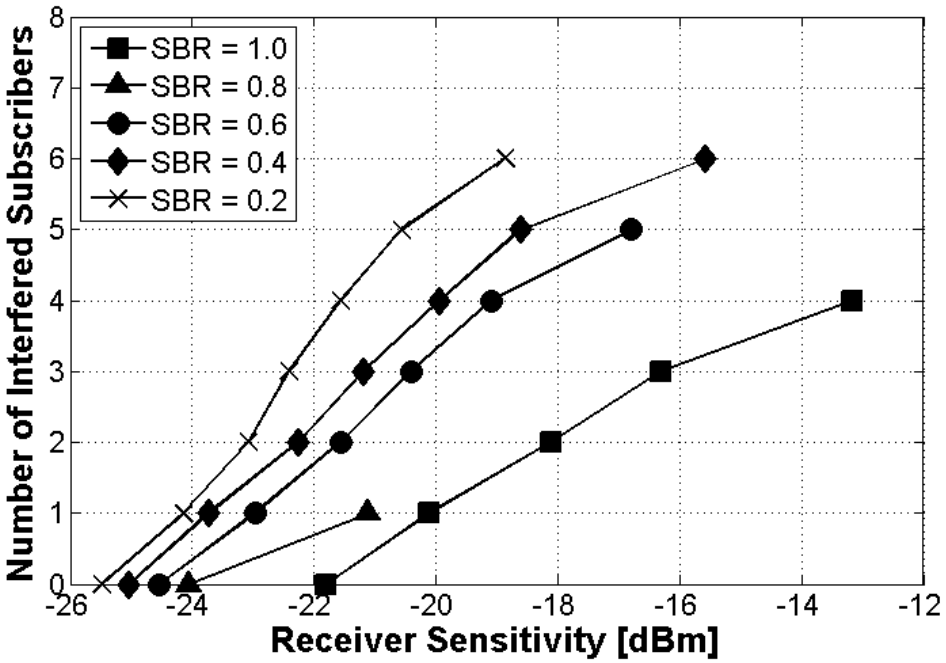

Fig. 4.14 The relation between m interfered subscribers and the receiver sensitivity for the average performance using the first method.

The noise variance of σ_{PBN}^2, σ_{MAI}^2, and σ_{SBN}^2 are calculate and shown as a function of m in Fig. 4.15. Since the σ_{PBN}^2 has depended on the position of the m interfered subscribers with respected to the desired subscribers, the average values of σ_{PBN}^2 through the uniform distribution from all chips in one bit period can mitigate the effects of the PBN. On the other hand, the σ_{MAI}^2 does not change significantly in comparison with the worst performance because its variances depend on the magnitude of the CCPs themselves. Therefore, the σ_{MAI}^2 at each chip position over one bit period is nearly the same. Finally, the σ_{SBN}^2 is illustrated in Fig. 4.15(c). in this case, the σ_{SBN}^2 is as same as the value we have in the worst case due to we have locked the position of the m interfered subscribers to have the strongest CCP.

In the asynchronous manner of the OCDMA system, we can conclude from our results that the noise variances can be mitigated. The largest noise variance that limit the performance is the σ_{PBN}^2.

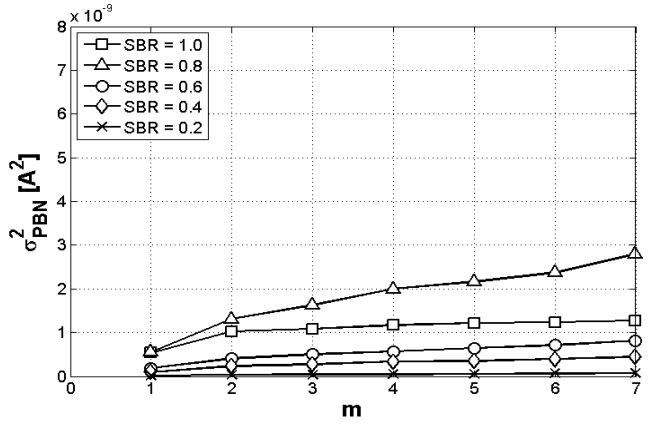

(a)

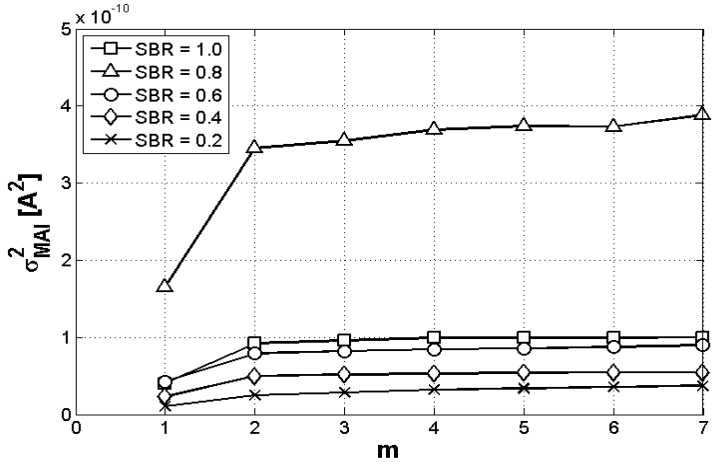

(b)

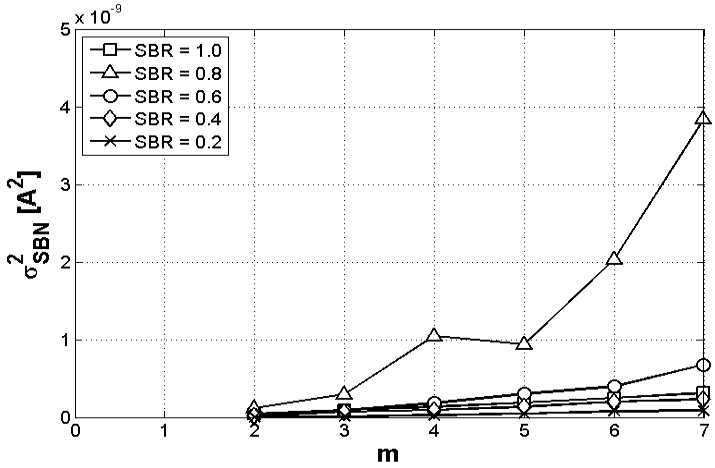

(c)

Fig. 4.15 Noise variance as a function of interfered subscriber obtained from the first method (a) σ_{PBN}^2, (b) σ_{MAI}^2, and (c) σ_{SBN}^2.

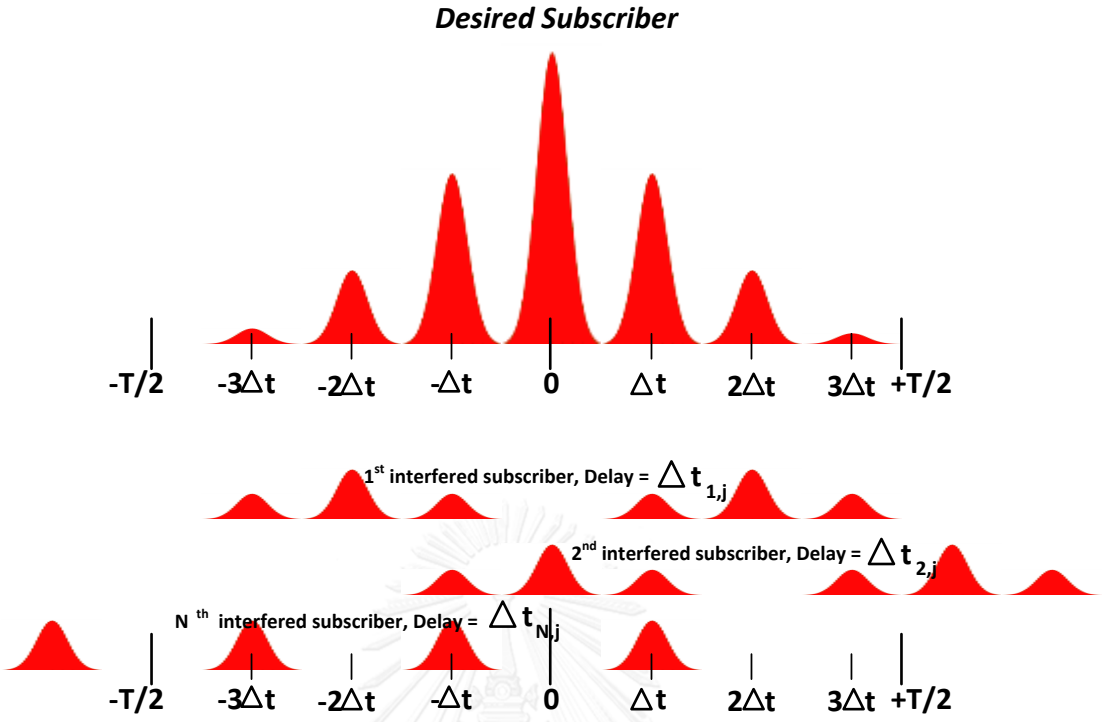

Fig. 4.16 Using random delay in an asynchronous transmission.

4.4.2.2 The second method

In this case, all m interfered subscribers were launched together randomly with random delays to obtain a truly asynchronous scenario. The random delay for each interfered subscribers is

$$\Delta t_{i,j} = n_{i,j} \cdot t_{chip} \tag{4.38}$$

, where n is the number of delayed chips started from 0 to total chips in one bit period N/SBR, i is the index number of interfered subscriber and j is the number of iteration which is started from 0 and bounded by 4 times of total chips in one bit period. Therefore, at each number of subscribers, we perform total 32, 40, 56, 80 and 160 random cases for the case of SBR = 1.0, 0.8, 0.6, 0.4 and 0.2, respectively. Then, we use the average value obtained from these events to represent the characteristic of the average performance in the asynchronous transmission. The simple graphical of an asynchronous transmission is illustrated in Fig. 4.16.

Since the interfered subscribers have launched randomly, the generation of SBN and especially PBN in each case changes due to the position of each interfered subscribers with respected to the desired subscribers are varied. Unfortunately, for the case of SBR = 1.0, we have mentioned early in the previous section that PBN is generated at all delay $\Delta t_{i,j}$ and causes high PBN all time. Nevertheless, for the case of SBR = 0.4 and 0.2 which their total available chips in a bit period are 20 and 40,

there are 5 and 25 chips outside the 15-chip decoding period of ACP that cannot produce PBN so that the σ^2_{PBN} can be reduced effectively through these cases. Moreover, the σ^2_{SBN} can be mitigated effectively as well since there are available 5 and 25 chips outside the 15-chip decoding period of each interfered subscribers themselves.

Therefore, from our numerical value, the average BERs as a representative of an asynchronous transmission for all SBR for the case of 1-8 subscribers are shown in Fig. 4.17. For the case of m = 1, the receiver sensitivity at BER = 10^{-3} is found to be -19.63, -20.51, -22.32, -23.28 and -23.81 dBm, respectively. The BERs obtained from all SBRs are lower and the total subscribers with BER lower than = 10^{-3} are increased in comparison with the worst case.

Moreover, we also plot the relation of the receiver sensitivity and m in Fig. 4.18. The power penalty in each case can be obtained from this figure. The total numbers under the FEC limit are 4, 2, 5, 6, and 8 for the case of SBR = 1.0, 0.8, 0.6, 0.4, and 0.2, respectively. These results obtained from this calculation can meet an agreement with the results from section 4.4.2.1.

The calculated noise variances are shown in Fig. 4.19. In comparison to the worst performance, all noise terms are smaller significantly. This improvement of the noise variances is resulting in the lower BER and the more number of subscribers under the FEC limit. In comparison to the average performance by using the weighted-probability in section 4.4.2.1, the σ^2_{PBN}, shown in Fig. 4.19(a), is approximately improved by 33% due to the generated PBN signals from the random access of the interfered subscribers are not the largest values as obtained in section 4.4.2.1. The σ^2_{MAI}, shown in Fig. 4.19(b), is nearly the same. Finally, the σ^2_{SBN}, shown in Fig. 4.19(c), is reduced lower than the variance obtained from the first method. It can be explained that the random access reduces the probability that each interfered subscriber will be beat each other and therefore the σ^2_{SBN} is reduced, respectively. Moreover, for all kind of noise variances, the SBR = 0.8 experiences the greatest noise among the others. By applying lower SBR can mitigate the noise variance effectively.

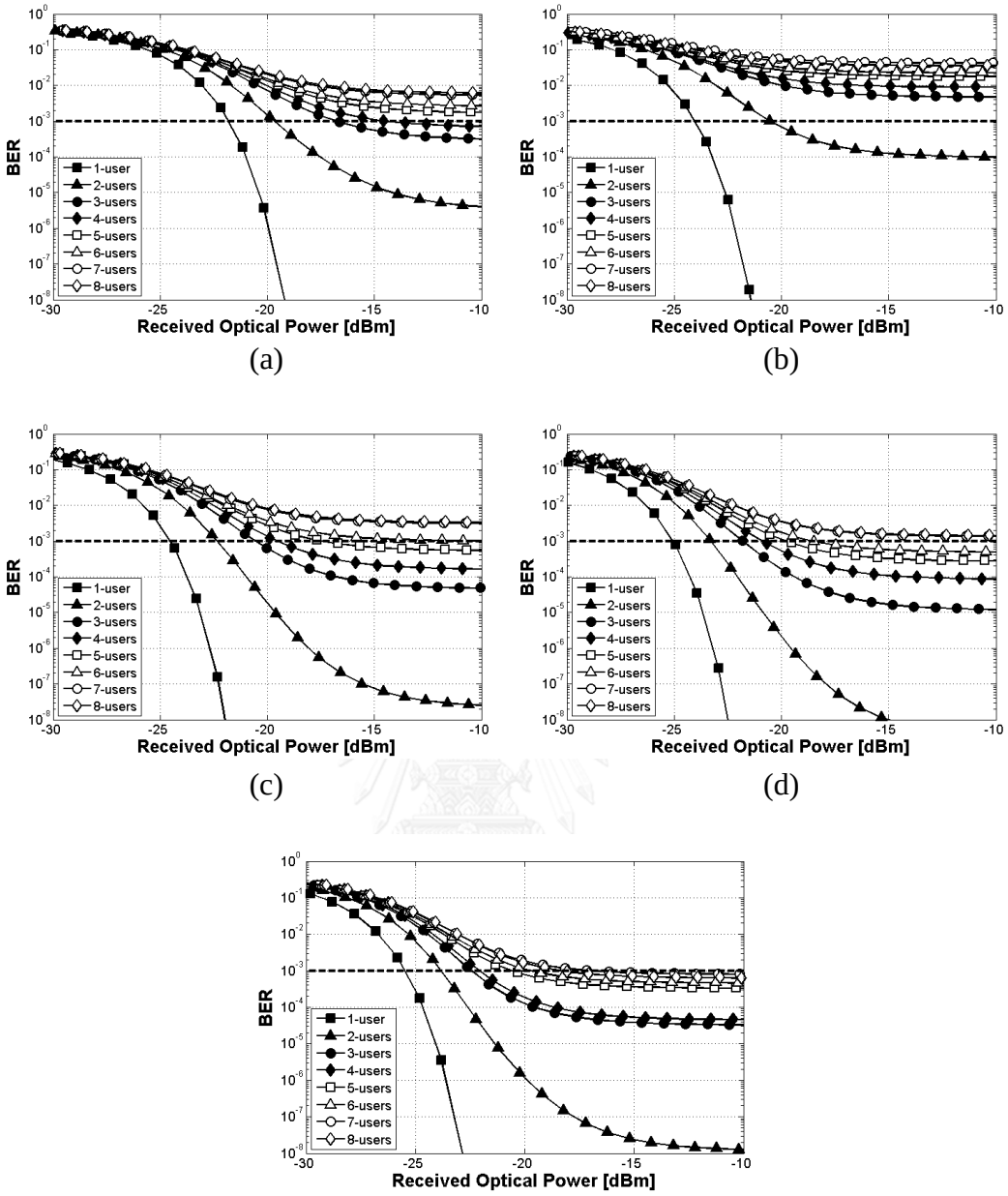

Fig. 4.17 Relation between numerical BER and ROP of the average performance from the second method (a) SBR = 1.0, (b) SBR = 0.8, (c) SBR = 0.6, (d) SBR = 0.4 and (e) SBR = 0.2.

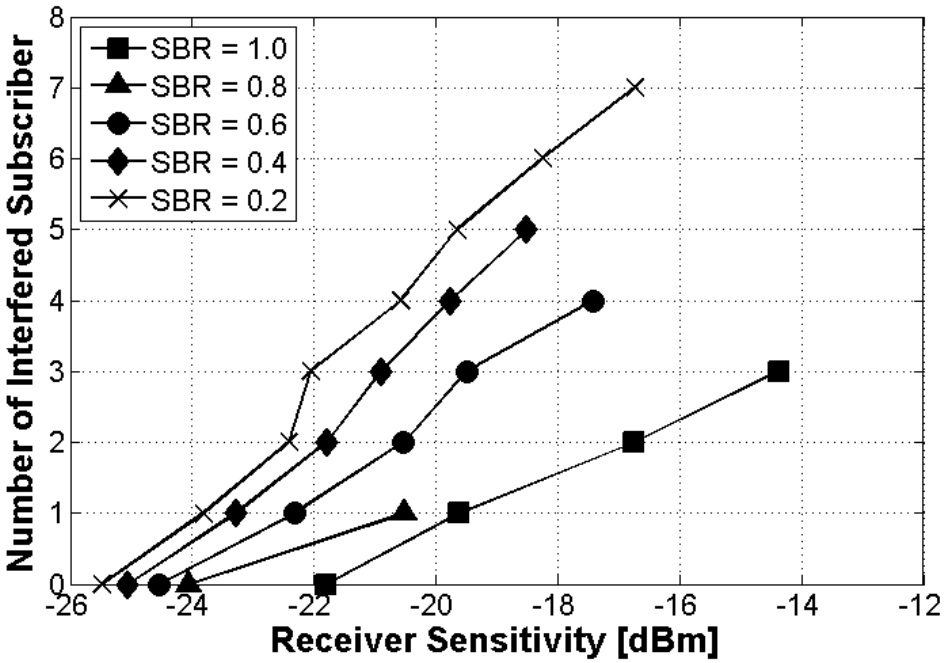

Fig. 4.18 The relation between *m* interfered subscribers and the receiver sensitivity for the average performance using the second method.

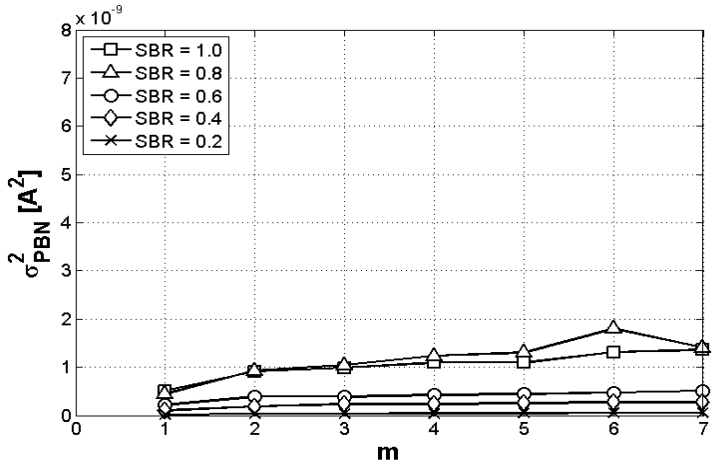

(a)

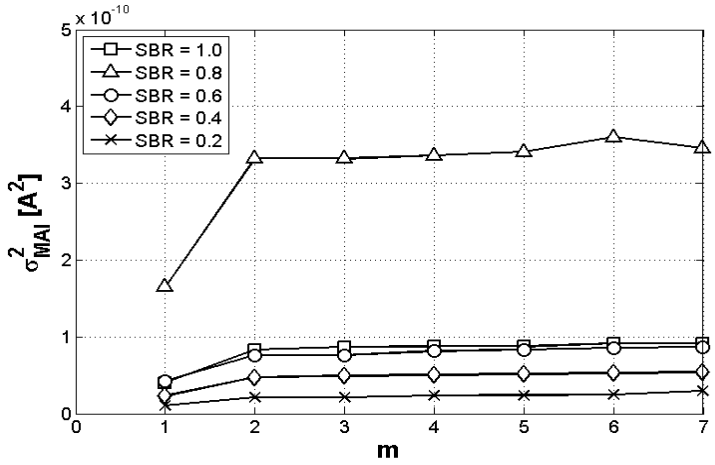

(b)

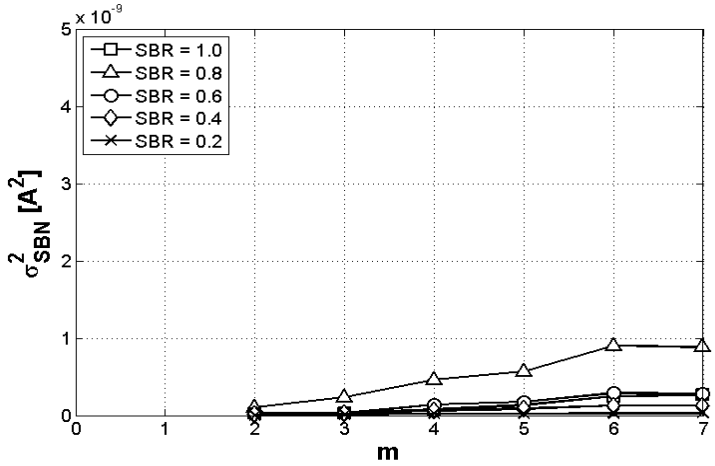

(c)

Fig. 4.19 Noise variance as a function of interfered subscriber obtained from the second method (a) σ_{PBN}^2, (b) σ_{MAI}^2, and (c) σ_{SBN}^2.

4.5 Spectral Efficiency

In communication theory, the spectral efficiency is defined as the total amount of information rate (data bits per second: bit/s) that can be transmitted to the destination with a given bandwidth. It represents, in a specific network, how many bits that a given bandwidth can send to the recipient in one second, as shown in (4.39).

$$S.E. = \frac{R}{BW}, \tag{4.39}$$

where R is the information rate or bit rate (bit/s) and BW refers to the bandwidth of the system. Therefore, in an OCDMA networks, to total bits sent depends on the total active subscribers and the spectral efficiency (S.E.) are

$$S.E. = \frac{N \times R}{B_0}, \tag{4.40}$$

where N is the total number of active subscribers that achieved an error-free BER and B_0 is the optical bandwidth, respectively.

The SE is an another important parameter to determine the system performance without any bias since the low SBR such as SBR = 0.2 can transmit simultaneously 8 subscribers by reducing the chip period of the en/decoder which is corresponding to handling very large optical bandwidth of the laser source. Therefore, the SE is appropriated to describe how efficient of each SBR is, respectively.

We collect the number of subscribers that can achieve an FEC limit from the previous section. The SE obtained from both the worst and the average cases are shown in Fig. 4.31. For the worst case, SBR = 0.6 can transmit 4 subscribers simultaneously with the total bit rate of 160 Gbps and can achieve the maximum SE of 0.29 b/s/Hz. The lowest SE of 0.074 b/s/Hz belongs to SBR = 0.2 since it owes the largest optical bandwidth and can transmit only 3 simultaneous subscribers with total bit rate of 120 Gbps. By performing an asynchronous transmission, the SE is improved clearly since the number of error-free subscribers is increased. Therefore, the greatest SE of the average case in an asynchronous transmission comes from SBR = 1.0. The SE, obtained from the first and second method, are found to be 0.62 and 0.49 b/s/Hz with total 5 and 4 error-free subscribers and the total bit rates are 200 and 160 Gbps. Finally, the smallest SE in this case comes from SBR = 0.8. It can transmit only 2 subscribers simultaneously with total bit rate of 80 Gbps, respectively.

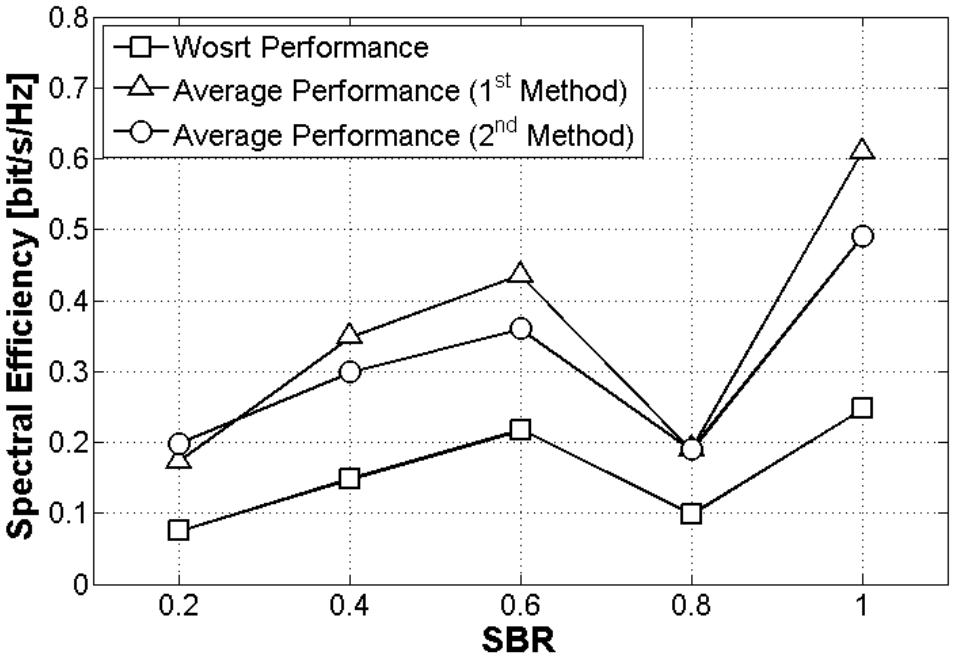

Fig. 4.20 The spectral efficiency as a function of SBR.

CHAPTER 5 OCDMA Signal Transmission with Various SBR System Verification Using The Simulation Software

In chapter 4, we have introduced our mathematical calculation of transmitting OCDMA signals with various SBRs. The results from the average performance in an asynchronous transmission show that, by reducing SBR, it can especially mitigate σ_{PBN}^2 effectively. We can earn from SBR = 0.2 that the σ_{PBN}^2 is suppressed most among employing another SBRs. Therefore, by employing low SBR of 0.6, 0.4 and 0.2 also resulting in greater BER in comparison with the conventional OCDMA system using SBR = 1.0 and 0.8, respectively. The excellence in low noise variances brings the better BER so that we can launch the more number of subscribers simultaneously in comparison with the conventional system.

Nevertheless, our proposed model should be corroborated by performing the experimental setup. Lots of optical sources and specific components are required in order to perform OCDMA signal transmission. Moreover, in each SBR, 8 pairs of a specific en/de based SSFBG should be prepared to perform a complete demonstration. Due to this complexity in the experiment setup, we would like to verify our OCDMA model with a simulation software Optisystem.

Optisystem is a comprehensive simulation software for optical communication system that is being used worldwide by many research groups. It is a virtual optical communication system so that you can plan, design, test and monitor the system performance in advance before setting up a real system. Most components in Optisystem are created based on the approval mathematical models and equations from many reference textbooks and some of specific components are created based on the models from scientific papers and periodical journals. Therefore, this simulation software is trusted by many researchers and engineers in the field of optical communication. Many of papers using Optisystem are published by very well-known publishers like Journal of Lightwave Technology, IEEE/OSA Journal of Optical Communication and Networking, IEEE Photonics Journal, IEEE Photonics Technology Letters and so on [53-70].

Consequently, we are going to verify our mathematical calculation by using Optisystem in this chapter. Fisrt, we introduce the system setup and some of important parameters in Optisystem. Then, we will show the BER as a function of ROP obtain from eye-diagram analyzer and we will make a comparison with our mathematical calculation as well. Finally, the signal transmission over a fiber with a complete compensation of the 2nd order dispersion is demonstrated in the last section.

5.1 System Model

Basic OCDMA system configuration in Optisystem is shown in Fig. 5.1. We can categorize basically into 4 parts. They are transmitter part, encoding part, transmission part, decoding and receiver part. First of all, a global parameter such as a system bit rate, sequence length and sample per bit should be set. In our setup, we set

system bit rate = 40 Gbps, sequence length = 1024 bit and sample per bit = 1024 samples, respectively.

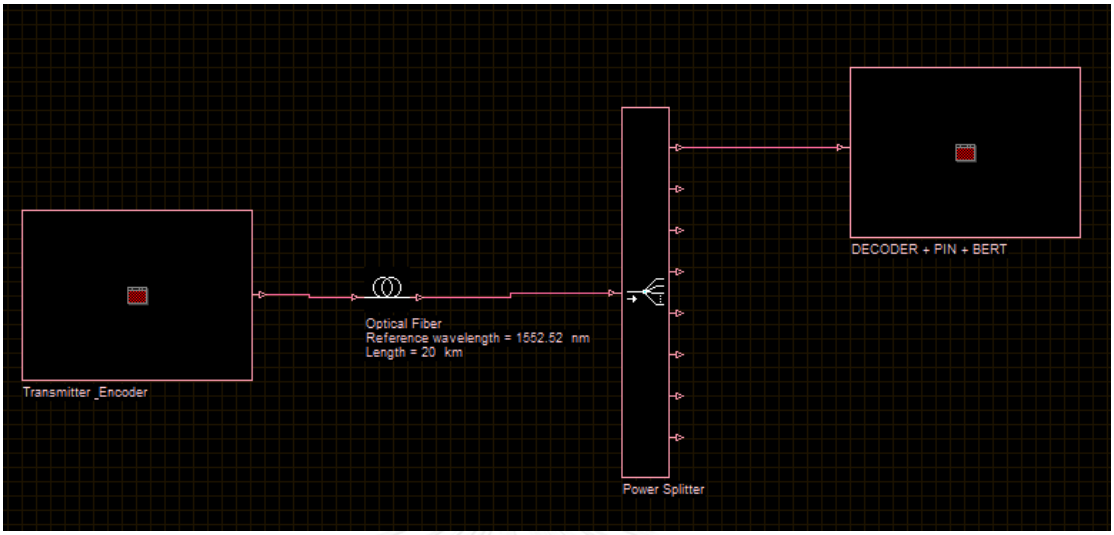

Fig. 5.1 OCDMA system configuration in the simulation software.

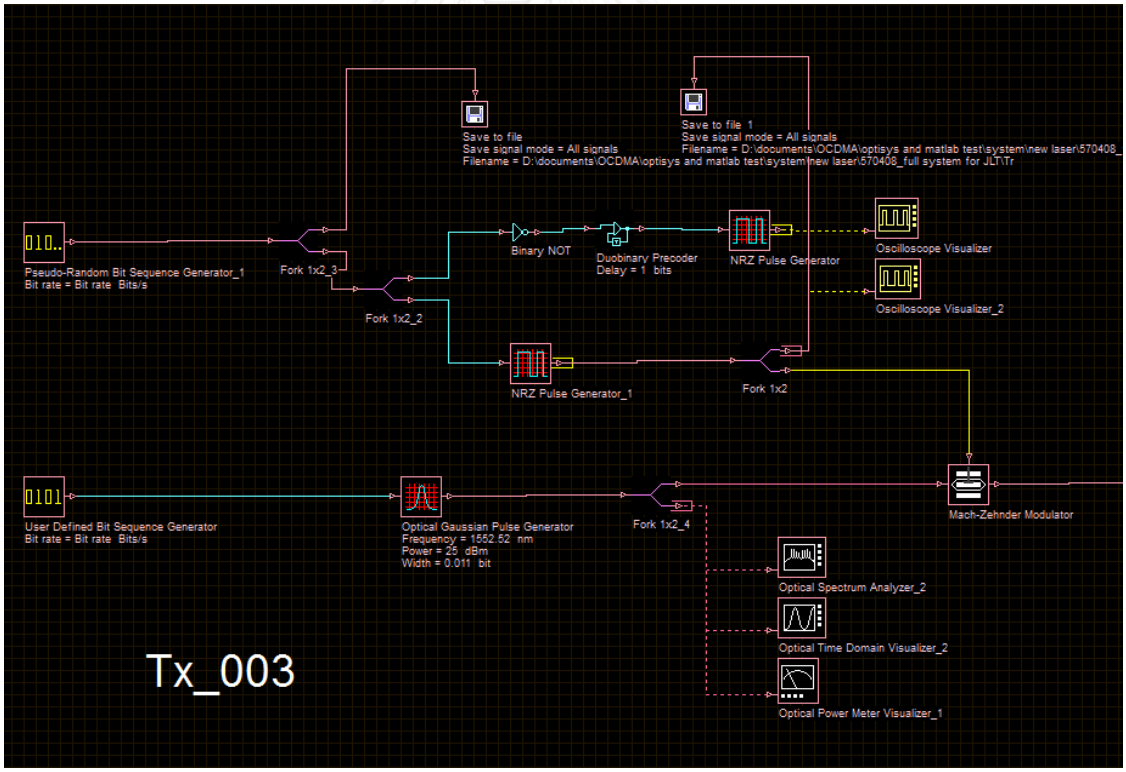

Fig. 5.2 The simulation layout of the transmitter part.

Table 5.1 Parameters of the transmitter part.

Attributes	Pulse Width (ps)	Optical Bandwidth (GHz)	Coherence Time τ_c (ps)	Chip Period T_{chip} (ps)	Coherent Ratio kt
SBR = 1.0	1.33	323.73	3.09	3.125	1.01
SBR = 0.8	1.07	402.00	2.49	2.50	1.00
SBR = 0.6	0.82	531.47	1.88	1.875	0.99
SBR = 0.4	0.55	802.80	1.25	1.25	1.00
SBR = 0.2	0.28	1605.6	0.623	0.625	1.00

Table 5.2 Specifications of the SMF and the DCF.

Fiber Type	Chromatic Dispersion ($ps/nm \cdot km$)	Dispersion Slope ($ps/nm^2 \cdot km$)	RDS (nm^{-1})	SC Rate
SMF	17.57	0.058	0.00330	-
DCF-1	-152.003	-0.2508	0.00165	0.5
DCF-2	-152.003	-0.5016	0.00330	1.0
DCF-3	-152.003	-1.0032	0.00660	2.0

5.1.1 Transmitter

The first part is the transmitter part, we use a Gaussian pulse generator as a mode-lock laser diode (MLLD) that can generate optical pulses at a constant repetition rate. The width of the pulse is adjusted to fit kt = 1in each SBR. Therefore, the widths of optical pulse and T_{chip} for en/decoders are demonstrated in Table 5.1, respectively. Then, optical pulse train will be intensity modulated by a Mach-Zhender modulator with random non-return to zero (NRZ) electrical signal and we finally get optical signal to be further encoded. The system layout of this part is shown in Fig. 5.2.

5.1.2 Encoder

The second part is the encoder and its layout is shown in Fig. 5.3. Each optical signal will be encoded by a unique code from an 8-level phase-shifted coherent time-spreading encoder. The pulse before the encoding process is a single pulse with a specific FWHM as described in Table 5.1 and it will be time-spread by the encoder so that the output from the encoder is a series of 8 optical pulses and the total encoded period is restricted to SBR, as depicted in Fig. 4.

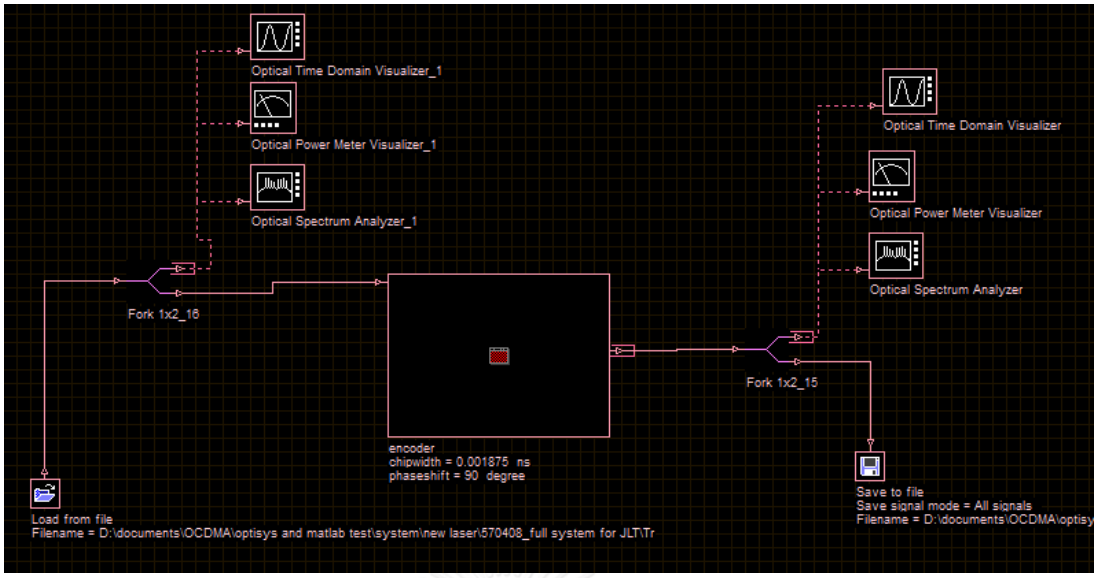

Fig. 5.3 The simulation layout of encoding part

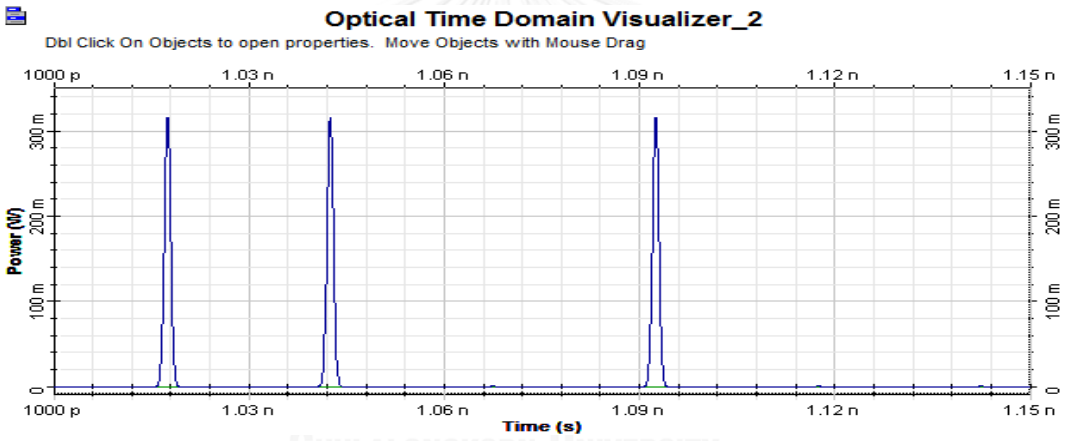

(a)

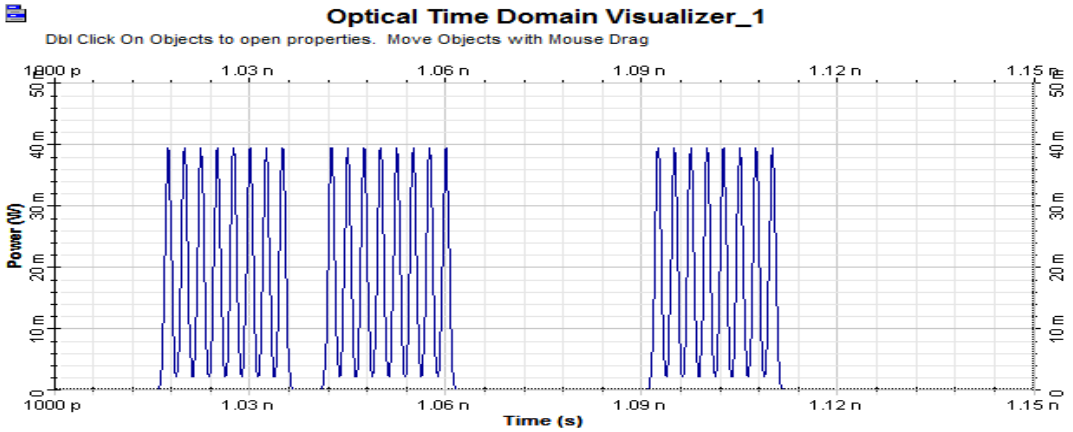

(b)

Fig. 5.4 Optical signal in time-domain (a) before encoding (b) after encoding.

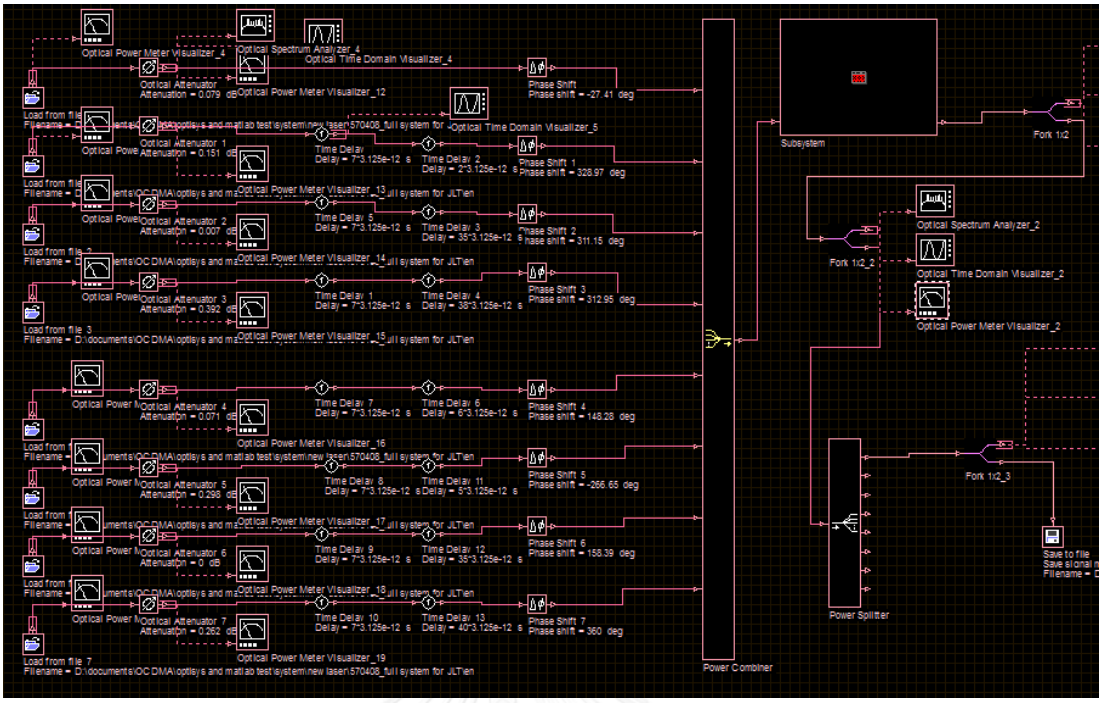

Fig. 5.5 The simulation layout of the transmission part.

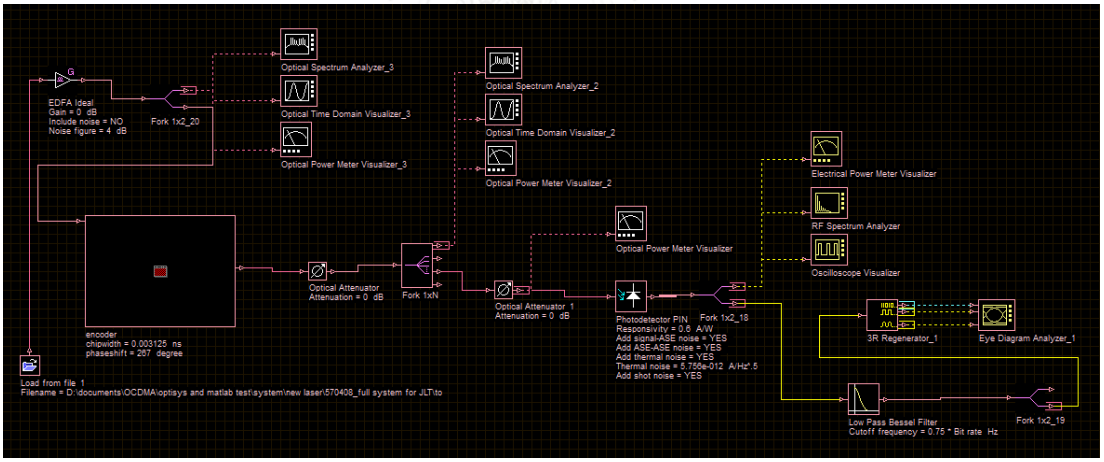

Fig. 5.6 The simulation layout of the decoder and signal detection part.

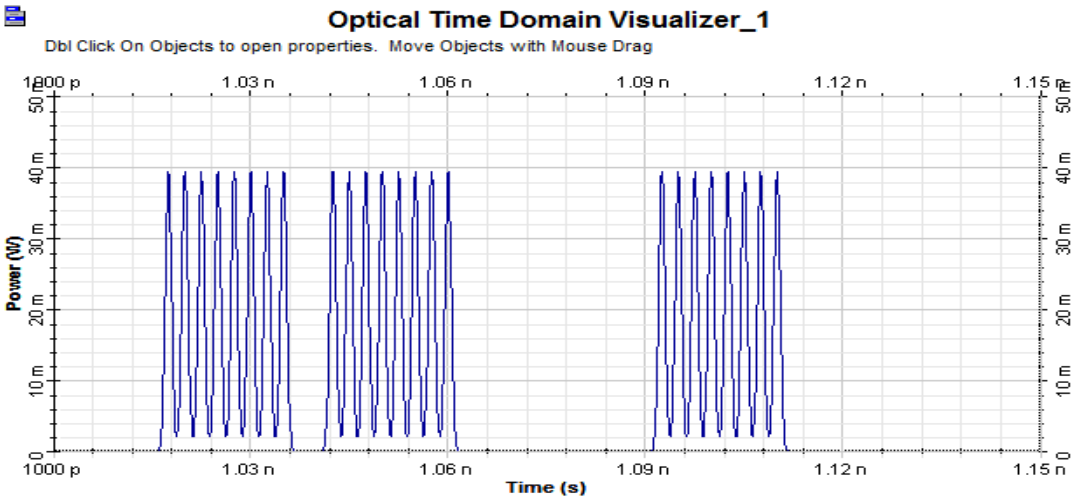

(a)

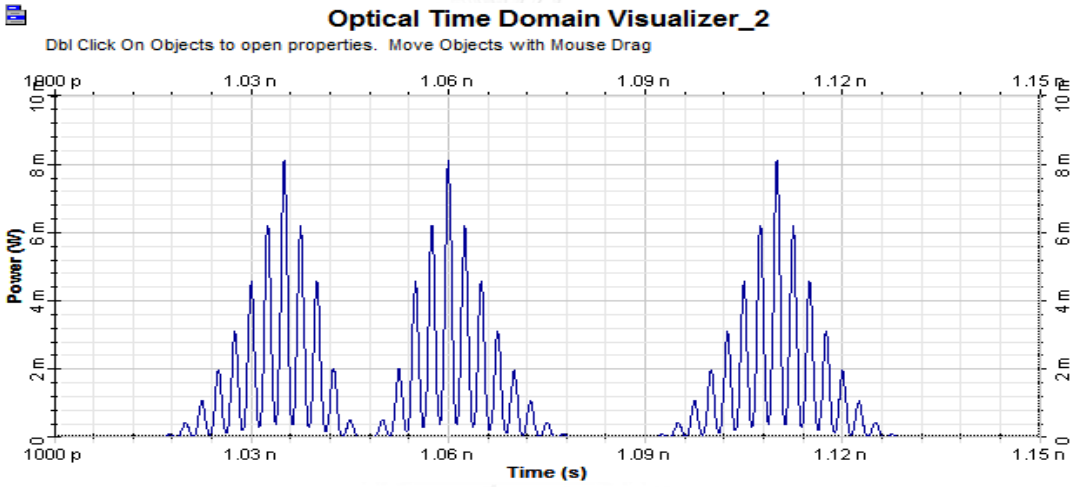

(b)

Fig. 5.7 Optical signal in time-domain (a) before decoding (b) after decoding.

5.1.3 Transmission Part

The power obtained from each subscriber is adjusted to have the equal level by a variable optical attenuator (VOA) and its initial phase is randomly added as well. The time delay added to each subscriber is different and it depends on the transmission scheme that will be discussed further. Then, each subscriber will be multiplexed together by a power combiner and then will be launched to the optical fiber. In the fiber link, it consists of a 20 km of standard SMF ITU-T G.652 and followed by an appropriate length of a DCF in order to cancel accumulated chromatic dispersion. The SMF G.652 has an attenuation coefficient of 0.2 dB/km at 1552.52 nm, a chromatic dispersion of 17.577 ps/nm·km at 1552.52 nm and a dispersion slope of 0.0581 ps/nm·km^2 at 1550 nm. The 2.7 km of DCF also has an attenuation coefficient of 0.47 dB/km at 1550 nm, a chromatic dispersion of -152.003 ps/nm·km at 1552 nm and we use 3 different dispersion slopes in order to measure the difference

between the perfect and imperfect dispersion compensation as shown in Table. 5.2. Then, at the distribution point, signals will be split by a 1:8 power splitter and sent to each decoder, respectively. The layout of the this part is illustrated in Fig. 5.5.

5.1.4 Decoder and Signal Detection

After the signal is split by a power splitter, it will be decoded by a decoder. The specification of a decoder is also shown in Table 5.1 already. Each subscriber will be received only their own data from the correctly decoded pulses whereas incorrectly decoded pulses are considered as the OCDM noises. Then, the decoded signal will be converted to the electrical signal by a PIN photodetector. The PIN photodetector has the dark current of 50 nA and thermal noise of 5.76 pA/Hz$^{1/2}$. The other kinds of receiver noise, like shot noise, will be calculated automatically using the dark current, respectively. Then, the high frequency of electrical signal is filtered out by a 30 GHz LPF which exhibits Bessel shape. Finally, this filtered electrical signal will be checked with the reference bit sequence in order to calculate BER by an eye-diagram analyzer and a BER tester, respectively. The layout of this part is shown in Fig. 5.6 and the signal waveforms at this part are shown in Fig. 5.7, respectively.

5.2 System Performance

We also categorize the simulation into 2 parts, the worst performance and the average performance. We consider only the back-to-back case in this section. The system architecture and the simulation result are discussed in the rest of this part.

5.2.1 Worst Performance

Since we have launched all m interfered subscribers simultaneously without random delays between them in the last chapter and we have just added the additional delay from 0-n as described in (4.29)-(4.31) in order to pick the worst case scenario, respectively. Therefore, the relation between BER and ROP obtained from the simulation is shown in Fig. 5.8. The results obtained from the simulation are illustrated by a dash-line whereas the results from the mathematical calculation are illustrated by a solid line. The trends of BER as a function of ROP for all SBR from the simulations are well compatible to the results from our proposed mathematical calculation.

The receiver sensitivity obtained at BER = 10^{-3} is plotted in Fig. 5.9. For the case of single subscriber, the receiver sensitivity from the simulation is found to be -20.62, -22.84, -23.73, -24.34 and -24.22 dBm for the case of SBR = 1.0, 0.8, 0.6, 0.4 and 0.2, respectively. Moreover, the maximum number of subscriber with the FEC limit is 2, 1, 3, 4, and 3 for the case of SBR = 1.0, 0.8, 0.6, 0.4 and 0.2, respectively. The total numbers of error-free subscribers are almost the same in comparison with the results from the mathematical calculation as discussed in Chapter 4.

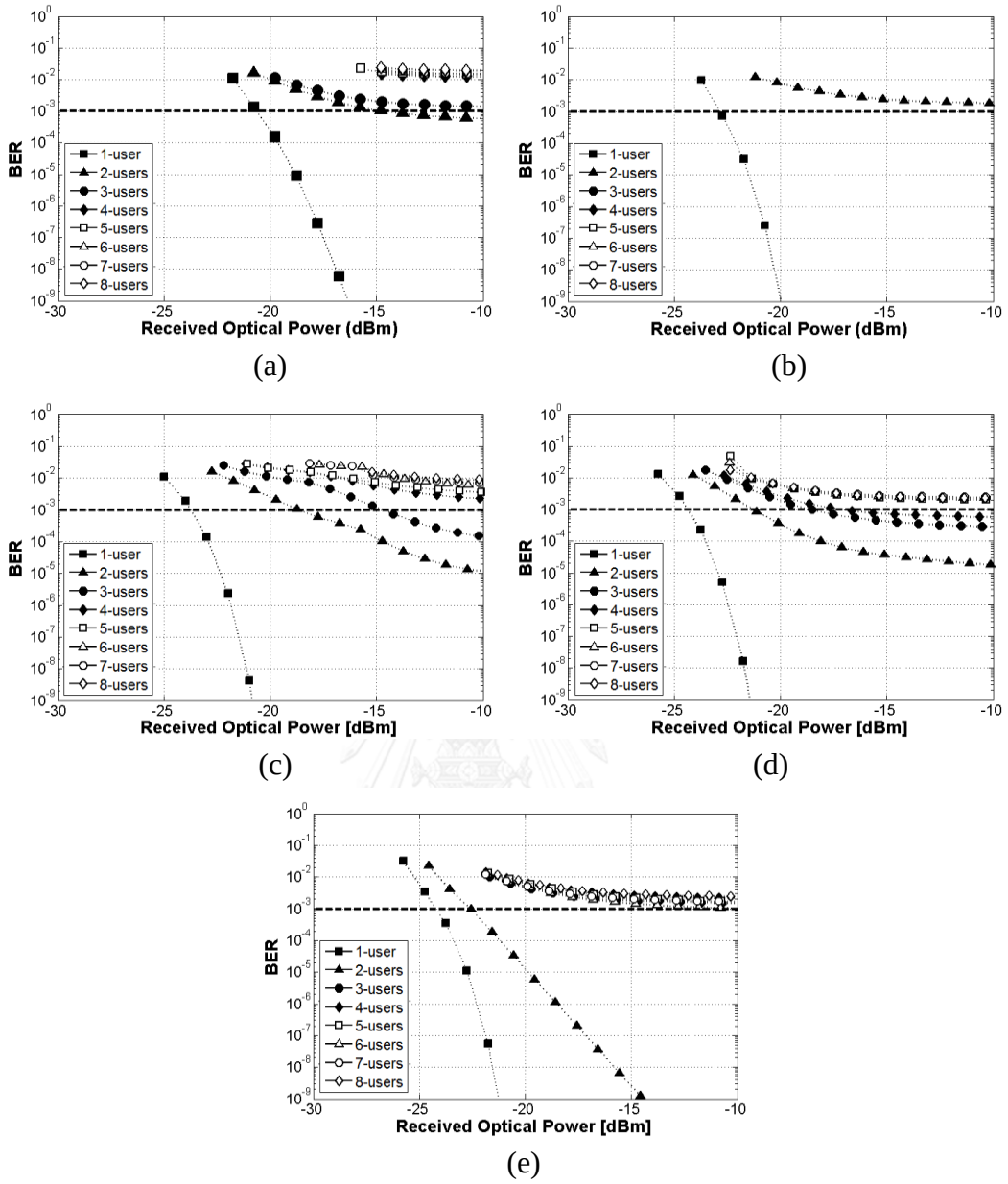

Fig. 5.8 Relation between numerical BER and ROP of the worst case transmission (a) SBR = 1.0, (b) SBR = 0.8, (c) SBR = 0.6, (d) SBR = 0.4 and (e) SBR = 0.2.

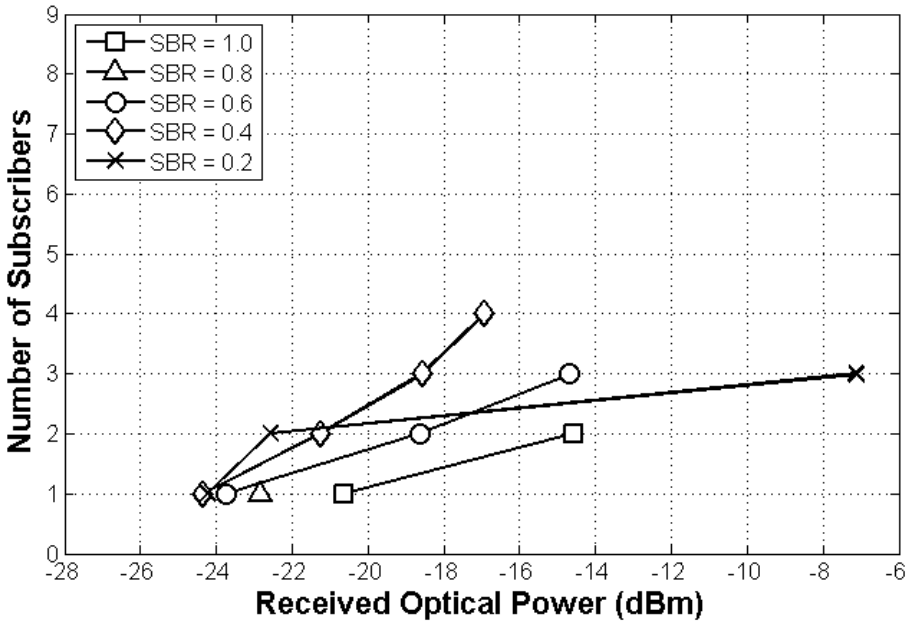

Fig. 5.9 Relation between ROP and the numbers of achieved error-free subscribers from the worst case.

5.2.2 Average Performance

In this case, we have randomly set time delay from 0-n to each subscriber to confirm the truly-asynchronous transmission. The relation between BER and ROP in an average case is represented in Fig. 5.10, respectively. As we can see from Fig. 5.10, the BERs obtained from the calculation and the simulations are nearly the same and this can guarantee the results from our mathematical calculation as well. Then, the receiver sensitivity at the BER = 10^{-3} at each number of subscriber is collected and represented in Fig. 5.11, respectively.

For the case of single subscriber, the receiver sensitivity is -20.63, -22.34, -23.72, -24.35 and -24.21 dBm for the case of SBR = 1.0, 0.8, 0.6, 0.4 and 0.2, respectively. Then, the receiver sensitivity is deteriorated mainly by σ^2_{PBN}, σ^2_{SBN} and σ^2_{MAI} as a function of number of interfered subscriber as shown in Fig. 5.11 and the total subscribers which can achieve an FEC limit at BER = 10^{-3} are found to be 3, 3, 7, 8 and 8 for the case of SBR = 1.0, 0.8, 0.6, 0.4 and 0.2, respectively. These numbers of FEC limit subscriber obtained from the simulation results are compatible with the numbers of error-free subscriber obtained from our mathematical calculation as discussed in Chapter 4.

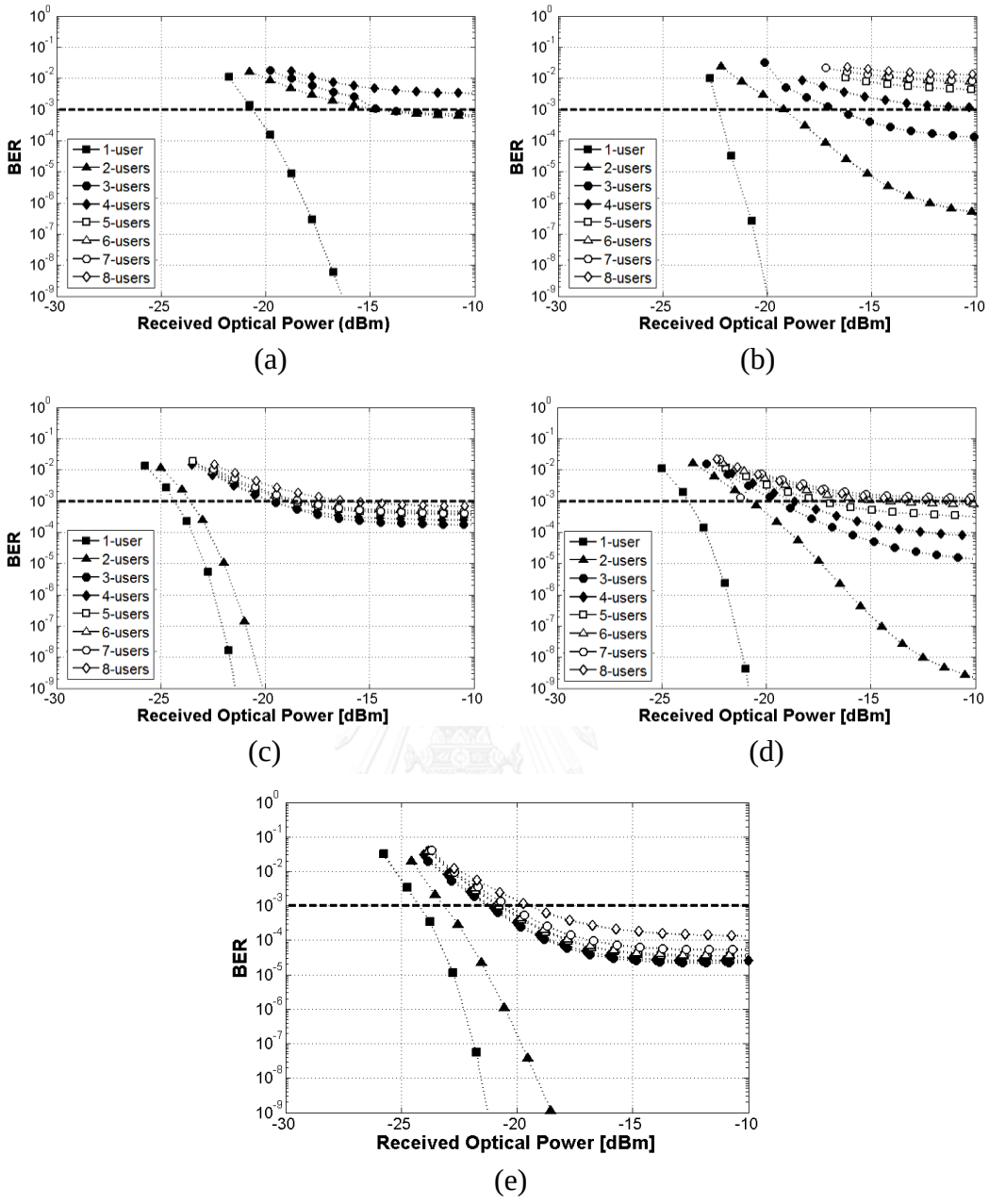

Fig. 5.10 Relation between numerical BER and ROP of the worst case from an asynchronous transmission (a) SBR = 1.0, (b) SBR = 0.8, (c) SBR = 0.6, (d) SBR = 0.4 and (e) SBR = 0.2.

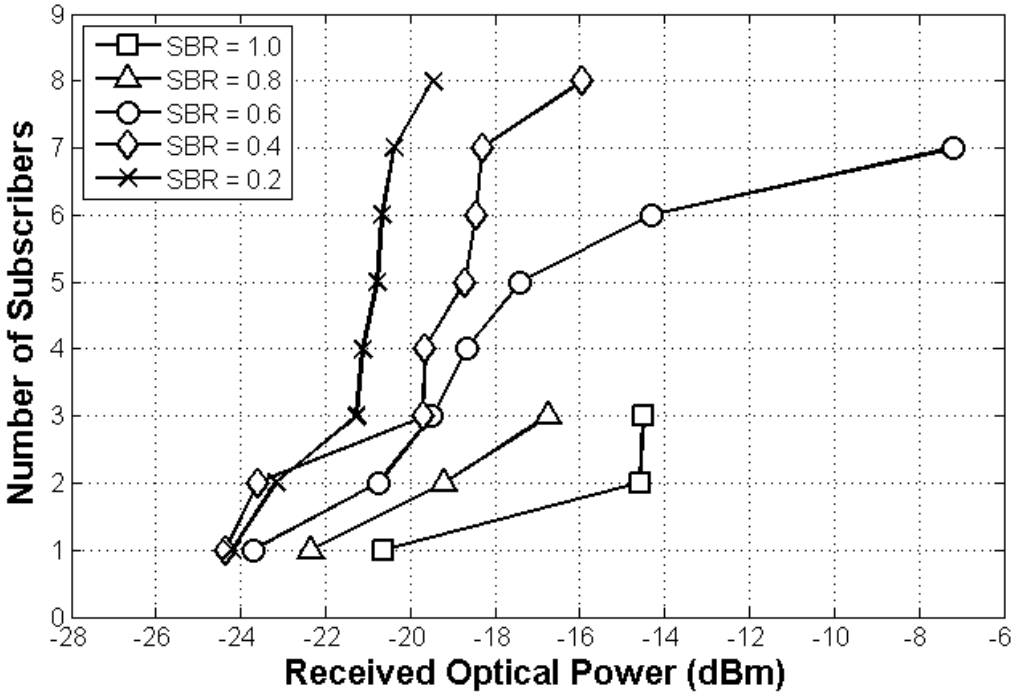

Fig. 5.11 Relation between ROP and the numbers of achieved error-free subscribers from the average performance.

5.3 Eye-Diagram

The decoded optical signal will be converted to electrical signal by a PIN photodetector with a specific bandwidth of the receiver. The electrical signal after the low-pass filtering process will be collected and displayed on the oscilloscope repetitively every 3 bits long or more, depended on the desired signal intervals. Therefore, we can see the bit transition from bit "0" to "1" or from bit "1" to "0" or all possible realizations of the desired signals superimpose themselves on the screen. The ideal eye diagram of the NRZ pulse should be obtained as a rectangular shape. Nevertheless, the imperfection of the communication channel causes an unclear shape, depended on signal distortion level and the received power of a signal. Therefore, we can determine the BER of the system by the numerical method. In additions, the simulation software also uses this method in order to compute the BER.

In this part, we show the eye-diagrams for all SBRs at their maximum number of error-free subscriber from our mathematical calculation and the simulation for both the worst and the average case, respectively.

5.3.1 Worst Performance

The detected electrical signal at PIN photodetector is filtered by a 30-GHz low-pass filter in order to recover the baseband signal. Therefore, the desired filtered

signal in Fig. 5.12 shows the eye diagrams at BER = 10^{-3} obtained from the calculation for the case of SBR = 1.0, 0.8, 0.6, 0.4 and 0.2, respectively. Moreover, the maximum numbers of the error-free subscribers for each eye-diagram in Fig. 5.12 (a)-(e) are found to be 2, 1, 4, 4 and 3, respectively. In Fig. 5.12(a), the eye-diagram looks chaotically because there are the overlapped pulses between consecutive decoded bits. These overlapped pulses bring the higher signal intensity in comparison with non-overlapped pulses and resulting in higher amplitude after have been filtered by an LPF. Moreover, with the suffering from σ_{PBN}^2 and σ_{MAI}^2, the interference can distort the shape of the received signal, respectively. The eye-diagram for the case of SBR = 0.8 is illustrated in Fig. 5.12(b). It looks quite clear because there is no any noise variances from the OCDM system since this case can provide only 1 of desired subscriber. Therefore, the eye-diagram is mainly suffered from σ_{Rx}^2. For the case of SBR = 0.6, the eye-diagram still looks unclear due to the overlapped between consecutive decoded pulses are still existed. Fortunately, the ytr is acceptable for the BER = 10^{-3}. For the case of SBR = 0.4 and 0.2 in Fig. 5.12(d)-(e), there is no any overlapped between consecutive bits so the eye-diagram exhibits a clear Gaussian shape. Nevertheless, the existence of σ_{PBN}^2, σ_{SBN}^2 and σ_{MAI}^2 causes the very high peak at the sampling point so the bit "1" of ACP signal of the desired subscriber can be detected as bit "0" since the noise variance is high enough to make a mistake in the bit detection.

Then, by computer simulation, we use a low-pass filter with 30 GHz of cut-off frequency and the obtained eye-diagrams at BER = 10^{-3} are illustrated in Fig. 5.13(a)-(e) for the case of SBR = 1.0, 0.8, 0.6, 0.4 and 0.2, respectively. The total error-free subscribers in each case are found to be 2, 3, 4, 3 and 3, respectively. For the case of SBR = 1.0 expressed in Fig. 5.13(a), the eye-diagram is unclear as same as obtained from the calculation. The eye-diagrams from SBR = 0.8 and 0.6 are still suffered from the overlapped pulses and the noise variances, resulting in an unclear eye-diagrams as shown in Fig. 5.13(b)-(c). As expected, the eye-diagrams obtained from SBR = 0.4 and 0.2 shown in Fig. 5.13(d)-(e) are suffered from only σ_{PBN}^2, σ_{SBN}^2 and σ_{MAI}^2 since there is no any interferences between each consecutive bit. Therefore, the eye-diagrams look quite clear but the BER unfortunately reaches the limit at 10^{-3} due to the great amount of noise variances.

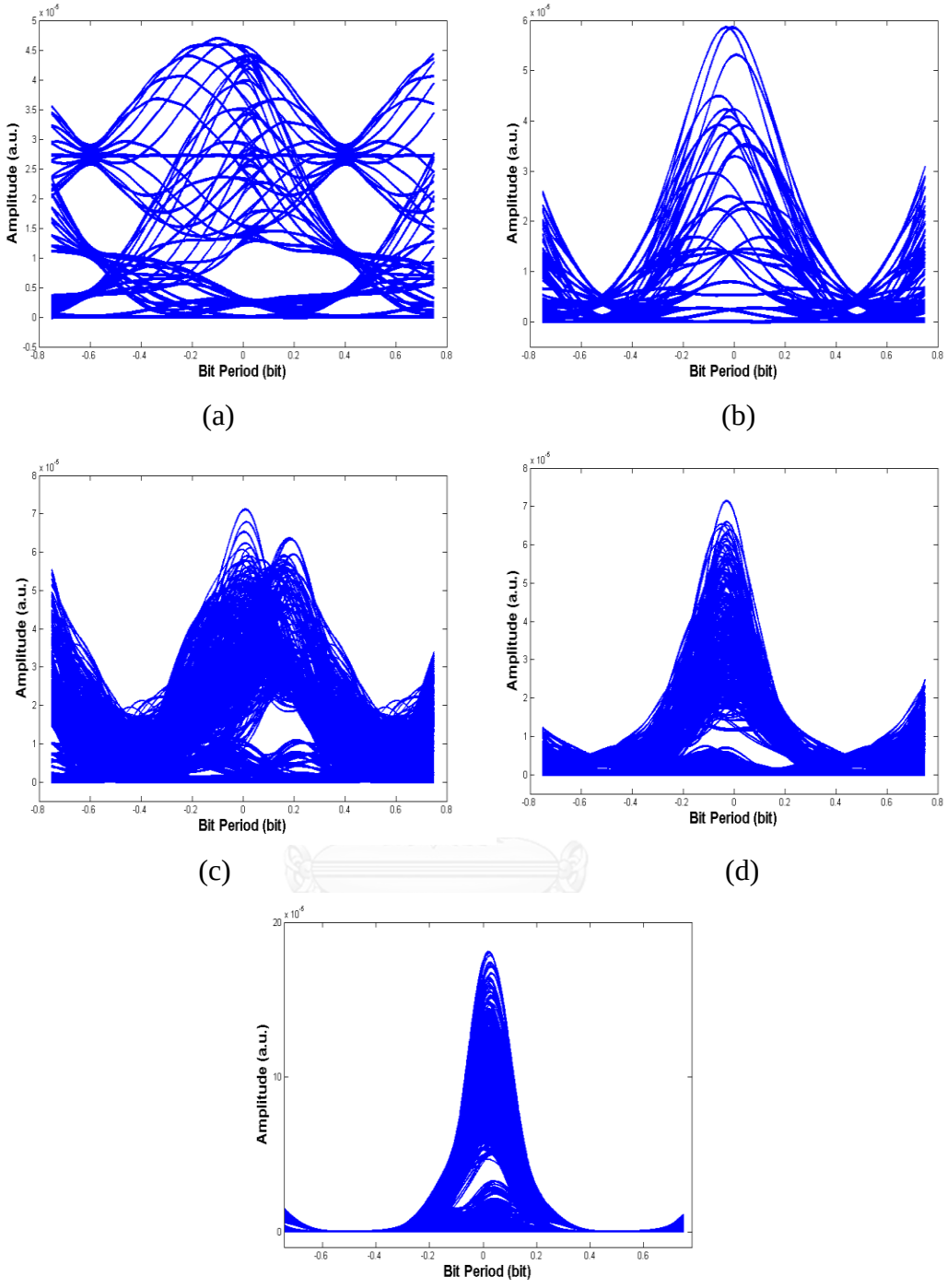

Fig. 5.12 Eye-diagrams of a worst case obtained by our mathematical calculation (a) SBR = 1.0, (b) SBR = 0.8, (c) SBR = 0.6, (d) SBR = 0.4 and (e) SBR = 0.2.

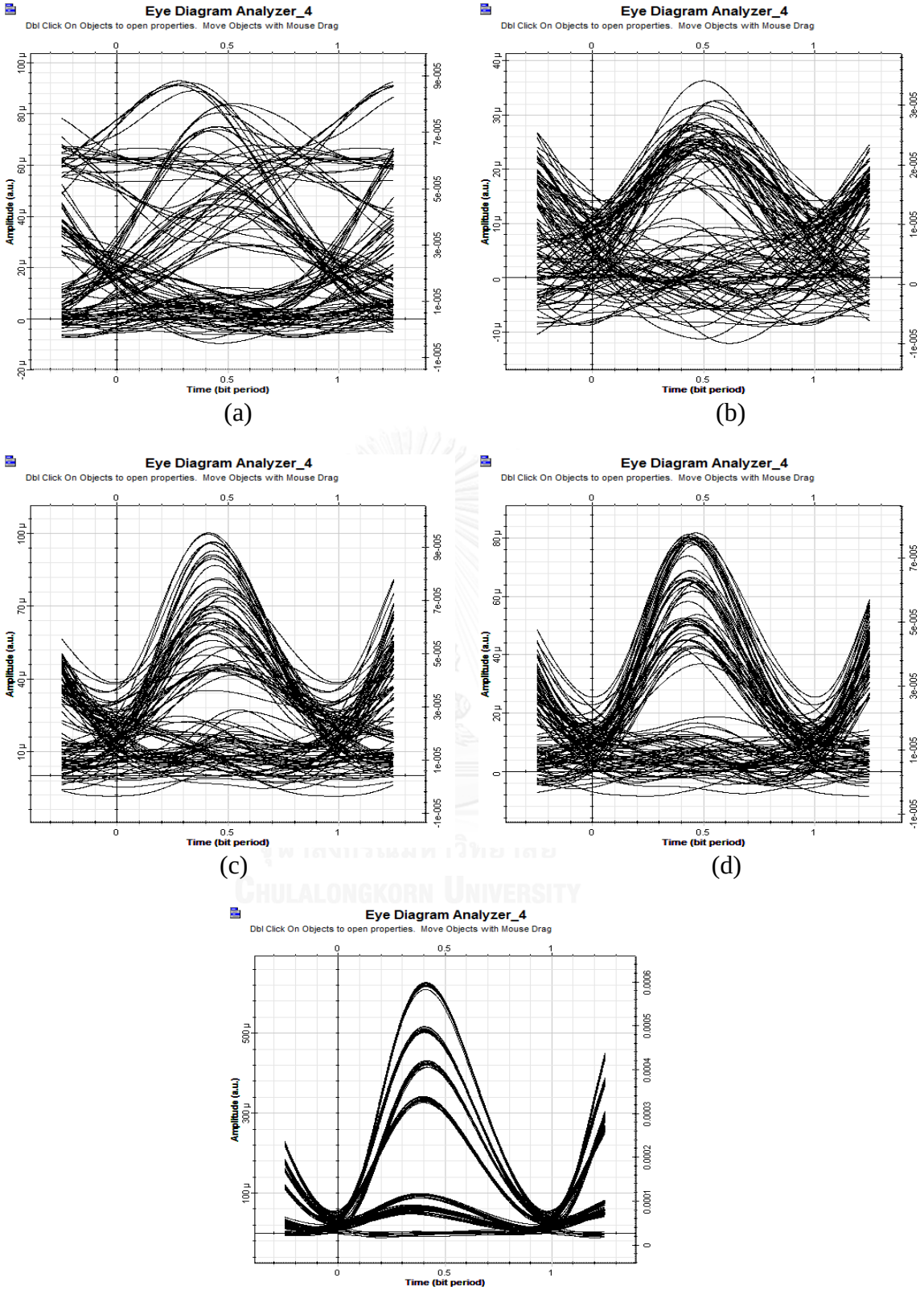

Fig. 5.13 Eye-diagrams of the worst case obtained by a simulation software.

5.3.2 Average Performance

The random access of the interfered subscribers can improve the BER since the dominant noise variance σ_{PBN}^2 is depended on the position related to the desired subscriber. Therefore, from our result, the signal transmission in an asynchronous case can enhance the BER as discussed in Chapter 4. The eye-diagram for each SBR at the BER = 10^{-3} obtained from both the mathematical calculation and the computer simulation is shown in Fig. 5.14 and Fig. 5.15, respectively.

The eye-diagrams from the calculation are obtained at their maximum error-free subscribers of 2, 2, 6, 6 and 8, respectively. For the case of SBR = 1.0 in Fig. 5.14(a), it is more clear in comparison with the worst case obtained in Fig. 5.12(a). This is because the effect of σ_{PBN}^2, σ_{SBN}^2 and σ_{MAI}^2 is mitigated through the random access of interfered subscribers. The disorder in an eye-diagram caused by σ_{PBN}^2, σ_{SBN}^2 and σ_{MAI}^2 is loosened and the amplitude of the eye-diagram at BER = 10^{-3} is decreased. This means that the BER is bound by the effect of σ_{Rx}^2 more than the worst case. For the case of SBR = 0.8 shown in Fig. 5.14(b), some of the overlapped pulses are remained that resulting in the unclear lines during the bit transition. Although the eye-opening is quite wide, the σ_{PBN}^2 is high and resulting in its limit of the BER. For the case of SBR = 0.6, 0.4, and 0.2 shown in Fig. 5.14(c)-(e). The σ_{PBN}^2 is mitigated since we have performed with low value of SBR since the waveform fluctuation at the level of bit "1" is decreased. Nevertheless, the effects from σ_{SBN}^2 and σ_{MAI}^2 shown in the thickness of eye-diagram at bit level "0" become more aggressive than the worst case. These two noises source become the dominant noises that can limit the BER of the system.

For the case of using the computer simulation, the eye-diagrams obtained at 3, 3, 7, 7 and 8 error-free subscribers for the case of SBR = 1.0, 0.8, 0.6, 0.4 and 0.2 are illustrated in Fig. 5.15(a)-(e), respectively. In Fig. 5.15(a), the eye looks chaotic as same as we can obtain from our numerical results. Furthermore, for the case of SBR = 0.8, 0.6, 0.4 and 0.2, the eye-diagrams present clearly bell-shaped pulses and the thickness in eye-diagrams are cause by σ_{PBN}^2, σ_{SBN}^2 and σ_{MAI}^2, respectively.

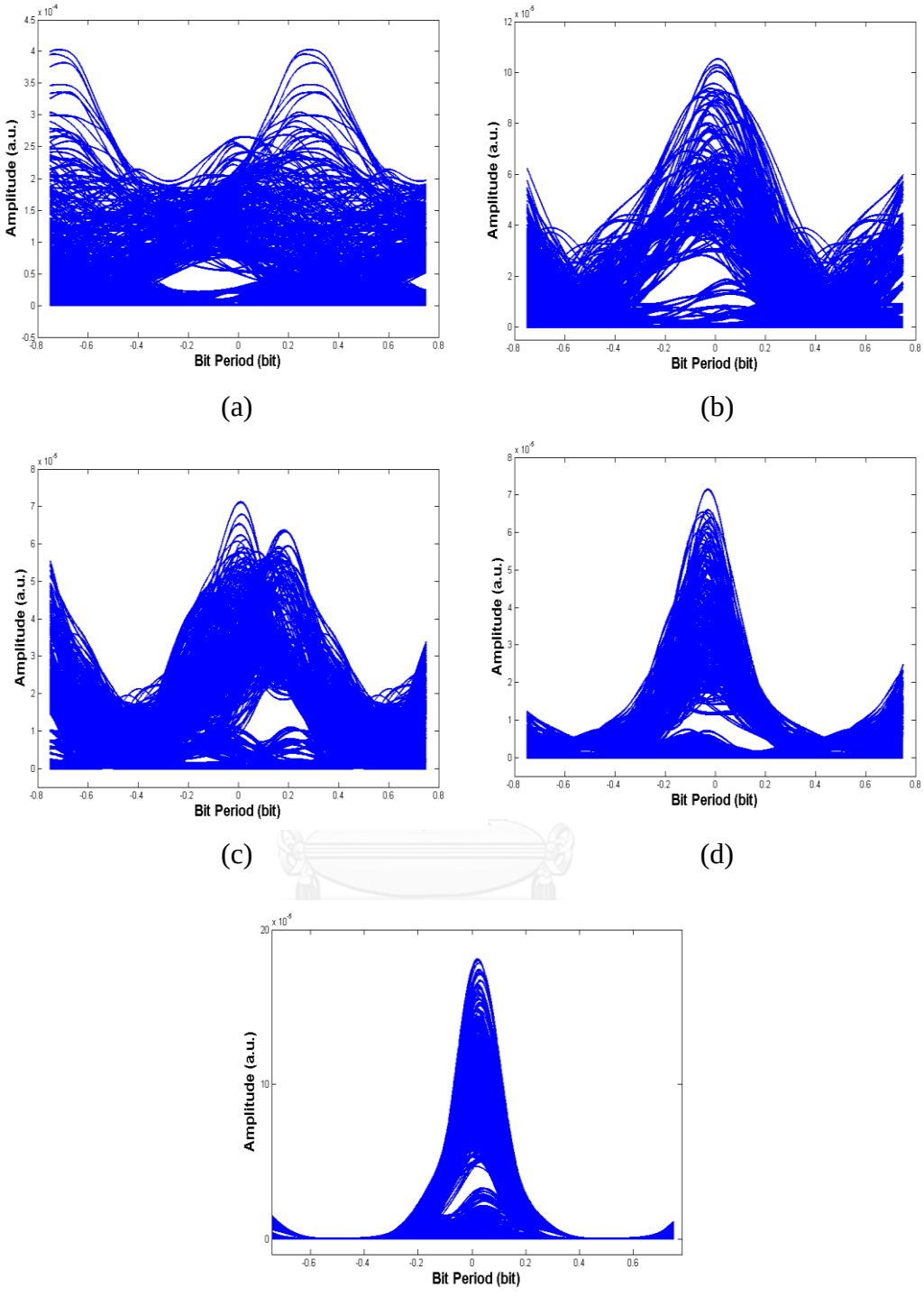

Fig. 5.14 Eye-diagrams of an average case obtained by our mathematical calculation (a) SBR = 1.0, (b) SBR = 0.8, (c) SBR = 0.6, (d) SBR = 0.4 and (e) SBR = 0.2.

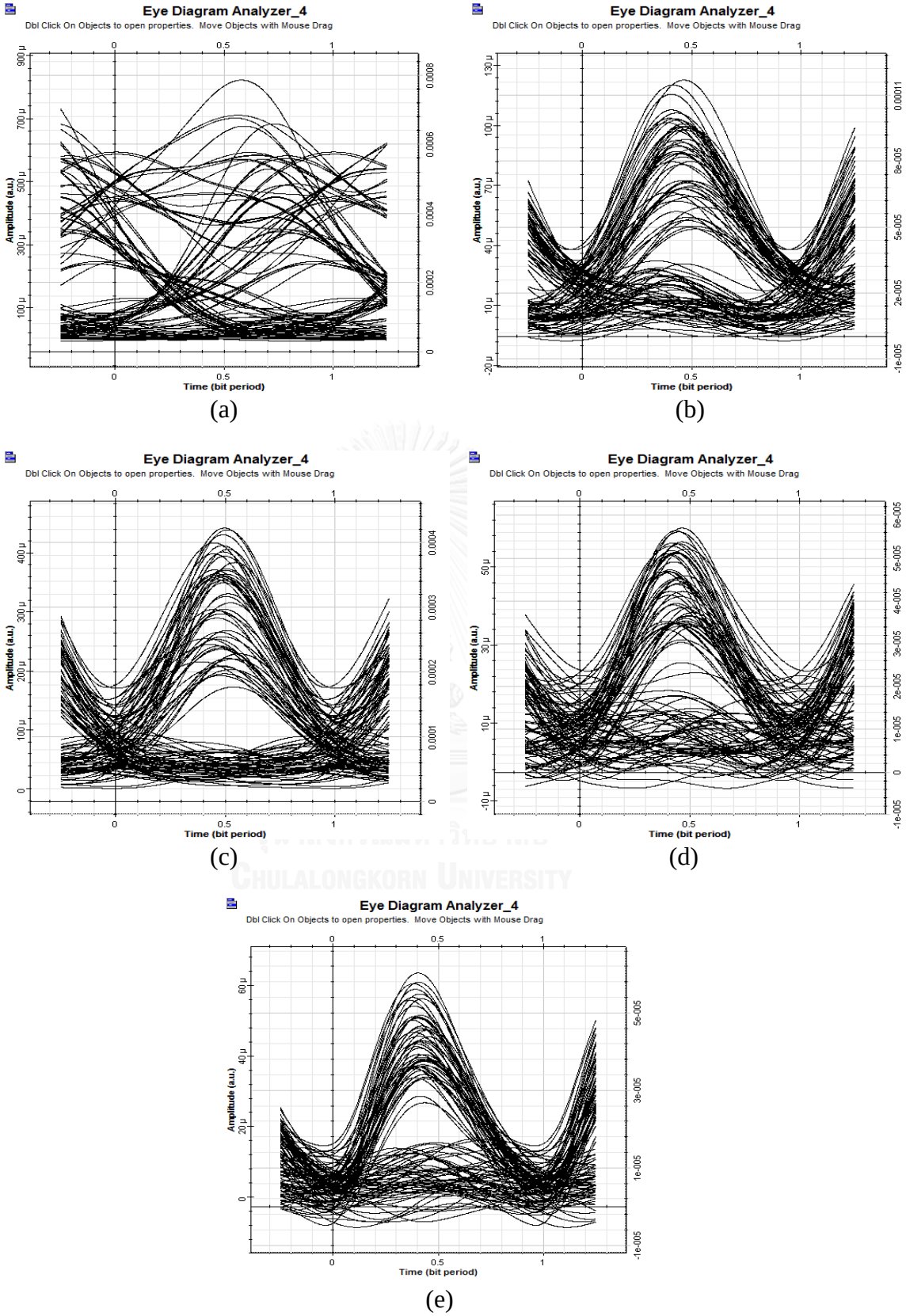

Fig. 5.15 Eye-diagrams of an average case obtained from the simulation.

5.4 Signal Transmission over 20-km of SMF.

In this case, we also run a simulation over a 20-km of SMF in order to find the power penalty cause by the transmission part. Since the optical pulse is very narrow, the optimal length of a DCF is used to compensate the chromatic dispersion. Nevertheless, in the real system, it is difficult to make perfect dispersion compensation because we cannot find a DCF which its dispersion slope is perfectly matched to the SMF's. Therefore, we'd like to find the power penalty caused by imperfect dispersion slope compensation so that this penalty can be used for power budget calculation.

One of the important parameter for a DCF is a ratio of a dispersion slope to chromatic dispersion (RDS). Its unit is nm^{-1}. The ratio between RDS of the DCF to RDS of transmission fiber is called slope compensation (SC) rate as shown in (5.1).

$$SC = \frac{RDS_{DCF}}{RDS_{SMF}} \tag{5.1}$$

If we have a DCF with RDS as same as the RDS of a transmission fiber, the SC rate is equal to 1. Therefore, we can have nearly 100% of dispersion compensation. A brief specification of SMF and DCF modules at 1552.52 nm used for the simulation are listed in Table. 5.2, respectively.

We repeat the simulation in 5.2.2 with a transmission fiber and 3 types of DCF module. After we have measure the BER as a function of ROP, a receiver sensitivity at BER = 10^{-3} is collected to investigate the power penalty as a function of the SBR and the number of OCDMA subscribers. We show, the relation between the SBR and the power penalty, for the case of single subscriber in Fig. 5.16. The maximum power penalties of 2.672, 2.501, and 2.072 dB belong to SBR = 0.2 for all 3 types of DCF whereas the minimum penalties of 0.043, 00.193, and 0.142 come from SBR = 1.0, respectively. It is a fact that the optical signal of SBR = 0.2 experiences more effect from the dispersion slope mismatched in comparison to the SBR = 1.0 due to its large optical bandwidth. Therefore, in low SBR, it is very sensitive to the dispersion effect.

The receiver sensitivity is measured again after the signal is transmitted over a fiber and the DCF. Then, the differences in the receiver sensitivity in comparison to the back-to-back case are obtained as the power penalty due to the dispersion slope mismatched. The power penalties of each DCF are depicted in Fig. 5.17, respectively. Most of the power penalties are no more than 3 dB for the case of SBR = 1.0, 0.8, 0.6, and 0.4 whereas it is approximately 3-5.5 dB for the case of SBR = 0.2. The results in Fig. 5.17 confirm that low SBR experiences more effect of the dispersion slope mismatched than the high SBR, and the power penalties obtained from all 3 types of the DCF are in the same range. Nevertheless, the total number of subscriber for the case of SBR = 0.2 is reduced from 3 in the back-to-back case to 2 by the dispersion slope effect. Moreover, the eye-diagrams of each SBR at its maximum subscribers are shown in Fig. 5.18. All eye-diagrams seem to be nearly the same in comparison to the back-to-back case because the pulse broadening due to the dispersion slope in the optical signal is filtered by the LPF.

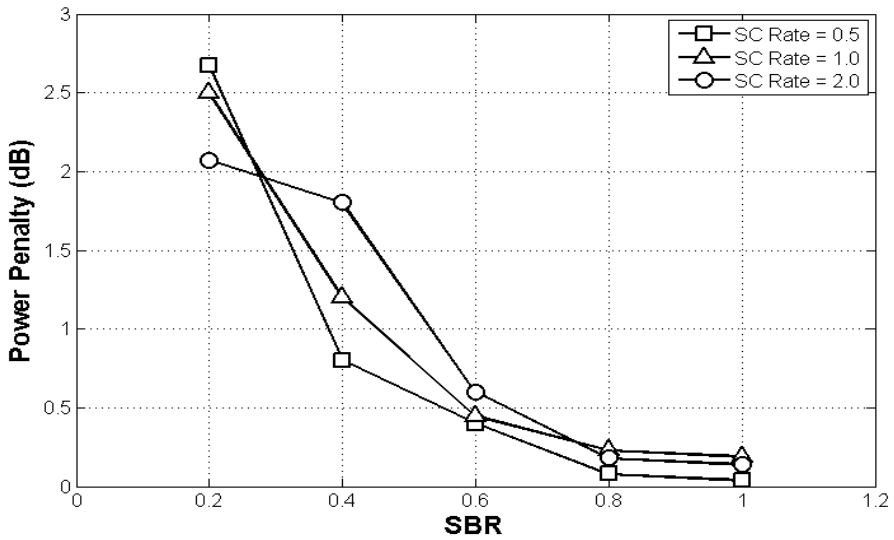

Fig. 5.16 The power penalty of the case of single-subscriber, as a function of the SBR.

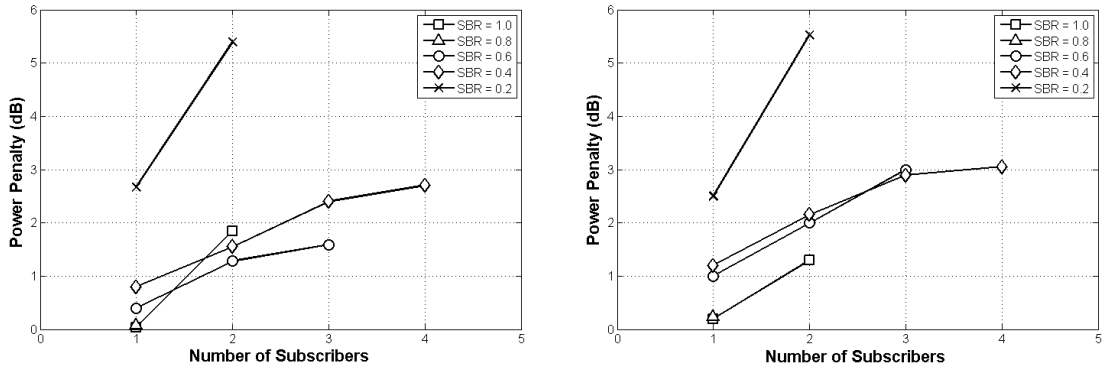

(a)

(b)

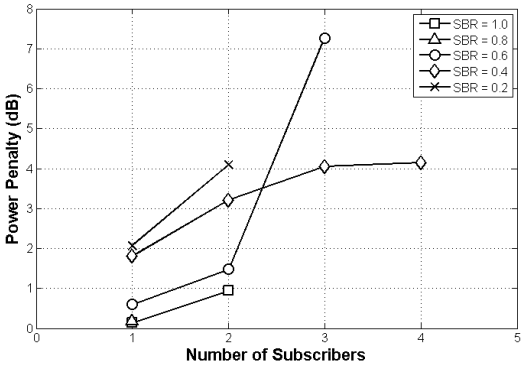

(c)

Fig. 5.17 Power penalty from the dispersion slope mismatched at each number of subscribers with different types of the DCF (a) SC rate = 0.5, (b) SC rate = 1.0, and (c) SC rate = 2.0

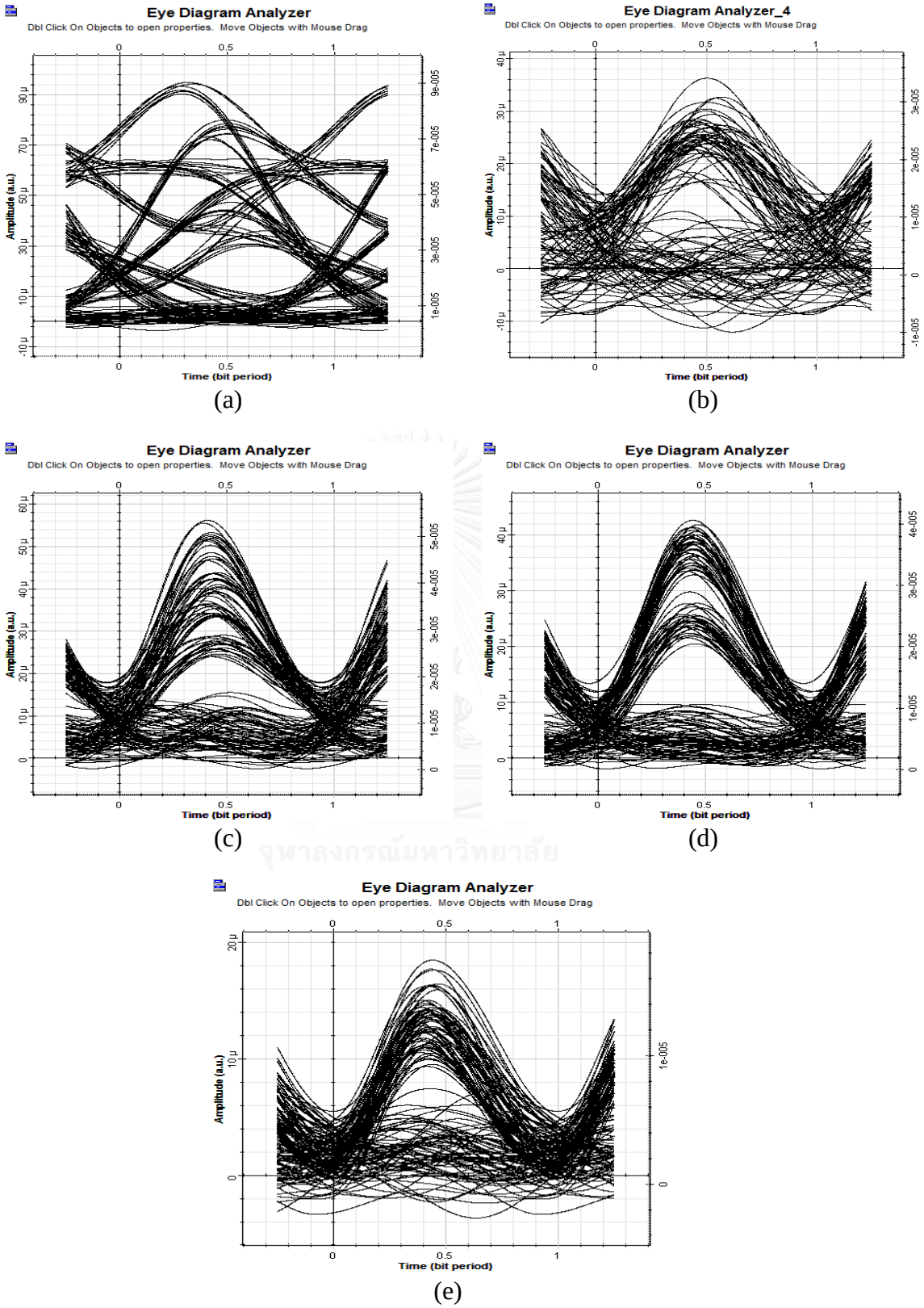

Fig. 5.18 Eye-diagram after the fiber transmission of an SMF and a DCF with SC rate = 0.5 (a) SBR = 1.0, (b) SBR = 0.8, (c) SBR = 0.6, (d) SBR = 0.4 and (e) SBR = 0.2.

5.5 System Power Budget

Since the transmitted power for all cases of SBRs are 9 dBm and we can obtain the receiver sensitivity from our results, we can calculate the power budget of the system by using (2.11). For the worst case scenario, we use the receiver sensitivity from section 5.4 to calculate the power budget. Nevertheless, the access of each subscriber to the system is the random process. Furthermore, we cannot perform the simulation under the average performance of the system. Therefore, we use the receiver sensitivity from chapter 4.4.2 as the representative of the average performance of the OCDMA-PON, respectively.

The receiver sensitivities and the power budget of each SBR for the worst case and are shown in Table 5.3. We can see that, the maximum power budget of 33.798 dB comes from the case of SBR = 0.2 whereas the minimum power budget of 25.201 comes from the case of SBR = 0.6 with 3 subscribers. Moreover, the power budget calculated from the asynchronous transmission as the representative value for the average performance is shown in Table 5.4. In the average case, the receiver sensitivities are improved for all SBRs. Therefore, the power budget in increased to 35.03 dB as the maximum, obtained from the single subscriber of the case of SBR = 0.2. On the other hand, the minimum power budget is found to be 24.92, obtained from SBR = 0.6 with total 6 subscribers, respectively.

Table 5.3 Power budget calculated from the worst case scenario.

Specification	OCDMA-PON				
	SBR = 1.0	SBR = 0.8	SBR = 0.6	SBR = 0.4	SBR = 0.2
Transmitted Power (dBm)	+10 dBm				
Receiver Sensitivity (dBm)					
▪ 1-Subscriber	-20.813	-23.031	-23.45	-23.687	-23.798
▪ 2-Subscribers	-13.776	N/A	-17.878	-20.797	-22.355
▪ 3-Subscribers	N/A	N/A	-15.201	-18.018	N/A
▪ 4-Subscribers	N/A	N/A	N/A	-16.835	N/A
Power Budget (dB)					
▪ 1-Subscriber	30.813	33.031	33.45	33.687	33.798
▪ 2-Subscribers	23.776	N/A	27.878	30.797	32.355
▪ 3-Subscribers	N/A	N/A	25.201	28.018	N/A
▪ 4-Subscribers	N/A	N/A	N/A	26.835	N/A

Table 5.4 Power budget calculated from the average case.

Specification	OCDMA-PON				
	SBR = 1.0	SBR = 0.8	SBR = 0.6	SBR = 0.4	SBR = 0.2
Transmitted Power (dBm)	+10 dBm				
Receiver Sensitivity (dBm)					
▪ 1-Subscriber	-20.52	-23.78	-23.96	-24.67	-25.03
▪ 2-Subscribers	-16.79	-20.37	-22.55	-23.39	-23.86
▪ 3-Subscribers	N/A	N/A	-20.92	-21.88	-22.38
▪ 4-Subscribers	N/A	N/A	-19.89	-21.08	-21.97
▪ 5-Subscribers	N/A	N/A	-15.21	-19.21	-21.22
▪ 6-Subscribers	N/A	N/A	-14.92	-18.41	-20.88
▪ 7-Subscribers	N/A	N/A	N/A	N/A	-19.3
▪ 8-Subscribers	N/A	N/A	N/A	N/A	-18.81
Power Budget (dB)					
▪ 1-Subscriber	30.52	33.78	33.96	34.67	35.03
▪ 2-Subscribers	26.79	30.37	32.55	33.39	33.86
▪ 3-Subscribers	N/A	N/A	30.92	31.88	32.38
▪ 4-Subscribers	N/A	N/A	29.89	31.08	31.97
▪ 5-Subscribers	N/A	N/A	25.21	29.21	31.22
▪ 6-Subscribers	N/A	N/A	24.92	28.41	30.88
▪ 7-Subscribers	N/A	N/A	N/A	N/A	29.3
▪ 8-Subscribers	N/A	N/A	N/A	N/A	28.81

CHAPTER 6 The System Performance Comparison between OCDMA and TDMA over PON

In this chapter, we show, the system performance comparison between the conventional PON based time-division multiple access (TDMA) technology and the proposed OCDMA-PON using various SBR. The receiver sensitivity of the TDMA-PON at various bit rates is shown. Moreover, the spectral efficiency, the system complexity and the power budget are discussed in the rest of this chapter, respectively.

6.1 System Configuration of TDMA-PON

The TDMA-PON system configuration is setup as shown in Fig. 6.1. The main components in the transmitter side are consisted of the continuous wave (CW) laser, the NRZ pulse generator, and the Mach-Zehnder Intensity modulator. The CW laser has the center wavelength of 1552.52 nm with a linewidth of 10 MHz, and the transmitted power of 10 dBm. The extinction ratio of the modulator is 30 dB. Then, the optical signal is launched into the optical fiber ITU G.652.D, followed by a dispersion compensating fiber. At the distribution unit, the optical signal is split by a power splitter and sent into each ONU. In front of the photodetector, a variable optical attenuator (VOA) is used to attenuate the input optical signal in order to prevent the overload signal power at the photodetector. Moreover, we adjust the VOA to find the relation between the ROP and the BER, respectively. We use PIN photodetector with a responsivity of 0.6 A/W with the dark current of 50 nA, respectively. The detected electrical signal will be filtered high component frequencies out by an LPF with a cut-off frequency of 75% of the system bit rate. Finally, the electrical filtered signal is used to find the BER by using the BER analyzer, respectively.

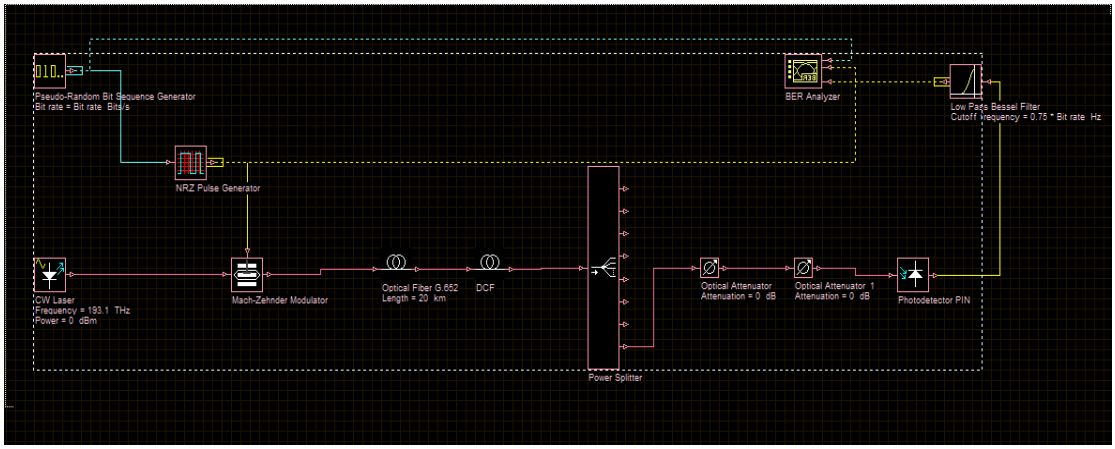

Fig. 6.1 TDMA-PON system configuration.

6.2 System Performance of TDMA-PON

We organize the simulation into a 8 cases. The system bit rates are organized as 40, 80, 120, 160, 200, 240, 280, and 320 Gbps, respectively. Therefore, the bit period of each case is found to be 25, 12.5, 6.25, 3.125, 1.56, 0.78, 0.39, and 0.195 ps, respectively. It should be noted that, in the TDMA-PON, the transmission mechanism is based on time-slot sharing among subscribers. In the ultra-high bit rate, the bit period is inversely proportional to the system bit rate. Unlike the WDMA and OCDMA-PON that we can add more wavelengths or codes to the system in order to increase the total bit rate whereas the bit period of each subscriber is still the same. In each case, the cut-off frequencies of the LPF are 30, 60, 90, 120, 150,180, 210, and 240 GHz, respectively. For the back-to-back case, the filtered electrical eye-diagrams at the BER $= 10^{-3}$ are shown in Fig. 6.2 and Fig. 6.3, respectively.

As we can see in Fig. 6.2-6.3, the eye-opening of the eye-diagram is almost closed for every system bit rate. Since the electrical NRZ waveform is ideal with the perfect rectangular shape, the shape of the eye-diagrams are almost the same. The thickness of the eye-diagram at the level of bit “0 and “1” are very large. Therefore, we can conclude that the signal distortion in the eye-diagrams is caused by the photodetector noise, especially the thermal noise and shot noise.

The BER as a function of ROP for each system bit rate is shown in Fig. 6.4. The receiver sensitivities are increased since the system bit rate is increased as well. This is because, at the same amplitude, the high bit rate with the small pulse width experienced lower ROP in comparison to the low bit rate. In the back-to-back case, the receiver sensitivities at the FEC limit of BER $= 10^{-3}$ for the case of 40-320 Gbps are -21.79, -20.05, -19.15, -18.61, -18.03, -17.75, -17.0, and -16.93 dBm, respectively.

For the signal transmission over 20 km of the optical fiber, the effect of chromatic dispersion is a serious issue for the high bit rate system. The pulse broadening of the optical signal is the cause of ISI that can limit the speed of the signal transmission. Therefore, in this case, we place the DCF with an appropriate length that can make a complete compensation for the 2^{nd} dispersion. Nevertheless, the effect of the dispersion slope is still remained for the case of imperfect dispersion slope compensation. In this case, we simulate the signal transmission over a fiber with 3 cases of the DCF in order to find the power penalty caused by the dispersion slope mismatched at each system bit rate. The specification of the DCF is already discussed in Table 5.2. The eye-diagrams for the case of 40 and 320 Gbps TDMA-PON with various SC rate of the DCF are illustrated in Fig. 6.5 and Fig. 6.6, respectively. For the case of 40 Gbps system, the bit period is 25 ps and the pulse broadening caused by the dispersion slope mismatched is so small that the shape of the eye-diagrams are nearly the same. On the other hand, for the case of 320 Gbps TDMA-PON, the bit period is found to be 0.195 ps. It is 8 times smaller in comparison to the 40 Gbps system. Therefore, the effect of the slope mismatched can be seen clearly for the case of employing the DCF with the SC rate of 0.5 and 2.0. The shapes of the eye-diagrams, shown in Fig. 6.6, are not symmetric because of the dispersive effect.

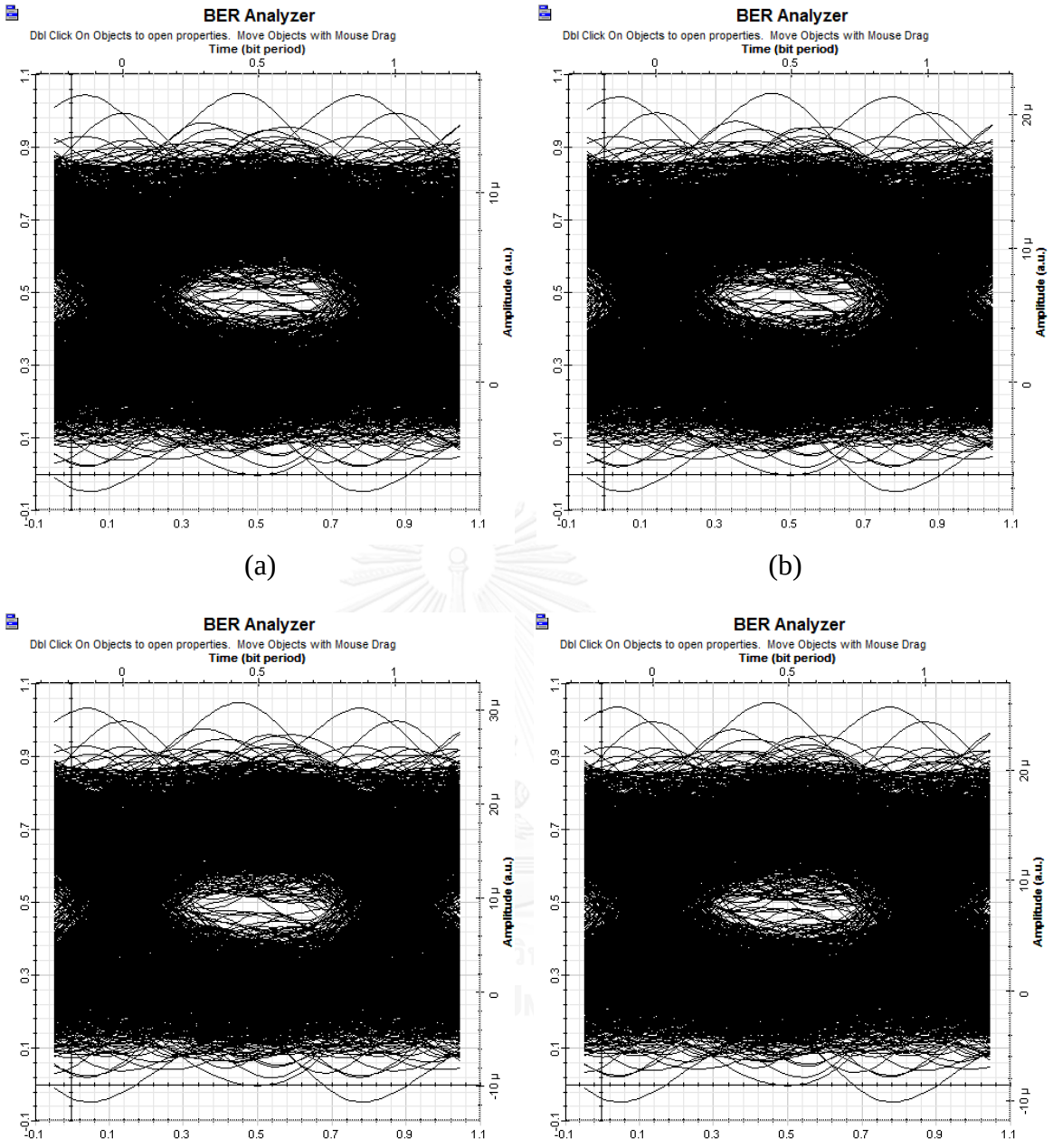

Fig. 6.2 The filtered electrical signal, obtained at BER = 10 for the case of (a) 40, (b) 80, (c) 120, and (d) 160 Gbps of TDMA-PON, respectively.

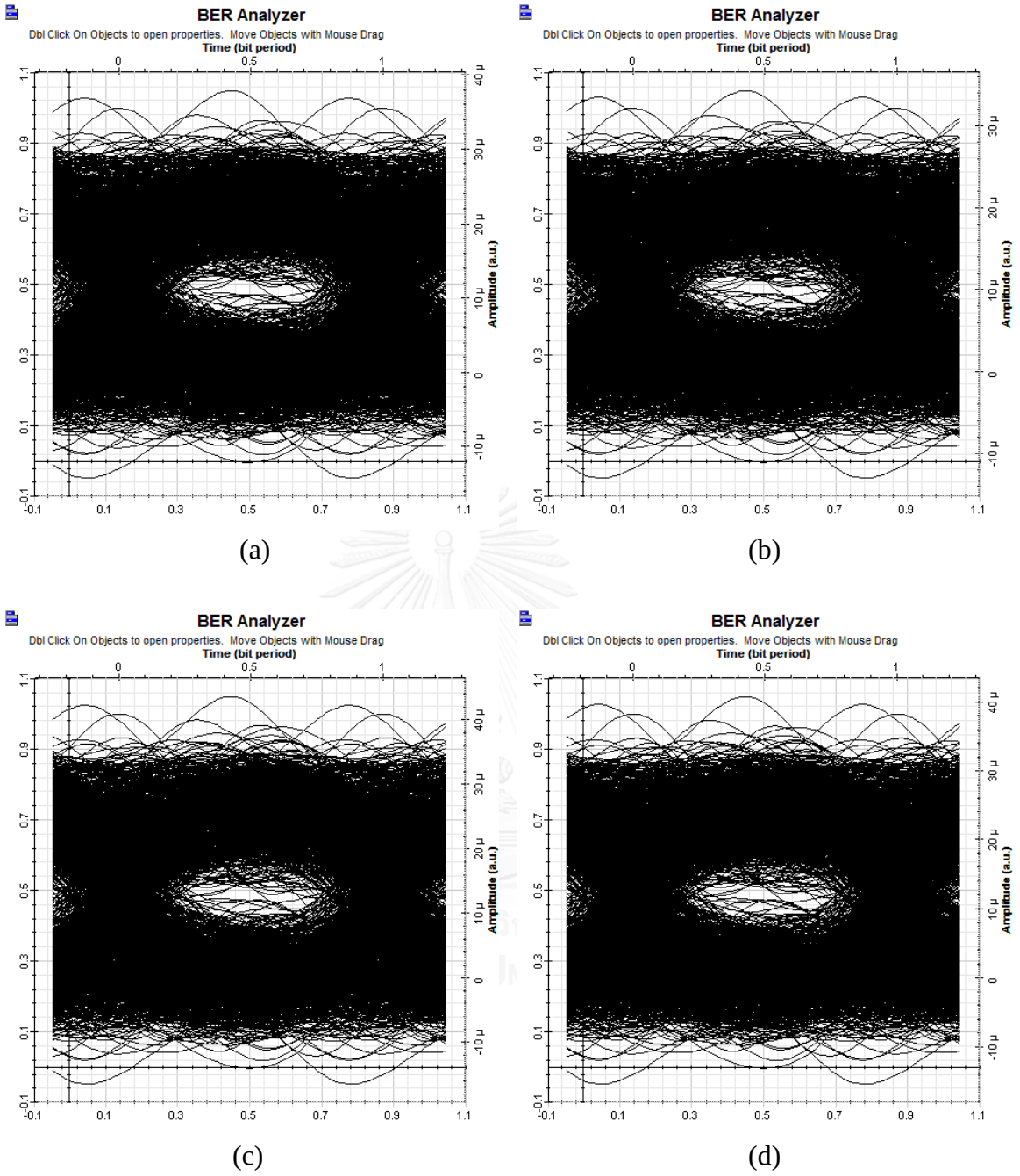

Fig. 6.3 The filtered electrical signal, obtained at BER = 10 for the case of (a) 200, (b) 240, (c) 280, and (d) 320 Gbps of TDMA-PON, respectively.

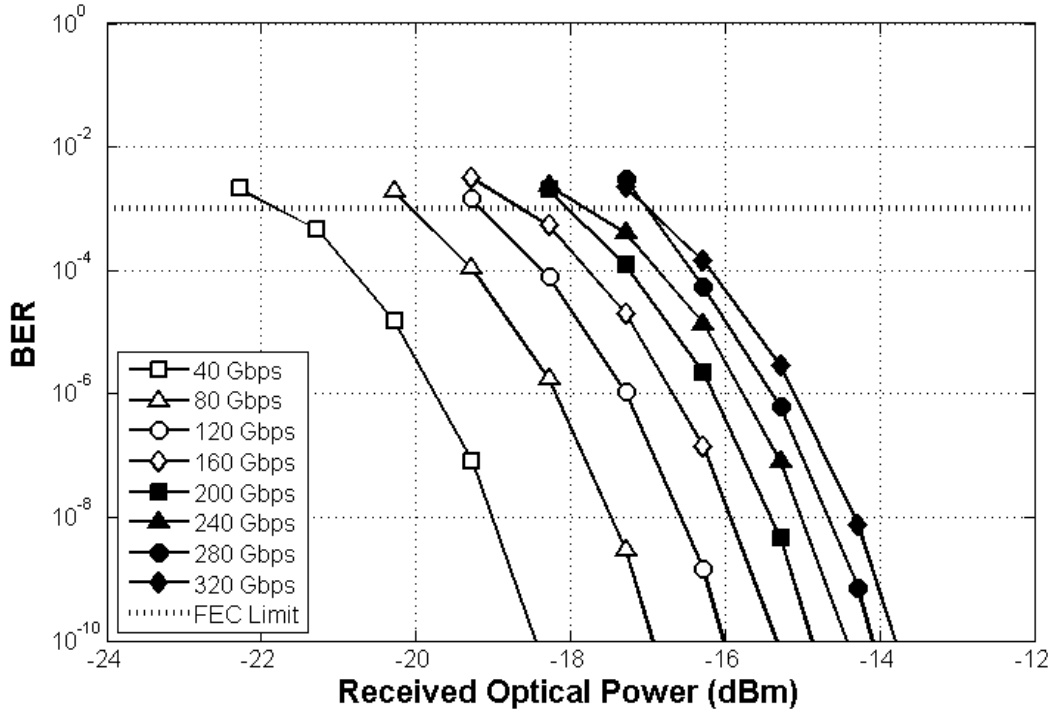

Fig. 6.4 The relation between ROP and BER for the back-to-back case.

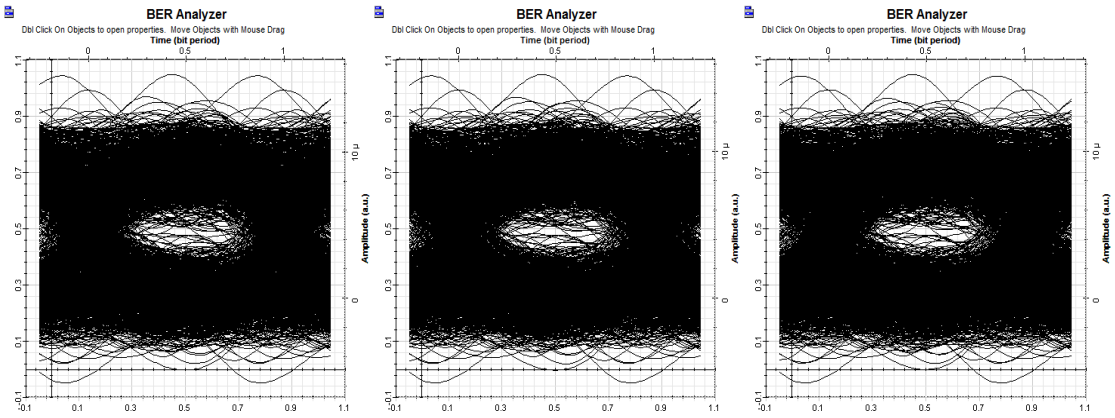

(a) (b) (c)

Fig. 6.5 Eye-diagrams of the 40G TDMA-PON with various SC rate of (a) 0.5, (b) 1.0, and (c) 2.0.

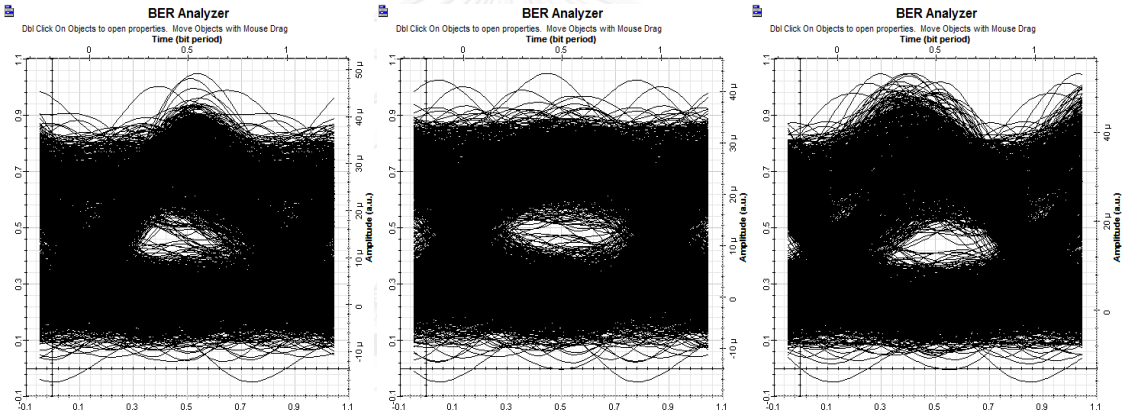

(a) (b) (c)

Fig. 6.6 Eye-diagrams of the 320G TDMA-PON with various SC rate of (a) 0.5, (b) 1.0, and (c) 2.0.

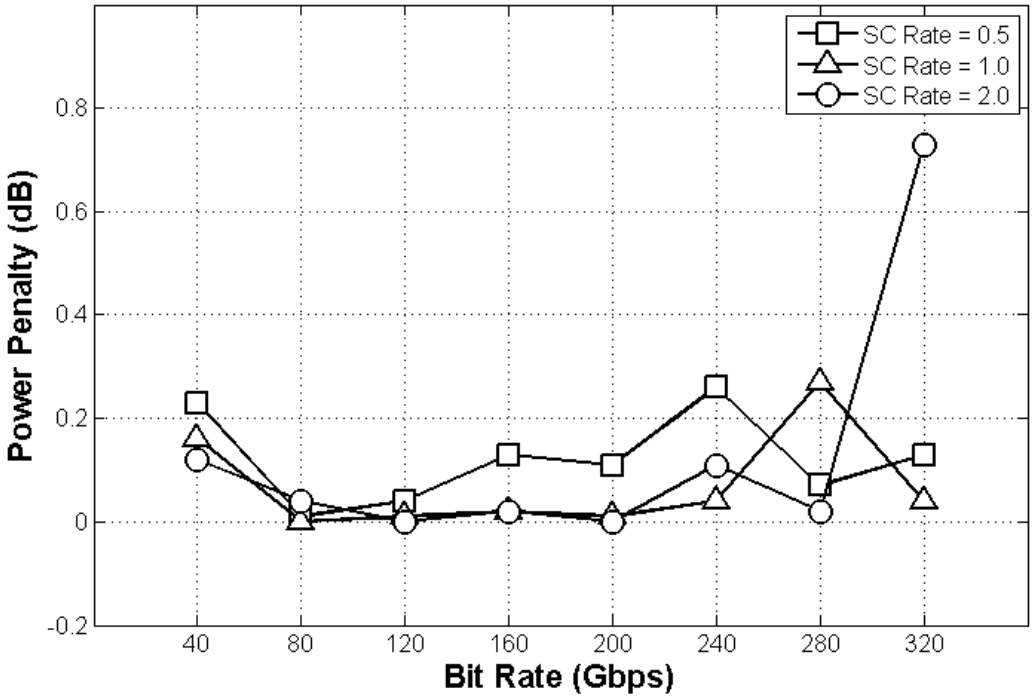

Fig. 6.7 Power penalty caused by the dispersion slope mismatched.

The power penalty, caused by the dispersion slope mismatched, of each system bit rate is obtained from the receiver sensitivity of the transmission case and subtracted by the receiver sensitivity of the back-to-back case, respectively. We can see that, the power penalties are quite small with the range of 0.01-0.27 dB, shown in Fig. 6.7. Nevertheless, by increasing the system bit rate, the power penalty is increased due to suffering from the ISI effect so that the maximum power penalty is approximately 0.73 dB for the case of 320G TDMA-PON using DCF with SC rate = 2.0, respectively.

6.3 System Performance Comparison between TDMA and OCDMA-PON

We discuss the number of subscribers, total bit rate, spectral efficiency, and the system complexity between the TDMA-PON and the OCDMA-PON in order to compare the efficiency of the system.

6.3.1 System Power Budget

The power budget calculation is stated in eq. (2.11). Since we know the transmitted power and the receiver sensitivity, we can calculate the power budget. For each system bit rate, the power budget of the TDMA-PON after transmitted over 20 km of a fiber and a DCF with SC rate of 1.0, is shown in Table 6.1. The maximum power budget 31.63 dB is obtained from the 40G TDMA-PON whereas the minimum power budget of 26.97 dB is obtained from the 320G TDMA-PON, respectively.

Table 6.1 TDMA-PON Power Budget.

Attributes	Bit Rate							
	40G	80G	120G	160G	200G	240G	280G	320G
Transmitted Power (dBm)	+10							
Receiver Sensitivity (dBm)	-21.63	-20.05	-19.14	-18.59	-18.02	-17.71	-17.27	-16.97
Power Budget (dB)	31.63	30.05	29.14	28.59	28.02	27.71	27.27	26.97

6.3.2 Number of Subscribers

The number of actual subscribers is actually depended on the receiver sensitivity. In the PON design, the ROP of each subscriber must be at least equal to the receiver sensitivity in order that we can guarantee the BER under the FEC limit. Therefore, we can split optical signal into many branches, or ports, by using the passive optical power splitter. Each branch of splitter is connected to one ONU located at each subscriber's home. In this case, the total number of subscribers is based on the number of a power splitter and the number of ports of the power splitter. Nevertheless, the bit rate per subscriber is inversely proportional to the number of ports. Although we can have many subscribers in the system, the bit rate per subscriber is also reduced.

To find the number of total ports that can be assigned to the subscribers. We have to calculate to optical power in front of the power splitter so that we can further estimate the number of total subscribers. Then, in order to select the appropriate power splitter, the insertion loss of the splitter must lower than the input optical power in front of the power splitter. The number of ports and the insertion loss of the splitter, obtained from the commercial product, are shown in Table 6.2. Moreover, the power at each stage of the PON is shown in Table 6.3, respectively.

Then, we can calculate the remaining power budget by subtracting the input power in front of the power splitter with the receiver sensitivity. Finally, the remaining power budget is used to find the total subscribers support by the TDMA-PON. The power budget in front of the splitter and the total number of subscribers are shown in Table 6.4. The maximum number of subscriber for the 40G and 80G TDMA-PON are 16, the maximum subscribers of the 120G and 160G TDMA-PON are 12, and the maximum subscribers supported by the 200G, 240G, 280G, and 320G are 8, respectively.

Table 6.2 The specification of the optical power splitter.

Operate Wavelength (nm)	1260-1625							
Number of Ports	1×2	1×4	1×6	1×8	1×12	1×16	1×32	1×64
Insertion Loss at 23° C (dB)	3.5	6.8	9.3	10.1	12.3	13.2	16.7	20.2

Table 6.3 Optical Power Distribution at each stage of PON.

Attributes	Value
Transmitted Power (dBm)	+10
• Optical Modulator Insertion Loss (dB)	-7
• Fiber Attenuation for 20 km (dB)	-4
• Fiber Attenuation for a DCF (dB)	-1.25
• Total Splice Loss (dB)	-1
• Total Connector Loss (dB)	-3
Total Loss (dB)	16.25
Input Power to the Optical Power Splitter (dBm)	-6.25

Table 6.4 Total Subscribers of the TDMA-PON.

Attributes	Bit Rate							
	40G	80G	120G	160G	200G	240G	280G	320G
Input Power to the Power Splitter (dBm)	-6.25							
Receiver Sensitivity (dBm)	-21.63	-20.05	-19.14	-18.59	-18.02	-17.71	-17.27	-16.97
Remaining Power Budget (dB)	15.38	13.80	12.89	12.34	11.77	11.46	11.02	10.72
Total Subscribers	16	16	12	12	8	8	8	8

For the case of OCDMA-PON, we organize the power budget into 2 cases, the worst case scenario and the average case scenario. From the worst case scenario, the power budget in front of the power splitter, and the power at the output port of the 1st stage power splitter are shown in Table 6.5. Since the input signal at the power splitter is code-multiplexed, the first power splitter is used to split the power to total N OCDMA subscribers of the system. At the 1st stage, the power splitters that are assigned to each SBR are depended on the number of OCDMA subscriber. Therefore, the maximum numbers of OCDMA subscribers are 2, 1, 3, 4, and 3, respectively. Then, in order to expand the capacity of the system, with the remaining power budget, we can further split the signal power by using the 2nd stage power splitter so that we can share the total bit rate of each OCDMA as the OCDM/TDMA-PON. By applying the appropriate power splitter based on the power budget, the total subscribers supported by OCDMA/TDMA-PON are already shown in Table 6.5. With the maximum value, the total subscribers are 16, 32, 32, 32, and 32 for the case of SBR = 1.0, 0.8, 0.6, 0.4, and 0.2, respectively.

In the average case scenario obtained from the asynchronous case, we can gain more power budget because the receiver sensitivities are improved in comparison to the worst case as already shown in Table 5.4. The maximum numbers of the OCDMA subscribers at the 1st stage power splitter are 2, 2, 6, 6, and 8 and the remaining power budgets at each SBR are shown in Table 6.6, respectively. After the 2nd stage power

splitter, the maximum numbers of subscribers supported by OCDMA/TDMA-PON are 16, 32, 32, 32, and 32 for the case of SBR = 1.0, 0.8, 0.6, 0.4, and 0.2, respectively.

For conclusion, the total numbers of subscribers of all TDMA-PONs are greater in comparison to the number of subscribers supported by OCDMA-PON due to the limit of the total codes. Nevertheless, the number of subscribers of the OCDMA-PON can be further increased by splitting the remaining power budget to other subscribers using TDMA technique, can be named as OCDMA/TDMA-PON. The total numbers of subscribers are depended on the combination between the number of OCDMA subscribers and the total ports of the 2^{nd} stage power splitter, respectively.

Table 6.5 Remaining power budget, type of power splitter and total subscribers of the OCDMA-PON for the worst case scenario.

Specification	OCDMA-PON				
	SBR = 1.0	SBR = 0.8	SBR = 0.6	SBR = 0.4	SBR = 0.2
Input Power to the Power Splitter (dBm)	-6.25				
Receiver Sensitivity (dBm)					
▪ 1-OCDMA Subscriber	-20.813	-23.031	-23.45	-23.687	-23.798
▪ 2-OCDMA Subscribers	-13.776	N/A	-17.878	-20.797	-22.355
▪ 3-OCDMA Subscribers	N/A	N/A	-15.201	-18.018	N/A
▪ 4-OCDMA Subscribers	N/A	N/A	N/A	-16.835	N/A
Remaining Power Budget (dB)					
▪ 1-OCDMA Subscriber	14.563	16.781	17.2	17.437	17.548
▪ 2-OCDMA Subscribers	7.526	N/A	11.628	14.547	16.105
▪ 3-OCDMA Subscribers	N/A	N/A	8.951	11.768	N/A
▪ 4-OCDMA Subscribers	N/A	N/A	N/A	10.585	N/A
1st Power Splitter					
▪ 1-OCDMA Subscriber	NO	NO	NO	NO	NO
▪ 2-OCDMA Subscribers	YES (1×2)	N/A	YES (1×2)	YES (1×2)	YES (1×2)
▪ 3-OCDMA Subscribers	N/A	N/A	YES (1×4)	YES (1×4)	N/A
▪ 4-OCDMA Subscribers	N/A	N/A	N/A	YES (1×4)	N/A
Total OCDMA-PON Subscribers	2	1	3	4	2
Remaining Power Budget					
▪ 1-OCDMA Subscriber	14.563	16.781	17.2	17.437	17.548
▪ 2-OCDMA Subscribers	4.026	N/A	8.128	11.047	12.605
▪ 3-OCDMA Subscribers	N/A	N/A	2.151	4.968	N/A
▪ 4-OCDMA Subscribers	N/A	N/A	N/A	3.785	N/A
2nd Power Splitter (For OCDMA/TDMA-PON)					
▪ 1-Subscriber	YES (1× 16)	YES (1× 32)	YES (1× 32)	YES (1× 32)	YES (1× 32)
▪ 2-Subscribers	YES (1×2)	N/A	YES(1×4)	YES (1×6)	YES (1×8)
▪ 3-Subscribers	N/A	N/A	N/A	YES (1×4)	N/A
▪ 4-Subscribers	N/A	N/A	N/A	YES (1×4)	N/A
Total OCDMA/TDMA PON Subscribers					
▪ 1-OCDMA Subscriber	16	32	32	32	32
▪ 2-OCDMA Subscribers	4	N/A	8	12	16
▪ 3-OCDMA Subscribers	N/A	N/A	3	12	N/A
▪ 4-OCDMA Subscribers	N/A	N/A	N/A	16	N/A

Table 6.6 Remaining power budget, type of power splitter and total subscribers of the OCDMA-PON for the average case scenario.

Specification	OCDMA-PON				
	SBR = 1.0	SBR = 0.8	SBR = 0.6	SBR = 0.4	SBR = 0.2
Input Power @ Power Splitter	-6.25 dBm				
Receiver Sensitivity (dBm)					
▪ 1-OCDMA User	-20.52	-23.78	-23.96	-24.67	-25.03
▪ 2-OCDMA Users	-16.79	-20.37	-22.55	-23.39	-23.86
▪ 3-OCDMA Users	N/A	N/A	-20.92	-21.88	-22.38
▪ 4-OCDMA Users	N/A	N/A	-19.89	-21.08	-21.97
▪ 5-OCDMA Users	N/A	N/A	-15.21	-19.21	-21.22
▪ 6-OCDMA Users	N/A	N/A	-14.92	-18.41	-20.88
▪ 7-OCDMA Users	N/A	N/A	N/A	N/A	-19.3
▪ 8-OCDMA Users	N/A	N/A	N/A	N/A	-18.81
Remaining Power Budget (dB)					
▪ 1-OCDMA User	14.27	17.53	17.71	18.42	18.78
▪ 2-OCDMA Users	10.54	14.12	16.30	17.14	17.61
▪ 3-OCDMA Users	N/A	N/A	14.67	15.63	16.13
▪ 4-OCDMA Users	N/A	N/A	13.64	14.83	15.72
▪ 5-OCDMA Users	N/A	N/A	8.98	12.96	14.97
▪ 6-OCDMA Users	N/A	N/A	8.67	12.16	14.63
▪ 7-OCDMA Users	N/A	N/A	N/A	N/A	13.05
▪ 8-OCDMA Users	N/A	N/A	N/A	N/A	12.56
1st Power Splitter					
▪ 1-OCDMA User	NO	NO	NO	NO	NO
▪ 2-OCDMA Users	YES (1×2)	YES (1×2)	YES (1×2)	YES (1×2)	YES (1×2)
▪ 3-OCDMA Users	N/A	N/A	YES (1×4)	YES (1×4)	YES (1×4)
▪ 4-OCDMA Users	N/A	N/A	YES (1×4)	YES (1×4)	YES (1×4)
▪ 5-OCDMA Users	N/A	N/A	YES (1×4)	YES (1×6)	YES (1×6)
▪ 6-OCDMA Users	N/A	N/A	YES (1×4)	YES (1×6)	YES (1×6)
▪ 7-OCDMA Users	N/A	N/A	N/A	N/A	YES (1×8)
▪ 8-OCDMA Users	N/A	N/A	N/A	N/A	YES (1×8)
Total OCDMA-PON Users	2	2	6	6	8
Remaining Power Budget					
▪ 1-OCDMA User	14.27	17.53	17.71	18.42	18.78
▪ 2-OCDMA Users	7.04	10.62	12.80	13.64	14.11
▪ 3-OCDMA Users	N/A	N/A	7.87	8.83	9.33
▪ 4-OCDMA Users	N/A	N/A	6.84	8.03	8.92
▪ 5-OCDMA Users	N/A	N/A	2.16	3.66	5.67

▪ 6-OCDMA Users	N/A	N/A	1.87	2.86	5.33
▪ 7-OCDMA Users	N/A	N/A	N/A	N/A	2.95
▪ 8-OCDMA Users	N/A	N/A	N/A	N/A	2.46
2^{nd} Power Splitter (For OCDMA/TDMA-PON)					
▪ 1-OCDMA User	YES (1 × 16)	YES (1 × 32)	YES (1 × 32)	YES (1 × 32)	YES (1 × 32)
▪ 2-OCDMA Users	YES (1 × 4)	YES (1 × 8)	YES (1 × 12)	YES (1 × 16)	YES (1 × 16)
▪ 3-OCDMA Users	N/A	N/A	YES (1 × 4)	YES (1 × 4)	YES (1 × 6)
▪ 4-OCDMA Users	N/A	N/A	YES (1 × 4)	YES (1 × 4)	YES (1 × 4)
▪ 5-OCDMA Users	N/A	N/A	N/A	YES (1 × 2)	YES (1 × 2)
▪ 6-OCDMA Users	N/A	N/A	N/A	N/A	YES (1 × 2)
▪ 7-OCDMA Users	N/A	N/A	N/A	N/A	N/A
▪ 8-OCDMA Users	N/A	N/A	N/A	N/A	N/A
Total OCDMA/TDMA PON Users					
▪ 1-OCDMA User	16	32	32	32	32
▪ 2-OCDMA Users	8	16	24	32	32
▪ 3-OCDMA Users	N/A	N/A	12	12	18
▪ 4-OCDMA Users	N/A	N/A	16	16	16
▪ 5-OCDMA Users	N/A	N/A	5	10	10
▪ 6-OCDMA Users	N/A	N/A	6	6	12
▪ 7-OCDMA Users	N/A	N/A	N/A	N/A	7
▪ 8-OCDMA Users	N/A	N/A	N/A	N/A	8

6.3.3 Bit Rate

The maximum bit rate of the each TDMA-PON is its full capacity of its own system of 40, 80, 120, 160, 240, and 320 Gbps. On the other hand, the maximum bit rate of each OCDMA subscriber is fixed at 40 Gbps and the maximum bit rates of the system are based on the number of subscribers that can achieved the FEC limit. For the worst case, the maximum bit rates of the OCDMA-PON are 80, 40, 120, 160, and 120 Gbps for the case of SBR = 1.0, 0.8, 0.6, 0.4, and 0.2, respectively. Moreover, the maximum bit rates of the average performance are 80, 80,240, 240, and 320 Gbps, respectively.

In additions, the bit rate per subscriber is obtained by dividing the total bit rate of the system by the numbers of subscribers. For the TDMA-PON, the bit rates per subscriber are shown in Table 6.7. On the other hand, for the case of OCDMA-PON and OCDMA/TDMA-PON, the bit rates per subscriber are reported in Table 6.8, respectively. With the various combinations between OCDMA and TDMA techniques, the bit rates are varied from 1.25-40 Gbps.

Table 6.7 Bit rates per subscribers of the TDMA-PON.

Attribute	Bit Rate							
	40G	80G	120G	160G	200G	240G	280G	320G
Bit Rate per Subscriber (Gbps)	2.5	5	10	13.3	25	30	35	40

Table 6.8 Bit rate per subscriber of the OCDMA-PON and OCDMA/TDMA-PON.

Bit Rate per Subscriber (Gbps)	Specification				
	SBR = 1.0	SBR = 0.8	SBR = 0.6	SBR = 0.4	SBR = 0.2
OCDMA-PON	40	40	40	40	40
OCDMA/TDMA-PON (Worst)					
▪ 1-OCDMA Subscriber	2.5	1.25	1.25	1.25	1.25
▪ 2-OCDMA Subscribers	20	N/A	10	6.67	5
▪ 3-OCDMA Subscribers	N/A	N/A	N/A	10	N/A
▪ 4-OCDMA Subscribers	N/A	N/A	N/A	7.5	N/A
OCDMA/TDMA-PON (average)					
▪ 1-OCDMA Subscriber	2.5	2.5	1.25	1.25	1.25
▪ 2-OCDMA Subscribers	10	5	3.33	2.5	2.5
▪ 3-OCDMA Subscribers	N/A	N/A	10	10	6.67
▪ 4-OCDMA Subscribers	N/A	N/A	10	10	10
▪ 5-OCDMA Subscribers	N/A	N/A	40	20	20
▪ 6-OCDMA Subscribers	N/A	N/A	40	40	20
▪ 7-OCDMA Subscribers	N/A	N/A	N/A	N/A	40
▪ 8-OCDMA Subscribers	N/A	N/A	N/A	N/A	40

6.3.4 Spectral Efficiency

The spectral efficiency (S.E.) which is the ratio between the total information rate divide by the given optical bandwidth, is discussed already in chapter 4.5. For the case of TDMA-PON, the measured 3-dB drop optical bandwidth after the modulator is shown in Fig. 6.8. We can see that the optical bandwidth of the OOK signal is increased linearly by the function of the system bit rate. Therefore, after the calculation, the S.E. of the TDMA-PON at each system bit rate with the maximum value of 1.24 b/s/Hz for the case of 40 Gbps TDMA-PON and the S.E. of the OCDMA-PON are illustrated in Fig. 6.9, respectively. The S.E. of the TDMA-PON is obviously greater that the OCDMA-PON for all cases.

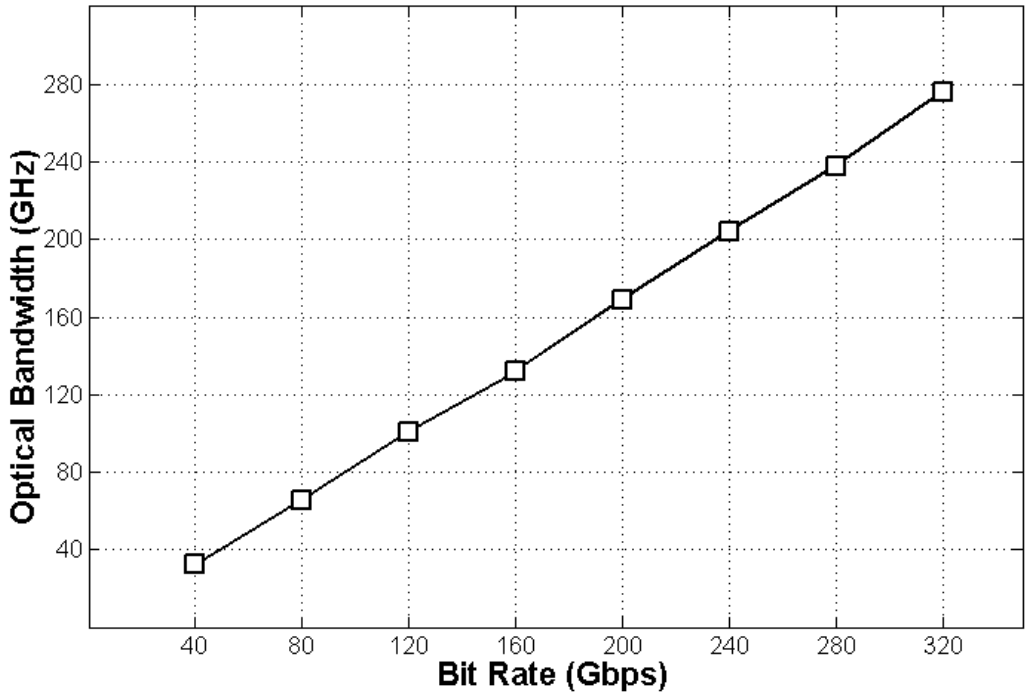

Fig. 6.8 Optical bandwidth of the TDMA-PON.

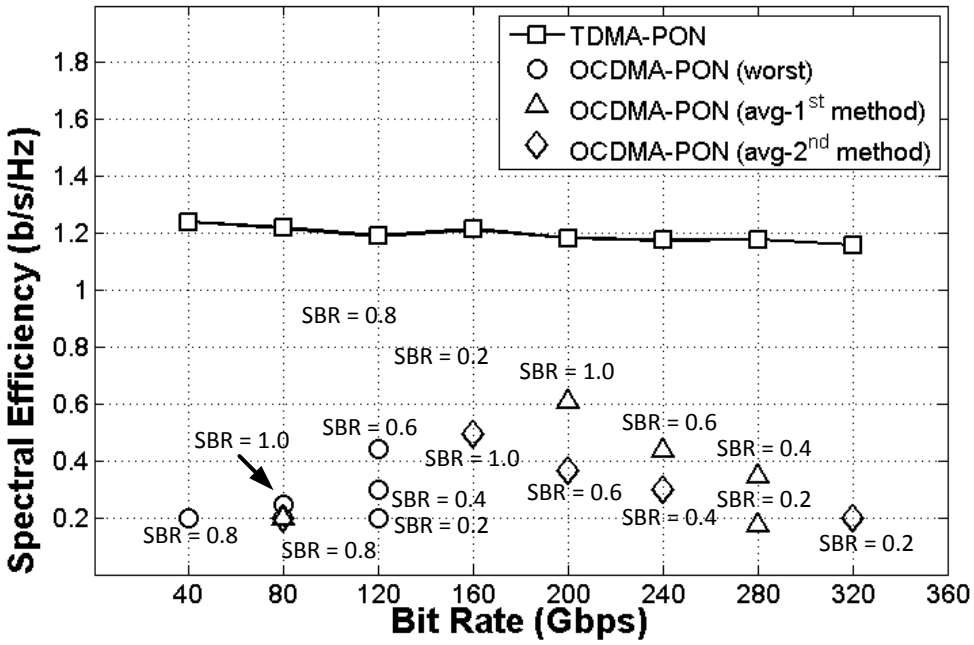

Fig. 6.9 Spectral efficiency of the TDMA-PON and the OCDMA-PON.

CHAPTER 7 The OCDMA System Verification by Performing the Experimental Setup

We have verified the system performance by using the simulation software in chapter 5 already. Therefore, we can first conclude that the reduction of SBR can reduce the σ_{PBN}^2. The BER can be improved and the total error-free subscribers can be increased when employing low SBR.

In this chapter, we would like to show the system performance by performing the experiment. The results from the experiment setup can be used to confirm the concept of our mathematical model. All of the experiments are performed at the Photonic Network System Laboratory, National Institute of Communication Technology (NICT), Japan.

First, we will introduce the system setup. Then, we will show the system performance by obtaining the BER as a function of ROP and the eye-diagram the desired BER of each SBR, respectively.

7.1 System Configuration

This experiment will be performed by using 2 types of the en/decoders. The first one is the 16-port AWG en/decoder with the chip period of 5 ps. Another is the 16-chip planar ligtwave circuit (PLC) based en/decoder with the chip period of 40 ps. The total encoding period of the AWG and the PLC en/decoder is 80 and 640 ps, respectively. With these two available types of the en/decoder, we decided to perform the experiment at the system bit rate of 1.25 Gbps with a total bit period of 800 ps. Therefore, the SBR of the AWG en/decoder is found to be 0.1 and the SBR of the PLC en/decoder is 0.8, respectively. The AWG and the PLC en/decoders are shown in Fig. 7.1

The system configuration of the SBR = 0.1 case (AWG case) is illustrated in Fig. 7.2. Since the chip period of AWG en/decoder is 5 ps, we need approximately 1.6 nm for optical bandwidth of the light source to keep the kt ratio equal to 1. This amount of the bandwidth is corresponding to nearly 2 ps of a pulse width. Therefore, we use a mode-locked laser diode (MLLD) that can generate 1.97 ps optical pulse with a repetition rate of 10 GHz. The center wavelength of the MLLD is 1552.52 nm. The pulse train is modulated by electrical signal, generated by a pulse pattern generator (PPG), in order to generate 1.25 Gbps optical signal. Then, the signal will be amplified by an erbium-dope amplifier (EDFA) and fed into a 1x4 coupler. Each branch of the coupler, the random length of fiber delay line is added to perform the experiment in an asynchronous transmission. Then, all branches are adjusted to have the same power and same polarization by a variable optical attenuator (VOA) and a polarization controller (PC), respectively.

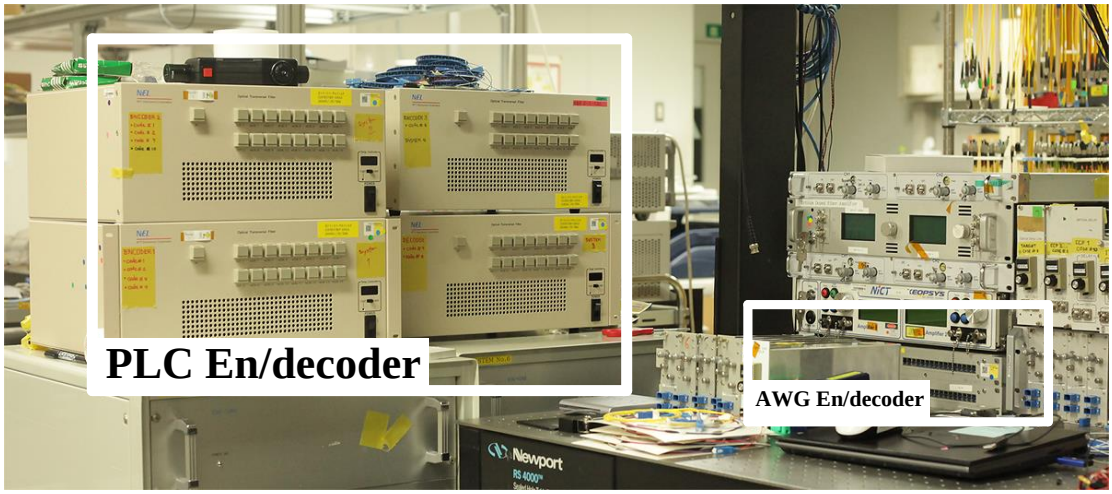

Fig. 7.1 The en/decoder used in the experiment (a) AWG en/decoder, and (b) PLC en/decoder.

The desired signal is launched into port #9 of the AWG and the interfered signal is launched into port #10 (or #7) for the case of 2-users and port # 7 and #11 for the case of 3-users, respectively. The output-port of the encoder is port #9. All encoded signals from the output-port #9 will be then decoded by AWG decoder using port #9 as the input-port and port #9 as the output-port in order to recover the target ACP signal, respectively. The ACP signal is then amplified and split into 2 branches to power meter 1 to observe received optical power (ROP), and to the EDFA-cascading section to maintain the same optical power of 0 dBm in front of the photodiode (PD) by using the VOA. The optical signal is converted to electrical signal by PD and followed by the 2.2 GHz low-pass filter (LPF) which exhibits Bessel shape in order to eliminate the high frequency components. Finally, the signal after filtering process is measured the BER by using an error detector (ED), respectively. It should be concerned that, the system performance must satisfy the requirement of BER lower than 10^{-9}.

For the case of SBR = 0.8, we need the optical pulse train at a repetition rate of 1.25 GHz and the approximate optical bandwidth of the light source of 0.2 nm. Therefore, we use the continuous wave (CW) laser with the center wavelength of 1552.52 nm, the first PPG, and the electro-absorption modulator (EAM) in order to generate the optical pulse train with a repetition rate of 40 GHz as shown in Fig. 7.3. The second PPG in corresponding with Mach-Zhender Intensity modulator (MZI) is used to down-convert the bit rate of the optical signal to 1.25 Gbps, as same as the case of SBR = 0.1, respectively. Then, the optical signal will be amplified and fed into a 1x4 coupler. After the addition of random delay and the polarization adjustment, each optical signal is encoded by a 16-chip PLC. The amplitude and the phase of each chip obtained in the encoded signal are manually adjusted by a built-in heater controlled by the injected current inside the PLC devices. All of the encoded signals will be adjusted to have the same power and polarization state by using VOA and PC, respectively. After all of the encoded signals are combined together by a 4:1 coupler, we need to maintain the polarization of the combined signals by using a polarizer. The decoder is phase-adjusted by using the target code. After that, the decoded signal is

launched to the cascaded-EDFA section in order to maintain the ROP in front of the PD as used in the case of SBR = 0.1. Finally, we measure the BER to obtain the system performance by using the ED.

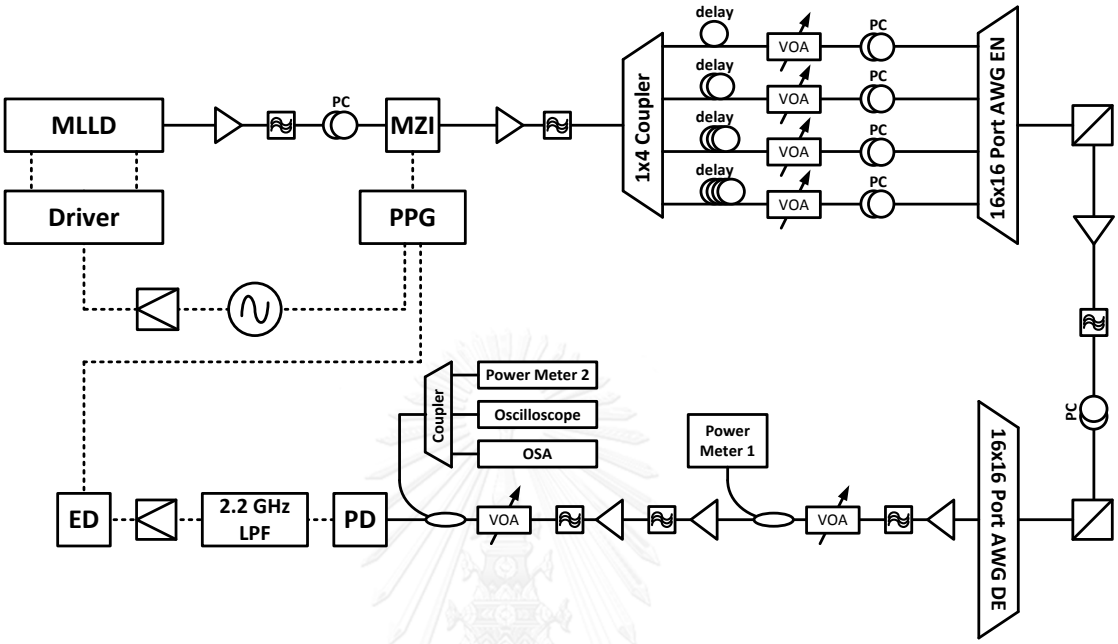

Fig. 7.2 OCDMA system configuration with SBR = 0.1 using 16-chip AWG en/decoder.

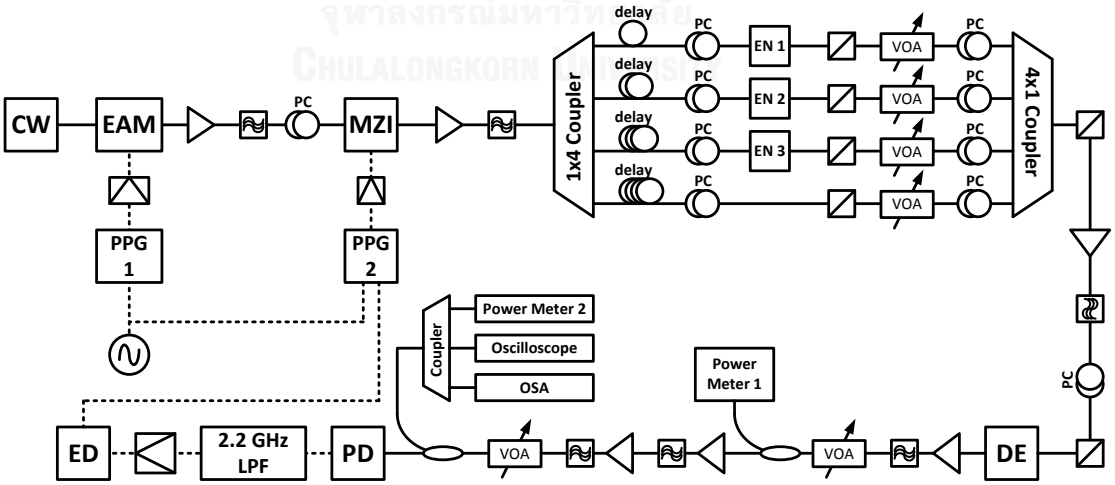

Fig. 7.3 OCDMA system configuration with SBR = 0.1 using 16-chip AWG en/decoder.

7.2 System Performance of the Single Subscriber Case

We show the difference in the en/decoded waveform of the en/decoded signal between the AWG and PLC case. The BER as a function of ROP of this single-subscriber case will be used as a reference result for the multi-subscriber cases, respectively.

7.2.1 AWG case

In this case, we use only the signal obtained from input-port #9/output-port #9 of the encoder. The total period of the encoded signal, measured by the Agilent 86100C oscilloscope with the receiver bandwidth of 40 GHz, is 80 ps as shown in Fig. 7.4(a), respectively. As a result, the SBR of this case is found to be 0.1. The effect of the slab diffraction of the AWG causes the power imbalance in each chip. The encoded signal spectrum is also measured and shown in Fig. 7.4(b). Since the chip period of the encoder is 5ps, the free spectral range (FSR) of the AWG encoder is 200 GHz, respectively. This encoded signal is decoded by the input-port #9/output-port #9 of the decoder in order to obtain only the ACP signal. The ACP signal waveform is illustrated in Fig. 7.5(a) with the triangle-like shape. The total period of the decoded signal is approximately 155 ps. By using the matched decoder, the filter shape of the decoder is matched to the spectrum of the encoded signal, resulting in the high power in each target spectrum as shown in Fig. 7.5(b). Therefore, all of the en/decoded signal waveforms are reached an agreement with the theory. It should be noted that, both waveforms obtained from the screen is bandwidth-limited by the oscilloscope.

In order to measure the system performance, the ACP signal will be first converted to the electrical signal at the PD. Then, the LPF will remove the high frequency components in order to recover the original data. Therefore, the filtered electrical signal waveform is broadened as a function of the filter response. This filtered electrical signal will be sent to the ED to measure the BER. The eye-diagrams of the signals, observed at BER = 10^{-3} and 10^{-9} are depicted in Fig. 7.6. The peak-to-peak voltage (V_{p-p}) of Fig. 7.6(a) and 7.6(b) are 40 and 84 mV, respectively.

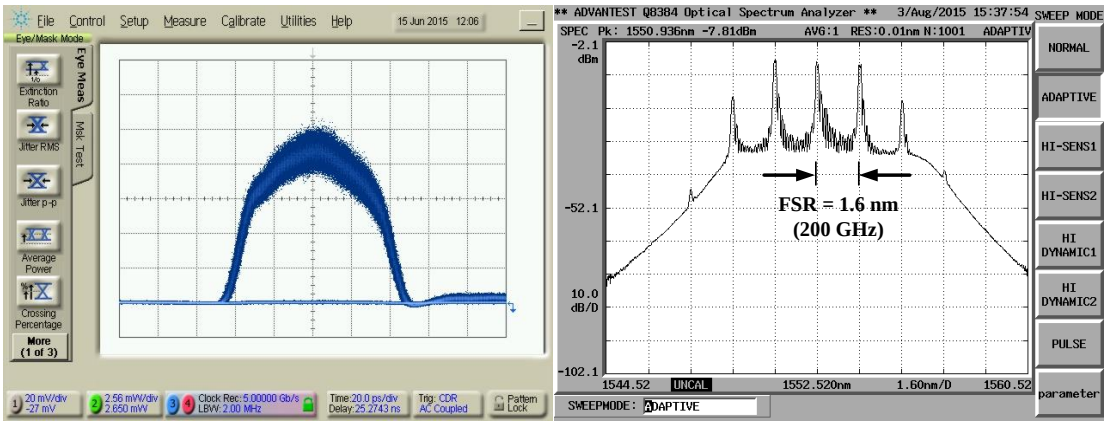

(a) (b)

Fig. 7.4 Encoded signal of the 16-chip AWG en/decoder (a) optical waveform, and (b) optical spectrum.

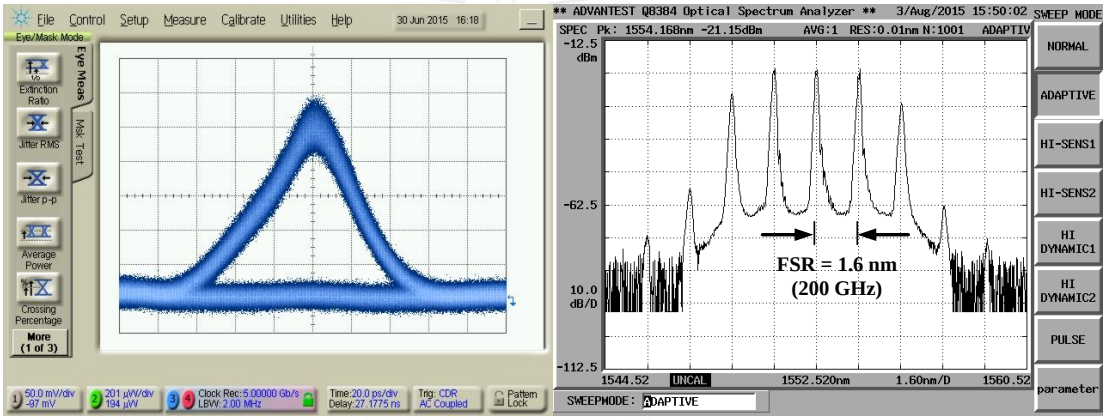

(a) (b)

Fig. 7.5 Decoded signal of the 16-chip AWG en/decoder (a) optical waveform, and (b) optical spectrum.

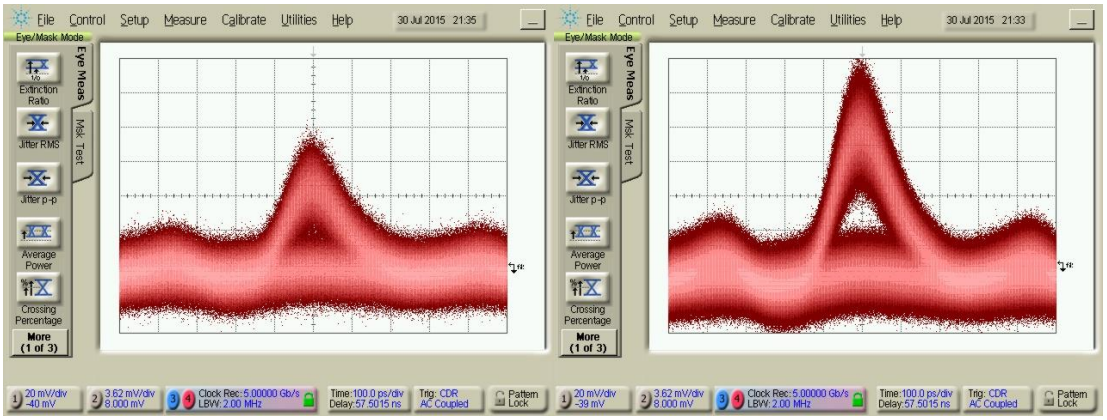

(a) (b)

Fig. 7.6 Eye-diagrams of the single-subscriber case using AWG (a) BER = 10^{-3} , and (b) BER = 10^{-9} .

7.2.2 PLC case

The power of all 16 chips is adjusted to be equal. Moreover, in each chip, we need to adjust the phase difference between each adjacent chip by a step of $7\pi/8$ (code #8). Unfortunately, both the amplitude and the phase are controlled by the built-in heater. Therefore, the adjustment in each parameter will affect another one. The encoded waveform is shown in Fig. 7.7(a) with the total encoding period of 640 ps. The SBR in this case is 0.8. In this case, we can see all 16 chips of the encoded signal clearly because the bandwidth of the oscilloscope is higher than the chip rate of the encoder. The measured spectrum is shown in Fig. 7.7(b) with the FSR of 0.2 nm. Both signals in the time-domain and the frequency domain in Fig. 7.7 are compatible to the theory.

After the decoding process, the ACP waveform is shown in Fig. 7.8(a) with the triangle-like shape. We can measure the period of the ACP, and it is approximately 1200 ps. The spectrum of the ACP is also shown in Fig. 7.8(b). After the LPF, the filtered electric signal, measured at BER = 10^{-3} and 10^{-9} with the period of 1200 ps is shown in Fig. 7.9 respectively. The measured voltages V_{p-p}, obtained from Fig. 7.9(a) and 7.9(b), are 136.3 and 262.4 mV, respectively.

We observed the optical power in front of the cascade-EDFA section as the ROP, and we also collected the BER at each ROP, respectively. The ROP as a function of the measure BER of the single-subscriber case, obtained from the AWG and the PLC case, is shown in Fig. 7.10. The receiver sensitivities of the system, measured at the BER of 10^{-9} are found to be -42.58 and -41.54 dBm, respectively. We can see that, by using the AWG with the SBR of 0.1 can improve the receiver sensitivity in comparison to the PLC case with the total power penalty of 1.04 dB.

The BER performance of the AWG case is steeper than the PLC case because the amplitude of the AWG case is dropped drastically due to most of the signal power is distributed over only 30% of the bit period. We can obtain from Fig. 7.6, at the point of BER = 10^{-9} and BER =10^{-3}, the difference in the ROP is 2.6 dB. As a result, in the signal amplitude, the V_{p-p} is decreased from 84 to 40 mV. For the PLC case, most of the signal power is distributed over all of the bit period. Therefore, we need 6 dB of the attenuation in order to reduce the V_{p-p} from 262.4 mV at BER = 10^{-9} down to 136.3 mV at BER = 10^{-3}, respectively.

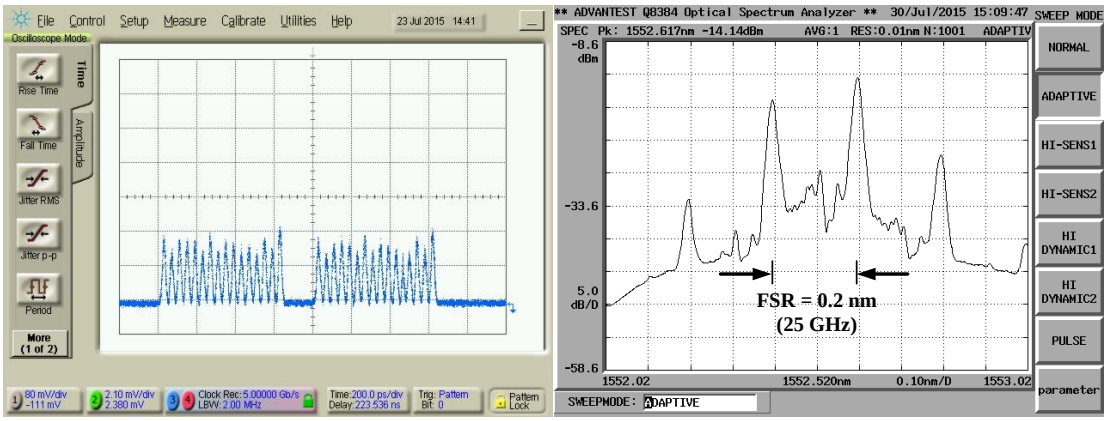

(a) (b)

Fig. 7.7 Encoded signal of the 16-chip AWG en/decoder (a) optical waveform, and (b) optical spectrum.

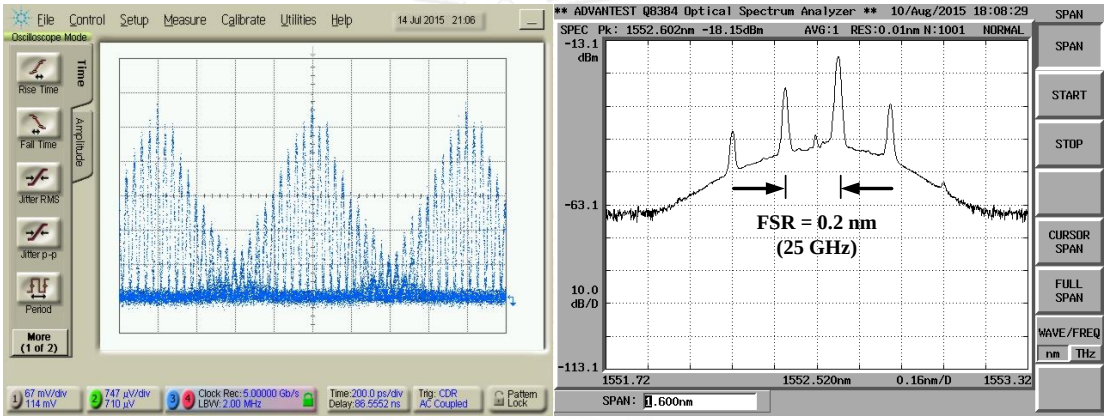

(a) (b)

Fig. 7.8 Decoded signal of the 16-chip AWG en/decoder (a) optical waveform, and (b) optical spectrum.

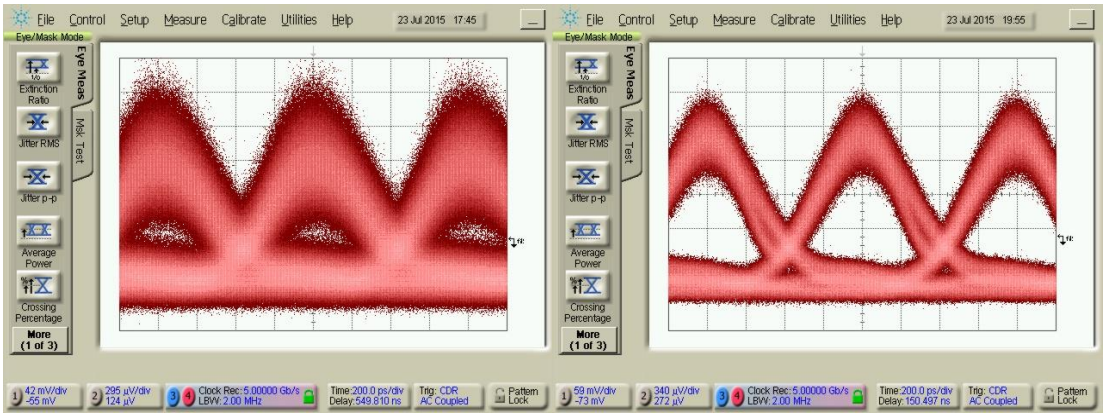

(a) (b)

Fig. 7.9 Eye-diagrams of the single-subscriber case using PLC (a) BER = 10^{-3} , and (b) BER = 10^{-9} .

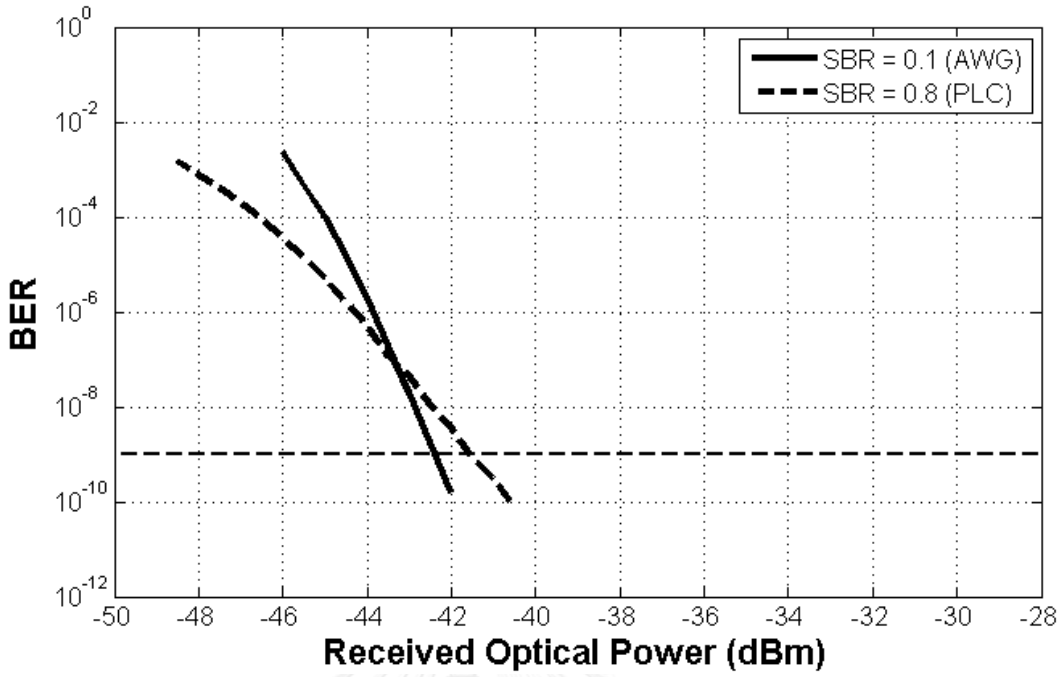

Fig. 7.10 Measured BER as a function of ROP.

7.3 System Performance of the 1-Interfered Subscriber Case (Adjacent Code)

In this case, we add the interfered subscriber using the adjacent code in order to investigate the BER under the worst case scenario. We have proposed the BER performance, by our mathematical calculation, in chapter 4 already. The results show that, by employing SBR = 0.6, 0.4, and 0.2, we can achieve the BER under FEC limit whereas the BERs of SBR = 1.0 and 0.8 are higher than the requirement of the FEC. Moreover, we have performed the simulation under the same scenario and the results are compatible to our mathematical calculation.

The optical waveform of the encoded signals, obtained from both the desired and the subscribers, are shown in Fig. 7.11. Since the two encoded signals are multiplexed together, the strong signal interference can be seen. At the decoder, the multiplexed signals will be decoded as the ACP and the CCP, respectively. The power of the CCP is dependent on the phase-difference of the code between the desired and the interfered subscriber. Therefore, by using the adjacent code, the phase-difference is the smallest and the power of the CCP is found to be the maximum. Fig. 7.12 shows the decoded signal after have decoded by the desired decoder. The bit sequence of the desired subscriber is “1110010001”, represented by the very clear shape with high power of the ACP, is shown in Fig. 7.12(a). On the other hand, we also transmit the bit with the sequence of “0100001110”, using the adjacent code. The CCP is represented in Fig. 7.12(b) with the low power in comparison to the ACP. As we can see in Fig. 7.12(c), the second bit, the ACP is distorted by the PBN caused by the beat terms between the ACP and the CCP. Moreover, at the 7^{th}-9^{th} bit, the desired

subscriber transmitted bits with mark “000” whereas the interfered subscriber transmitted bits with mark “111”. We can see the CCP or MAI signal very clearly. As a result, with these severe OCDM noise terms, they can lead to the error in the bit-pattern recognition at the receiver.

7.3.1 AWG Case

In this case, we use the input-port #9/output-port #9 and the input-port #9/output-port #10 of the AWG encoder as the desired and the interfered subscriber, respectively. The input-port #9/output-port #9 of the AWG decoder is assigned as the desired decoder. After the decoder, the measured PCR between these two codes is 7.75 dB. The eye-diagrams of the decoded signal are shown in Fig. 7.13.

The different delays, adjusted by the optical delay line, are added to the interfered subscriber in order to obtain the eye-diagrams and the BERs at various positions over one bit-period. The worst case scenario which the highest peak of the CCP is aligned at the center of the ACP is shown in Fig. 7.13(a). At this point, the strongest constructive and destructive interferences between two optical fields can be seen. The extremely strong fluctuations of the optical waveform cause no eye-opening. Nevertheless, by the employing various delays, we can see very small eye-openings due to the interferences are still high as we can see in Fig. 7.13(b)-(c). All V_{p-p} obtained from Fig. 7.13 can be measured as 148.5, 170.5, 187.1, and 192.5 mV, respectively. Furthermore, we also shift the CCP to both the left and the right side of the ACP. The left-shift and the right-shift of the CCP cause the mitigation of the interference due to the overlapped period between the ACP and the CCP is reduced. Therefore, the eye-opening of the ACP is loosened as stated in Fig. 7.14. The maximum peak of the CCP obtained in Fig. 7.14(a) is left-shifted from the ACP and most of the CCP is place outside the ACP. In this case, the serious PBN cannot be generated and the total noise sources of this signal transmission are MAI and receiver noise, respectively. As a result, the eye-opening of Fig. 7.14(a) is nearly the same height as shown in Fig. 7.5(a) for the case of single-subscriber. Nevertheless, the BER in this case is worse than the single-subscriber due to suffering from various noise sources.

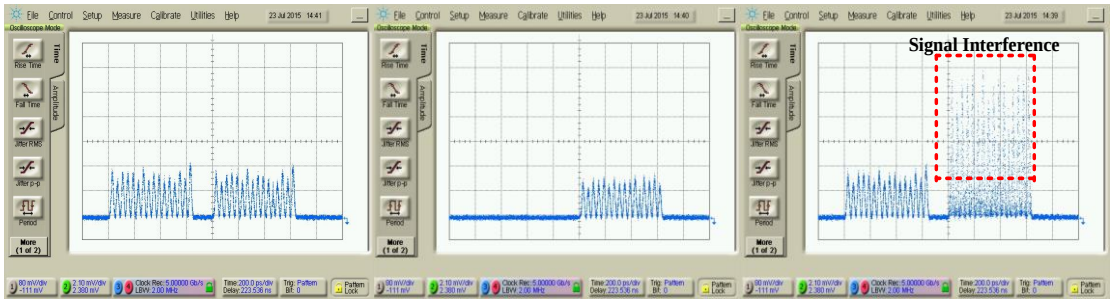

(a) (b) (c)

Fig. 7.11 Encoded waveform obtained from (a) desired subscriber, (b) interfered subscriber and (c) multiplexed signal.

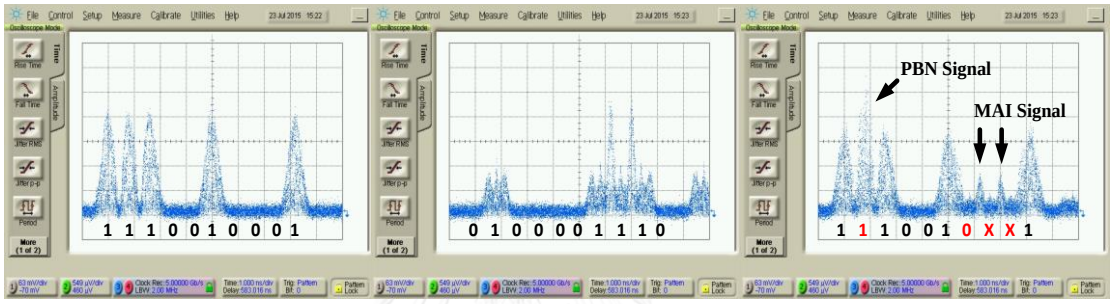

(a) (b) (c)

Fig. 7.12 Decoded signal obtained from (a) desired subscriber, (b) interfered subscriber and (c) multiplexed signal of the desired and interfered subscriber.

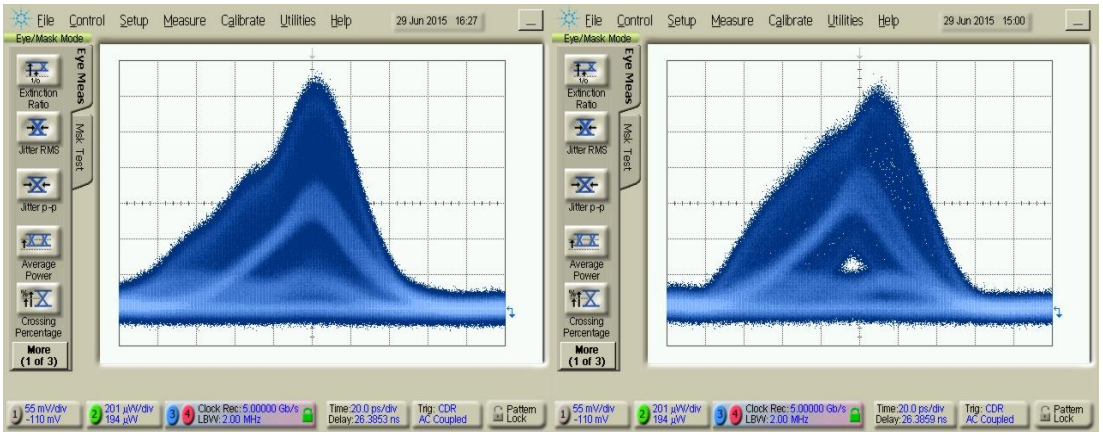

(a) (b)

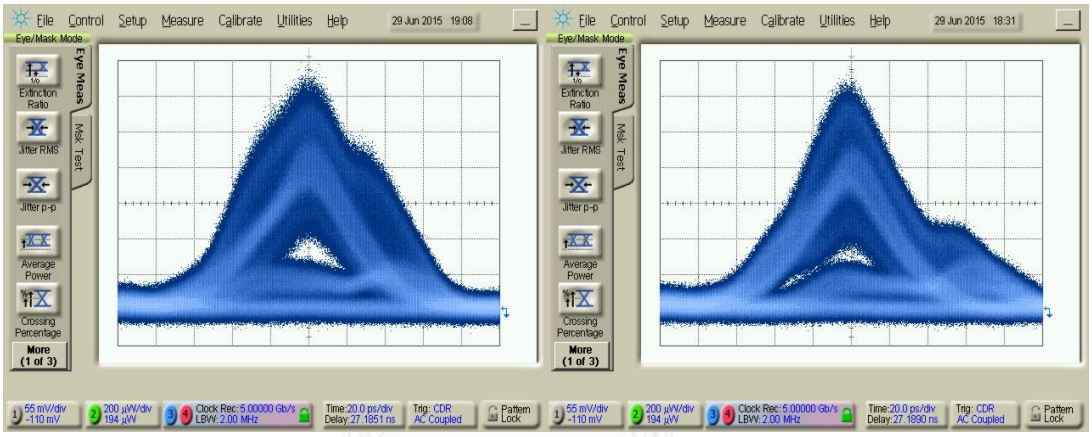

(c) (d)

Fig. 7.13 Eye-diagrams of the decoded optical signals with various delays (a) 0 ps, (b) +20 ps, (c) +40 ps and (d) +60 ps.

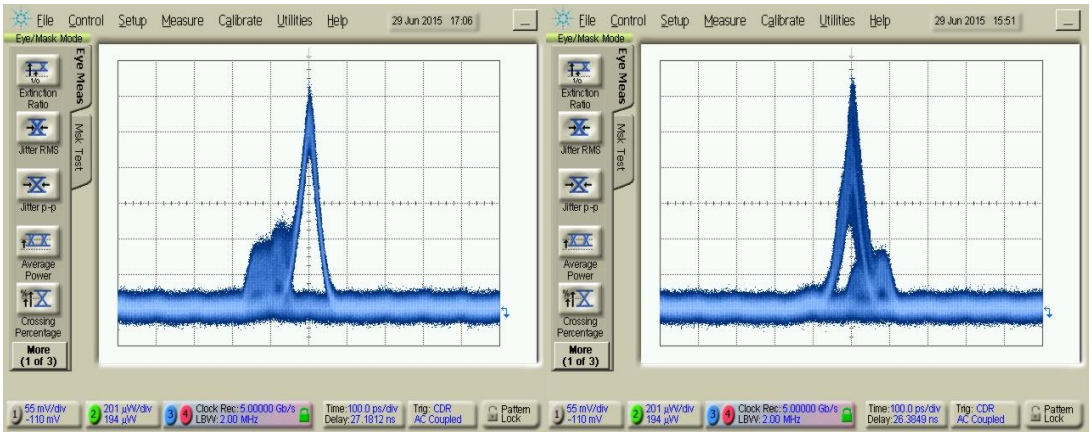

(a) (b)

Fig. 7.14 Eye-diagrams of the decoded signals at various delay (a) -80 ps and (b) +80 ps.

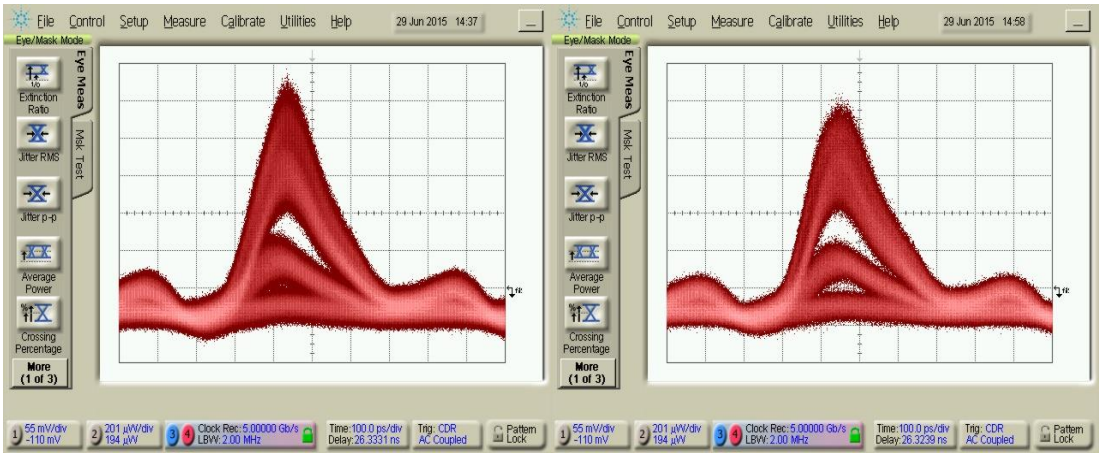

(a) (b)

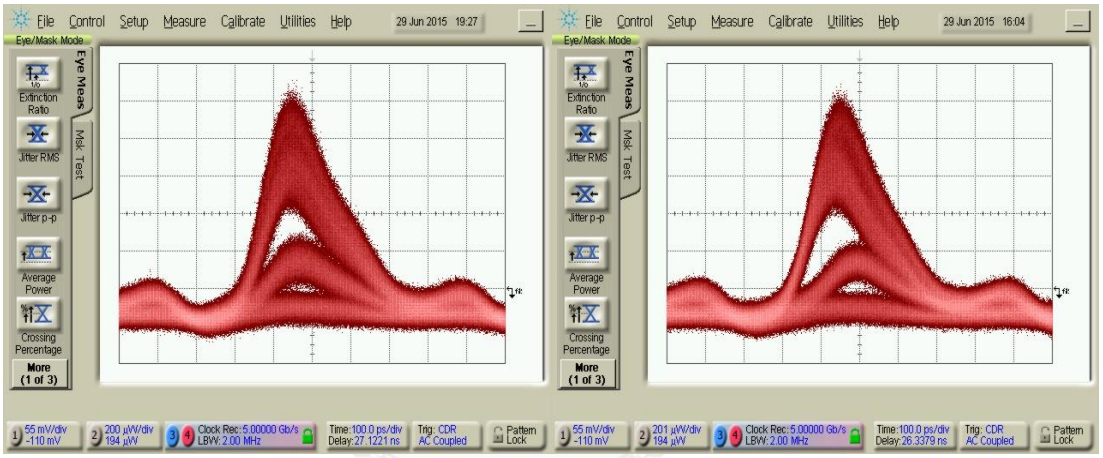

(c) (d)

Fig. 7.15 Eye-diagrams of the filtered electrical signal with various delays at the BER = 10^{-9} (a) 0 ps, (b) +20 ps, (c) +40 ps and (d) +60 ps.

The eye-diagrams of the filtered electrical signal at various delays of the interfered subscriber are illustrated in Fig. 7.15. Note that, all figures are obtained at BER = 10^{-9}. The high frequency components of the decoded optical signal, especially the beat terms of each 5-ps chip between the desired and the interfered subscribers which is corresponding to a 200 GHz of bandwidth, are filtered out by a 2.2 GHZ LPF. Although the eye-opening of the optical eye-diagrams in Fig. 7.13 are suffered from the severe interference, we still can obtain the eye-opening in the filtered electrical signal.

We measure the BER of the 1-interfered subscriber case by employing the adjacent code. The measured BERs of this experiment are reported in Fig. 7.16 as a function of ROP. Each line represents the system performance at each position of the highest peak of CCP with respected to the center of the ACP. The worst case scenario is obtained at the point which the highest peak of CCP is aligned at the center of the ACP. The receiver sensitivity at BER = 10^{-9} is found to be -30.34 dBm. The shift of

the CCP away from the center of the ACP resulting in the reduction of the overlapped period between the CCP and the ACP, and the PBN is reduced. As a result, the BERs are improved and the receiver sensitivities are lower in comparison to the worst case. The power penalties in order to achieve the BER = 10^{-9} as a function of delay, in comparison to the receiver sensitivity of the single-subscriber case, are observed and shown in Fig. 7.17, respectively. Moreover, with the delay of -400 and +400 ps, the CCP from these two cases is completely placed outside the ACP. Only the MAI noise is generated. Therefore, the BERs obtained from these two cases are limited by the MAI with the power penalty of 2.45 dB. In additions, the BER of the worst case is limited by the MAI and the PBN with the power penalty of 12.75 dB. Therefore, we can conclude that the power penalty caused by only the PBN is found to be 9.79 dB, respectively.

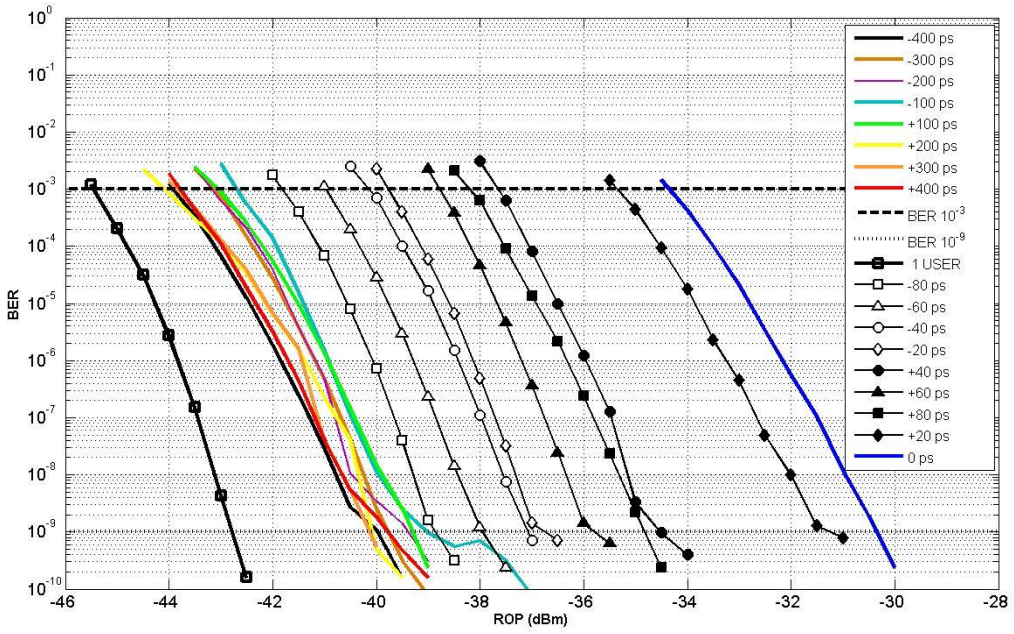

Fig. 7.16 BER performance from the case of 1-interfered subscriber using the adjacent code as a function of ROP.

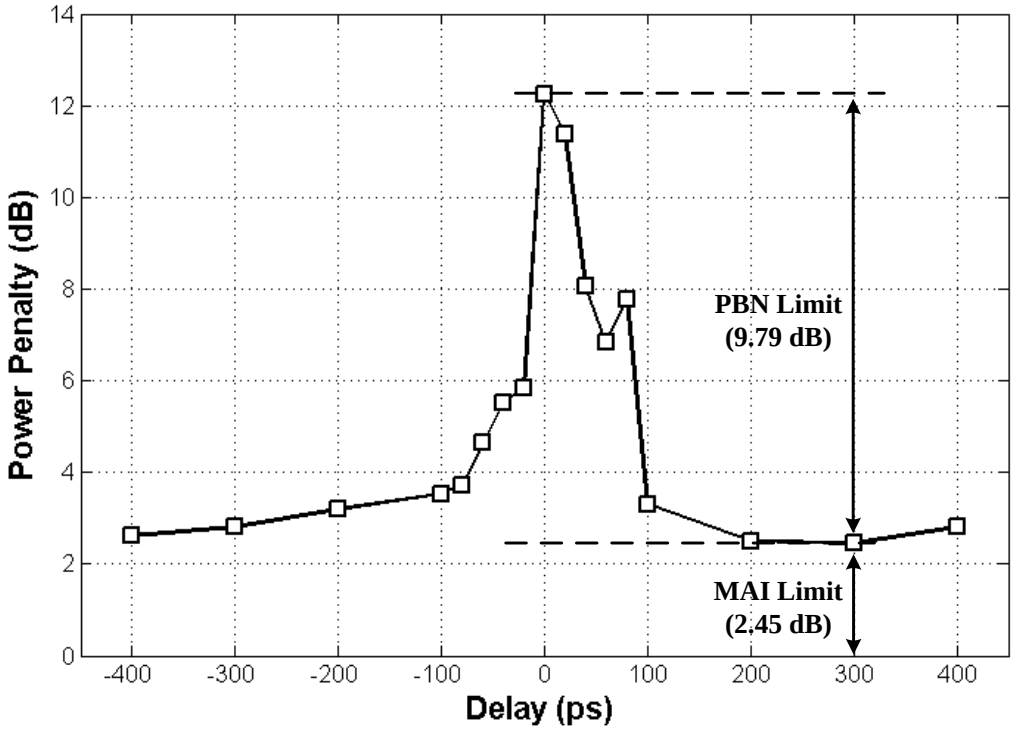

Fig. 7.17 The relation between the power penalty and the delay of the CCP.

7.3.2 PLC Case

We have manually adjusted 2 of the PLC encoders using code #8 with the phase difference between each consecutive chip of $7\pi/8$ as the desired subscriber, and code #9 which its phase difference between each consecutive chip is π as the interfered subscriber, respectively. The measured PCR between two codes, after decoded by the decoder with code #8, is approximately 6.91 dB. Therefore, the code performance of this manually adjusted en/decoder is worse than the AWG case by 0.84 dB. Fig. 7.18 shows the filtered electrical waveform of the ACP, CCP and the decoded signal obtained from the multiplexed signal between the desired and the interfered subscriber, respectively. The PBN signal from the beat terms causes the severe signal fluctuation that can lead to the error in the bit pattern recovery. Moreover, the strong MAI signal from the adjacent code can also bring the failure in the bit pattern recovery

The eye-diagram of the decoded optical signal and the filtered electrical signal is shown in Fig.7.19. This optical eye-diagram in Fig. 7.19(a) is captured from the worst case scenario. We cannot see the eye-opening around the center area of the ACP because of the strong signal interference, mainly from the PBN. This decoded optical signal is then filtered by the LPF and the electrical eye-diagram is shown in Fig. 7.19(b) with none of any eye-openings. The cut-off frequency of the LPF cannot eliminate all of the PBN caused by the 40-ps chip of the en/decoder. Moreover, the

cut-off frequency is 1.76 times higher than the system bit rate and this can bring more amount of receiver noise than usual. As a result, the eye-opening is closed for all available ROPs and we cannot measure the BER in this case.

Therefore, in this section, we can conclude that, by using the en/decoder with SBR = 0.8, we are unable to achieve the BER = 10^{-9}. On the contrary, by using the en/decoder with SBR = 0.1, we can achieve the BER = 10^{-9} with the maximum power penalty of 12.24 dB.

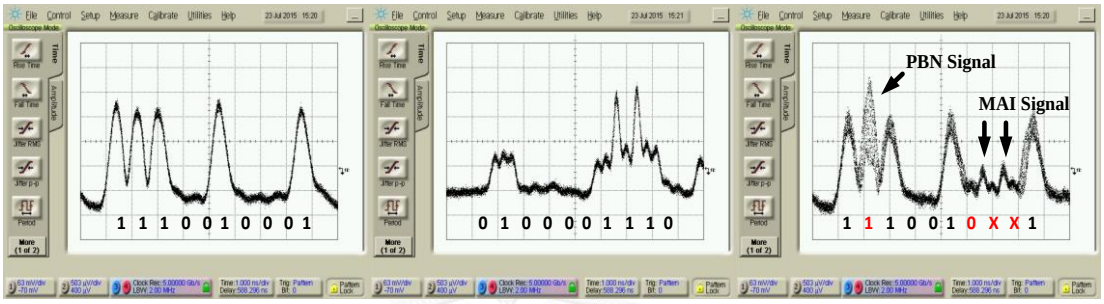

(a) (b) (c)

Fig. 7.18 Filtered electrical signal obtained from (a) desired subscriber, (b) interfered subscriber and (c) multiplexed signal of the desired and interfered subscriber.

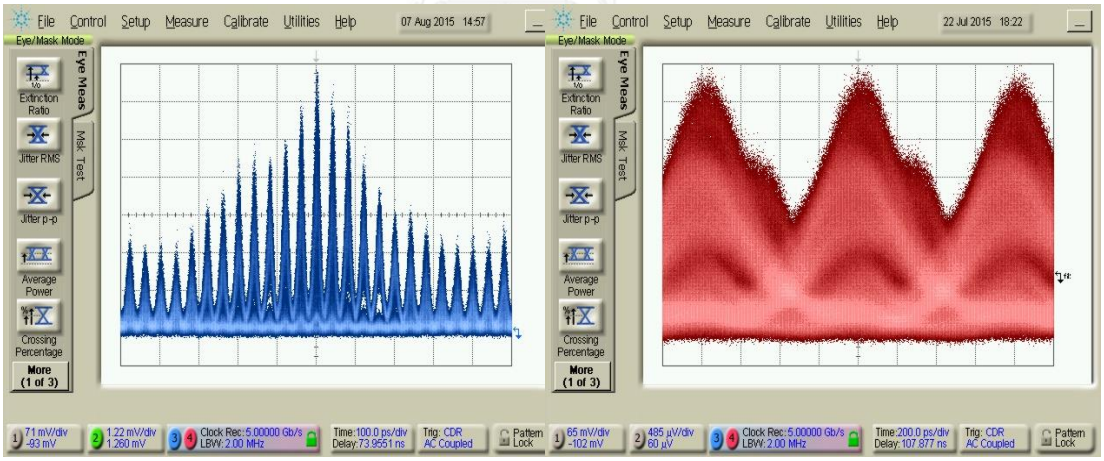

(a) (b)

Fig. 7.19 Eye-diagram of the decoded signal (a) optical waveform and (b) electrical waveform.

7.4 System Performance of 1-Interfered Subscriber Case (Non-Adjacent Code)

In the previous section, we show the experiment setup and its results for the case of 1-interfered subscriber using the adjacent code is already discussed. It is clearly seen that the PBN is very strong for the case of SBR so that we cannot measure the BER. Therefore, in this case, we skip the adjacent code and use the next code instead. Since the PCR level of the skipped code is lower than the adjacent code, the interference level can be reduced so that we can measure the BER and can make a comparison of the system performance between the AWG and the PLC case, respectively.

7.4.1 AWG Case

We use the signal obtained from the input port #11/output port #9 of the AWG encoder as an interfered subscriber in this case. After we have multiplexed the desired and the interfered subscriber together, the optical spectrum is shown in Fig. 7.20(a). The channel spacing between these two codes, also known as the code spacing, is 0.2 nm which is in agreement with the theory. At the AWG decoder, the optical spectrum of the signal after decoded by decoder using input-port #9/output-port #9 is shown in Fig. 7.20(b). The spectrum of the interfered subscriber is attenuated by the frequency response of the decoder. Therefore, the dominant spectrum comes from the desired subscribers, respectively.

The optical eye-diagrams at various delays of the interfered subscriber are shown in Fig. 7.21. As expected, the eye-opening of the worst case in Fig. 7.21(a) is wider than Fig. 7.13(a). The reason is the power of the CCP in this case is lower than the CCP employing the adjacent code. Therefore, the beat terms in this case are not as severe as stated in the case of using the adjacent code. The left shift of 60 ps in Fig. 7.21(b) represents the eye-diagram with the clear eye-opening because the highest peak of the CCP is shifted to the left and most of the interference is occurred at the left side of the ACP. Moreover, eye-diagrams in Fig. 7.21(c)-(d) look like the case of single-subscriber since the right shift of the CCP cause only the MAI signal outside the ACP period.

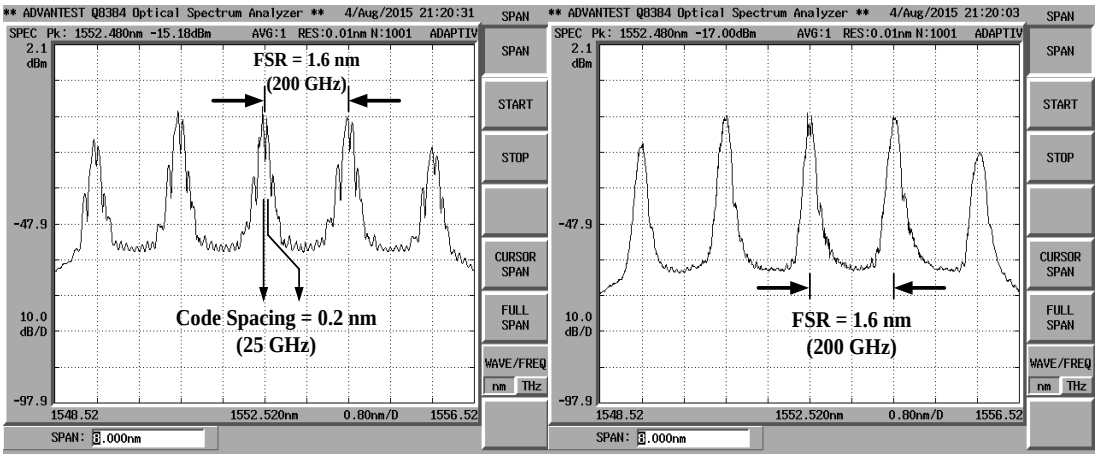

(a) (b)

Fig. 7.20 Optical spectrum (a) encoded signals (b) decoded signal.

Fig. 7.22 shows the filtered electrical eye-diagram of the desired subscriber at various delays of the interfered subscriber. Most of the PBN caused by the interfered subscriber can be removed by the LPF, resulting in the large eye-opening in Fig. 7.22(a)-(b) with the average V_{p-p} of 193.2 and 156.0 mV, respectively. On the other hand, the eye-diagrams in Fig. 7.22(c)-(d) represent the case which the CCPs are placed outside the ACP with the delay of 200 and 400 ps. Therefore, there is no any PBN at the ACP so that we can obtain lower V_{p-p} than the case in Fig. 7.22(a)-(b). The V_{p-p} in Fig. 7.22(c) and (d) are 93.6 and 97.5 mV, respectively.

The BER of this case is already shown in Fig. 7.23. By using the skipped code, we can achieved the BER = 10^{-9} for all delays of the interfered subscriber. In the worst case, the receiver sensitivity is -39.07 dBm. As expected, the BER and the receiver sensitivity are improved in comparison to the adjacent-code case. For the case of the CCP which its position is placed outside the ACP, the signal distortion caused by MAI is very small. The BER performance is very close to the BER line which is obtained from the single-subscriber case.

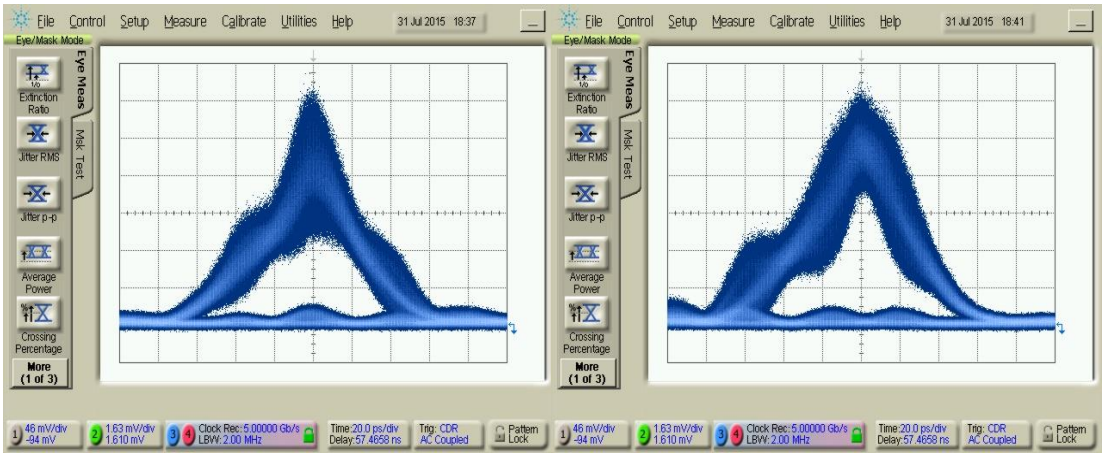

(a) (b)

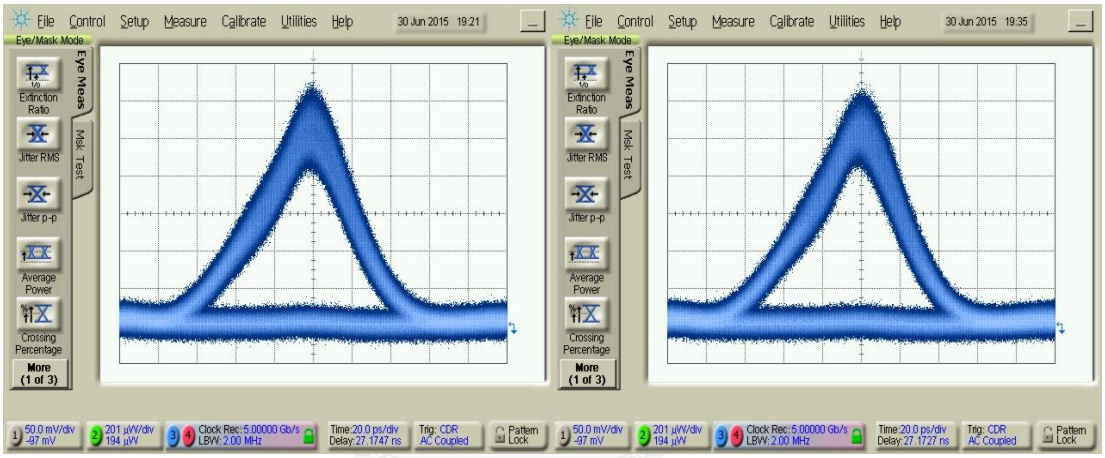

(c) (d)

Fig. 7.21 Eye-diagrams of the decoded optical signals with various delays (a) 0 ps, (b) +60 ps, (c) +200 ps and (d) +400 ps.

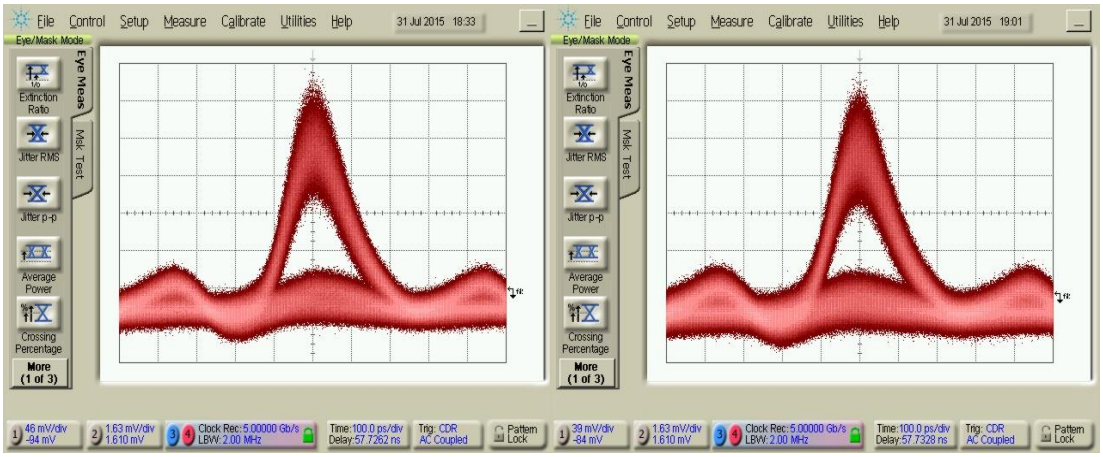

(a) (b)

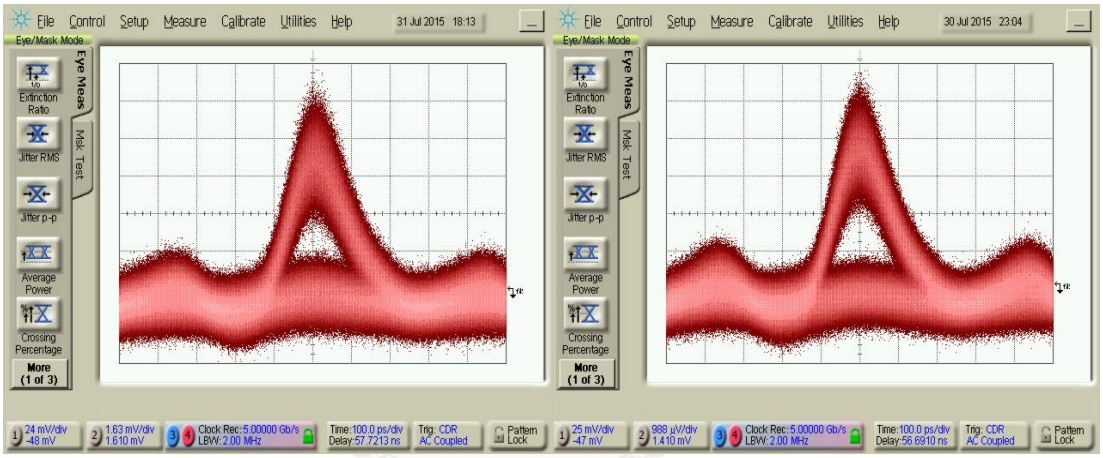

(c) (d)

Fig. 7.22 Eye-diagrams of the decoded optical signals with various delays, obtained at (a) 0 ps, (b) +60 ps, (c) +200 ps and (d) +400 ps.

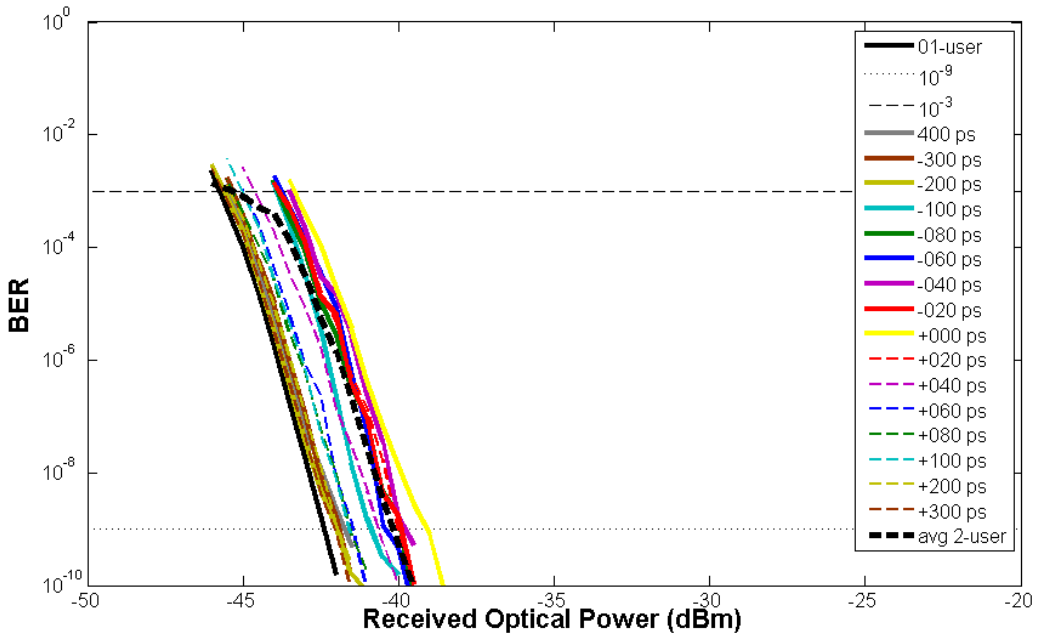

Fig. 7.23 BER performance as a function of ROP, obtained from the case of 1-interfered subscriber (non-adjacent code) using AWG device.

7.4.2 PLC Case

The third PLC encoder device is added into the experiment setup as the interfered subscriber. We adjust the phase difference between each consecutive chip is $9\pi/8$ so that we can generate the encoded signal with code #10. The optical spectrum of the multiplexed signal is shown in Fig. 24. The code spacing between code #8 and #10 of 0.025 nm is according to the theory. Then, after the decoding process, the spectrum of code #10 is attenuated by the frequency response of the desired decoder. Therefore, the spectrum of the desired subscriber is dominant as shown in Fig. 7.24(b).

The interference caused by the interfered subscriber using code #10 is reduced so that we can obtain the eye-opening in the electrical eye-diagram. Fig. 7.25 shows the filtered electrical eye-diagram obtained at various delays of the interfered subscriber. All of the eye-diagrams are observed at BER = 10^{-9}. Nevertheless, all eye-diagrams are suffered from the interference caused by PBN and the LPF cannot remove these beat terms so that it resulting in the thickness in the eye-diagrams. The V_{p-p} in Fig. 7.25(a)-(d) are 292.0, 284.7, 262.2, and 285 mV, respectively. We also measure the BER, as a function of ROP, and it is shown in Fig. 7.26, respectively. From our best case, obtained at the left shift with the delay of 160 ps, the receiver sensitivity is -33.36 dBm. The power penalty of this case in comparison to the single-subscriber case is 8.1 dB. Since the SBR = 0.8 has no of any guard-time periods, at all chip positions, the PBN is generated and all of the BERs for the case of 1-interfered subscriber are limited by the effect of the PBN and the MAI, respectively.

The observed receiver sensitivities at BER = 10^{-9}, for both the AWG and PLC devices, at various delays of the interfered subscriber are collected and then plotted in Fig. 7.27 as a power penalty in comparison to the single-subscriber case. The maximum power penalty, at the delay of 0 ps, obtained from SBR = 0.1 and 0.8 are 3.31 and 13.99 dB, respectively. This also confirms that by employing SBR = 0.1 is capable of reducing the effect of PBN. Moreover, for the case of SBR = 0.1, the incoming signal from the interfered subscriber has the probability to launch to the system outside the ACP period of the desired subscriber. As a result, we can avoid the PBN generation and the desired ACP will be deteriorated by the MAI only. For the case of SBR = 0.8, the PBN can be generated at any available chip positions over one bit period so that the power penalty in this case is limited by the effect of PBN and MAI, respectively.

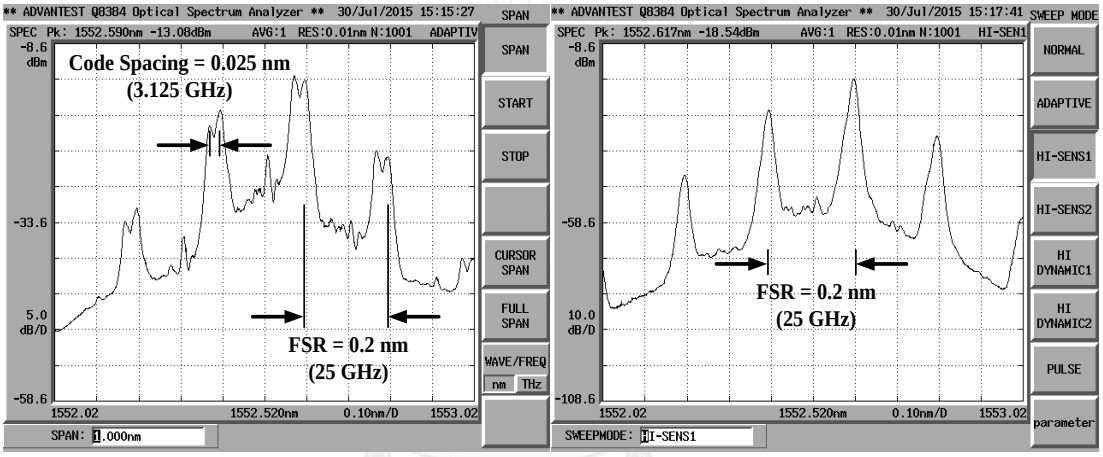

(a) (b)

Fig. 7.24 Optical spectrum (a) encoded signals (b) decoded signal.

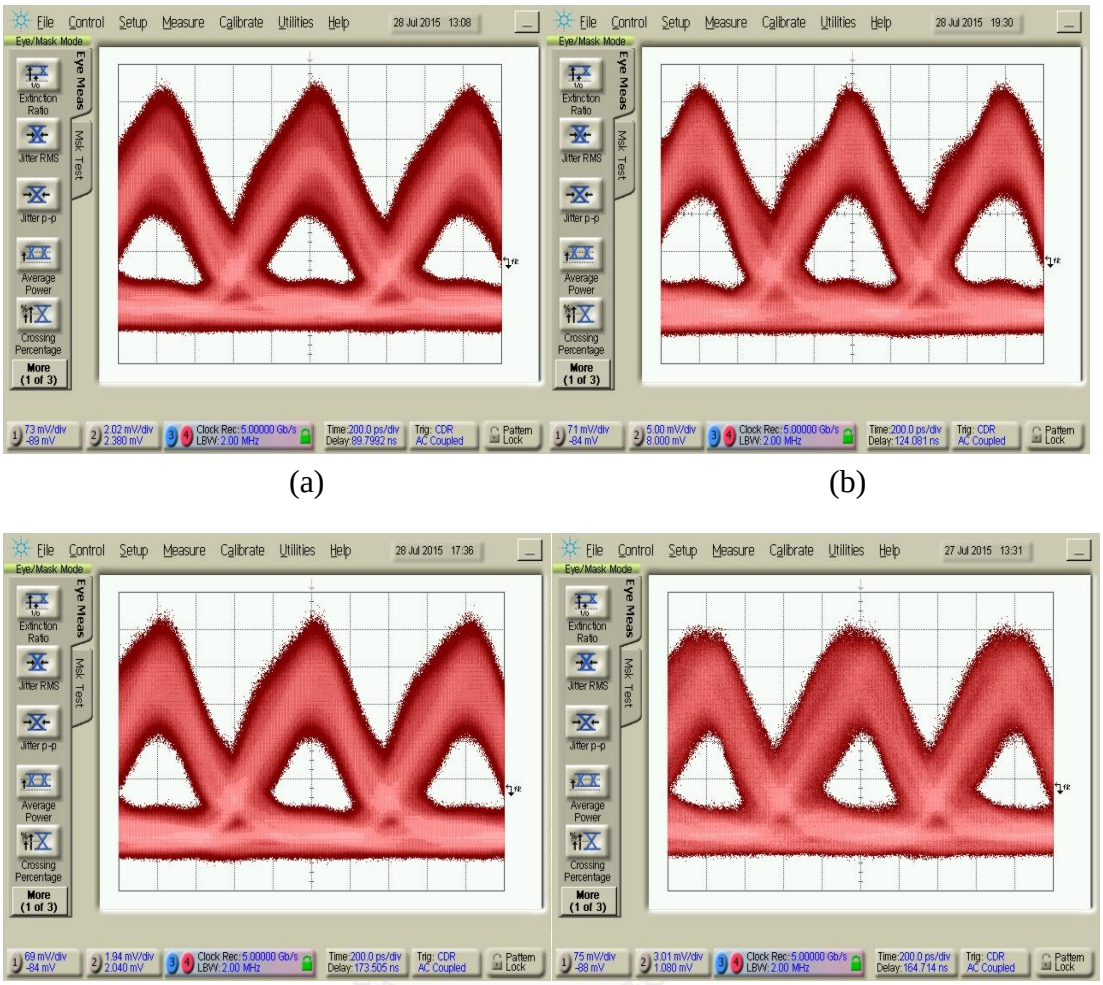

Fig. 7.25 Eye-diagrams of the filtered electrical signals with various delays, obtained at BER = 10 (a) 0 ps, (b) +240 ps, (c) +320 ps and (d) +400 ps.

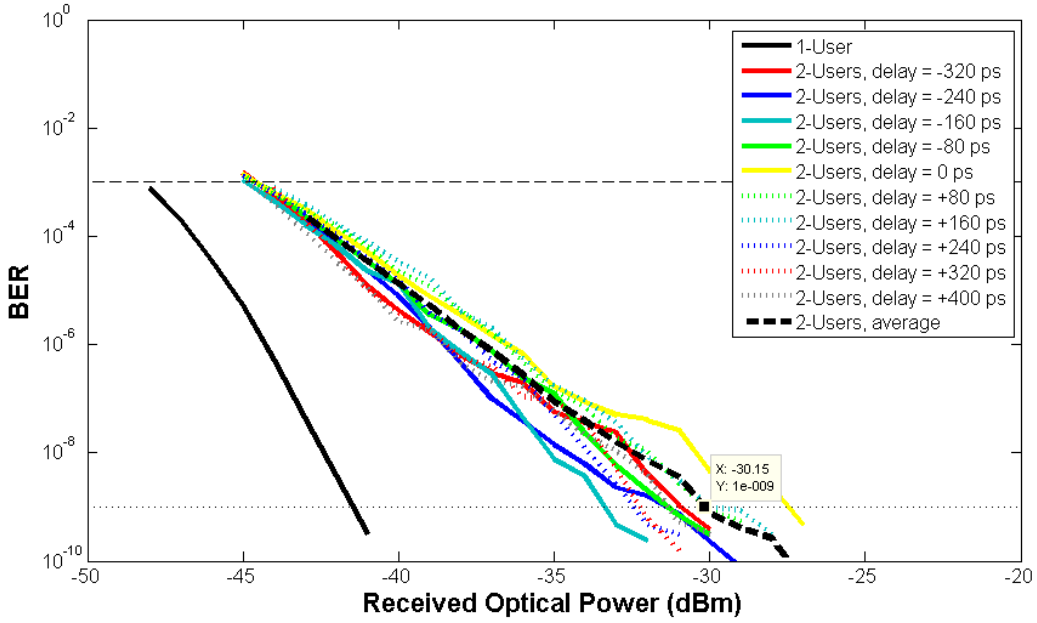

Fig. 7.26 BER performance as a function of ROP, obtained from the case of 1-interfered subscriber (non-adjacent code) using PLC device.

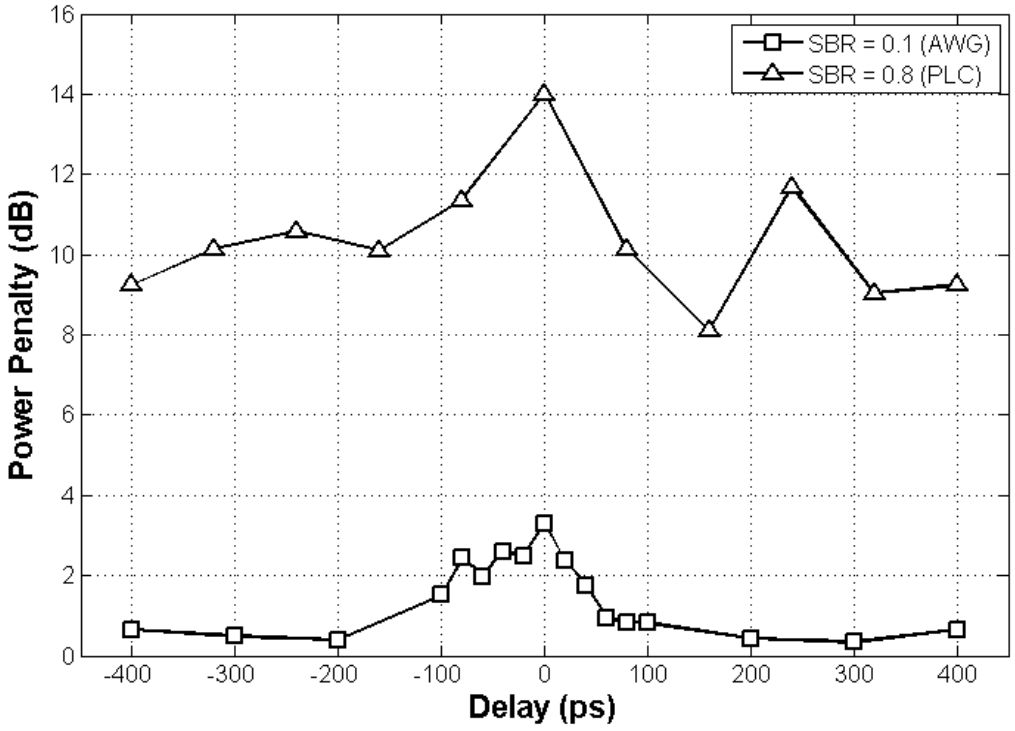

Fig. 7.27 Power penalty for the case of 1-interfered subscriber in comparison to the single-subscriber case, obtained at various delays in one bit period.

7.5 System Performance of 2-Interfered Subscriber Case

In order to confirm that the performance of the desired subscriber is performed under the worst case, we setup the experiment by adding the 2nd interfered subscriber to the system. In this case, the signal quality of the desired subscriber is degraded by two interfered subscribers. Therefore, the signal interferences are mainly governed by the PBN, the MAI, and the SBN, respectively. It should be note that, the code spacing between the desired and the 1st and the 2nd interfered subscriber must be the same.

7.5.1 AWG Case

In this case, we use the input port #7/output port #9 of the AWG encoder as the 2nd interfered subscriber. The optical spectrum of all encoded signals after multiplexing is shown in Fig. 7.28(a). In each FSR, the spectrum of the desired subscriber is the center peak whereas the spectrums of the interfered subscribers are placed at the left and the right side of the center peak the equal code spacing of 0.2 nm, respectively. After the decoding process, both spectrums of the interfered subscribers are attenuated by the frequency response of the decoder. Only the spectrum of the desired subscriber is matched to the frequency response of the decoder. Consequently, the decoded spectrum shown in Fig. 7.28(b) is dominated by the spectrum of the desired subscriber.

The alignment of each interfered subscriber must be considered to guarantee the worst case scenario. Therefore, we adjust the highest peak of the CCP from the 1st and the 2nd interfered subscriber to be the center of the desired ACP. The most severe fluctuation in the optical waveform mainly caused by the PBN at the center of the desired ACP is captured and shown in Fig. 7.29(a). The destructive interference at the center of the ACP is so strong that we cannot achieve the eye-opening in this case. The left shift of these two CCPs by 20 ps also causes the strong interference, but the most severe point is shifted to the left and we can achieve the small eye-opening in this case, as shown in Fig. 7.29(b). Moreover, in Fig. 7.29(c), the CCPs are shifted by 100 ps to the left. Only few parts of the CCPs cause the PBN around the left part of the CCP. Nevertheless, at the center of the ACP, the eye-opening is large due to none of any PBN, MAI, and SBN signals around this area. In Fig. 7.29(d), the CCPs are completely shifted outside the ACP period. There is only MAI and SBN in this case. Obviously, the eye-diagram of the ACP in Fig. 7.29 is very clear due to there is no PBN, MAI and SBN around the ACP.

At the receiver, the filtered electrical signals, obtained at BER = 10^{-9}, at various delays of the CCPs are shown in Fig. 7.30. Since the signal distortion in the optical waveform, mainly caused by the PBN, MAI, and SBN, is maximized in Fig. 7.29(a), we should obtain the largest difference in V_{p-p} in order to achieve the BER = 10^{-9}. Moreover, the degrees of the interference in the optical waveform are mitigated in Fig. 7.29(b)-(c) and it is minimized as shown in Fig. 7.29(d), in comparison to the worst case, respectively. Therefore, the V_{p-p} in each case is decreased due to the noises are reduced. As a result, the measured V_{p-p} obtained from Fig. 7.30(a)-(d) are 332.1, 176.3, 142.8, and 110.5 mV, respectively.

For the worst case, as we can see that the optical waveform in Fig. 7.29(a) has the extremely strong interference so that the electrical waveform obtained in Fig. 7.30(a) has the largest V_{p-p} among the other cases in order to achieve the BER = 10^{-9}. The measured BER, shown in Fig. 7.31, for the case of 2-interfered subscribers, at the delay of 0 ps, confirms the performance of the worst case with the receiver sensitivity at BER=10^{-9} of -37.76 dBm. Furthermore, the BER is improved when the highest peak of 2 CCPs is shifted away from the center of the ACP and the effect of the PBN can be reduced. As a result, the best BER can be obtained at the delay of 400 ps. Since there is no PBN signal generation, the BER of the best case is limited by the MAI at the receiver sensitivity of -43.63 dBm.

The power penalty of all cases, with respected to the single-subscriber case, is illustrated in Fig. 7.32. All of the power penalties obtained in the case of 2-interfered subscribers are obviously higher than the 1-interfered subscriber case due to suffering from the greater interference level. The maximum power penalty is 5.87 dB. At this point, the power penalty is mainly caused by the PBN, the MAI, and the SBN. On the other hand, the minimum power penalty of 0.91 dB which is caused by only the MAI and the SBN, can be seen at the delay of 400 ps.

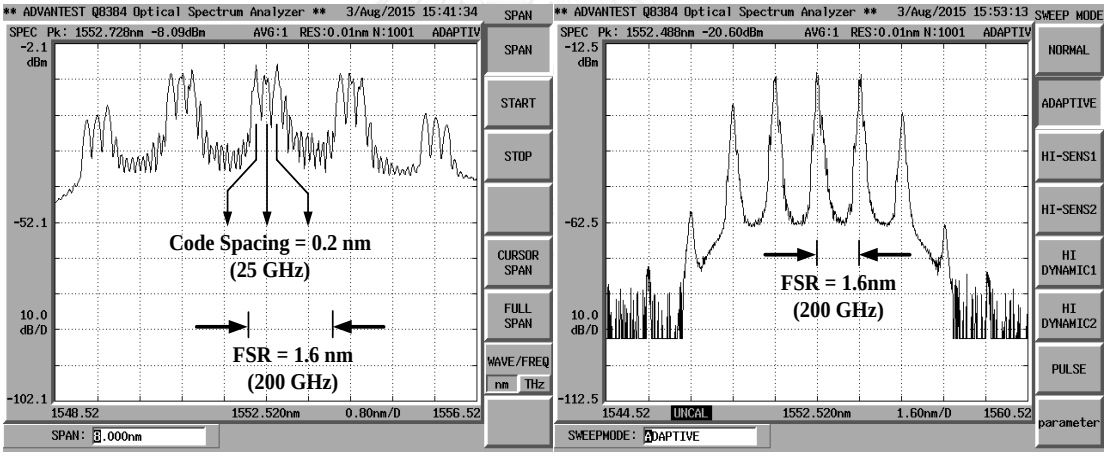

(a) (b)

Fig. 7.28 Optical spectrum of the 2-interfered subscribers case obtained from the AWG device (a) encoded signal and (b) decoded signal.

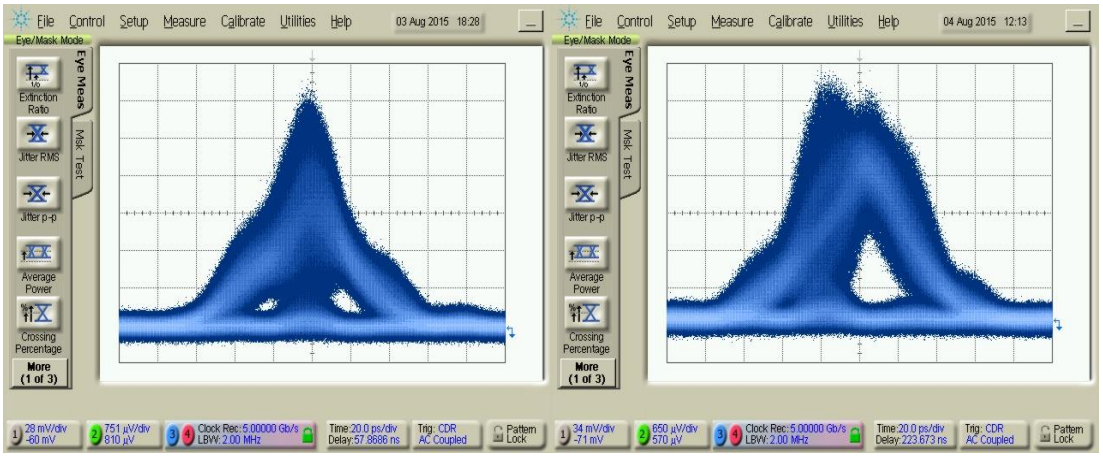

Fig. 7.29 Eye-diagrams of the decoded optical signals with various delays (a) 0 ps, (b) -20 ps, (c) -100 ps and (d) -400 ps.

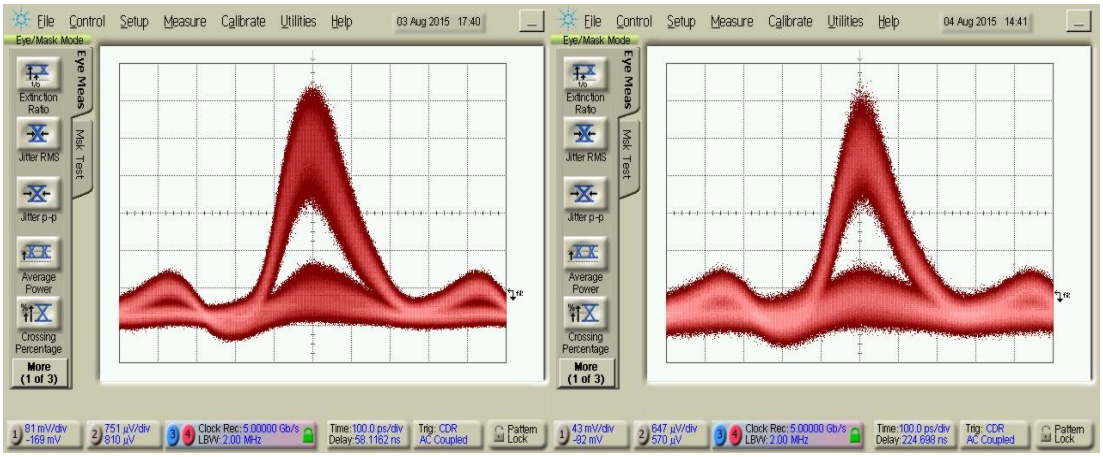

Fig. 7.30 Eye-diagrams of the filtered electrical signals with various delays, obtained at BER = 10 (a) 0 ps, (b) -20 ps, (c) -100 ps and (d) -400 ps.

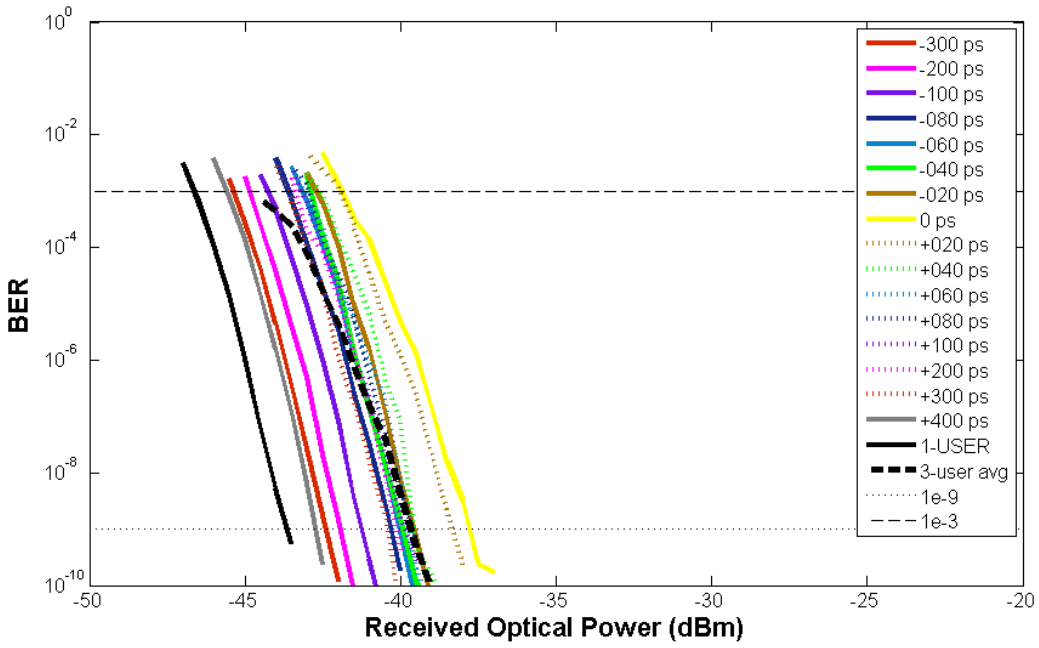

Fig. 7.31 BER performance as a function of ROP, obtained from the case of 2-interfered subscriber (non-adjacent code) using AWG device.

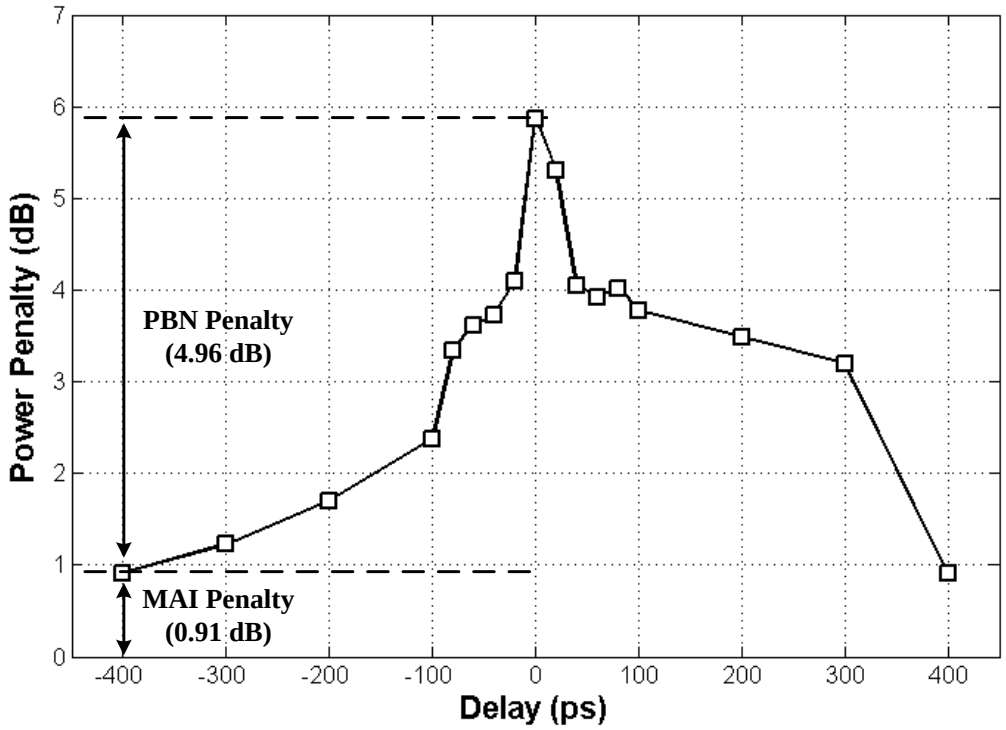

Fig. 7.32 Power penalty for the case of 2-interfered subscriber using AWG device, in comparison to the single-subscriber case, obtained at various delays in one bit period.

7.5.2 PLC Case

The 2nd interfered subscriber is assigned to use code #6. Therefore, both two interfered subscribers employing code #6 and code #10 have the code spacing of 0.0125 nm with respected to the desired subscriber employing code #8. The optical spectrum of all encoded signals is shown in Fig. 7.33(a). Then, after the decoding process, the decoded spectrum is shown in Fig. 7.33(b). In order to obtain the worst case scenario, in the time domain, the highest peak of each CCP is aligned at the center of the ACP. The strong interference causes the fluctuation in the optical signal as shown in Fig. 7.34. At the center peak of the ACP, we cannot obtain the eye-opening in the optical eye-diagram. Although we have adjusted the delay of two CCPs, the eye-opening at the center of the ACP is still closed. Therefore, the interference caused by the PBN, the MAI, and the SBN is very strong at every available chip of one bit period.

The filtered electrical signal at each delay of two CCPs is captured and shown in Fig. 7.35. We can see that, in all sub-figures, the thickness of the amplitude of bit with mark "1" is very large and the eye-opening is very small. This is because the interference from PBN is very strong at every delay of the two CCPs and the LPF cannot remove the PBN signal. Furthermore, all eye-diagrams in Fig. 7.35 with the V_{p-p} of 249, 226.3, 262.4, and 92 mV cannot achieve the BER = 10^{-9}. The BER of all cases is shown in Fig. 7.36 with the error floor approximately at BER = 10^{-3}, respectively.

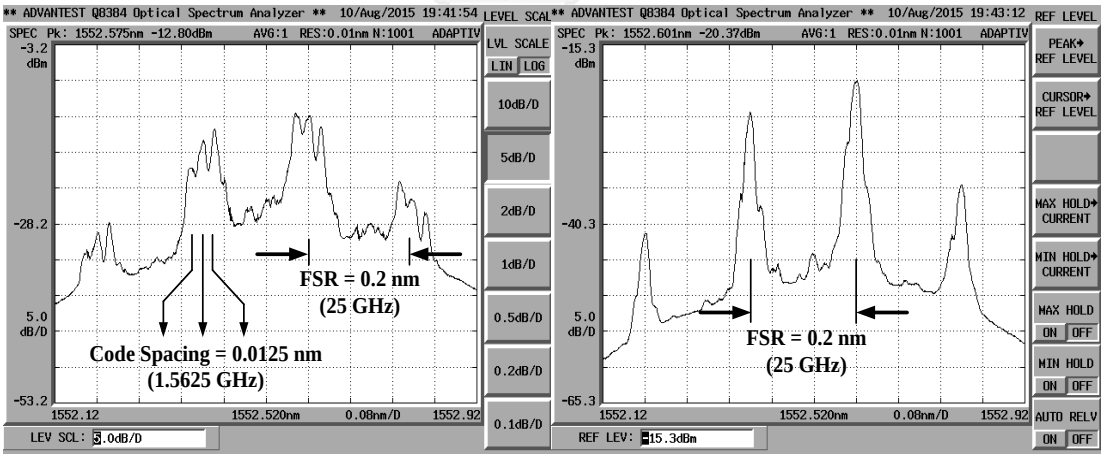

(a) (b)

Fig. 7.33 Optical spectrum of the 2-interfered subscribers case obtained from the PLC device (a) encoded signal and (b) decoded signal.

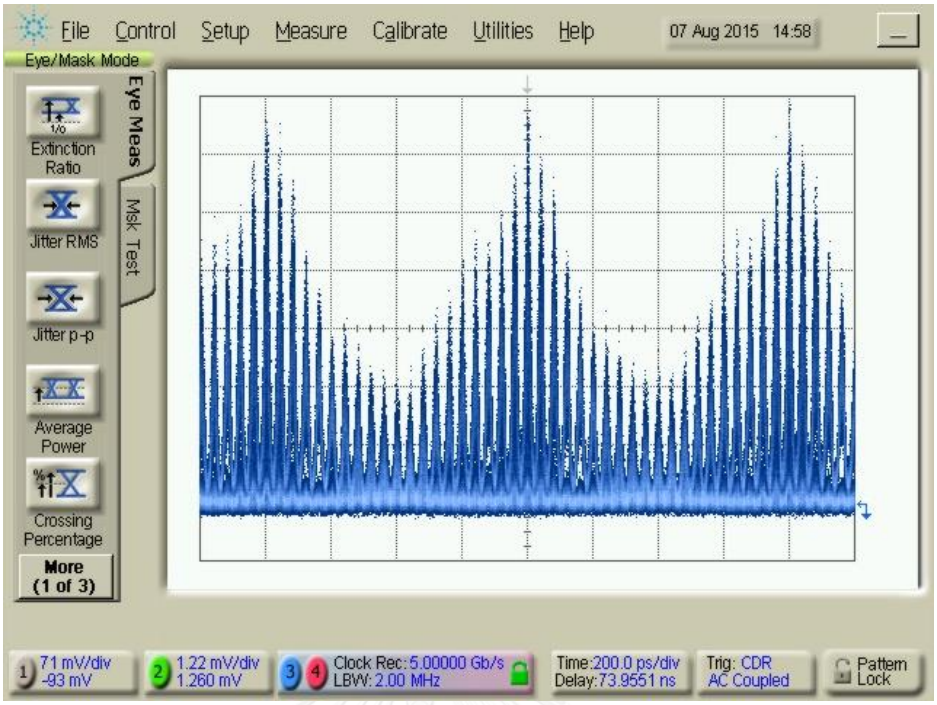

Fig. 7.34 Optical eye-diagrams for the case of 2-interfered subscribers with the delay of 0 ps.

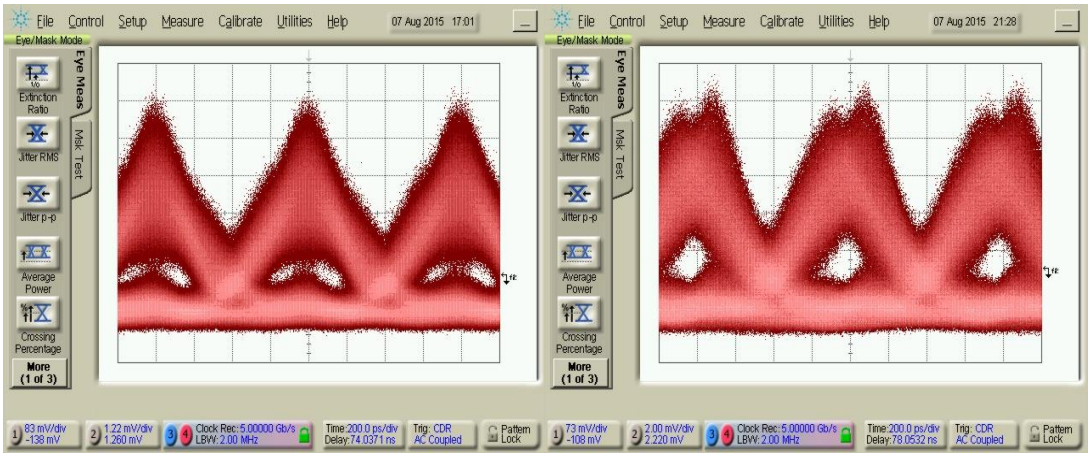

(a) (b)

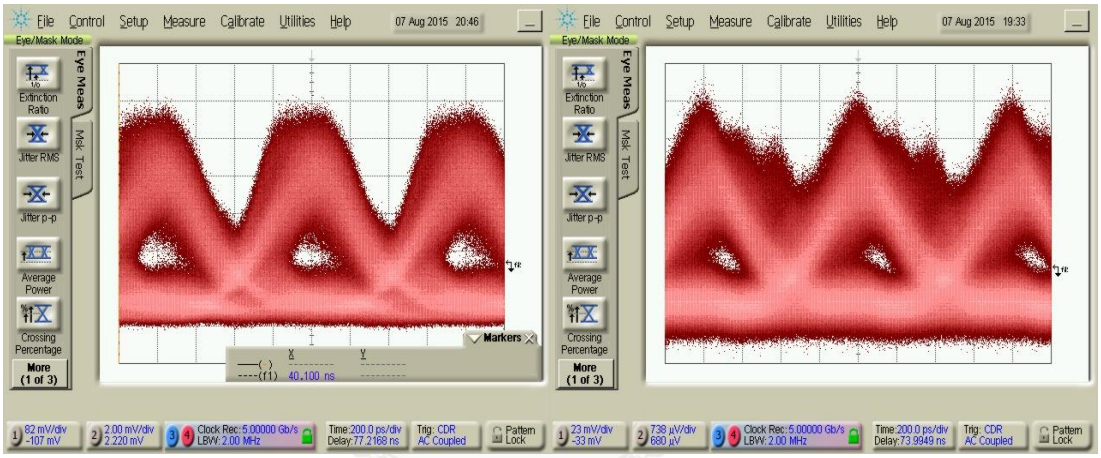

(c) (d)

Fig. 7.35 Eye-diagrams of the filtered electrical signals with various delays (a) 0 ps, (b) +160 ps, (c) -160 ps and (d) -80 ps.

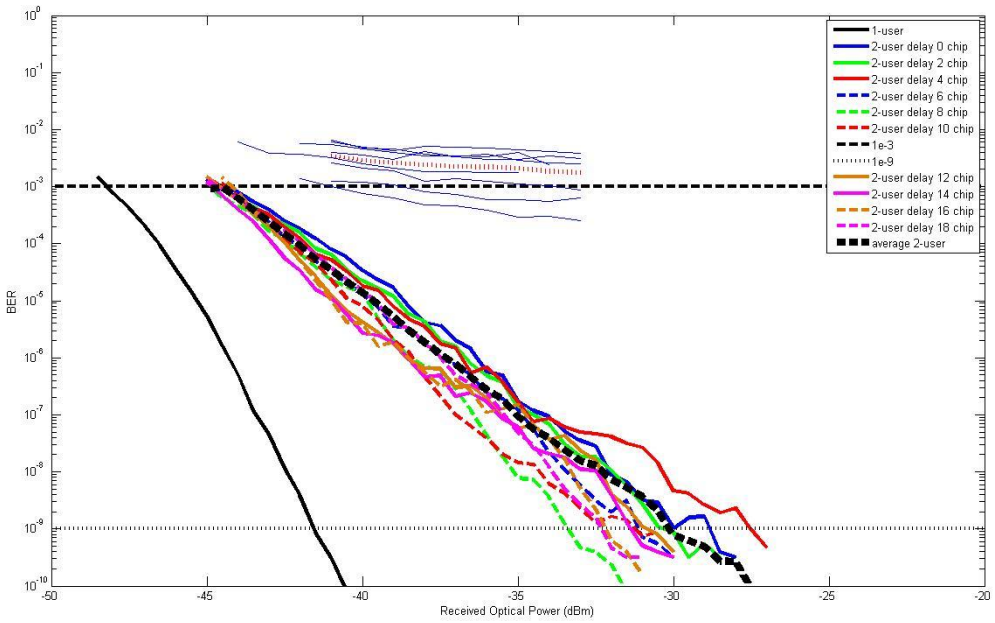

Fig. 7.36 BER performance as a function of ROP, obtained from the case of 2-interfered subscriber (non-adjacent code) using PLC device.

7.6 Average Performance of the system

One of the most advantages of the OCDM system is the asynchronous transmission which the subscribers can access to the system at any time. There is no need for the strict-time synchronization between the OLT and the ONUs. Therefore, the random access of each ONU resulting in various interference levels at the desired ONU. The BER measurements in section 7.3-7.5 show that, the BER is depended on the position of the interfered subscriber. Since each position of the CCP generates different amount of the interference level caused by the PBN and the MAI, at each position of the CCP, we can obtain different BER. We have already shown the BER at the worst case scenario which the peak of the CCP is aligned at the center of the ACP in order to confirm the greatest interference. All of the worst cases from our three experiment setups are already stated in section 7.3-7.5. Furthermore, we have shown the possibly best cases which are suffered from the lowest amount of the interference in each experiment.

Therefore, in this section, we would like to introduce the average BER of the system computed by using our measurement results. The average BER can be used to represent the average performance of the OCDM system in an asynchronous transmission. We will discuss, in section 7.6.1, the numerical BER based on the probability of m interfered subscribers access to the system at each delay. Then, the average BER for the case of 1-interfered subscriber using the adjacent code, 1-interfered subscriber using non-adjacent code, and 2-interefered subscribers are shown and discussed in section 7.6.2, respectively.

7.6.1 Average BER Expression

In order to calculate the average BER of the system at m interfered subscribers, we define the average BER of the system as,

$$BER = \sum_{i=1}^{k} p(i) \cdot BER(i), \tag{7.1}$$

where i is the index number from 0 to total number of the measurement cases. $p(i)$ is the probability that group of m interfered subscribers can be located on the specific point over one bit period. $BER(i)$ is the measured BER of the case with index number i.

From our experiments, we have divided the point of interest to be measured into many points. For examples, we perform the BER measurement at the point which the group of interfered subscribers is delayed by 0, -20, -40, and -60 ps and so on with respected to the center of the ACP. Since we cannot measure the BER at all points over one bit period, we must take into account the specific point that can be used to represent the individual BER over a small period of occupying time Δt_i. Therefore, the probability $p(i)$ can be calculate as,

$$p(i) = \frac{\Delta t_i}{T_b}, \tag{7.2}$$

where T_b is the bit period. Moreover, it should be noted that, the cumulative distribution function (CDF) of the probability $p(i)$ must be equal to 1.

7.6.2 The Average BER for the Case of 1 and 2-Interfered Subscribers

The point of interests to be measured for the case of AWG and PLC device are shown in Fig. 7.37. For the AWG case, the period of the ACP is approximately 155 ps and the most of the interference from PBN occurs around this period. Therefore, we pay much attention over this period and we divide the point of interests by a step of 20 ps ranging from -100 to 100 ps. Then, outside the ACP period, most of the interference comes from the MAI and most of the BERs in this period are nearly the same so that we can divide our point of interests with the larger step of 100 ps, respectively. For the PLC case, the ACP which its period of 1240 ps is exceeded from one bit period of 800 ps, the interference from PBN can be generated all over a bit period. Consequently, the division of the point of interests is performed equally by a step of 80 ps over a whole bit period.

The occupying period Δt_i of each point of interest should be obtained so that we can calculate the probability $p(i)$. The middle point between each consecutive point of interest is considered as the boundary. Therefore, we measure the width between each boundary and defined as the occupying period Δt_i. For the AWG case, the boundary of each point of interest is illustrated by the dash line in Fig. 7.38 and

the occupying periods are also shown. Similarly, the boundary of each point of interest and its occupying period for the PLC case is shown in Fig. 7.39. Finally, the probability of the group of m interfered subscribers can access to each position over one bit period is calculated and shown in Table 7.1-7.2, respectively.

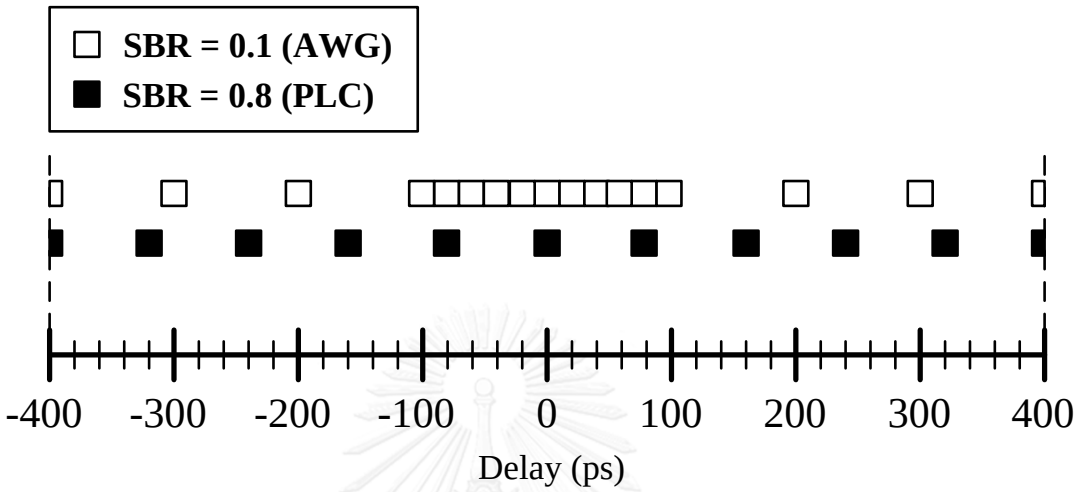

Fig. 7.37 The measurement point for both the AWG and the PLC case.

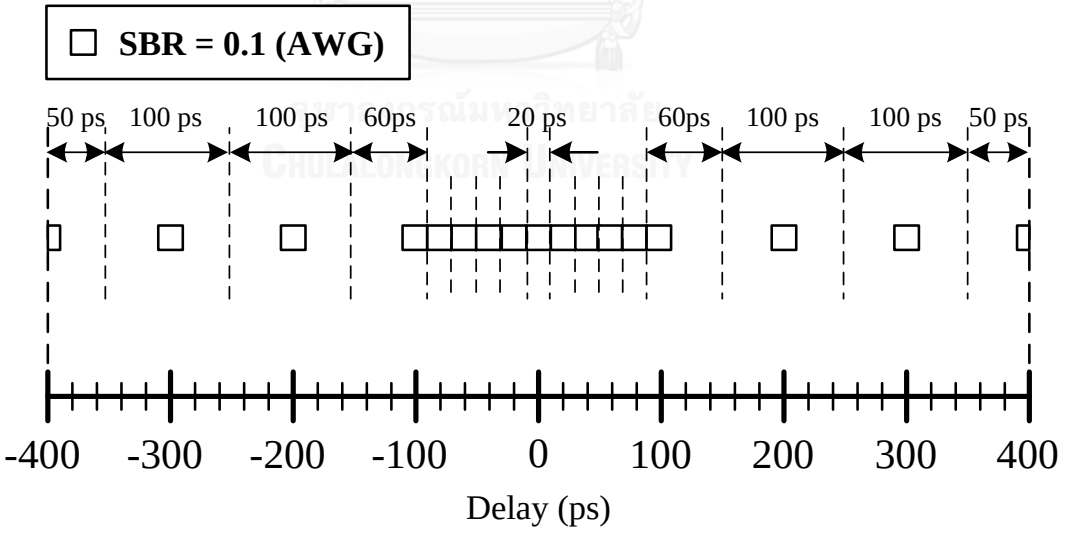

Fig. 7.38 The boundary and the occupying time of each point of interest for the case of AWG en/decoder.

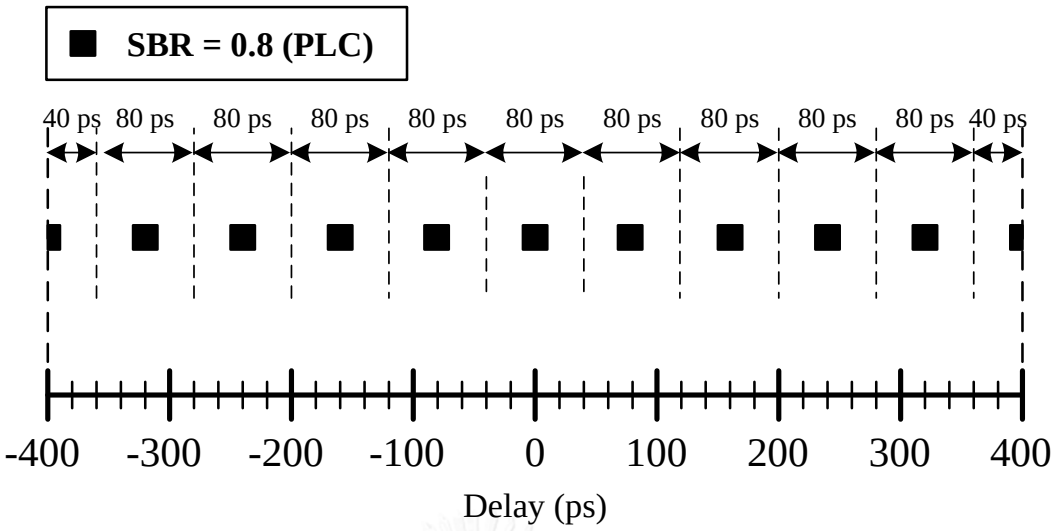

Fig. 7.39 The boundary and the occupying time of each point of interest for the case of PLC en/decoder.

Table 7.1 Calculated probability for the case of AWG en/decoder.

Case Number i	Position (ps)	Occupying Time Δt_i (ps)	Probability p_i	CDF
1	-400	50	0.0625	0.0625
2	-300	100	0.125	0.1875
3	-200	100	0.125	0.3125
4	-100	60	0.075	0.3875
5	-80	20	0.025	0.4125
6	-60	20	0.025	0.4375
7	-40	20	0.025	0.4625
8	-20	20	0.025	0.4875
9	0	20	0.025	0.5125
10	20	20	0.025	0.5375
11	40	20	0.025	0.5625
12	60	20	0.025	0.5875
13	80	20	0.025	0.6125
14	100	60	0.075	0.6875
15	200	100	0.125	0.8125
16	300	100	0.125	0.9375
17	400	50	0.0625	1.000

Table 7.2 Calculated probability for the case of PLC en/decoder.

Case Number i	Position (ps)	Occupying Time Δt_i (ps)	Probability p_i	CDF
1	-400	40	0.05	0.05
2	-320	80	0.1	0.15
3	-240	80	0.1	0.25
4	-160	80	0.1	0.35
5	-80	80	0.1	0.45
6	0	80	0.1	0.55
7	80	80	0.1	0.65
8	160	80	0.1	0.75
9	240	80	0.1	0.85
10	320	80	0.1	0.95
11	400	40	0.05	1.00

For the AWG case, Fig. 7.40 shows the BERs of the worst case scenario for the case of 1 and 2-interfered subscribers. Moreover, the average BERs of those cases are also shown. It reveals that, all BERs of the average case are improved. The receiver sensitivities are -31.26, -40.18, and -39.66 dBm so that the improvement in the receiver sensitivities in comparison with the worst cases are 0.93, 1.11, and 1.90 dB, for the case of 1-interfered subscriber with adjacent code, 1-interfered subscriber with non-adjacent code, and 2-interfered subscribers respectively.

For the PLC case, the average BERs are shown in Fig. 7.41. We found that, by employing 1-interfered subscriber, the average case can improve the receiver sensitivity by 2.69 dB in comparison with the worst case with the receiver sensitivity of -30.16 dBm. Nevertheless, for the case of 2-interfered subscriber, the BER of the average case is improved with the error floor of BER = 10^{-3}, respectively.

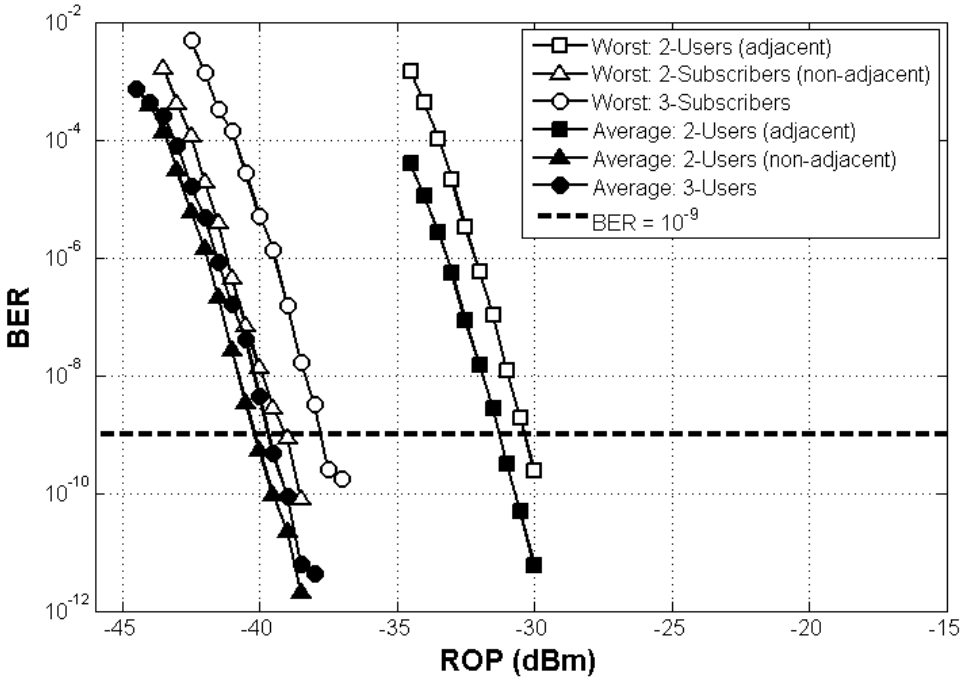

Fig. 7.40 The worst and the average BER obtained from the AWG device.

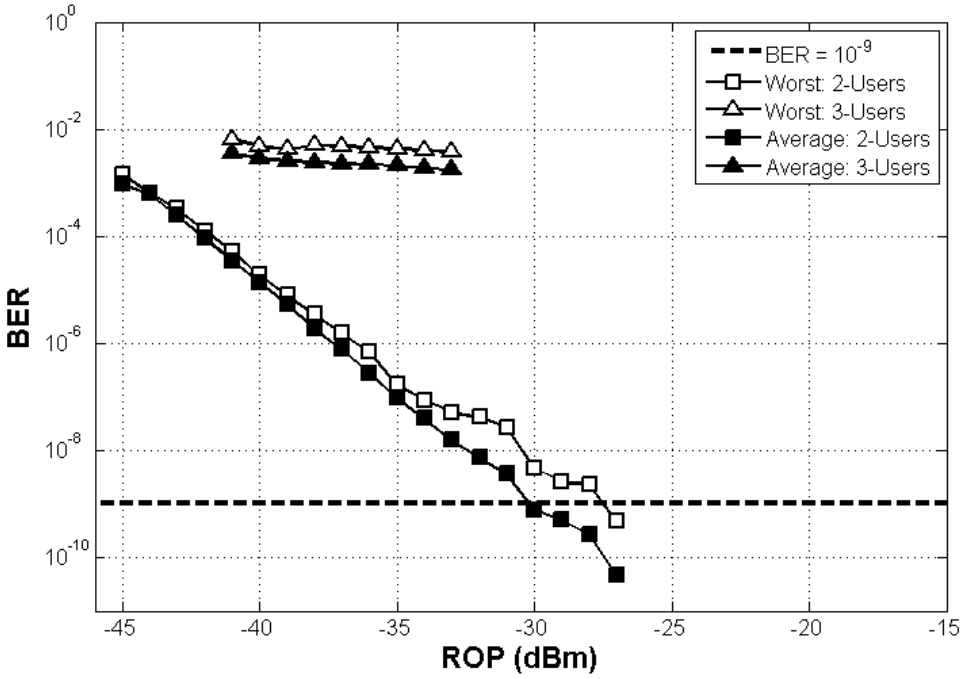

Fig. 7.41 The worst and the average BER obtained from the PLC device.

CHAPTER 8 Thesis Conclusion

The aim of this thesis is to propose the solution to suppress the noise in the coherent time-spreading OCDMA-PON at a bit rate per subscriber of 40 Gbps. The Fourier code which the phase difference between each consecutive chip of π / N was used in this thesis due to its greater PCR with small number of chips in comparison to the other types of code. The en/decoding process was performed by a programmable multi-level phase-shifted en/decoder. In chapter 3, we show that the more number in number of chips brought a greater PCR value in comparison to the case of low number of chips. In chapter 4, a novelty mathematical model in order to shape the length of the total encoding period with the factor SBR was proposed. In this case, the number of chips for each SBR was constant. We showed the calculated BER under Gaussian approximation of the signals obtained at each SBR from the worst and the average case. The mathematical calculation results from chapter 4 were verified by using simulation software in chapter 5. We found that the results from both the mathematical calculation and the simulation were in a good agreement. Furthermore, in chapter 6, the performance of the PON using OCDMA technique was compared with the TDMA technique in terms of the power budget, number of subscribers, the number of subscribers, and the spectral efficiency, respectively. Finally, we performed the experiment setup of the 1.25G OCDMA system using the en/decoder with the SBR = 0.8, and 0.1, respectively. The results from the experiment confirmed our mathematical results and the simulation results that the using of en/decoder with low SBR is greater in the noise suppression in comparison to the higher SBR.

8.1 Contributions from chapter 3

The first method to reduce the effects of noise in OCDMA system was to use the more number of chips. We investigated the effects of using different number of chips of 8, 16, and 32, respectively. The optical waveform of the ACP employing Fourier code was a triangle-like consisted of $2N-1$ chips. On the other hand, the optical waveforms of the CCP are depended on the distance between the desired and the interfered code. Then, the received power of the ACP and each CCP were used to find the PCR. At the adjacent code, the PCRs from the simulation for the case of 8, 16, and 32 chips are approximately 7 dB. Nevertheless, at the maximum distance between the desired and interfered codes, the PCRs for the case of 8, 16, and 32 are found to be 16.33, 22.33, and 28.33 dB, respectively. This result confirmed that the increase in number of chips is able to reduce the OCDMA noise effectively. Since the PCRs of the adjacent code are low, the interferences are so strong that we should avoid using the adjacent code. The simulation of 4 OCDMA signals employing code #1, #3, #5, and #7 were sent into the system simultaneously and the BER could achieve the BER under FEC limit. On the other hand, by adding the 5^{th} subscriber to the system, the BER of the 5^{th} subscriber was exceeded the FEC limit because it was suffered from the low PCR of the adjacent code.

8.2 Contributions from chapter 4

In this chapter, we proposed the mathematical model that used to shape the length of the total encoding period under the factor SBR. The en/decoded signals under various SBRs were used to calculate the signal power, noise power, and the numerical BER, respectively. We organized the calculation under the synchronous and the asynchronous transmission in order to find the performance of the desired subscriber under the worst case and the average case as the representative of the random access of the interfered subscribers.

The first advantage of the employing low SBR is the enhancement in the receiver sensitivity which is clearly seen for the case of single subscriber. For the multi-subscriber case, under the worst case scenario where all of interfered subscribers were aligned to obtain the strongest interference at the center of the ACP, the total numbers of subscribers that could achieve the BER under the FEC limit for the case of SBR = 0.6, 0.4, and 0.2 are greater than the case of conventional OCDMA system using SBR of 1.0 and 0.8, respectively. Moreover, in the asynchronous transmission, the average BERs for the case of SBR = 0.6, 0.4, and 0.2 are lower than the case of SBR = 1.0 and 0.8. The total numbers of subscribers of 8 can be achieved by only SBR = 0.2 with the full capacity of 320 Gbps.

In depth analysis of the OCDMA noise sources, we found that the most severe noise is the PBN. The variance of the PBN can be reduced effectively in the case of SBR = 0.6, 0.4, and 0.2 through the statistical independent in the asynchronous transmission. We also considered the system performance by using the S.E. The S.E. from the average case is improved for all SBR in comparison to the worst case. Moreover, the maximum S.E. of 0.62 b/s/Hz is obtained at SBR = 1.0, respectively.

The main contributions from this chapter are the solutions how to operate the OCDMA-PON in the real scenario with the maximum number of subscribers and the best point of SBR in order to operate the system under the maximum spectral efficiency, respectively.

8.3 Contributions from chapter 5

We showed the system verification of the OCDMA-PON employing various SBRs by using a simulation software. All components with the main system parameters used in the simulation and the system architecture including the screen layout are illustrated. The BER performances, the receiver sensitivities, the total number of subscribers obtained from the mathematical calculation and the simulation are in a good agreement. Moreover, we also showed the dispersive effect from the dispersion slope mismatched which are obtained from 3 SC rates of the DCF modules. The power budgets of each SBR are also report.

8.4 Contributions from chapter 6

First, the system architecture of the TDMA-PON was shown and we further described briefly about the main system parameters that were used in the simulation.

The signal transmission for the B-B case and the 20km with the DCF were shown. Then, the power penalties caused by the dispersion slope mismatched of the TDMA-PON were report. We compared the system performance of both TDMA-PON and OCDMA-PON by considering the power budget, the number of subscribers, the bit rate, and the S.E., respectively. The OCDMA-PON is greater than the TDMA-PON in the power budget, and the system complexity under the same bit rate. On the other hand, the TDMA-PON is greater than the OCDMA-PON in the number of subscribers and the S.E., respectively.

Nevertheless, at the bit rate over 80 Gbps, it is onerous to operate the PON using the TDMA technique since it needs the extremely fast electronic devices at the transmitters and the receiver. Moreover, the effect of pulse broadening caused by the dispersion slope mismatched is a serious problem that can cause the ISI effect. On the other side, for the case of OCDMA-PON with low SBR, we need a light source with a very good stability that can generate the ultra-short pulse with a desired repetition rate.

8.5 Contributions from chapter 7

We performed the experiment setup of the OCDMA signal transmission at the Photonic Network System Laboratory, National Institute of Communication Technology (NICT), Japan. The en/decoders that were used to verify our mathematical model are the AWG and the PLC which their SBRs are 0.8 and 0.1, respectively. First, the experiment was performed the use of the adjacent code for the case of 1-interfered subscriber in order to check the PBN suppression performance. The results of the first experiment show that, by using the SBR = 0.1 can suppress the beat noise and the BER is able to achieve the FEC limit with the power penalty of 12.75 dB. On the other hand, the case of SBR = 0.8 has the poor performance and the BER cannot achieve the FEC limit.

The second experiment, the distance between codes are 2. We showed the power penalty caused by the PBN and the MAI. The results confirmed that the case of SBR = 0.1 is capable of suppressing the PBN better than the case of SBR = 0.8. The power penalties of the 1-interfered subscriber are 3.31 and 13.99 dB for the case of SBR = 0.1 and 0.8, respectively.

The last experiment, we performed with 2-interfered subscribers owing the codes which the distance of code respected to the desired subscriber are 2. The results still confirmed our mathematical results that the case of SBR = 0.1 is better than the case of SBR = 0.8 in the noise suppression. The measured of power penalties are found to be 5.87 dB for the case of SBR = 0.1 whereas it is impossible to achieve the BER lower that 10^{-9} for the case of SBR = 0.8, respectively. Moreover, the average BER calculation using the measured BER is used to represent the average performance of the system.

8.6 Research Suggestion

The main scope of this thesis is to reduce the SBR of the OCDMA signal in order to reduce the noise variance. By using low SBR can decrease the electrical waveform fluctuation due to the high frequency components of the PBN is filtered out by the LPF. Nevertheless, by reducing the SBR, we also need to use the light source that have to generate the optical pulse width with the ultra-short FWHM. The nature of the short FWHM pulse can spread the optical spectrum and this could bring the poor S.E. The further analysis should be focused on the optimal point of the SBR in order to maximize the S.E. Furthermore, the chromatic dispersion and the dispersion slope effect can be solved by using the digital signal processing (DSP).

The other dimensions of the multiplexing schemes to increase the system capacity of the OCDMA are a challenge. The polarization division multiplexing (PDM) which each set of the OCDMA subscribers are transmitted via the same time and frequency, but different in the polarization axis, is being studied by many research groups. Moreover, the coherent detection with the aid of DSP may improve the performance of the OCDMA over PON by the advance modulation techniques.

In the upcoming year, the trend of the flexible network will bring an enormous breakthrough in the system bit rate, spectral efficiency and the capacity of the optical communication. The OCDMA technique with the good correlation property could be one of the candidates to be used in the next generation platform of the optical communication systems, respectively.

REFERENCES

1. Finnie, G. and S. ANALYST, *FTTH in Europe: Forecast & Prognosis, 2006-2011*. Heavy Reading, 2006.
2. Shinohara, H., *FTTH in Japan: Strategy, technology and implementation.* Plenary talk of ECOC2011, Geneva, Switzerland, 2011.
3. Wong, E., *Next-generation broadband access networks and technologies.* Lightwave Technology, Journal of, 2012. **30**(4): p. 597-608.
4. Specifications, P.L., *Management Parameters for 10 Gb/s Passive Optical Networks.* IEEE Std. **802**.
5. Rec, I., *G. 987.1," 10-Gigabit-Capable Passive Optical Networks (XG-PON): General Requirements,"*. 2009, ITU-T.
6. Luo, Y., et al., *Time-and wavelength-division multiplexed passive optical network (TWDM-PON) for next-generation PON stage 2 (NG-PON2).* Lightwave Technology, Journal of, 2013. **31**(4): p. 587-593.
7. Effenberger, F.J., et al., *Next-generation PON-part II: candidate systems for next-generation PON.* Communications Magazine, IEEE, 2009. **47**(11): p. 50-57.
8. Shumate, P.W., *Fiber-to-the-home: 1977–2007.* Journal of Lightwave Technology, 2008. **26**(9): p. 1093-1103.
9. Senior, J., S. Cusworth, and A. Ryley. *Wavelength division multiple access in fibre optic LANs*. in *Fibre Optic LANS and Techniques for the Local Loop, IEE Colloquium on*. 1989. IET.
10. Effenberger, F.J., *The XG-PON system: Cost effective 10 Gb/s access.* Journal of lightwave technology, 2011. **29**(4): p. 403-409.
11. Prucnal, P.R., *Optical code division multiple access: fundamentals and applications*. 2005: CRC press.
12. Prucnal, P.R., M. Santoro, and T.R. Fan, *Spread spectrum fiber-optic local area network using optical processing.* Lightwave Technology, Journal of, 1986. **4**(5): p. 547-554.
13. Kitayama, K., *State of the art and applications of optical code division multiple access.* European Cnference of Optical Communication (ECOC'04),(Stockholm, Sweden), 2004.
14. Kitayama, K.-i., X. Wang, and N. Wada, *OCDMA over WDM PON-solution path to gigabit-symmetric FTTH.* Lightwave Technology, Journal of, 2006. **24**(4): p. 1654-1662.
15. Teh, P., et al., *Demonstration of a four-channel WDM/OCDMA system using 255-chip 320-Gchip/s quarternary phase coding gratings.* Photonics Technology Letters, IEEE, 2002. **14**(2): p. 227-229.
16. Wang, X., et al., *Field trial of 3-WDM× 10-OCDMA× 10.71-Gb/s asynchronous WDM/DPSK-OCDMA using hybrid E/D without FEC and optical thresholding.* Lightwave Technology, Journal of, 2007. **25**(1): p. 207-215.
17. Kataoka, N., et al. *2.56 Tbps (40-Gbps x 8-wavelength x 4-OC x 2-POL) asynchronous WDM-OCDMA-PON using a multi-port encoder/decoder*. in

European Conference and Exposition on Optical Communications. 2011. Optical Society of America.

18. Kitayama, K.-i. and N. Wada, *Photonic IP routing.* Photonics Technology Letters, IEEE, 1999. **11**(12): p. 1689-1691.
19. Yoo, S., *Optical packet and burst switching technologies for the future photonic internet.* Lightwave Technology, Journal of, 2006. **24**(12): p. 4468-4492.
20. Furukawa, H., et al., *Demonstration of 10 Gbit ethernet/optical-packet converter for IP over optical packet switching network.* Journal of Lightwave Technology, 2009. **27**(13): p. 2379-2390.
21. Furukawa, H., N. Wada, and T. Miyazaki, *640 Gbit/s (64-wavelength 10 Gbit/s) data-rate wide-colored NRZ-DPSK optical packet switching and buffering demonstration.* Lightwave Technology, Journal of, 2010. **28**(4): p. 336-343.
22. Matsumoto, R., et al., *40G-OCDMA-PON system with an asymmetric structure using a single multi-port and sampled SSFBG encoder/decoders.* Journal of Lightwave Technology, 2014. **32**(6): p. 1132-1143.
23. Wada, N., K.-I. Mitayama, and H. Kurita. *10 Gbit/s optical code division multiplexing using 8-chip BPSK-code with time-gating detection*. in *Optical Communication, 1998. 24th European Conference on*. 1998. IEEE.
24. Kitayama, K.-i., *Code division multiplexing lightwave networks based upon optical code conversion.* Selected Areas in Communications, IEEE Journal on, 1998. **16**(7): p. 1309-1319.
25. Wang, X. and K.-i. Kitayama, *Analysis of beat noise in coherent and incoherent time-spreading OCDMA.* Journal of Lightwave Technology, 2004. **22**(10): p. 2226.
26. Lee, J.H., et al., *A grating-based OCDMA coding-decoding system incorporating a nonlinear optical loop mirror for improved code recognition and noise reduction.* Journal of lightwave technology, 2002. **20**(1): p. 36.
27. Tsuda, H., et al. *Photonic spectral encoder/decoder using an arrayed-waveguide grating for coherent optical code division multiplexing*. in *Wavelength Division Multiplexing Components*. 1999. Optical Society of America.
28. Ebrahimi, P., et al. *A 10-μs-tuning MEMS-actuated Gires-Tournois filter for use as a tunable Wavelength Demultiplexer and a tunable OCDMA encoder/decoder*. in *Optical Fiber Communication Conference*. 2004. Optical Society of America.
29. Jiang, Z., et al., *Four-user, 2.5-Gb/s, spectrally coded OCDMA system demonstration using low-power nonlinear processing.* Journal of lightwave technology, 2005. **23**(1): p. 143.
30. Hamanaka, T., et al., *Ten-user truly asynchronous gigabit OCDMA transmission experiment with a 511-chip SSFBG en/decoder.* Journal of lightwave technology, 2006. **24**(1): p. 95.
31. Cincotti, G., *Full optical encoders/decoders for photonic IP routers.* Journal of lightwave technology, 2004. **22**(2): p. 337.
32. Cincotti, G., *Design of optical full encoders/decoders for code-based photonic routers.* Journal of lightwave technology, 2004. **22**(7): p. 1642.

33. Wang, X., et al., *Demonstration of over 128-gb/s-capacity (12-User/spl times/10.71-gb/s/user) asynchronous OCDMA using FEC and AWG-based multiport optical encoder/decoders.* Photonics Technology Letters, IEEE, 2006. **18**(15): p. 1603-1605.
34. Hanawa, M. *Fourier code: A novel orthogonal code for OCDM systems*. in *OECC/ACOFT 2008-Joint Conference of the Opto-Electronics and Communications Conference and the Australian Conference on Optical Fibre Technology*. 2008.
35. Choi, Y.-K., et al., *Upstream transmission of WDM/OCDM-PON in a loop-back configuration with remotely supplied short optical pulses.* Journal of Optical Communications and Networking, 2013. **5**(3): p. 183-189.
36. Kataoka, N., et al., *Demonstration of asynchronous, 40Gbps x 4-user DPSK-OCDMA transmission using a multi-port encoder/decoder.* Optics express, 2011. **19**(26): p. B965-B970.
37. Wang, X., et al. *Flexible 10 Gbps, 8-User DPSK-OCDMA System with 16* 16 Ports Encoder and 16-Level Phase-Shifted SSFBG Decoders*. in *Optical Fiber Communication Conference*. 2008. Optical Society of America.
38. Matsumoto, R., et al. *Apodized SSFBG Encoder/Decoder for 40G-OCDMA-PON System*. in *OptoElectronics and Communications Conference and Photonics in Switching*. 2013. Optical Society of America.
39. Gao, Z., et al., *Stealth transmission of time-domain spectral phase encoded OCDMA signal over WDM network.* Photonics Technology Letters, IEEE, 2010. **22**(13): p. 993-995.
40. Yoshima, S., et al., *Full-duplex, extended-reach 10G-TDM-OCDM-PON system without En/decoder at ONU.* Lightwave Technology, Journal of, 2013. **31**(1): p. 43-49.
41. Tanaka, Y., et al. *100-km uplink transmission of 10G-and 1G-ONU co-existing TDM-OCDMA-PON system using dual-rate burst-mode receiver*. in *Optical Fiber Communication Conference*. 2011. Optical Society of America.
42. ITU, T., *Recommendation G. 652.* Characteristics of a singlemode optical fibre and cable, 2003.
43. Agrawal, G.P., *Lightwave technology: telecommunication systems*. 2005: John Wiley & Sons.
44. Keiser, G., *Optical fiber communications*. 2003: Wiley Online Library.
45. Koonen, A. *Technologies and applications of FTTx*. in *IEEE Lasers & Electro-Optics Society*. 2006.
46. Keiser, G., *FTTX concepts and applications*. Vol. 91. 2006: John Wiley & Sons.
47. Lee, C.-H., W.V. Sorin, and B.Y. Kim, *Fiber to the home using a PON infrastructure.* Journal of Lightwave Technology, 2006. **24**(12): p. 4568-4583.
48. DeCusatis, C., *Handbook of fiber optic data communication: a practical guide to optical networking*. 2013: Academic Press.
49. Wang, X., et al., *High reflectivity superstructured FBG for coherent optical code generation and recognition.* Optics express, 2004. **12**(22): p. 5457-5468.
50. Kodama, T., et al., *Asynchronous OCDM-based 10 G-PON using cascaded multiport E/Ds to suppress MAI noise.* Journal of Lightwave Technology, 2013. **31**(20): p. 3258-3266.

51. Amaya, W., D. Pastor, and J. Capmany, *Modeling of a time-spreading OCDMA system including nonperfect time gating, optical thresholding, and fully asynchronous signal/interference overlapping.* Journal of Lightwave Technology, 2008. **26**(7): p. 768-776.
52. Winzer, P.J. and R.-J. Essiambre, *Advanced optical modulation formats.* Proceedings of the IEEE, 2006. **94**(5): p. 952-985.
53. Diaz-Otero, F.J. and P. Chamorro-Posada, *Bundled solitons collision-induced frequency shifts in multiple-channel WDM dispersion managed systems.* Optics Communications, 2014. **332**: p. 1-8.
54. Bi, M., et al., *Power Budget Improved Symmetric 40-Gb/s Long Reach Stacked WDM-OFDM-PON System Based on Single Tunable Optical Filter.* Photonics Journal, IEEE, 2014. **6**(2): p. 1-8.
55. Li, X., et al., *Time-domain adaptive decision-directed channel equalizer for RGI-DP-CO-OFDM.* Photonics Technology Letters, IEEE, 2014. **26**(3): p. 285-288.
56. Li, Z., et al., *Aurora: A Cross-Layer Solution for Thermally Resilient Photonic Network-on-Chip.* Very Large Scale Integration (VLSI) Systems, IEEE Transactions on, 2015. **23**(1): p. 170-183.
57. Li, L., et al., *TWA-based channel estimation for CO-OFDM systems.* Optoelectronics Letters, 2014. **10**: p. 133-136.
58. Imtiaz, W.A., et al., *A Comparative Study of Multiplexing Schemes for Next Generation Optical Access Networks.* Journal of Optical Communications, 2014. **35**(3): p. 201-205.
59. Liu, Y.-h., et al., *A novel joint technique for PAPR reduction in CO-OFDM systems.* Optoelectronics Letters, 2014. **10**: p. 277-280.
60. Pandey, G. and A. Goel, *Long reach colorless WDM OFDM-PON using direct detection OFDM transmission for downstream and OOK for upstream.* Optical and Quantum Electronics, 2014. **46**(12): p. 1509-1518.
61. Han, X. and C.-H. Cheng, *Nonlinear filter based decision feedback equalizer for optical communication systems.* Optics express, 2014. **22**(7): p. 8712-8719.
62. You, H., et al., *Multi-Wavelength Optical Single-Sideband Modulated WDM Radio-over-Fiber Systems by Employing a Twin-Core Fiber.* Lightwave Technology, Journal of, 2014. **32**(20): p. 3868-3873.
63. Zhu, Z., et al., *A Linearized Optical Single-Sideband Modulation Analog Microwave Photonic Link Using Dual Parallel Interferometers.* Photonics Journal, IEEE, 2013. **5**(5): p. 5501712-5501712.
64. Zhu, Z., et al., *A Radio-Over-Fiber System With Frequency 12-Tupling Optical Millimeter-Wave Generation to Overcome Chromatic Dispersion.* Quantum Electronics, IEEE Journal of, 2013. **49**(11): p. 919-922.
65. Li, X., et al., *Fiber nonlinearity tolerance of APSK modulated DFT-S OFDM systems.* Photonics Technology Letters, IEEE, 2013. **25**(23): p. 2304-2307.
66. Minato, N., et al., *Inter-Band Crosstalk Reduction Using Sinc Apodization of Super-Structured Fiber Bragg Gratings for Hybrid WDM/OCDM Add/Drop Filters.* Photonics Technology Letters, IEEE, 2012. **24**(6): p. 446-448.
67. Karar, A.S., et al., *Electronic pre-compensation for a 10.7-Gb/s system employing a directly modulated laser.* Journal of Lightwave Technology, 2011. **29**(13): p. 2069-2076.

68. Zhang, F., et al., *A broadcast/multicast-capable carrier-reuse WDM-PON.* Lightwave Technology, Journal of, 2011. **29**(15): p. 2276-2284.
69. Pan, J. and C.-H. Cheng, *Nonlinear electrical predistortion and equalization for the coherent optical communication system.* Lightwave Technology, Journal of, 2011. **29**(18): p. 2785-2789.
70. Xia, H., et al., *Ultrafast and precise interrogation of fiber Bragg grating sensor based on wavelength-to-time mapping incorporating higher order dispersion.* Journal of lightwave technology, 2010. **28**(3): p. 254-261.

APPENDIX

PUBLICATIONS

International Periodical Journals

1. R. Maneekut and P. Kaewplung, "The BER Improvement of the Coherent Time Spreading OCDM-PON Using Various Spreading-Time to Bit-Period Ratio," submitted to the Journal of Lightwave Technology.
2. R. Maneekut, S. Shimizu, N. Wada, and P. Kaewplung, "The Enhancement of the Receiver Sensitivity in the 1.25 Gbps OCDM System Using Various Spreading-Time to Bit-Period Ratio En/Decoder," in the process of submitting to the IEEJ Transactions on Electrical and Electronic Engineering.

International Conference Proceedings

1. R. Maneekut and P. Kaewplung, "Performance of OCDMA signal transmission over passive optical network," in *proceeding of 16th OptoElectronics and Communications Conference (OECC),* 2011, pp.571-572.
2. V. Ket-Urai, R. Maneekut and P. Kaewplung, "Feasibility of 40-Gbps RZ-DQPSK Signal Transmission over PON," in *proceeding of 17th OptoElectronics and Communications Conference (OECC),* 2012, pp.319-320.
3. T. Sakchaichanchon, R. Maneekut and P. Kaewplung, "40-Gbps DPSK-OCDMA Transmission over PON Using 8, 16 and 32-Level Phase-Shifted En/Decoders," in *proceeding of 18th Asia-Pacific Conference on Communications (APCC), 2012.*
4. R. Maneekut, T. Sakchaichanchon, V. Ket-Urai and P. Kaewplung, "Recent Progress of the Next Generation 40-Gbps Signal Transmission over Passive Optical Network Using the Advance Modulation Formats," presented in *11th International Conference on Optical Communications and Networks (ICOCN), 2012.*
5. P. Kanjanopas, R. Maneekut, and P. Kaewplung, "FTTx with dynamic wavelength and bandwidth allocation," *in proceeding of The International Conference on Information Networking 2014 (ICOIN2014),* Feb, 2014, pp. 517-520.
6. R. Maneekut, and P. Kaewplung, "Feasibility of 40-Gbps DPSK-Based OCDMA PON Using a Programmable 8-Chip En/Decoder," in *proceeding of 29th International Technical Conference on Circuits/Systems, Computers and Communications (ITC-CSCC), July, 2014.*
7. T. Wiriyanitikorn, R. Maneekut, and P. Kaewplung, "An Algorithm for Balancing Traffic Load of Optical Network Units in Wireless-Optical Broadband Access Network," in *proceeding of 29th International Technical Conference on Circuits/Systems, Computers and Communications (ITC-CSCC), July, 2014.*

8. T. Jaemkarnjanaloha, R. Maneekut, and P. Kaewplung, “The Transmission Characteristics of Non- Coherent Optical OFDM signal on Optical Phase Conjugation System,” in *proceeding of 29th International Technical Conference on Circuits/Systems, Computers and Communications (ITC-CSCC), July, 2014.*
9. P. Vijarnstit, R. Maneekut, and P. Kaewplung, “Evolution in the Performance of Superchannel Coherent Optical OFDM Signal Transmission and Its Application to Fiber Access Network,” in *proceeding of 29th International Technical Conference on Circuits/Systems, Computers and Communications (ITC-CSCC), July, 2014.*
10. P. Pensri, R. Maneekut, and P. Kaewplung, “Superchannel N-WDM Signal Transmission,” in *proceeding of 29th International Technical Conference on Circuits/Systems, Computers and Communications (ITC-CSCC), July, 2014.*
11. P. Vijarnstit, R. Maneekut, and P. Kaewplung, “A flexible fiber access network using superchannel coherent optical orthogonal frequency division multiplexing,” *in proceeding of* 17th International Conference on Advanced Communication Technology (ICACT) , July, 2015, pp. 319-322.

National Conference Proceedings

1. R. Maneekut and P. Kaewplung, “Influence of System Parameters on OCDMA Signal Transmission over Passive Optical Network ,” in *proceeding of 34th Electrical Engineering Conference (EE-CON),* 2011
2. วราภรณ์ เกตุอุไร, รชฎ มณีขัติ และพสุ แก้วปลั่ง, “Feasibility of 40 Gbps transmission on passive optical network,” in *proceeding of* 7th National Conference on Optics and Applications (NCOA-5), 2012.

VITA

Rachata Maneekut was born in Chiang Mai, Thailand in December 1985, He received the B.E and M.E degrees in electrical engineering from Chulalongkorn University, Thailand, in 2007 and 2010, respectively. He is currently puesuing the Ph.D from the Microwave and Lightwave Communications Strategic Research Area, Department of Electrical Engineering, Faculty of Engineering, Chulalongkorn University. His research interests are including the advance modulation scheme over passive optical network, optical signal processing, and the next-generation optical elastic network technology.